Technical Report CERC-94-4
August 1994

US Army Corps
of Engineers
Waterways Experiment
Station

New York Bight Study

Report 1:
Hydrodynamic Modeling

by Norman W. Scheffner, S. Rao Vemulakonda,
David J. Mark, H. Lee Butler, Keu W. Kim

Prepared for U.S. Army Engineer District, New York

Technical Report CERC-94-4
August 1994

New York Bight Study

Report 1:
Hydrodynamic Modeling

by Norman W. Scheffner, S. Rao Vemulakonda,
David J. Mark, H. Lee Butler, Keu W. Kim

U.S. Army Corps of Engineers
Waterways Experiment Station
3909 Halls Ferry Road
Vicksburg, MS 39180-6199

Report 1 of a series

Approved for public release; distribution is unlimited

Prepared for U.S. Army Engineer District, New York
New York, NY 10278

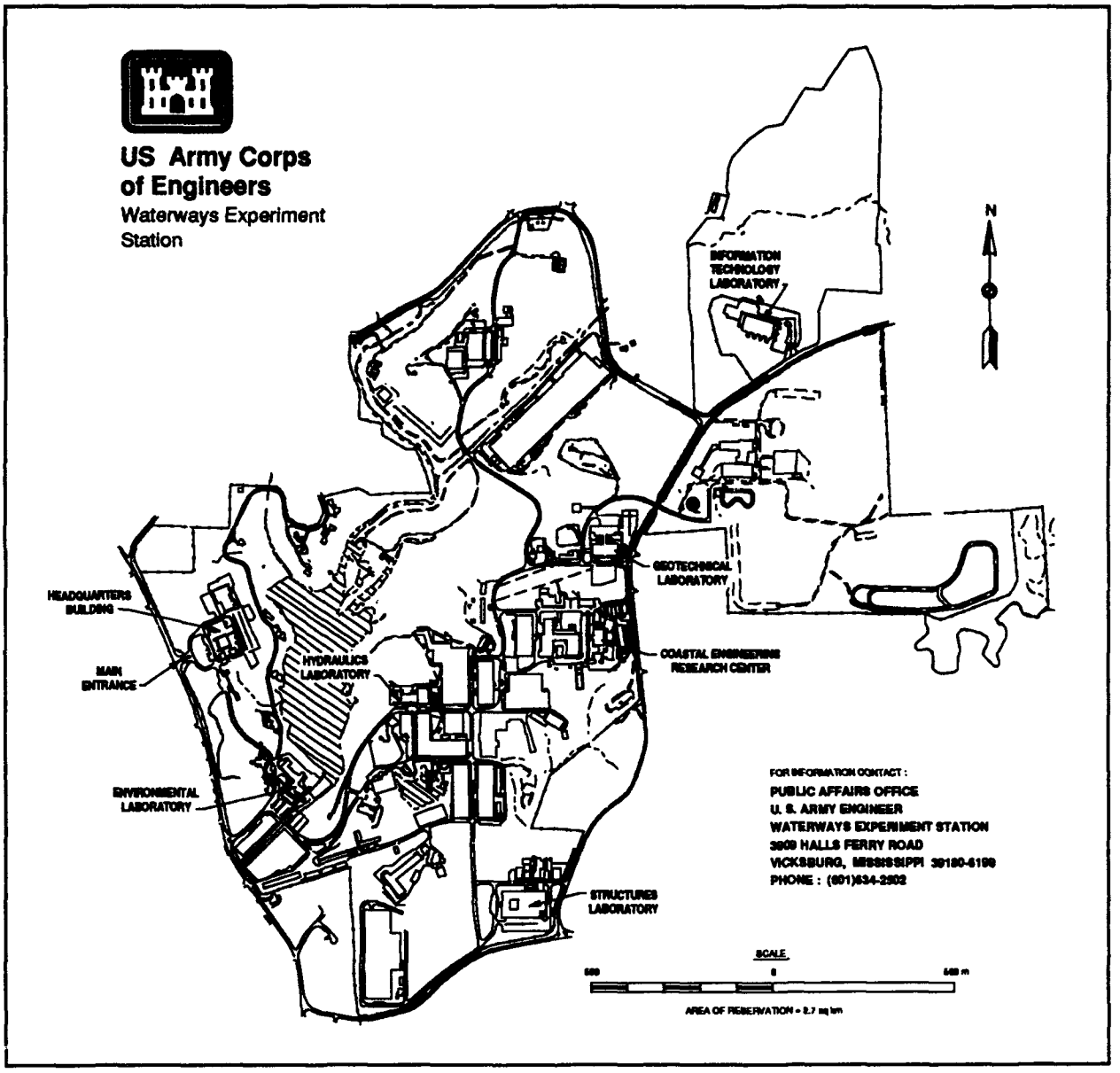

Waterways Experiment Station Cataloging-in-Publication Data

New York Bight Study. Report 1, Hydrodynamic modeling / by Norman W. Scheffner... [et al.] ; prepared for U.S. Army Engineer District, New York.
228 p. : ill. ; 28 cm. — (Technical report ; CERC-94-4)
Report 1 of a series
Includes bibliographic references.
1. Oceanography — New York Bight (N.J. and N.Y.) 2. Oceanic mixing — Long Island Sound Region (N.Y. and Conn.) 3. Hydrodynamics — Mathematical models. 4. New York Bight (N.J. and N.Y.) I. Scheffner, Norman W. II. United States. Army. Corps of Engineers. New York District. III. U.S. Army Engineer Waterways Experiment Station. IV. Title: Hydrodynamic modeling. V. Series: Technical report (U.S. Army Engineer Waterways Experiment Station) ; CERC-94-4.
TA7 W34 no.CERC-94-4

Contents

List of Tables

Preface

The New York Bight (NY Bight) Study is an investigation to determine the feasibility of using a numerical model to assess impacts to the NY Bight that may result from the various uses of the NY Bight. Potential uses include ocean disposal sites and the possible construction of offshore coastal structures. A combined hydrodynamic-environmental (hydro-environmental) modeling technique, used in conjunction with a monitoring plan and geographical information system, was identified as an approach that could be used to successfully satisfy the goals of the study. This approach was adopted and the feasibility of the coupled modeling technology was demonstrated. This report describes the implementation of the hydrodynamic modeling effort conducted to demonstrate that the dynamics of the NY Bight can be accurately simulated to provide water surface and current data to the environmental modeling component of the study.

The hydrodynamic modeling effort represents one aspect of the overall study. Additional reports will describe the water quality modeling effort, the development of a field monitoring plan, and the generation of a data-base/geographical information system. The overall objective of the investigation is to utilize numerical modeling techniques and information retrieval systems to evaluate potential impacts of the various uses of the NY Bight. Results of the study provide a means of estimating the response of the NY Bight to various hydrodynamic or environmental scenarios. This study provides the U.S. Army Engineer District, New York (CENAN) with a systematic approach to estimating future responses of the NY Bight to various hydrodynamic or environmental conditions.

The U.S. Army Engineer Waterways Experiment Station (WES) gratefully acknowledges the direction and assistance of Mr. John Tavolaro, Ms. Patricia Barnell-Pechko, Ms. Lynn Bocamazo, and Mr. Bryce Wisemiller (CENAN). In addition to those involved in the management of the study, the following contributions are gratefully acknowledged and highly appreciated: Dr. Henry Frey and his staff from National Ocean Service furnished 1990 field data for the Long Island Sound. Dr. Donald W. Prichard furnished 1990 salinity and temperature profile data and a summary on circulation in the Long Island Sound.

Hydrodynamic simulations were conducted by Drs. Keu W. Kim and S. Rao Vemulakonda, WES. The final report was prepared by Drs. Norman W. Scheffner, Rao Vemulakonda, and Keu Kim, WES.

General supervision was provided by Dr. James R. Houston and Mr. Charles C. Calhoun, Jr., Director and Assistant Director, respectively, of the WES Coastal Engineering Research Center (CERC). Direct supervision of the project was provided by Mr. H. Lee Butler, Chief of the CERC Research Division (RD) and overall manager of the NY Bight project, and Mr. Bruce A. Ebersole, Chief of the Coastal Processes Branch, RD, CERC, and Dr. Martin C. Miller, Chief of the Oceanography Branch, RD, CERC.

At the time of publication of this report, Director of WES was Dr. Robert W. Whalin. Commander was COL Bruce K. Howard, EN.

1 Introduction

Background

The New York Bight (NY Bight) is the area bounded by a line extending offshore of Cape May, New Jersey to the continental shelf, along the shelf, and offshore of Montauk Point, New York, to the continental shelf. The majority of waterborne traffic into and out of New York Harbor therefore passes through the NY Bight, making it one of the busiest waterways in the world. In addition to its role as a major commerce route, the NY Bight also provides suitable locations for the placement of dredged material generated in support of navigation. There are considerable concerns regarding the effects of these actions, as well as naturally occurring events, on the environmental resources of the NY Bight.

The NY Bight Study began as an investigation to determine the feasibility of assessing impacts to the NY Bight flow system that may result from the various uses of the NY Bight. The goal of the study, authorized under the authority of Section 728 of the Water Resources Act of 1986, was to identify a means of developing a comprehensive tool for effectively managing the resources of the NY Bight and Harbor estuaries with an emphasis on addressing environmental, economic, and societal needs. Areas of primary concern include ocean disposal of dredged material, disposal of pollutants, and possible future projects, such as containment islands.

A combined hydrodynamic-environmental (hydro-environmental) modeling technique, used with a monitoring plan and information system, was identified as the preferred approach to successfully investigate potential impacts to the NY Bight. This approach was adopted and a feasibility demonstration was developed as a proof of concept. This report describes the implementation of the hydrodynamic modeling effort conducted as a component of the overall study to demonstrate that the flow regime of the NY Bight can be successfully simulated to provide quantitative insight into the complex behavior of the flow system, including NY Bight, NY Harbor area, and Long Island Sound. The resulting currents can then be used to predict the transport and fate of both surface and sub-surface dissolved and suspended pollutants.

The following sections describe the physical complexities of the modeled system, i.e., NY Bight, NY Harbor, and Long Island Sound. Also presented are details of the scope of work, addressing pertinent problems and needs of the NY Harbor estuary. Subsequent sections describe the hydrodynamic model used to simulate the physical system; the analysis of prototype data collected within the NY Bight system; and the implementation of the numerical model to include calibration, verification, and application. Results of, and difficulties encountered during, the calibration and verification phase provide insight for recommendations concerning the implementation of a hydrodynamic/water quality monitoring system. Details of a recommended monitoring plan will be presented following the sections of the report documenting validation of the model. Conclusions reached as a result of the hydrodynamic modeling phase of this investigation are finally presented. The water quality modeling task of this study, as well as the executive summary on the overall project, are presented in subsequent reports.

Description of Area

The NY Bight occupies that portion of the Middle Atlantic Bight extending north from Cape May, New Jersey, to Montauk Point, New York. The present study is concerned with the hydrodynamically coupled NY Bight, Long Island Sound, and Hudson and East River flow s stems. The area of investigation therefore considers the entire coastal area extending from Cape May, New Jersey, to Nantucket Shoals, located south of Cape Cod, Massachusetts, as indicated in Figure 1. The study area is bounded by the interior coastline and extends approximately 160 km offshore to beyond the continental shelf break. Depths in the study area range from 3 m near Sandy Hook, New Jersey, to 900 m in the Hudson Canyon, to over 2,000 m seaward of the continental shelf. Average depths are approximately 60 m.

Circulation of water in the NY Bight is influenced by astronomical tide fluctuations, meteorological forcings, and large-scale oceanic circulation patterns affecting the entire Middle Atlantic Bight. Additional influences that can have significant local effects on the circulation include the bathymetric variations in the NY Bight and flow from the Hudson-Raritan Estuary. A comprehensive review of the physical oceanography of the Middle Atlantic Bight, from the earliest investigations through more contemporary studies, is presented by Beardsley and Boicourt (1981). The availability of historical current meter, wind, and sea level data sets for the Middle Atlantic Bight through 1982-1983 is summarized by Moody et al. (1984). A thorough description of data used in this study is presented in Chapter 3 of this report.

Scope of Work

The current study focuses on a coupled hydrodynamic and environmental (termed hydro-environmental) modeling effort, the development of a compre-

hensive environmental monitoring plan based (in part) on the findings of the modeling effort, and the development of a Geographic Information System (GIS) for the NY Bight. The GIS will utilize results from both the hydrodynamic and environmental numerical models as well as existing databases of information pertaining to the NY Bight. These data will provide a capacity for assessing various or multiple impacts to the NY Bight system.

Details of the scope of work developed to accomplish the goals of this study are presented below. Because this report represents only the hydrodynamic phase of the project, the scope concentrates on the tasks necessary for the completion of the hydrodynamic modeling and monitoring recommendation portions of the study. For continuity, however, major aspects of the environmental modeling effort, the monitoring plan, and the construction of the GIS will be itemized. Complete details of those additional efforts, as well as the conclusions and recommendations from those efforts, are presented in separate reports.

The majority of potential problems in the NY Bight are related to various aspects of water quality such as floatable and/or pollutant transport and anoxic conditions. Water quality constituents are, in general, transported and diffused by both local currents and large-scale circulation patterns. Water quality impacts in the NY Bight can not be successfully investigated without an accurate description of the hydrodynamic processes within the NY Bight. Therefore, the time-varying three-dimensional (3-D) hydrodynamic model (HM) Curvilinear Hydrodynamics in Three Dimensions - U.S. Army Engineer Waterways Experiment Station (CH3D-WES) was used to provide flow field input data for the 3-D environmental model.

A second aspect of the hydro-environmental study was the development of a monitoring plan. This plan will provide guidance for the collection of hydrodynamic boundary condition data for the HM, water quality related data for the environmental model, and biological data to increase our understanding of the overall NY Bight system. Because this report concentrates on the application of the HM, only the hydrodynamic monitoring recommendations are presented in detail. However, as will be described in a subsequent section of this report, the monitoring of certain key environmental parameters such as temperature, salinity, and dissolved oxygen are recommended to be taken in conjunction with the surface elevation and current hydrodynamic data.

Finally, all available data will be archived into a GIS database such that the effects of various impacts to the NY Bight can be anticipated by interrogation of available data. The following paragraphs briefly describe the major tasks and components of the scope of work identified as central to the hydrodynamic and environmental modeling, monitoring, and GIS components of this study.

Task A: Development of the 3-D hydrodynamic model

The work effort required for the hydrodynamic modeling effort involved grid generation, determination of appropriate boundary conditions and their locations. Subsequent tasks included calibration and verification of the model based on measured data and model results as well as resolution and discretization testing. Subtasks devoted to this component are briefly described as follows and are described in detail in Chapter 2.

A.1 Grid generation. A coarse, horizontally curvilinear grid was initially generated with sufficient resolution to represent both deep and shallow areas in the NY Bight. The grid extends from Cape May in the south to Nantucket Shoals in the north, and extends offshore to the 2,000-m contour. The initial grid was then modified to meet the fine horizontal and vertical resolution requirements necessary for modeling the NY Bight apex and East River.

A.2 Tidal boundary condition generation. Tidal time series data for lateral open water boundaries along the continental shelf were generated using existing global tide models as well as prototype time series. An analysis of results was used to select boundary conditions for application of the model.

A.3 Steady state diagnostic tests. A qualitative evaluation of the HM was made through analysis of time-averaged currents, surface elevations along the open water boundaries, riverine inflow, and surface wind stress.

A.4 Model calibration/verification. Model calibration and verification were accomplished by comparing measured prototype data to model predictions based on prototype freshwater inflow, tide, and wind data boundary conditions. These comparisons provide an evaluation of the capabilities of the HM to represent hydrodynamics in the NY Bight for a wide range of boundary and forcing conditions. Future data needs for specifying model boundary conditions are identified and expanded upon in the hydrodynamic monitoring section in Chapter 7 of this report.

A.5 Testing of boundary conditions. Various open-water boundary conditions such as cross-shelf elevation gradients, shelf-break elevation, river flow across boundaries, etc. are tested in order to evaluate model response to different boundary conditions.

Task B: Development of the 3-D water quality model

The work effort required for the water quality modeling phase of the study concentrates on reporting results on dissolved oxygen calibration, sensitivity tests, and model demonstration simulations. Subtasks devoted to this component are briefly described below because they interact with the hydrodynamic tasks described above. Details are described in a separate report.

B.1 Water quality model linkages. Hydrodynamic simulations including salt transport were compared to the similar transport computations in the Water Quality Model (WQM) to assure that HM and WQM simulations were in agreement.

B.2 Dissolved oxygen calibration. The WQM was coarsely calibrated for transport of dissolved oxygen and nutrients for the anoxia event which occurred in the summer of 1976.

B.3 Sensitivity testing. Tests were made on the sensitivity of the WQM to various boundary conditions.

B.4 Model demonstration simulations. The model was applied with nutrient load reductions for non-point source and point source loads.

Task C: Contaminant screening and particle tracking models

The Contaminant Screening model (RECOVERY) and the particle tracking model were developed for application to the NY Bight. Both models require flow field input from CH3D. The RECOVERY model simulates the concentration of trace metals in the water and bed sediment over long periods of time. The particle tracking model simulates the time-varying location of particles released on the water surface (i.e., floatables) as well as in the water column. Details of both models are presented in separate reports.

Task D: Hydrodynamic, water quality, and biological monitoring

The hydrodynamic and water quality monitoring efforts performed under this task were limited to identifying feasibility, instrumentation capability, and monitoring procedures which could be used in support of the recommended monitoring program. As previously stated, the hydrodynamic monitoring recommendations are presented in Chapter 7 of this report.

The biological monitoring effort was limited to identifying potential biological impacts, reviewing and evaluating existing data/modeling procedures, and recommending a plan to rectify data/model/program gaps. Results of both of the above subtasks are described in detail in a separate report.

Task E: Informational database

This task included the development of a relational database (RDB) and the development of interface procedures for linking the New York District's GIS to the RDB and the numerical model generated information. A detailed description of the database and associated subtasks are presented in a separate report.

2 Hydrodynamic Modeling

Background

The National Oceanic and Atmospheric Administration (NOAA) Marine EcoSystems Analysis (MESA) Program was formed in 1972 to help focus both government and non-government research on regional problems caused by man's use of marine and estuarine resources. In 1973, the MESA NY Bight Project was initiated with a goal of developing a comprehensive research program which would help provide an understanding of the NY Bight as a productive marine ecosystem.

The past 15 years (for example, 1977 - 1991) of modeling studies of the NY Bight have relied almost exclusively on data generated by earlier studies. The description of the NY Bight's dynamics and the interrelationships of various parameters have been greatly advanced by investigations in the mid-1980's reported by Beardsley and Boicourt (1981), Hopkins and Dieterle (1983, 1987), and others. They have succeeded in modeling, summarizing their data, and building upon data from previous studies to provide a clear picture of the circulation and dynamics within the NY Bight.

In recent years, hydrodynamic circulation models have become fully three-dimensional, and as such, they provide a physically realistic description of the complex behavior of large hydrodynamic systems such as the NY Bight. The models are based on primitive equations, are time-dependent, include free-surface variations, and use either a z-plane grid in which the vertical grid spacing is fixed or a sigma-coordinate system in which the vertical spacing is specified as a fixed percentage of the local depth. Examples include models developed by Leendertse, Alexander, and Liu (1973); Oey, Mellor, and Hires (1985a, b, c, d); and Blumberg and Mellor (1987). Oey, Mellor, and Hires (1985a, b, c, d) compared their time-dependent three-dimensional numerical simulation results within just the Hudson-Raritan Estuary with prototype observations. These observations included instantaneous salinity, water surface amplitudes and phases of the M_2 tidal constituent, mean current and mean salinity in the Hudson River, kinematic-energy spectra, response to wind forcing, salt fluxes, and volume transport. They concluded that future

estuarine modeling should be directed toward a model in which the estuary is coupled to the continental shelf. Therefore, the model selected for the present study was required to represent the entire coupled flow regime, to include the NY Harbor, Long Island Sound, and the NY Bight from the land boundary to beyond the break in the continental shelf with the focus on the NY Bight.

CH3D-WES Hydrodynamic Model

The numerical hydrodynamic model CH3D-WES was selected to provide detailed hydrodynamic flow field information for input to the environmental model. The basic model (CH3D) was developed by Sheng (1986) for WES but was extensively modified in its application to the Chesapeake Bay Study. These modifications have consisted of implementing different basic numerical formulations of the governing equations as well as substantial recoding of the model to provide more efficient computing. As its name implies, CH3D-WES makes hydrodynamic computations on a curvilinear or boundary-fitted planform grid. Physical processes impacting circulation and vertical mixing that are modeled include tides, wind, density effects (salinity and temperature), freshwater inflows, turbulence, and the effect of the earth's rotation.

An adequate representation of the vertical turbulence is crucial to a successful simulation of stratification and destratification. A second-order turbulence model based upon the assumption of local equilibrium of turbulence is employed. The boundary-fitted coordinate feature of the model provides grid resolution enhancement necessary to adequately represent deep navigation channels and irregular shoreline configurations of the flow system. The curvilinear grid also permits adoption of accurate and economical grid schematization software. The solution algorithm employs an external mode in which the free surface elevation and depth-averaged currents are computed as input to the internal mode, which provides the full 3-D solution.

Governing equations

The governing partial differential equations are based on the following assumption:

a. The hydrostatic pressure distribution adequately describes the vertical distribution of fluid pressure.

b. The Boussinesq approximation is appropriate.

c. The eddy viscosity approach adequately describes turbulent mixing in the flow.

The basic equations for an incompressible fluid in a right-handed Cartesian coordinate system (x,y,z) are (Johnson et al. 1991):

$$\frac{\partial u}{\partial x} + \frac{\partial v}{\partial y} + \frac{\partial w}{\partial z} = 0 \qquad (1)$$

$$\frac{\partial u}{\partial t} + \frac{\partial u^2}{\partial x} + \frac{\partial uv}{\partial y} + \frac{\partial uw}{\partial z} = fv - \frac{1}{\rho_o}\frac{\partial p}{\partial x} + \frac{\partial}{\partial x}\left(A_H \frac{\partial u}{\partial x}\right)$$

$$+ \frac{\partial}{\partial y}\left(A_H \frac{\partial u}{\partial y}\right) + \frac{\partial}{\partial z}\left(A_v \frac{\partial u}{\partial z}\right) \qquad (2)$$

$$\frac{\partial v}{\partial t} + \frac{\partial uv}{\partial x} + \frac{\partial v^2}{\partial y} + \frac{\partial vw}{\partial z} = -fu - \frac{1}{\rho_o}\frac{\partial p}{\partial y} + \frac{\partial}{\partial x}\left(A_H \frac{\partial v}{\partial x}\right)$$

$$+ \frac{\partial}{\partial y}\left(A_H \frac{\partial v}{\partial y}\right) + \frac{\partial}{\partial z}\left(A_v \frac{\partial v}{\partial z}\right) \qquad (3)$$

$$\frac{\partial p}{\partial z} = -\rho g \qquad (4)$$

$$\frac{\partial T}{\partial t} + \frac{\partial uT}{\partial x} + \frac{\partial vT}{\partial y} + \frac{\partial wT}{\partial z} = \frac{\partial}{\partial x}\left(K_H \frac{\partial T}{\partial x}\right) + \frac{\partial}{\partial y}\left(K_H \frac{\partial T}{\partial y}\right) + \frac{\partial}{\partial z}\left(K_v \frac{\partial T}{\partial z}\right) \qquad (5)$$

$$\frac{\partial S}{\partial t} + \frac{\partial uS}{\partial x} + \frac{\partial vS}{\partial y} + \frac{\partial wS}{\partial z} = \frac{\partial}{\partial x}\left(K_H \frac{\partial S}{\partial x}\right) + \frac{\partial}{\partial y}\left(K_H \frac{\partial S}{\partial y}\right) + \frac{\partial}{\partial z}\left(K_v \frac{\partial S}{\partial z}\right) \qquad (6)$$

$$\rho = \rho\,(T,S) \qquad (7)$$

where

(u,v,w) = velocities in (x,y,z) directions
t = time
f = Coriolis parameter defined as $2\Omega \sin \phi$

where

Ω = rotational speed of the earth
ϕ = latitude
ρ = density
p = pressure
A_H, K_H = horizontal turbulent eddy coefficients
A_v, K_v = vertical turbulent eddy coefficients
g = gravitational acceleration
T = temperature
S = salinity

Equation 4 implies that vertical accelerations are negligible and thus the pressure is hydrostatic. Various forms of the equation of state can be specified for Equation 7. In the present model, the formulation given below is used:

$$\rho = P/(\alpha + 0.698P) \tag{8}$$

where

$$P = 5890 + 38T - 0.375T^2 + 3S$$

$$\alpha = 1779.5 + 11.25T - 0.0745T^2 - (3.8 + 0.01T)S$$

and T is temperature in degrees Celsius, S is salinity in parts per thousand (ppt), and ρ is density in grams per cubic centimeter.

Non-dimensionalization of equations

The dimensionless forms of the governing equations are used to facilitate relative magnitude comparisons of the various terms in the governing equations. Therefore, the following dimensionless variables are used:

$$(u^*, v^*, w^*) = (u, v, wX_r/Z_r)/U_r$$

$$(x^*, y^*, z^*) = (x, y, zX_r/Z_r)/X_r$$

$$(\tau^*_x, \tau^*_y) = (\tau^w_x, \tau^w_y)/\rho_o f Z_r U_r$$

$$t* = tf$$

$$\zeta^* = g\zeta/fU_r X_r = \zeta/S_r$$

$$\rho^* = (\rho - \rho_o)/(\rho_r - \rho_o) \qquad (9)$$

$$T^* = (T - T_o)/(T_r - T_o)$$

$$A^*_H = A_H/A_{Hr}$$

$$A^*_v = A_v/A_{vr}$$

$$K^*_H = K_H/K_{Hr}$$

$$K^*_v = K_v/K_{vr}$$

where

(τ^w_x, τ_y) = wind stress in (x,y) directions

ζ = water surface elevation

These definitions yield the following dimensionless parameters in the governing equations:

Vertical Ekman Number: $E_v = A_{vr}/fZ_r^2$

Lateral Ekman Number: $E_H = A_{Hr}/fX_r^2$

Vertical Prandtl (Schmidt) Number: $Pr_v = A_{vr}/K_{vr}$

Lateral Prandtl (Schmidt) Number: $Pr_H = A_{Hr}/K_{Hr}$

Froude Number: $F_r = U_r/(gZ_r)^{1/2}$

Rossby Number: $R_o = U_r/fX_r$ (10)

Densimetric Froude Number: $Fr_D = F_r / \sqrt{\varepsilon}$

where $\varepsilon = (\rho_r - \rho_o)/\rho_o$

S_r, T_r, U_r, ρ_r, X_r, Z_r, A_{Hr}, A_{vr}, K_{Hr}, *and* K_{vr} are arbitrary reference values of the elevation, temperature, velocity, density, etc.

External-internal modes

The basic equations (Equations 1-4) can be integrated over the depth to yield a set of vertically integrated equations for the water surface ζ and unit flow rates U and V in the x and y directions. Using the dimensionless variables (asterisks have been dropped) and the parameters previously defined, the vertically integrated equations constituting the external mode are:

$$\frac{\partial \zeta}{\partial t} + \beta \left(\frac{\partial U}{\partial x} + \frac{\partial V}{\partial y} \right) = 0 \tag{11}$$

$$\frac{\partial U}{\partial t} = - H \frac{\partial \zeta}{\partial x} + \tau_{sx} - \tau_{bx} + V$$

$$- R_o \left[\frac{\partial}{\partial x} \left(\frac{UU}{H} \right) + \frac{\partial}{\partial y} \left(\frac{UV}{H} \right) \right]$$

$$+ E_H \left[\frac{\partial}{\partial x} \left(A_H \frac{\partial U}{\partial x} \right) + \frac{\partial}{\partial y} \left(A_H \frac{\partial U}{\partial y} \right) \right]$$

$$- \frac{R_o}{Fr_D^2} \frac{H^2}{2} \frac{\partial \rho}{\partial x} \tag{12}$$

$$\frac{\partial V}{\partial t} = - H \frac{\partial \zeta}{\partial y} + \tau_{sy} - \tau_{by} - U$$

$$- R_o \left[\frac{\partial}{\partial x} \left(\frac{UV}{H} \right) + \frac{\partial}{\partial y} \left(\frac{VV}{H} \right) \right]$$

$$+ E_H \left[\frac{\partial}{\partial x} \left(A_H \frac{\partial V}{\partial x} \right) + \frac{\partial}{\partial y} \left(A_H \frac{\partial V}{\partial y} \right) \right]$$

$$- \frac{R_o}{Fr_D^2} \frac{H^2}{2} \frac{\partial \rho}{\partial y} \qquad (13)$$

where $\beta = gZr/f^2X_r^2 \equiv (R_o/F_r)^2$

H = *total depth*

As will be discussed later, the major purpose of the external mode is to provide the updated water-surface field for input to the internal mode equations.

The internal mode equations from which the 3-D velocity, salinity, and temperature fields are computed are:

$$\frac{\partial hu}{\partial t} = - h \frac{\partial \zeta}{\partial x} + E_V \frac{\partial}{\partial z} \left(A_V \frac{\partial hu}{\partial z} \right) + hv$$

$$- R_o \left(\frac{\partial huu}{\partial x} + \frac{\partial huv}{\partial y} + \frac{\partial huw}{\partial z} \right)$$

$$+ E_H \left[\frac{\partial}{\partial x} \left(A_H \frac{\partial hu}{\partial x} \right) + \frac{\partial}{\partial y} \left(A_H \frac{\partial hu}{\partial y} \right) \right]$$

$$- \frac{R_o}{Fr_D^2} \left(\int_z^\zeta \frac{\partial \rho}{\partial x} \, dz \right) \qquad (14)$$

$$\frac{\partial hv}{\partial t} = - h \frac{\partial \zeta}{\partial y} + E_V \frac{\partial}{\partial z} \left(A_V \frac{\partial hv}{\partial z} \right) - hu$$

$$- R_o \left(\frac{\partial hvu}{\partial x} + \frac{\partial hvv}{\partial y} + \frac{\partial hvw}{\partial z} \right)$$

$$+ E_H \left[\frac{\partial}{\partial x} \left(A_H \frac{\partial hv}{\partial x} \right) + \frac{\partial}{\partial y} \left(A_H \frac{\partial hv}{\partial y} \right) \right]$$

$$- \frac{R_o}{Fr_D^2} \left(\int_z^\zeta \frac{\partial \rho}{\partial y} \, dz \right) \tag{15}$$

$$W_{k+1/2} = W_{k-1/2} - \left(\frac{\partial uh}{\partial x} + \frac{\partial vh}{\partial y} \right) \tag{16}$$

$$\frac{\partial hT}{\partial t} = \frac{E_v}{Pr_v} \frac{\partial}{\partial z} \left(K_v \frac{\partial T}{\partial z} \right) - R_o \left(\frac{\partial huT}{\partial x} + \frac{\partial hvT}{\partial y} + \frac{\partial hwT}{\partial z} \right)$$

$$+ \frac{E_H}{Pr_H} \left[\frac{\partial}{\partial x} \left(K_H \frac{\partial hT}{\partial x} \right) + \frac{\partial}{\partial y} \left(K_H \frac{\partial hT}{\partial y} \right) \right] \tag{17}$$

$$\frac{\partial hS}{\partial t} = \frac{E_v}{Pr_v} \frac{\partial}{\partial z} \left(K_v \frac{\partial S}{\partial z} \right) - R_o \left(\frac{\partial huS}{\partial x} + \frac{\partial hvS}{\partial y} + \frac{\partial hwS}{\partial z} \right)$$

$$+ \frac{E_H}{Pr_H} \left[\frac{\partial}{\partial x} \left(K_H \frac{\partial hS}{\partial x} \right) + \frac{\partial}{\partial y} \left(K_H \frac{\partial hS}{\partial y} \right) \right] \tag{18}$$

In these equations h is the thickness of an internal layer and $k+1/2$ and $k-1/2$ represent the top and bottom, respectively, of the k^{th} vertical layer and W is the transport in the z-direction.

Boundary-fitted equations

The CH3D model utilizes a boundary-fitted or generalized curvilinear planform grid which can be made to conform to flow boundaries, providing a detailed resolution of the complex horizontal geometry of the flow system. This necessitates the transformation of the governing equations into boundary-fitted coordinates (ξ,η). If only the (x,y) coordinates are transformed, a system of equations similar to those solved by Johnson (1980) for vertically averaged flow fields is obtained. However, in the CH3D model not only are the (x,y) coordinates transformed into the (ξ,η) curvilinear system but also the velocity is transformed such that its components are perpendicular to the (ξ,η)

coordinate lines. This is accomplished by employing the definitions below for the components of the Cartesian velocity (u,v) in terms of contravariant components $\bar{u}$ and $\bar{v}$.

$$u = x_\xi \bar{u} + x_\eta \bar{v}$$

$$v = y_\xi \bar{u} + y_\eta \bar{v} \tag{19}$$

along with the following expressions for replacing Cartesian derivatives

$$f_x = \frac{1}{J}\left[(fy_\eta)_\xi - (fy_\xi)_\eta\right]$$

$$f_y = \frac{1}{J}\left[-(fx_\eta)_\xi + (fx_\xi)_\eta\right] \tag{20}$$

where f is an arbitrary variable and J is the Jacobian of the coordinate transformation defined as

$$J = x_\xi y_\eta - x_\eta y_\xi$$

With the governing equations written in terms of the contravariant components of the velocity, boundary conditions can be prescribed on the boundary-fitted grid in the same manner as on a Cartesian grid because $\bar{u}$ and $\bar{v}$ are perpendicular to the curvilinear cell faces (e.g., at a land boundary, either $\bar{u}$ or $\bar{v}$ is set to zero).

The vertical dimension is represented through the use of what is commonly referred to as a sigma-stretched grid, illustrated in Figure 2. The vertical depth is discretized in a fixed number of layers, each layer equal in thickness to a fixed percentage of the local depth. The sigma-stretched grid is then transformed to a fixed-space grid where the computations are easily performed.

With both the Cartesian coordinates and the Cartesian velocity transformed, the following boundary-fitted equations for $\bar{u}$, $\bar{v}$, w, S, and T to be solved in each vertical layer are obtained.

$$\frac{\partial h\bar{u}}{\partial t} = -h\left(\frac{G_{22}}{J^2}\frac{\partial \zeta}{\partial \xi} - \frac{G_{12}}{J^2}\frac{\partial \zeta}{\partial \eta}\right) + \frac{h}{J}\left(G_{12}\bar{u} + G_{22}\bar{v}\right) + \frac{R_o x_\eta}{J^2}\left[\frac{\partial}{\partial \xi}\left(Jy_\xi h\bar{u}\bar{u}\right.\right.$$

$$+ Jy_\eta h\bar{u}\bar{v}\Big) + \frac{\partial}{\partial\eta}\left(Jy_\xi h\bar{u}\bar{v} + Jy_\eta h\bar{v}\bar{v}\right)\Big] - \frac{R_o y_\eta}{J^2}\left[\frac{\partial}{\partial\xi}\left(Jx_\xi h\bar{u}\bar{u} + Jx_\eta h\bar{u}\bar{v}\right)\right.$$

$$\left. + \frac{\partial}{\partial\eta}\left(Jx_\xi h\bar{u}\bar{v} + Jx_\eta h\bar{v}\bar{v}\right)\right] - R_o\left[(w\bar{u})_{top} - (w\bar{u})_{bot}\right]$$

$$+ E_v\left[\left(A_v\frac{\partial\bar{u}}{\partial z}\right)_{top} - \left(A_v\frac{\partial\bar{u}}{\partial z}\right)_{bot}\right] - \frac{R_o h}{Fr_D^2}\left[\int_z^\zeta\left(\frac{G_{22}}{J^2}\frac{\partial\rho}{\partial\xi}\right.\right.$$

$$\left.\left. - \frac{G_{12}}{J^2}\frac{\partial\rho}{\partial\eta}\right)dz\right] + \text{Horizontal Diffusion} \qquad (21)$$

$$\frac{\partial h\bar{v}}{\partial t} = -h\left(-\frac{G_{21}}{J^2}\frac{\partial\zeta}{\partial\xi} + \frac{G_{11}}{J^2}\frac{\partial\zeta}{\partial\eta}\right) - \frac{h}{J}\left(G_{11}\bar{u} + G_{21}\bar{v}\right) - \frac{R_o x_\xi}{J^2}\left[\frac{\partial}{\partial\xi}\left(Jy_\xi h\bar{u}\bar{u}\right.\right.$$

$$\left. + Jy_\eta h\bar{u}\bar{v}\right) + \frac{\partial}{\partial\eta}\left(Jy_\xi h\bar{u}\bar{v} + Jy_\eta h\bar{v}\bar{v}\right)\Big] + \frac{R_o y_\xi}{J^2}\left[\frac{\partial}{\partial\xi}\left(Jx_\xi h\bar{u}\bar{u} + Jx_\eta h\bar{u}\bar{v}\right)\right.$$

$$\left. + \frac{\partial}{\partial\eta}\left(Jx_\xi h\bar{u}\bar{v} + Jx_\eta h\bar{v}\bar{v}\right)\right] - R_o\left[(w\bar{v})_{top} - (w\bar{v})_{bot}\right]$$

$$+ E_v\left[\left(A_v\frac{\partial\bar{v}}{\partial z}\right)_{top} - \left(A_v\frac{\partial\bar{v}}{\partial z}\right)_{bot}\right] - \frac{R_o h}{Fr_D^2}\left[\int_z^\zeta\left(-\frac{G_{21}}{J^2}\frac{\partial\rho}{\partial\xi} + \frac{G_{11}}{J^2}\frac{\partial\rho}{\partial\eta}\right)dz\right]$$

$$+ \text{Horizontal Diffusion} \qquad (22)$$

$$w_{top} = w_{bot} - \frac{1}{J}\left(\frac{\partial J\bar{u}h}{\partial\xi} + \frac{\partial J\bar{v}h}{\partial\eta}\right) \qquad (23)$$

$$\frac{\partial hS}{\partial t} = \frac{E_v}{Pr_v}\left[\left(K_v \frac{\partial S}{\partial z}\right)_{top} - \left(K_v \frac{\partial S}{\partial z}\right)_{bot}\right] - \frac{R_o}{J}\left(\frac{\partial hJ\bar{u}S}{\partial \xi} + \frac{\partial hJ\bar{v}S}{\partial \eta}\right)$$

$$- R_o\left[(wS)_{top} - (wS)_{bot}\right] + \text{Horizontal Diffusion} \qquad (24)$$

$$\frac{\partial hT}{\partial t} = \frac{E_v}{Pr_v}\left[\left(K_v \frac{\partial T}{\partial z}\right)_{top} - \left(K_v \frac{\partial T}{\partial z}\right)_{bot}\right] - \frac{R_o}{J}\left(\frac{\partial hJ\bar{u}T}{\partial \xi} + \frac{\partial hJ\bar{v}T}{\partial \eta}\right)$$

$$- R_o\left[(wT)_{top} - (wT)_{bot}\right] + \text{Horizontal Diffusion} \qquad (25)$$

where

$$G_{11} = x_\xi^2 + y_\xi^2$$

$$G_{22} = x_\eta^2 + y_\eta^2 \qquad (26)$$

$$G_{12} = G_{21} = x_\xi x_\eta + y_\xi y_\eta$$

Similarly, the transformed external mode equations become:

$$\frac{\partial \zeta}{\partial t} + \beta\left(\frac{\partial \bar{U}}{\partial \xi} + \frac{\partial \bar{V}}{\partial \eta}\right) = 0 \qquad (27)$$

$$\frac{\partial \bar{U}}{\partial t} = -\frac{H}{J^2}\left(G_{22}\frac{\partial \zeta}{\partial \xi} - G_{12}\frac{\partial \zeta}{\partial \eta}\right)$$

$$+ \frac{1}{J}\left(G_{12}\bar{U} + G_{22}\bar{V}\right) + \frac{R_o x_\eta}{J^2 H}\left[\frac{\partial}{\partial \xi}\left(Jy_\xi \bar{U}\bar{U} + Jy_\eta \bar{U}\bar{V}\right) + \frac{\partial}{\partial \eta}\left(Jy_\xi \bar{U}\bar{V} + Jy_\eta \bar{V}\bar{V}\right)\right]$$

$$- \frac{R_o y_\eta}{J^2 H}\left[\frac{\partial}{\partial \xi}\left(Jx_\xi \bar{U}\bar{U} + Jx_\eta \bar{U}\bar{V}\right) + \frac{\partial}{\partial \eta}\left(Jx_\xi \bar{U}\bar{V} + Jx_\eta \bar{V}\bar{V}\right)\right]$$

$$+ \tau_{s\xi} - \tau_{b\xi} - \frac{R_o}{Fr_D^2} \frac{H^2}{2} \left(G_{22} \frac{\partial \rho}{\partial \xi} - G_{12} \frac{\partial \rho}{\partial \eta} \right)$$

$$+ \text{Horizontal Diffusion} \tag{28}$$

$$\frac{\partial \bar{V}}{\partial t} = - \frac{H}{J^2} \left(- G_{21} \frac{\partial \zeta}{\partial \xi} + G_{11} \frac{\partial \zeta}{\partial \eta} \right) - \frac{1}{J} \left(G_{11} \bar{U} + G_{21} \bar{V} \right)$$

$$- \frac{R_o x_\xi}{J^2 H} \left[\frac{\partial}{\partial \xi} \left(Jy_\xi \bar{U}\bar{U} + Jy_\eta \bar{U}\bar{V} \right) + \frac{\partial}{\partial \eta} \left(Jy_\xi \bar{U}\bar{V} + Jy_\eta \bar{V}\bar{V} \right) \right]$$

$$+ \frac{R_o y_\xi}{J^2 H} \left[\frac{\partial}{\partial \xi} \left(Jx_\xi \bar{U}\bar{U} + Jx_\eta \bar{U}\bar{V} \right) + \frac{\partial}{\partial \eta} \left(Jx_\xi \bar{U}\bar{V} + Jx_\eta \bar{V}\bar{V} \right) \right]$$

$$+ \tau_{s\eta} - \tau_{b\eta} - \frac{R_o}{Fr_D^2} \frac{H^2}{2} \left(- G_{21} \frac{\partial \rho}{\partial \xi} + G_{11} \frac{\partial \rho}{\partial \eta} \right)$$

$$+ \text{Horizontal Diffusion} \tag{29}$$

Equations 27-29 are solved first to yield water-surface elevations which are then used to evaluate the water-surface slope terms in the internal mode equations. The horizontal diffusion terms are quite lengthy and thus are omitted in this report. Full documentation of the terms is presented in Johnson et al. (1991) for the internal mode equations. Similar expressions for the diffusion terms in the vertically averaged equations can be inferred from those for the internal mode.

Boundary conditions

The boundary conditions at the free surface are

$$A_v \left(\frac{\partial \bar{u}}{\partial z} , \frac{\partial \bar{v}}{\partial z} \right) = \left(\tau_{s_\xi} , \tau_{s_\eta} \right) / \rho = \left(C W_\xi^2 , C W_\eta^2 \right)$$

$$\frac{\partial T}{\partial z} = \frac{Pr_v}{E_v} K (T - T_e) \tag{30}$$

$$\frac{\partial S}{\partial z} = 0$$

whereas the boundary conditions at the bottom are

$$A_v \left(\frac{\partial \bar{u}}{\partial z} , \frac{\partial \bar{v}}{\partial z} \right) = \left(\tau_{b_\xi} , \tau_{b_\eta} \right) / \rho$$

$$= \frac{U_r}{A_{vr}} Z_r C_d \left(\bar{u}_1^2 + \bar{v}_1^2 \right)^{1/2} \left(\bar{u}_1, \bar{v}_1 \right)$$

$$\frac{\partial T}{\partial z} , \frac{\partial S}{\partial z} = 0 \tag{31}$$

where

C = surface drag coefficient
W = wind speed
K = surface heat exchange coefficient
T_e = equilibrium temperature
C_d = bottom friction coefficient
$\bar{u}_1$, $\bar{v}_1$ = values of the horizontal velocity components next to the bottom

With z_1 equal to one half the bottom layer thickness, C_d is given by

$$C_d = k^2 \left[\ln \left(z_1 / z_o \right) \right]^{-2} \tag{32}$$

where

k = von Karman constant
z_o = bottom roughness height

Manning's formulation is employed for the bottom friction in the external mode equations if the model is used only to compute vertically averaged flow

fields. The surface drag coefficient is computed according to Garratt (1977) as follows

$$C = (0.75 + 0.067\ W) \times 10^{-3} \tag{33}$$

with the maximum allowable value being 0.003. The surface heat exchange coefficient K and the equilibrium temperature T_e are computed from meteorological data (wind speed, cloud cover, wet and dry bulb air temperatures, and relative humidity) as discussed by Edinger, Brady, and Geyer (1974).

Freshwater inflow and water temperature are prescribed along the shoreline where river inflow occurs; however, the salinity at the river boundary is specified according to a zero spatial gradient assumption (computed from the previous time-step). At an ocean boundary, the water-surface elevation is prescribed along with time-varying vertical distributions of salinity and temperature. Specified values of salinity and temperature are employed during flood flow, whereas during ebb, interior values are advected out of the grid. The normal component of the velocity, viscosity, and diffusivity are set to zero along solid boundaries.

Initial conditions

When initiating a run of CH3D-WES, the values of ζ, $\bar{u}$, $\bar{v}$, w, $\bar{U}$ and $\bar{V}$ are set to zero. Values of salinity and temperature are read from input files. These initial data are generated from prototype measurements at a limited number of locations. Once the values in individual cells are determined by interpolating from the field data, the resulting 3-D field is smoothed. Generally, the salinity and temperature fields are held constant for the first few days of a simulation.

Numerical solution algorithm

Finite differences are used to replace derivatives in the governing equations, resulting in a system of linear algebraic equations to be solved in both the external and internal modes. The external mode solution consists of the surface displacement and vertically integrated contravariant unit flows $\bar{U}$ and $\bar{V}$. All terms in the transformed vertically averaged continuity equation are treated implicitly whereas only the water-surface slope terms in the transformed vertically averaged momentum equations are treated implicitly. If the external mode is used only as a vertically averaged model, the bottom friction is also treated implicitly. Those terms treated implicitly are weighted between the new and old time-steps. The resulting finite difference equations are then factored such that a ξ-sweep followed by an η-sweep of the horizontal grid yields the solution at the new time-step.

Writing Equations 11-13 as

$$\frac{\partial \zeta}{\partial t} + \beta \left(\frac{\partial \bar{U}}{\partial \xi} + \frac{\partial \bar{V}}{\partial \eta} \right) = 0 \tag{34}$$

$$\frac{\partial \bar{U}}{\partial t} + \frac{H}{J^2} G_{22} \frac{\partial \zeta}{\partial \xi} = M \tag{35}$$

$$\frac{\partial \bar{V}}{\partial t} + \frac{H}{J^2} G_{11} \frac{\partial \zeta}{\partial \eta} = N \tag{36}$$

the ξ-sweep is

$$\xi\text{-sweep} \Rightarrow \zeta^{*}_{ij} + \frac{\beta \theta \Delta t}{\Delta \xi} \left(\bar{U}^{*}_{i+1,j} - \bar{U}^{*}_{ij} \right) = \zeta^{n}_{ij}$$

$$- (1-\theta) \frac{\Delta t}{\Delta \xi} \left(\bar{U}^{n}_{i+1,j} - \bar{U}^{n}_{ij} \right)$$

$$- \frac{\Delta t}{\Delta \eta} \left(\bar{V}^{n}_{i,j+1} - \bar{V}^{n}_{ij} \right) \tag{37}$$

and

$$\bar{U}^{n+1}_{ij} + \frac{\theta \Delta t H G_{22}}{\Delta \xi \, J^2} \left(\zeta^{*}_{ij} - \zeta^{*}_{i-1,j} \right)$$

$$= \bar{U}^{n}_{ij}$$

$$-(1-\theta)\frac{\Delta t HG_{22}}{\Delta\xi\, J^2}\left(\zeta_{ij}^{n} - \zeta_{i-1,j}^{n}\right) + \Delta t\, M^{n} \qquad (38)$$

The η-sweep then provides the updated ζ and $\bar{V}$ at the n+1 time level.

$$\eta\text{-sweep} \Rightarrow \zeta_{ij}^{n+1} + \frac{\beta\theta\Delta t}{\Delta\eta}\left(\bar{V}_{i,j+1}^{n+1} - \bar{V}_{ij}^{n+1}\right) = \zeta_{i,j}^{*}$$

$$- (1-\theta)\frac{\Delta t}{\Delta\eta}\left(\bar{V}_{i,j+1}^{n} - \bar{V}_{i,j}^{n}\right)$$

$$+ \frac{\Delta t}{\Delta\eta}\left(\bar{V}_{i,j+1}^{n} - \bar{V}_{i,j}^{n}\right) \qquad (39)$$

and

$$\bar{V}_{i,j}^{n+1} + \frac{\theta\Delta t HG_{11}}{\Delta\eta\, J^2}\left(\zeta_{i,j+1}^{n+1} - \zeta_{i,j}^{n+1}\right)$$

$$= V_{i,j}^{n}$$

$$-(1-\theta)\frac{\Delta t HG_{11}}{\Delta\eta\, J^2}\left(\zeta_{i,j+1}^{n} - \zeta_{i,j}^{n}\right) + \Delta t\, N^{n} \qquad (40)$$

A typical value of θ of 0.55 yields stable and accurate solutions.

The internal mode consists of computations from Equations 21-25 for the three velocity components $\tilde{u}$, $\tilde{v}$, and w, salinity, and temperature. The only

terms treated implicitly are the vertical diffusion terms in all equations and the bottom friction and surface slope terms in the momentum equations. Values of the water-surface elevations from the external mode are used to evaluate the surface slope terms in Equations 21 and 22. As a result, the extremely restrictive speed of a free-surface gravity wave is removed from the stability criteria. Roache's second upwind differencing scheme is used to represent the convective terms in the momentum equations, whereas a spatially third-order scheme developed by Leonard (1979) (called QUICKEST) is used to represent the advective terms in Equations 24 and 25 for salinity and temperature, respectively. For example, if the velocity on the right face of a computational cell is positive, then with QUICKEST the value of the salinity used to compute the flux through the face is

$$S_R = \frac{1}{2}\left(S_{i,j,k}+S_{i+1,j,k}\right)$$

$$-\frac{1}{6}\left[1-\left(\frac{\bar{U}_{i+1,j,k}\,\Delta t}{\Delta\xi}\right)^2\right]\left(S_{i+1,j,k}-2\,S_{i,j,k}+S_{i-1,j,k}\right)$$

$$-\frac{1}{2}\,\frac{U_{i+1,j,k}\,\Delta t}{\Delta\xi}\left(S_{i+1,j,k}-S_{i,j,k}\right) \qquad (41)$$

The more interested reader is referred to the paper by Leonard (1979).

It should be noted that once the $\bar{u}$ and $\bar{v}$ velocity components are computed, they are slightly adjusted to ensure conservation of mass. This is accomplished by forcing the sum of $\bar{u}$ over the vertical to be the vertically averaged velocity $\bar{U}/H$ and the sum of $\bar{v}$ over the vertical to equal $\bar{V}/H$, where H is the total water depth.

Turbulence parameterization

Vertical turbulence is handled by using the concept of eddy viscosity and diffusivity to represent the velocity and density correlation terms that arise from time averaging of the governing equations. These eddy coefficients are computed from mean flow characteristics using a simplified second-order closure model originally developed by Donaldson (1973). The closure model has been further developed and applied to various types of flows by Lewellen (1977) and Sheng (1982, 1986). A discussion of the implementation of the turbulence model taken from Sheng (1990) follows. For more details, the interested reader should refer to these references and to Johnson et al. (1991).

Assuming local equilibrium of turbulence, i.e., there is no time evolution or spatial diffusion of the second-order correlations, an equation relating the

turbulent kinetic energy and the macroscale of turbulence to the mean flow shear and stratification (given by the Richardson number *Ri*) can be derived as

$$3A^2b^2sQ^4 + A[(bs + 3b + 7b^2s)Ri - Abs(1 - 2b)]Q^2 + b(s + 3 + 4bs)Ri^2 + (bs - A)(1 - 2b)Ri = 0 \quad (42)$$

where

$b = 0.125$

$s = 1.8$

$A = 0.75$

and

$$Q = \frac{q}{\Lambda\sqrt{(\partial\bar{u}/\partial z)^2 + (\partial\bar{v}/\partial z)^2}} \quad (43)$$

In the above expression, q is defined as

$$q = (\overline{u'u'} + \overline{v'v'} + \overline{w'w'})^{1/2}$$

and Λ is the macroscale of turbulence. The quantities u', v', *and* w' are the turbulent velocity fluctuations and the overbar indicates time averaging.

It can also be shown that the following relations hold:

$$\overline{u'w'} = -\frac{\frac{\partial\bar{u}}{\partial z}\Lambda}{q}\frac{1 + \frac{\bar{\omega}}{A}}{1 - \omega}\overline{w'w'} \quad (44)$$

$$\overline{v'w'} = -\frac{\frac{\partial\bar{v}}{\partial z}\Lambda}{q}\frac{1 + \frac{\bar{\omega}}{A}}{1 - \omega}\overline{w'w'} \quad (45)$$

$$q^2 b = \left[\frac{(1 + \frac{\bar{\omega}}{A})}{Q^2(1 - \omega)} + \bar{\omega} \right] \overline{w'w'} \tag{46}$$

where

$$\omega = \frac{Ri}{AQ^2} \tag{47}$$

and

$$\bar{\omega} = \frac{\omega}{1 - \frac{\omega}{bs}} \tag{48}$$

Thus, after the velocity shear and flow stratification are determined, q can be computed from Equations 42 and 43. $\overline{w'w'}$ is then determined from

$$\overline{w'w'} = \frac{\frac{q^2}{2} - q^2 b}{\frac{3}{2}(1 - 2\omega)} \tag{49}$$

Finally, after Λ is prescribed, $\overline{u'w'}$ and $\overline{v'w'}$ can be computed from Equations 44 and 45 and the vertical eddy coefficients can be determined from

$$A_V = \frac{\overline{-u'w'}}{\frac{\partial \bar{u}}{\partial z}} = \frac{\Lambda}{q} \frac{A + \bar{\omega}}{A(1 - \omega)} \overline{w'w'} \tag{50}$$

$$K_V = \frac{\overline{-\rho'w'}}{\frac{\partial \rho}{\partial z}} = \frac{\Lambda}{q} \frac{bs}{(bs - \omega)A} \overline{w'w'} \tag{51}$$

In addition to setting $\Lambda = 0.65z$ near boundaries, three basic constraints are used to compute Λ at a vertical position z

$$\left|\frac{d\Lambda}{dz}\right| \leq 0.65 \tag{52}$$

$$\Lambda \leq \frac{q}{N} = q / \left(- \frac{g}{\rho} \frac{\partial \rho}{\partial z} \right)^{0.5} \tag{53}$$

$$\Lambda \leq Q_{cut} \left(z_{q=qmax} - z_{q=qmax/2} \right) \tag{54}$$

where N is the Brunt-Vaisala frequency. Equation 54 states that Λ is less than a fraction of the spread of turbulence as measured by the distance between the location of a maximum q^2 to where q^2 is equal to 25 percent of the maximum. The coefficient Q_{cut} is on the order of 0.15 to 0.25.

Computational grid

A staggered grid is used in both the horizontal and vertical directions of the computational domain schematized in Figure 3. In the horizontal directions, a unit cell consists of a ζ-point in the center ($\zeta_{i,j}$), a U-point to its left ($U_{i,j}$), and a V-point to its bottom ($V_{i,j}$). In the vertical direction, the vertical velocities are computed at the "full" grid points. Horizontal velocities, temperature, salinity, and density are computed at the "half" grid points (half grid spacing below the full points).

Two arrays, NS and MS, are set automatically by the model to flag cells in the horizontal. The array NS indicates the condition of the "west" and "east" cell boundaries, whereas the array MS denotes the condition of the "north" and "south" cell boundaries. Figure 4 illustrates typical values of the NS and MS array elements for different cell boundaries.

The boundary-fitted grid shown in Figure 5 was developed to provide a high-resolution representation of the complex geometry of the coupled NY Bight, NY Harbor, and Long Island Sound model domain focusing on the NY Bight. The computational grid contains a maximum of 76 cells in the alongshore direction and 45 cells in the offshore direction. The grid contains a total of 2,652 active horizontal cells and 10 vertical layers, resulting in 26,520 computational cells. The average horizontal grid resolution is 8 km in the alongshore direction with a minimum of 2 km in the Hudson Canyon and a maximum of 17 km near Cape May. Average offshore-directed resolution is 6 km with a minimum of 200 m in the East River and a maximum of 8 km near the shelf break. The Hudson River is parameterized as a two-dimensional, laterally integrated body of water and modeled as a river boundary input to the bight. Depths, specified at the center of each cell, were extracted from bathymetric data gathered from NOAA nautical charts based on mean low water. Although the resolution in Long Island Sound, New York-New Jersey Harbor, and the Hudson-Raritan Estuary system is coarse for detailed study, the grid resolution is sufficient to provide insight into the circulation and transport processes in the NY Bight.

3 Prototype Data Evaluation

Data Requirements

Calibration and verification of an HM are accomplished when model simulations, specified according to prototype measurement input boundary conditions, acceptably match measured prototype water surface elevations and currents at a variety of locations within the modeled domain. The general procedure begins with the selection of a calibration period during which model simulations are compared to prototype data. At this point, model variables such as friction coefficients, heat exchange coefficients, boundary condition implementation, and wind field transfer functions are adjusted to optimize the model simulation-to-prototype match. After an acceptable calibration has been achieved, verification of the model is accomplished by comparing model simulations of some alternate time period for which prototype data are available. In the verification phase, model coefficients and parameters are not adjusted, but maintained at the values used in the calibration phase. Both the calibration and verification phases require prototype data at a number of spatially separated locations. These data must extend through the simulation period and be of an acceptable quality such that a valid comparison between model and prototype conditions can be made.

Tides along the east coast of the United States are primarily semidiurnal in period, i.e., approximately two ebb and flood cycles per day. In addition to these daily fluctuations, longer period cycles of spring tide with a large surface elevation range and neap tide with a low tidal range occur approximately twice a month. This period, on the order of approximately 28 days, is termed a lunar month. A minimum two-week, and preferably one-month, simulation and comparison to prototype data were determined to be necessary for both the calibration and verification phase of the model. Necessary boundary condition and comparison data include river inflows, tides at open ocean boundaries as well as at various interior locations, meteorological data at one or more stations from which the surface wind stress and heat flux can be determined, and the three-dimensional structure of currents, temperature, and salinity.

Prototype Data

An extremely comprehensive database of hydrodynamic and environmental data were collected for, and in support of, the MESA project previously described. This database contains the information necessary to calibrate and verify both the HM and the environmental model. The MESA hydrodynamic, environmental, and water quality data were provided to the U.S. Army Engineer Coastal Engineering Research Center (CERC) by Dr. Andrew Stoddard of Creative Enterprises of Northern Virginia and Dr. Gregory Han of Han and Associates, Inc. The data were prepared for Evans-Hamilton, Inc. under contract to CERC (Stoddard and Han 1990). The supplied data generally correspond to the period of 1 September 1975 through 31 August 1976. The following sections provide a brief summary of the data used in the hydrodynamic modeling effort.

Water surface elevation

Water surface data were supplied in the form of hourly time series of surface elevation values. Data were provided for the 10 primary and secondary NOAA tidal stations shown in Figure 6. Gauge descriptors and corresponding durations of time series are shown below.

a)	The Battery, NY	9/75 - 8/76
b)	Montauk Point, NY	9/75 - 8/76
c)	Cape May, NJ	9/75 - 5/76
d)	Willets Point, NY	9/75 - 8/76
e)	Sandy Hook, NJ	9/75 - 12/75
f)	Shinnecock, NY	4/76 - 8/76
g)	Newport, RI	9/75 - 8/76
h)	Atlantic City, NJ	9/75 - 5/76
i)	Bridgeport, CT	9/75 - 8/76
j)	New London, CT	10/75 - 8/76

A 16-constituent harmonic analysis was performed on each of the tidal time series as a means of determining possible data gaps as revealed by unusually low values of reduction in variance (RV). The RV value equalled variance minus the root mean square (RMS) error estimate normalized by the variance. Values of 1.0 indicate a purely tidal signal while low values (below 0.5, for example) indicate the presence of either a significant nonastronomical component of the signal (for example, wind or storm surge effects) or abrupt phasing problems caused by gaps in the data. As an additional indication of the relative percentage of tidal to non-tidal energy in the signal, a high-pass filter was applied to the data to separate the non-astronomical component of the signal from the tidal portion. The period of separation was selected at 40 hr.

An example of frequency separation is shown in Figure 7 in which the raw prototype data as well as the low-frequency component of the Battery and Montauk tidal stations for the month of April 1976 are shown. Note that the spring and neap tidal cycles of high and low tidal range are shown in the data.

The corresponding RV values, 0.957 and 0.895 respectively, provide a quantitative estimate of the percentage of the signal which is of tidal origin. These RV values are typical for water surface elevations in a tidally dominated system. For comparison purposes, values of 0.40 or 0.50 indicate a wind-dominated regime. As shown in the figure, the tidal amplitudes at Montauk are less than those at the Battery, but the non-tidal energy is approximately the same, hence the lower RV value for Montauk. In both cases, however, the percentage of the total signal attributable to tidal action is high, i.e., approximately 90 percent. As will be addressed at a later point, the non-astronomical low-frequency component can represent a significant percentage of the peak flood or ebb tidal magnitude, particularly when the event occurs during neap tide conditions of small tidal range. Results of harmonic analyses, RV computation, and filtering do, however, confirm the fact that the NY Bight is tidally dominated with the M_2 semidiurnal constituent as the primary component.

Current and temperature measurements

Time series of velocity and temperature data were supplied for seven sampling sites located throughout the central portion of the NY Bight. Gauge locations are indicated on Figure 6. Data collected at multiple depths through the water column at various times were provided for each station. Time periods during which data are available are indicated in Figure 8. The data are sufficiently dense to describe the vertical structure of the temperature as well as velocity magnitudes, directions, and vertical distributions. These data are used for model-to-prototype comparisons in the calibration and verification phase of the HM development.

Harmonic analyses of each U- and V-component time series of the currents as well as high/low pass filtering have been completed as a means of investigating the overall characteristics of the signals. An example presentation of the data corresponding to station LT6 at a height of 49 m from the bottom (a total depth of 70 m) is shown in Figure 9.

The low-frequency component included in both the U (positive to the east) and V (positive to the north) component plots shows the presence of non-astronomical low-frequency energy. The percentage of the total velocity signal which can be attributed to tidal motion is indicated in the computed RV values of 0.411 for U and 0.287 for V. As previously described, non-astronomical energy can substantially affect the signal magnitude. This effect is particularly noticeable in the currents because of both their directionality and low magnitudes. For example, the V component remains negative through both ebb and flood during the low-frequency event on days 20-22 of the record shown in Figure 9. The possible origin of this source of energy will be discussed in the following section.

Water temperature and salinity

In addition to the time series data obtained from moored instruments, a substantial number of ship measurements were obtained. These data include temperatures and salinities recorded at multiple depths throughout the water column. A total of 1,064 sets of vertical temperature and salinity profile data were provided for analysis. Locations of the stations within the NY Bight are shown in Figure 10. Because the locations at which data were collected vary in space and time, rigorous analyses of the data can not be performed. However, the data are used to provide offshore boundary and initial conditions for running the numerical model. For example, data were scanned to locate stations in which the total depth exceeds 150 m. These data were then used to develop monthly salinity-versus-depth and temperature-versus-depth relationships for the model offshore boundary. Examples for the entire period of April through September 1976 are shown in Figure 11. Note that the salinity is generally within 35.0 to 35.5 ppt at depths below approximately 150 m and that it remains nearly constant at 35.0 ppt below 400 m. Also, temperatures decrease quadratically from approximately 11.0 ^{o}C at 200 m to 4.0 ^{o}C at depths below 1,000 m. Data from each month were analyzed separately to provide the depth-temperature/salinity relationship for each month. For example, the plot for the month of April 1976 is shown in Figure 12. For this period, near surface salinity averages approximately 34.0 ppt and temperature approximately 10.0 ^{o}C.

Meteorologic data

Supplied meteorologic data include wind direction and magnitude, air temperature, and atmospheric pressure for the four weather stations of Nantucket, MA, Providence, RI, Atlantic City, NJ, and Bridgeport, CT. Locations of these stations are indicated on Figure 6. The data cover the period 1 September 1975 through 31 August 1976. Temperature and pressure data have been plotted and examined for consistency. Wind velocity data have been plotted and probability histograms of the wind direction have been computed and plotted. Example plots of wind magnitude (including low frequency), direction, and probability distribution are shown in Figure 13 for the Atlantic City, NJ, airport. Data from all four airports were similar in magnitude and directionality. Wind magnitude, atmospheric pressure, and surface temperature for the same period for Atlantic City are shown in Figure 14.

The correlation between low-frequency energy in the water surface and current data and the wind field can be seen in a comparison of Figures 7, 9, and 14. In all cases, a low-frequency event is measured on approximately 9-12 April and 24-27 April 1976. At this time, a distinct drop in atmospheric pressure is observed at the airport. Although the precise mechanism relating wind and pressure to surface elevation and sub-surface currents is not known, the fact that they are correlated in some sense is clear. A more detailed discussion of the interaction process will be given in the next section.

Additional wind data were available through the WES Wave Information Study (WIS). This database contained time series of hindcast wind fields at increments of 2.5 deg in latitude and longitude. Although rigorous correlations between the onshore meteorological station data and the WIS data were not performed, the data were in qualitative agreement. Because the WIS data corresponded to locations closer to the offshore model boundaries, these data were selected to drive the model. Wind field hindcasts for three boundary locations for the months of April through October 1976 are shown in Appendix A.

Freshwater inflow

Freshwater inflow data were provided for the Hudson River. These hydrographs are presented in Appendix A for the period of April through October 1976.

Boundary Condition Selection

Before numerical model output was compared to prototype data, the model was tested to multiple hypothetical boundary conditions. This procedure is referred to as the diagnostic or sensitivity testing phase. At that time, simulations were analyzed to determine if the model was behaving correctly and reproducing known circulation patterns within the flow region. For the case of the NY Bight, sensitivity tests demonstrated, for example, global circulation patterns as a response to constant wind stress or surface slope and tidal propagation due to single constituent forcing. These generic testing procedures assure that the model is reproducing the gross features of the flow system. Satisfactory completion of this phase was followed by the calibration and verification process in which model results were compared to prototype data.

Proper calibration and verification demonstrate that a numerical model is capable of acceptably reproducing the hydrodynamic behavior of the entire flow system such that the flow characteristics at all portions of the system are reliably predicted by imposing only boundary and external forcings begun with appropriate initial conditions. Because the primary purpose of this study was to investigate various long-term aspects of water quality transport within the NY Bight, the ultimate role of the HM is to provide the water surface and current distribution for input to the environmental (water quality) model. The six-month period of 1 April through 30 September 1976 was selected as the period for which hydrodynamic data would be generated and supplied to the water quality study. Therefore, the lead-in periods of April 1976 and May 1976 were selected for the times of calibration and verification. During these periods, prototype data were used as boundary conditions for the model. These conditions include offshore tidal fluctuations, river inflows, wind fields, salinity, and temperature. A complete description of the methodology used to define these conditions on the outer boundary is presented in Chapter 4.

4 CH3D-WES Model Implementation

Implementation of CH3D begins by specifying the initial surface elevation and flow field distribution throughout the computational domain. Thereafter, the simulation is driven by the following time-varying boundary conditions: a prescribed change in surface elevation at the ocean boundaries, an imposed surface wind stress, and river inflow from the Hudson River. All conditions are specified even though they may be zero; for example, no wind. This section of the report describes preliminary diagnostic testing in which various combinations of boundary conditions are imposed on the model. These simulations are used to confirm that model results are in acceptable agreement with known behavior patterns in the NY Bight. This section is followed by a description of the calibration and verification comparisons and an analysis of the cross-shelf and along-shelf surface and current response to low-frequency disturbances. The 6-month simulation, driven by hindcast wind fields and astronomical tidal forcing generated from a global tidal model, is next described. This long-term simulation represents the flow field used for the simulation of water quality parameters via the environmental model. Finally, an extended application of the model to circulation in the Long Island Sound is presented to further demonstrate the ability of the model to acceptably reproduce the hydrodynamics over the entire modeled domain, not just the NY Bight.

Diagnostic/Steady-State Tests

The purpose of the diagnostic/steady-state tests was to provide estimates of circulation and mixing in the NY Bight under different imposed boundary conditions. Because potential pollutants are dispersed through a system as a function of large-scale circulation patterns, these estimates provide direct input to the environmental modeling studies of contaminant fate. Circulation tests were also used to confirm and demonstrate model performance and accuracy. For example, hydrodynamic results produced with CH3D-WES must be consistent with results obtained from previous studies. The following paragraphs describe the diagnostic tests used to check the response and performance of the

model. These include tests to: (a) simulate average summer circulation patterns, (b) investigate the effects of constant wind stress over the NY Bight, and (c) verify model response and stability to single (M_2) and multiple constituent tidal forcing.

Summer circulation simulation

The summer circulation application of the model was performed to demonstrate that the model can reproduce general circulation features observed within the entire NY Bight. Although circulation patterns are "not always in the same general direction" (Bumpus 1973), certain persistent characteristics have been reported. For example, circulation is generally parallel to the contour lines of the continental shelf, directed from northeast to southwest. However, velocities within the Hudson Canyon are, on the average, directed toward the apex of the NY Bight. Nearshore current reversals along the New Jersey shore north of the entrance to Delaware Bay and easterly flows along Long Island have been observed to generate large-scale circulation cells. The purpose of the circulation test was to demonstrate the model's ability to reproduce these features.

Steady-state water surface elevation boundary conditions were specified according to the results of Hopkins and Dieterle (1987). Their study indicates that for the typical summer period of August 1978, a difference of 13 cm in water level exists between Narragansett Bay and the shelf break and a difference of 11 cm exists between Cape May and the shelf break. Therefore, a steady-state nearshore head differential of 2 cm from northeast to southwest and a zero elevation boundary along the shelf break is consistent with observed summer circulation patterns. A zero wind, zero initial current, and zero river inflow contribution from the Hudson River were specified as initial conditions. The initial water surface elevation was specified as mean sea level. Model simulations were then conducted for a period of time sufficiently long that start-up approximations are not reflected in model results. For the initial steady-state tests, computations were stopped when model results became stabilized.

Results for the initial simulation are shown in Figures 15a-15c, the flow is shown to be forced to the southwest by the imposed cross-shelf elevation gradient. Some northerly flow along the coast of New Jersey is evident. Currents in Long Island Sound are seen to be weak (i.e., quiescent conditions occurring in Long Island Sound and areas offshore of the NY Bight apex). The Hudson Canyon bathymetry acts as a trough, such that the current has a dominant shoreward component on the northern side and an offshore component on the southern side of the canyon. Figures 15a-15c show surface, mid-depth, and bottom currents, respectively, at a time of 720 hr from the beginning of simulation. Results are consistent with a circulation pattern of contour parallel flow from the northeast to the southwest.

Wind stress response

The effect of wind field forcing over the NY Bight was investigated by imposing a constant wind stress uniformly over the entire modeled area. The imposed along-shelf and cross-shelf water surface slope and zero initial current boundary conditions described in the previous section for the summer circulation test were specified in all wind field simulations. Because the general circulation patterns created by near constant wind are known, these series of tests provide confirmation that the wind stress boundary condition segment of the model is performing correctly and that the model is reproducing known wind-initiated system responses.

The surface wind stress was specified to correspond to mean summer wind conditions with a magnitude of 0.14 dyne/cm^2 (Saunders 1977). In this series of tests, selected wind conditions were applied to demonstrate the hydrodynamic flow field that develops in response to differing wind conditions. The wind stress is applied uniformly over the entire computational grid. Selected wind conditions represent winds from the southwesterly, northeasterly, southeasterly, and northwesterly directions. Results are in general agreement with those obtained by other investigators (Blumberg et al. 1988, Hopkins and Dieterle 1983). Water density, salinity, and temperature computations were not performed in this series of model evaluations.

The following numerical experiments describe the various tests used to evaluate model response to wind forcing. Results are discussed in terms of their effect on the hydrodynamic circulation within the NY Bight. Although the examples chosen depict characteristic cases rather than exact phenomena, they represent realistic wind field conditions for which a system response is known. Six sets of test cases are presented to assess the impact of different wind and river inflow conditions on circulation within the NY Bight.

Case 1. The first simulation is performed with a uniform wind stress (0.14 dyne/cm^2) from the southwest. Figures 16a-16c show surface, mid-depth and bottom currents, respectively, at a simulation time of 720 hr. These figures show the influence of wind on the overall current pattern, causing a strong reversed northwestward flow near the New Jersey shore. A clockwise circulation in Long Island Sound is shown in which flows on the north and south shores of Long Island Sound are reversed. This rotation of currents is evident at all levels of computation. It is interesting to note that the quiescent zone east of the NY Bight apex observed during the no-wind simulation has moved eastward along the shoreline of Long Island. Also, the weak clockwise circulation zone offshore of New Jersey has become stronger, especially at the mid-depth and bottom layers.

Case 2. The primary effect of a wind field from the northeast, shown in Figures 17a-17c, is to force a strong flow to the southwest. Currents in the southern part of the Hudson Canyon are directed offshore (down the canyon), indicating that northeasterly winds are ideal for driving water offshore of the

northern New Jersey coast. Results show that eddies do not develop near the northern New Jersey coast as in Case 1.

Case 3. A southeasterly wind produces northwest surface currents toward the Long Island coast in the vicinity of the NY Bight apex as shown in Figure 18a. Currents decrease toward the mid-depth and there appear to be no wind effects on bottom currents because of the relative magnitude of opposing boundary elevations (Figures 18b and 18c). The flow south of the Canyon is directed offshore in the bottom layer, while surface flow near the New Jersey coast is weak, developing circulation eddies. Onshore surface currents remain on the north side of the Hudson valley.

Case 4. The effects of a northwesterly wind are shown in Figures 19a-19c. Surface currents in the NY Bight apex are consistently in an offshore direction but diminish to near zero in the mid-depth layer. The bottom flow in the apex shows a general up-valley direction. It is interesting to note that no eddies develop near the water surface off the New Jersey coast and that eastward currents are generated along the New England coast along the north boundary of Long Island Sound. The model indicates that circulation on the inner shelf region offshore of New Jersey is weak and spatially variable near the bottom layer. Under these conditions, northwesterly winds tend to drive water offshore from the New Jersey coast, similar to the effects of winds from the northeast; however, a more pronounced circulation zone offshore of New Jersey is seen.

Case 5. The fifth case imposes an average daily summer river inflow of 200 m^3/sec from the Hudson River with zero wind conditions. Figures 20a-20c show little change from the average summer circulation case, although the offshore directed currents in the apex are slightly greater than the no-flow summer case. Few flow field effects are shown in the Long Island Sound.

Case 6. Case 6 specifies a wind stress that is double that of the Case 3 (i.e., southwesterly winds). Results of this simulation are shown on Figures 21a-21c. The effects of the wind appear to be primarily confined to the nearshore regions. The stronger winds enhance the northward flow along the Long Island ocean coast.

The objective of the wind response testing is to demonstrate the effect of wind forcing on the steady-state circulation pattern along the shelf and within the NY Bight. Figures 16-21 show that the winds have an impact on the surface flow patterns but little effect on the bottom flow. The external or ocean sea-level gradients and wind forcings are considered to be the primary forcing functions for the system, having a greater influence than other factors such as bottom stresses or salinity and temperature effects on density. However, density structures and large-scale oceanic circulation patterns can have noticeable effects on circulation in the NY Bight.

Tidal response

Time-varying applications of the model were performed by simulating tidal propagation throughout the NY Bight and Long Island Sound. Required input to the model included time series of water surface elevations at the outer boundary of the computational grid; therefore, hourly tidal boundary elevations were specified at the following locations (Figure 22):

Lat. 39.35 N, Long. 74.70 W
Lat. 38.48 N, Long. 74.00 W
Lat. 38.42 N, Long. 73.88 W
Lat. 38.23 N, Long. 73.57 W
Lat. 38.92 N, Long. 72.83 W
Lat. 39.38 N, Long. 72.12 W
Lat. 39.83 N, Long. 71.33 W
Lat. 39.95 N, Long. 70.22 W
Lat. 41.50 N, Long. 71.33 W

The water surface elevation time series used to define these open water boundaries were computed from the Naval Surface Weapons Center's Global Ocean Random-Point Tide (RPTIDE) program (Schwiderski 1979, Schwiderski and Szeto 1981). At nearshore open-water boundaries in the vicinity of Nantucket and Cape Cod, where ocean tides undergo significant distortion, time series boundary data were computed from the coastal tide generation program TIDEGEN (Cialone 1991) developed by CERC. The standard tidal harmonic constants obtained from the NOAA were used for input to the TIDEGEN program. Intermediate cell boundary elevations were computed by linear interpolation between the offshore and nearshore boundaries. Additional boundary and initial conditions included the specification of an initial zero velocity distribution, zero wind and inflow, and a water surface elevation specified at zero mean sea level.

Two levels of testing for tidal response were performed. The first was a simulation to a single M_2 constituent tidal signal. Because the M_2 represents the dominant astronomical constituent in the NY Bight, this initial simulation was performed to demonstrate that model simulations are correct in both amplitude and phase and that the computed tidal envelope remains uniform in amplitude, i.e., the computed tidal signal does not fluctuate in maximum flood tide elevation, but maintains a clear and uniform signal. Comparisons of computed to prototype data were made by comparing computed M_2 time series to tides reconstructed from tidal constituents. Tidal stations at which comparisons were made are listed below:

The Battery, NY
Montauk Point, NY
Willets Point, NY
Sandy Hook, NJ
Newport, RI

Atlantic City, NJ
Bridgeport, CT
New London, CT
Buzzards Bay, RI

Example comparisons for the nine NOAA tide gauges listed above are shown in Figure 23. As shown, model results are stable and compare well to reconstructed prototype conditions. Successful completion of this task led to a simulation of a tidal signal reconstructed from eight primary tidal constituents. This comparison demonstrates the model's ability to reproduce spring and neap tidal fluctuations as well as the ebb/flood cycle of the tide.

The mixed tide signal generated for input to the model is based on the semidiurnal and diurnal constituents M_2, S_2, N_2, K_2, K_1, O_1, Q_1, and P_1. These constituents represent the dominant tidal components for the bight. Harmonic analysis of prototype data, performed under Task A.2 of the scope of work and described in Chapter 3 of this report, confirm these constituents to represent the majority of astronomical tidal energy in the tidal signal at stations located in NY Bight, NY Harbor, and Long Island Sound.

As was the case with the single constituent tide, a comparison of model results to prototype data is made by comparing computed time series to prototype time series reconstructed from published harmonic constituents.

Comparisons of simulation results versus harmonic reconstructed time series of tidal elevations are shown in Figure 24. As shown, model reproduction of astronomic tides is excellent. These comparisons show the model to be ready for the calibration and verification phase in which the model is driven by and results compared to actual prototype data.

Model Calibration/Verification

Boundary condition selection

The tidal time series boundary conditions for the tidal constituent simulation phase of the diagnostic tests were based on published harmonic constituent data. These data include the amplitude and equilibrium arguments for each constituent of the tide and reflect both the location of the specified tide station and the time at which the time series was initiated. Therefore, phase and amplitude information between adjacent boundary condition locations shown in Figure 22 are automatically specified as a function of time and location. Because prototype time series of water surface elevation are not available at the outer boundary of the grid for the periods of calibration and verification, an alternate method of boundary condition selection was adopted.

The methodology selected to specify boundary conditions for the April and May 1976 time periods was to drive the outer boundary water surface with time series corresponding to recorded tidal elevation time series at Atlantic City, NJ and Newport, RI. In each case, the amplitudes and phases of the boundary time series were adjusted until the computed time series at Atlantic City and Newport were in agreement with the recorded measurements. The amplitude transfer function and phase lag for tidal forcing were determined from harmonic analyses of the M_2 constituent simulations described previously. Boundary conditions were specified at the four corner locations shown in Figure 25. Intermediate tidal boundary control points at each boundary cell were specified according to linear interpolation between these points. The Atlantic City time series was used for specifying stations 1-3, while the Newport data were used to specify station 4 according to the following criteria.

Results of the M_2 analysis indicated that the tidal component of the Atlantic City data could be translated without change in phase or amplitude to station 1 but should be reduced by a factor of 0.70 for translation to stations 2 and 3. The phase of the signal was advanced by 15 min for both stations. Station 4 was specified as identical in amplitude to the time series recorded at Newport; however, the phase was advanced by 5 min. For stations 1 and 4, the phase-shifted full tidal signal at Atlantic City and Newport (both tidal and low-frequency components) was used for boundary conditions. However, due to the amplitude reduction for stations 2 and 3, an alternate procedure was followed.

The low-frequency non-tidal component of the prototype tide signal was removed from the Atlantic City and Newport data with the filtering technique discussed in Chapter 3. The full tide (tidal plus low-frequency) signal was then multiplied by the factor of 0.70; however, the computed low-frequency component of the time series was added to the reduced time series. This new time series was then phase shifted as discussed above. This procedure produces a water level elevation boundary condition in which the tidal portion has been reduced by a factor of 0.70 and the non-tidal component amplified by a factor of 1.70. This procedure maintains a positive cross-shore gradient for positive elevation, low-frequency events and a negative cross-shore gradient for low-frequency water level depressions. This procedure was developed through a trial-and-error iteration in an attempt to optimize model-to-prototype comparisons of both tidal and non-tidal components of the signal. Examples of the success of this procedure are shown in the calibration and verification section.

Wind stress for the calibration and verification phases of the model were specified as the numerical average of the three WIS hindcast wind fields presented in Appendix A. The WIS data were selected to minimize land boundary layer effects contained in meteorological data measured at airports. Figures A4, A5 and A7 represent wind fields for the three locations for the month of April 1976. Figures A8-A13 present data for just the location 72.5W longitude, 40.0N latitude for the months of May through October 1976. River

inflow was specified according to the Hudson River hydrographs included in Appendix A (Figure A1).

Calibration - April 1976

April 1976 was selected as the time period for calibration of the model. Tidal data from the Atlantic City gauge were found to contain a gap which extended from 3 April through 10 April 1976; therefore, the calibration time period began on 11 April 1976 and extended through 30 April 1976. The specified water surface elevation boundary conditions are shown in Appendix A (Figures A2 and A3). Wind field and river inflow data are also shown in Appendix A.

It is not always possible for model results to match prototype data to the accuracy shown in the tidal constituent comparisons of Figures 23 and 24. The degree of acceptability must be determined through examination of the data which the model is expected to reproduce. In the case of Figures 23 and 24, the data are purely tidal in origin. Figure 26 is a plot of raw data for April 1976 for the Atlantic City, Newport, and Montauk Point tide stations. Included in each plot is the superimposed low-frequency contribution to the signal as determined with the low pass filter. The data gap for 3-10 April for Atlantic City has been filled with zero values. Events of interest in the record are the low-frequency fluctuations on 10 April (day 223) and 25 April (day 238). In each episode, a significant increase in the mean sea level is experienced over the entire bight which persists for over 24 hr. The spatial extent of the impact of this low-frequency energy can be seen in Figure 27 in which the April-May 1976 tidal signal at the Battery is plotted above the concurrent velocity components measured at current station LT2A. The spatial separation of the two locations can be seen in Figure 6. As shown, the non-tidal contribution is significant and can be seen to be generally correlated at all stations. Unfortunately, the correlation between low-frequency energy in the water surface elevation and in the currents is variable. For example, tides and currents are approximately in phase on day 10 while they are out of phase on day 25. This discrepancy in phasing demonstrates the difficulty in attempting to model low-frequency events with estimated boundary conditions. The following will describe the degree of success achieved by backing out surface elevation boundary conditions from nearshore data and will show that low-frequency events can not be precisely reproduced without accurate offshore boundary measurements.

The subtidal low-frequency fluctuations observed in the data are commonly experienced on the east coast of the United States and have a period on the order of 5-7 days. However, this low-frequency energy is difficult to quantify since its exact origin is due to an unknown combination of such forcing functions as pressure deficits, wind fields, and/or large-scale ocean current patterns. Because surface elevation data are not available at or beyond the continental shelf break at the computational boundaries of the model, the adjustment of

low-frequency energy previously described was used to provide a best model-to-prototype match. The following describes model-to-prototype comparisons of water surface elevation and currents.

Comparsions of computed water surface elevation to prototype data are presented in Appendix B. An example plot is reproduced in Figure 28 for the Battery tide gauge. As shown, the match between model and prototype results is excellent. Similar results shown in Appendix B demonstrate that the model provides an excellent reproduction of water surface elevations, including the low-frequency events shown on 10 and 25 April 1976.

In hydrodynamic modeling, currents are recognized to be more difficult to predict than water surface elevations. This difficulty is due in part to the directionality of currents and the influence of local bathymetry, which often can not be adequately resolved by the discrete computational grid. Comparisons of computed currents to prototype measurements recorded at the approximate equivalent depth are presented in Appendix B. Examination of the plots shows that the model provides a very acceptable reproduction of currents corresponding to stations LT2 and LT3, somewhat less acceptable comparison for stations LT4 and LT7, and a rather poor fit for station LT6. The poor fit for station LT6 can probably be attributed to local bathymetric effects because the station is located on the edge of the Hudson Shelf Valley. Station LT7 may also be similarly affected by local bathymetry. Note from Figures 16 through 21 that stations LT4, LT6, and LT7 are located in areas that are prone to current reversals and large-scale eddy formations. In view of their locations and the uncertainty of the low-frequency boundary conditions, it is not unusual that the low-frequency events are not well-reproduced. In contrast, the low-frequency events are more accurately described at stations LT2 and LT3, areas not prone to current reversals.

General observations concerning the comparison of model-to-prototype current data indicate that matching of low-frequency events is difficult to accomplish due to the fact that the exact amplitude and phasing of boundary conditions for the outer boundary of the model are not known but are assumed from nearshore measurements. An example of this difficulty is shown in Figure 26, which graphically demonstrates differences in low-frequency phasing between tidal stations at different locations within the modeled domain. As a result, it is difficult to determine the outer boundary elevation time series or the precise along- and cross-shore surface gradients and therefore difficult to precisely match the current vectors. The following conclusions can be drawn from the calibration process:

1. Simulations with steady-state boundary conditions such as wind stress, freshwater inflow, and imposed surface elevation gradients indicate that the model successfully reproduces large-scale circulation patterns that are generally known to exist. This conclusion is based on both quantitative and qualitative observations of the behavior of the system.

2. Calibration of the model to astronomical tidal forcings produced excellent comparisons for tidally driven water surface elevations. The basis of evaluation is comparisons of model predictions of surface time elevation series versus surface elevation time series reconstructed from tidal constituents. Results were obtained for single-constituent tides to demonstrate model stability and repeatability and for multiple-constituent tides to demonstrate accurate reproduction of long-term spring and neap tidal cycles. In all cases, surface elevations are well-reproduced.

3. Calibration of the model to observed prototype conditions was also very successful but indicated that the lack of prototype data for the offshore boundary condition leads to uncertainties and/or inaccuracies in the model-to-prototype comparisons. Although comparisons of surface elevation were excellent, comparisons of currents often exhibited errors in phasing. These differences are shown to be due, to a large extent, to the presence of low-frequency energy in the system, which has not been accurately specified at the offshore boundary. An additional source of error may be due to localized bathymetry effects, especially in the vicinity of the Hudson Canyon where depth differences between adjacent computational cells can be on the order of a hundred meters. If, for example, the location of the model gauge does not correspond to the location of its prototype counterpart, then differences in current magnitude and direction will occur. Despite known inaccuracies in the specified boundary conditions, the model simulation comparisons are considered very good.

4. Non-astronomical energy is shown to be present in the system. It is observed in the data as low-frequency oscillations in the surface elevation, sub-surface current, wind velocity, and atmospheric pressure time series data and has a period on the order of several days to a week. Because the exact boundary conditions are not known, simulated conditions were based on observed surface elevation time series at NOAA tide stations on shore. Therefore, phasing errors in model-to-prototype comparisons are due to errors introduced in simulating offshore boundary conditions. It is concluded that, in order to improve the model-to-prototype comparisons, it is necessary to know the precise water surface fluctuation in the field corresponding to the numerical grid boundaries, as well as the wind and pressure distribution over the area. This would require gathering prototype meteorological and surface elevation data offshore at depths of over 500 m.

5. The purpose of this feasibility study is to demonstrate that the HM can simulate the flow characteristics of the NY Bight and coupled flow system and to show that model output can be used in a comprehensive environmental model to demonstrate how various uses of the bight may impact the surrounding region. Because water quality simulation comparisons are made over time scales on the order of months, the short-term (daily to weekly) low-frequency fluctuations are not significant as long as weekly to monthly mean values are consistent with local inflow

and weather conditions. The ability of the model to reflect wind conditions was adequately demonstrated. Therefore, the hydrodynamic modeling effort involved reproduction of the 6-month period of April 1976 through September 1976. It is during this time period that the summer of 1976 hypoxia event occurred. Because prototype data were not available at Atlantic City and Newport during this entire period, long-term computations were specified as constituent-based tides corresponding to the period and to actual seasonal river inflow and wind conditions.

6. The goal of the HM application is to demonstrate the capability of the model to simulate the flow regime in the NY Bight. Even though differences in current phasing are shown to exist, these differences are due to inability to exactly specify prototype boundary conditions. However, current magnitudes and tidal phasing are correct. If precise boundary phasing were imposed on the model, then low-frequency phasing would probably be in agreement. The purpose of the study is to show the model capable of reproducing the prototype system, which has been accomplished with available data.

7. A more rigorous comparison of low-frequency events will require additional boundary condition measurements. Because the low-frequency events have a long-term average of zero, and the model has been shown to respond properly to wind field forcing superimposed on mean conditions, the use of a constituent-based tide and observed wind fields will provide valid long-term data for input to and verification of the environmental model.

The following section will describe the verification procedure in which prototype data for the month of May 1976 are compared to the hydrodynamic simulation results.

Verification - May 1976

The month of May 1976 was selected as the period for model verification. All aspects of the modeling process, including the specification of boundary and initial conditions, were identical to the procedures described in the calibration description. The tidal signal comparisons for May for the NOAA gauges are shown in Appendix C. An example comparison is presented in Figure 28, representing the Battery. Note the reproduction of the two low-frequency events of 6 and 19 May. Both events are well-reproduced by the model. In fact, as is evidenced by all comparisons shown in Appendix C, the tidal elevation verification can be considered excellent.

Comparisons of model to prototype velocity data are also shown in Appendix C. Inspection of the comparisons shows very good reproduction of stations LT2, LT3, and LT4. A slightly less acceptable reproduction is shown for stations LT5 and LT6, although station LT5 appears to be somewhat out of phase. The degree of match for these stations is generally valid for all depths

shown in the appendix. As with the calibration comparison, station LT6 shows a rather poor fit. As noted in the calibration section, this poor fit is most likely due to bathymetry and/or location discrepancies between the location of the model gauge and the prototype gauge.

It can be seen in all comparisons that the storm/low-frequency events of 6 May and 19 May are not well-reproduced by the model. This lack of reproduction is due to the fact that the origin of the disturbance is not modeled, only its water surface response. As was described in the previous section, low-frequency events such as this can not be modeled unless the proper forcing function (hence, boundary conditions) are used to drive the model.

Conclusions - calibration and verification

Conclusions of the calibration and verification process are that the model acceptably reproduces water surface elevations and currents as a function of tidal forcing, wind forcing, and river inflow forcing. As is common with a well-behaved hydrodynamic model, the elevation comparisons are excellent. The current comparisons are also acceptable; however, differences do occur, one of which (LT6) is extreme but explainable. The majority of error shown in all but one current station occurs when low-frequency disturbances occur over the entire NY Bight. As discussed, it is not possible to reproduce these effects (or responses) without specifying the forcing boundary conditions. However, all low-frequency events, which persist only a day or two, have an approximate zero mean over periods of time on the order of a month or more. Because the goal of this modeling effort is to ultimately provide input to the environmental model, which is concerned with water quality constituents that change over months, it is not critical that short-term hydrodynamics are reproduced. If this were necessary, additional prototype data would be necessary. Therefore, for the purposes and goals of the NY Bight study, the HM has been rigorously tested and proved to be capable of reproducing the hydrodynamics of the NY Bight. The following section describes the 6-month long-term simulation of the period of April through October 1976. The flow fields generated in this simulation were provided to the environmental model to compute the transport and dispersion of water quality constituents and surface floatables.

5 Long-term Simulation

Introduction

For purposes of the long-term simulation, the six-month period from April 1 to October 1, 1976 was selected for the following reasons. MESA and other field data on currents and temperature were available for this period to validate model results, and this period included the summer hypoxia event of 1976. The hypoxia condition was of great interest for water quality modeling, as it provided a means of verifying the environmental model to a known environmental event.

In performing realistic long-term simulations, it is necessary to consider density effects in addition to tides, winds, and river flows because the long-term flows also respond to density gradients. Initial testing of the model with density gradients revealed the model results tended to become unstable near the offshore boundary of the grid due to rapid increases in depth at the shelf break. In view of this, depths in the first three rows of cells near the offshore boundary were made equal to the depths of the corresponding cells in the fourth row. Ten sigma layers were used for the long-term simulation. As in model calibration and verification, a time-step of 2.5 min was used for both external and internal mode calculations.

Most of the MESA sensors stopped functioning during the period of 9-14 August 1976. This malfunction is believed to have resulted from the passage of Hurricane Belle through the NY Bight area during that period. Initially, when WIS winds were directly used in the numerical model, the model tended to become unstable in the shallow areas of the grid at approximately 9 August. This instability is due to the fact that there is no provision in the model for flooding and drying of low-lying areas. In view of this, the input winds were smoothed and their magnitude was limited during the passage of the hurricane. The smoothing should not have had an adverse effect in terms of long-term results, especially as they relate to water quality. This view is supported by Mayer, Hansen, and Minton (1979), who, on the basis of a study on water movement in the bight during 1975 and 1976, "conclude that despite strong winds and surface waves, Hurricane Belle was too small and passed too rapid-

to have had a lasting effect on either the advection or vertical mixing processes in the Bight."

Boundary Conditions

For the long-term simulation, the HM was forced with tide, wind, inflow at the Hudson River boundary, and density gradients due to salinity and temperature. Offshore and lateral (open-water) surface boundary conditions were obtained for the same eight tidal constituents used in the mixed tide comparison. Referring to Figure 30, the surface elevation signals at stations 2 through 8 were obtained using Schwiderski's global tidal model. Surface elevation at station 1 was obtained by computing the tidal signal at Atlantic City from published constituents and translating the signal without change in amplitude or phase to station 1. Similarly, the surface elevation at station 11 was obtained by computing the tidal signal at Newport from published constituents and translating it to station 11 without change in amplitude or phase. In every boundary segment located between two boundary stations, the elevation signals for boundary cells were determined by linear interpolation between the boundary stations.

As in the calibration and verification runs, wind velocities and directions were interpolated from WIS stations located offshore (Appendix A). Freshwater flows were prescribed at the Hudson River boundary from available field data (Figure A1). Vertical distribution of temperature at the river boundary was estimated from available data and prescribed as a function of time, as were vertical distributions of temperature and salinity at the offshore and lateral boundaries.

As indicated in Chapter 2, computation of surface heat flux required input of equilibrium temperature T_e and surface heat exchange coefficient K as a function of time. Values of these parameters, averaged daily, were computed from meteorological data recorded at the John F. Kennedy (JFK) Airport for the period under consideration, using the procedure of Edinger, Brady, and Geyer (1974). They are shown in Figures 31 and 32.

Initial Conditions

The model was started from rest, with the surface elevation and velocities set to zero. The initial vertical distributions of salinity and temperature at all water cells were estimated from all available measurements, including MESA gauges, ship observations, etc. The following procedure was used. At each grid location where measurements of salinity and temperature were available, values at different sigma layers were obtained by interpolation. Each grid cell was assigned the value of the nearest measurement location. For Long Island Sound, because synoptic field data were not available, salinity and temperature were assigned uniformly constant values. Next, three-point smoothing was

performed in each of the two horizontal coordinate directions to obtain smoothly varying fields. Care was taken to ensure that boundary and interior cell values were consistent with each other and that there were no sudden jumps between adjacent cells.

Long-term simulations were repeated using alternate initial conditions, as a check on sensitivity to specification of initial conditions. The alternate procedure was based on z-plane interpolation as follows. At the measurement stations, salinity and temperature were interpolated to pre-determined depths below the free surface. The pre-determined depths chosen were 1, 5, 10, 15, 20, 25, 30, 40, 50, 60, 70, 100, 150, 300, and 500 m. As before, grid cell values were based on those of the nearest measurement station. For each constant depth layer (z-plane), values were smoothed in both horizontal coordinate directions several times. Finally, at each cell, values for different sigma layers were obtained by interpolation from the z-plane values for that cell.

Model results obtained using the two different initial conditions did not differ significantly when compared with field data for temperature. However, the latter procedure yielded smoother starts. In what follows, only results obtained from the first procedure will be discussed. In the model simulation, computation of salinity and temperature transport was not initiated until 5 days after the start of computation of hydrodynamic quantities (surface elevations and velocities), in order to minimize any start-up transients. During the first 5 days, the HM used forcing due to tides, wind, river flow, and density gradients computed from the initially prescribed salinity and temperature gradients.

Ideally, to achieve successful simulations, it is necessary to prescribe realistic and accurate boundary and initial conditions to the model. Effects of boundary conditions continue throughout the simulation, because they are used to force the model. Depending on the phenomena of interest and the areal extent of the region studied, the effect of initial conditions may persist for days to months after the start of the simulation. In the present case, since there were no boundary surface elevation measurements available, surface elevations computed from the eight major tidal constituents were used. They contain most of the tidal contribution but not the effect of winds or other low-frequency energy. Nor do they contain cross-shelf gradients, which are known to exist in the NY Bight area. There were no measurements of salinity and temperature at the offshore and lateral boundaries. Therefore, estimates had to be made for boundary values based on available interior measurements and judgement.

In regard to initial conditions for salinity and temperature, there were very few measurements corresponding to April 1. Those that were available were mostly temperature values at the MESA gauge locations. Because ship cruise observations were taken at discrete point locations at discrete times, values for April 1 had to be interpolated based on temporally closest values. Boundary/initial conditions are difficult to define because temperature varies during the course of each day and from day to day. This is true for salinity to a lesser

extent. In summary, there was some uncertainty in prescribing both boundary and initial conditions.

Discussion of Results

Because comparisons of computed surface elevations and currents with prototype data were performed during the model calibration and verification phases, long-term simulation comparisons were primarily limited to temperature and salinity. The following paragraphs describe these results.

Temperature

Time series. The MESA gauges had time series measurements of temperature taken at different levels in the water column. No salinity measurements were taken. For the period under consideration, continuous measurements were available (Figure 8) only at gauges LT2, LT4, LT5, LT6 and LT7. Field measurements were taken every hour, whereas model results are more representative of daily averaged values. Temperature can vary by several degrees during the course of a day, especially in summer months. Therefore, a daily average condition should be used for comparison to model results. Comparisons at gauges LT2 and LT4 at two different levels are shown in Figures 33-36. These gauges are selected for display because they are located in open water, on either side of the Hudson Shelf Valley, in an intermediate depth of water and are representative of conditions offshore of the New Jersey and Long Island coasts. The total water depth at station LT2 was 32 m. At LT2C located 1 m above the bottom, the computed results follow the trend of the measurements very well but are higher by about 2 deg. At LT2A, located 19 m above the bottom, model results follow the trend of the observed data very well up to approximately day 84. The deviation is within 2 deg. However, a change in the trend of measurements is shown after day 84 where the sensor behaves erratically, exhibits large oscillations, and effectively stops functioning after day 110. As indicated previously, most of the temperature sensors stopped functioning around day 130 (9 August).

At station LT4, the water depth was 49 m. At location LT4C, located 1 m above the bottom, the computed results generally follow the flat trend of measurements but are higher in value, the deviation being within 4 deg. At LT4S, 47 m above the bottom, model results follow the trend of measurements and the transients very well, although model transients are much larger than those observed. This is true for the entire length of record until the sensor fails in August. Results obtained at all other gauges (Appendix D) show similar behavior at the bottom and surface layers.

In general, model results follow the trend of prototype measurements but are higher in value. This deviation is only within a few degrees. Occasionally, the measurements depart from the trends of model results after some time

and exhibit quite a different behavior (e.g., LT4A, LT6A, and LT7A). This could be due to other phenomena not modeled such as flow reversals and the fact that both LT6 and LT7 are located in regions of rapidly varying bathymetry, i.e., at the edge of the Hudson Shelf Valley.

The large oscillations in model results near the free surface can be directly related to variations in equilibrium temperature T_e (Figure 31). Computation of surface heat flux is very sensitive to T_e and K (Equation 30), with surface temperatures responding immediately to variations in T_e. It is believed that the sudden large variations in daily equilibrium temperature input to the model may not be realistic. This aspect needs to be investigated in future studies. Also, the generally higher model predictions of temperature in lower layers indicate that, in the model, heat energy may not be transmitted from the surface to the lower layers realistically. This may indicate that improvements may be needed in the vertical turbulence closure model used in CH3D-WES.

Vertical profiles. As a consistency check on the model computations, vertical profiles at different MESA gauge locations were plotted corresponding to September 1, 1976. Figures 37 and 38 show the computed profiles at LT2 at 120 hr (at the start on April 6) and at 3672 hr (on September 1, after nearly 5 months of simulation). Figures 39 and 40 show the profiles at LT4 at corresponding times. As comparisons at each gauge location indicate, the profiles evolve from the simple profiles of early spring to summer profiles with a characteristic thermocline structure. In the later profiles, the temperature is uniform near the surface but shows an abrupt decrease near the 8-m depth for LT2 and the 6-m depth for LT4. Thereafter, the temperature decreases more gradually with depth below free surface. Similar behavior is observed at other gauge locations (Appendix D). All the profiles are stable, with temperature decreasing as elevation decreases.

Salinity

The only salinity measurements available were those from ship cruises, which were not convenient for comparing with model results because they were spot measurements taken at discrete times and locations. Therefore, the salinity results were examined for reasonable trends in behavior.

Time series. Salinity time series at the bottom (layer 1), near mid-depth (layer 5), and near the surface (layer 9) are shown in Figures 41-43 for LT2 and Figures 44-46 for LT4. At each location, salinity increases very slowly with time for a given layer. This is characteristic of typical seasonal change from spring to summer. At each location and time, salinity increases with depth. Time series plots for other gauge locations (Appendix D) exhibit similar behavior. These trends are reasonable.

Vertical profiles. Vertical profiles of salinity at different gauge locations were plotted at the beginning of the simulation (120 hr) and at September 1 (3672 hr). These profiles are shown in Figures 47-48 for LT2 and 49-50 for

LT4. Profiles for other gauge locations are given in Appendix D. Results show that computed salinity increases with depth and time. The increase with time is shown to be small at the surface and larger at the lower layers. This may indicate that the initial conditions chosen deviated considerably from the actual values occurring at the bottom layers.

Conclusions from the Long-term Simulation

In summary, the computed temperatures match the trend of time series observations but are somewhat greater in value. Computed vertical profiles of temperature are stable and show typical seasonal variation. Model results for salinity exhibit typical slow seasonal change from spring to summer and stable vertical profiles. Overall, in view of the good comparisons achieved to hydrodynamic field data, and the reasonable matching of model results and trends to prototype conditions, the long-term simulation is considered successful. Most of the observed deviations from prototype data may be attributed to uncertainties in the specification of initial and boundary conditions.

6 Extended Validation to Long Island Sound

Introduction

The calibration and verification of the CH3D hydrodynamic model described in the previous section utilized existing water surface elevation, current, salinity, and temperature data collected for the MESA project conducted during the period of 1975 to 1976. Because the calibration and verification data were primarily concentrated offshore, in the region of the NY Bight extending from the apex to the continental shelf break, verification of the model to water surface elevations was achieved at selected NOAA tide stations both within and adjacent to the NY Bight. Therefore, the primary verification effort for the model was made to offshore currents, temperatures, and salinities located throughout the NY Bight.

In FY91, an extended verification effort was proposed to demonstrate the capability of the model to reproduce the hydrodynamic circulation as well as the salinity and temperature structure within the major subsystems of the computational grid. Specifically, it was felt that an extended validation of the model should be made for the Long Island Sound and the East River hydrodynamic connection between the Sound and NY Harbor at the Battery. This region of interest is shown in Figure 51. Because data were not collected in these areas during the MESA studies, additional data sets were acquired and analyzed for use in this extended verification effort. The following sections describe the data selected for this purpose and the manner in which these data were analyzed, edited, and reduced to a form appropriate for comparison to model-generated data.

Data Acquisition and Analysis

Two sources of data were available for use in the extended effort: (a) NOAA and (b) the Marine Sciences Research Center of the State University of New York (SUNY) at Stony Brook, NY. These data include: (a) time series of water surface elevations, (b) time series of current measurements,

(c) time series of salinity and water temperature, and (d) vertical salinity and temperature profiles. Both sets of data were collected as a part of the Long Island Sound Oceanographic Project (Earwaker 1990) and were used by NOAA for the short-term validation of its Long Island Sound hydrodynamic model.

The following paragraphs describe each data type, its respective spatial and temporal distribution, and the manner in which it will be used in the extended verification procedure.

Water surface elevations

Water surface time series were provided by NOAA for the tide stations shown in Figure 52. The NOAA station numbers corresponding to each station name, the location in latitude and longitude, and the time span of the data are indicated in Table 1. In general, data are available beginning on 1 April 1988; however, CERC obtained only data corresponding to the May through July 1990 period of interest. Available data for this period are shown in Table 1. All times are referenced to Eastern Standard Time.

Table 1
Water Level Station Summary

Station Name	Station Number	Latitude (d-m-s N)	Longitude (d-m-s W)	Start-End Date d/m/yr-d/m/yr
Bridgeport, NY	846-7510	41-09-54	73-10-54	1/5/90-31/7/90
The Battery, NY	851-8750	40-42-06	74-01-00	1/5/90-31/7/90
Fishers Is., NY	851-0719	41-15-24	72-01-48	1/5/90-25/7/90
Point Judith, RI	845-5083	41-21-48	71-29-18	4/5/90-24/7/90
Montauk Point, NY	851-0560	41-02-48	71-57-36	1/5/90-31/7/90
New London, CT	846-1490	41-21-54	72-05-42	1/5/90-31/7/90
Port Jefferson, NY	851-4560	40-57-00	73-04-36	1/5/90-31/7/90
Willets Point, NY	851-6990	40-47-42	73-46-54	1/5/90-31/7/90

Water surface data were provided in two forms, a time series file of hourly residual water surface elevations and a table of harmonic constituent amplitudes and local epochs (κ'). The residual file represents the observed water surface time series corresponding to the period indicated in Table 1 with the tidal harmonic constituent contribution removed. An example of the residual data can be seen in Figure 53 for the Bridgeport, CT tide station. This time series covers the period of 1 May 1990 through 31 July 1990.

Although the number of constituents varies slightly between stations as a function of the length of available data for the analysis, amplitudes and local epochs for approximately 23 harmonic constituents were provided for each

location shown in Figure 52. These data permitted the reconstruction of the actual time series of data as the sum of the tidal constituent contribution shown in Figure 54 and the residual files. An example of tidal reconstruction for the Bridgeport gauge is shown in Figure 55.

A tidal verification based on actual data (Figure 55, for example) would limit the comparison period to the periods shown in Table 1. The alternate approach used in the extended verification effort is to drive the model's offshore computational boundary with a time series of water levels reconstructed from only tidal constituents. This approach was adopted so that the model boundary elevation could be computed with respect to the same gauges used in the original calibration and verification process previously described - gauges for which actual time series were not readily available. This identical verification procedure is necessary to preserve continuity and consistency between the initial and extended efforts.

Therefore, offshore surface elevation boundaries were defined in terms of phase lag and amplitude corrections to tides that were reconstructed for the Atlantic City and Newport gauges from NOAA published harmonic constituents. These time series were then adjusted to the time period during which prototype data are available for Long Island Sound. No attempt is made to include the low-frequency, non-astronomical component of the water surface in the boundary conditions because they are not known for the Atlantic City and Newport stations for the time at which data are available in Long Island Sound.

Although the extended effort must necessarily be driven by a constituent-only surface elevation, the verification comparisons of model data were made to prototype currents, temperature, and salinity. This procedure was selected because the temperature and salinity data do not contain a measurable (thus removable) tidal component. Prototype temperature and salinity are strongly influenced by currents; therefore, the decision was made to use actual current data for comparison to model data. This seemingly inconsistent procedure introduced error that was unavoidable without additional tidal data corresponding to the Table 1 time periods.

Currents

Time series of velocities at four locations along the central axis of Long Island Sound were provided to CERC by NOAA. Data were sampled with an Acoustic Doppler Current Profiler (ADCP). Locations of these Residual Acoustic Doppler Sampling (RADS) stations are shown in Figure 56, along with locations of additional data types to be described later. Each data set contains residual currents corresponding to three bins within the water column. Data are provided at 10-min increments and referenced to Eastern Standard Time. A summary of the contents of each file, the location of the mooring, and the depth of each respective bin in meters from the surface are shown in Table 2.

Current meter data are in the same format as the water surface elevation data. The time series for each depth bin is separated into a residual time series and a table of harmonic constituent amplitudes and local epochs. Reconstruction of the actual current time series is accomplished identically to the example presented above, by superimposing the tidal constituent based signal on the residual signal. Example data are presented in the section describing verification.

Table 2
Current Meter Station Summary

Station Number	Latitude (d-m-s)	Longitude (d-m-s)	Depth (m)	Bin Depth (m) Below Surface	Start-End Date d/m/yr-d/m/yr
01	40-48-26	73-47-10	16.0	12.5,8.5,4.5	07/05/90-30/07/90
07	40-59-44	73-24-36	45.0	38.5,28.5,13.5	06/05/90-10/07/90
10	41-04-44	72-33-55	22.5	16.0,11.0,6.0	13/05/90-22/7/90
12	41-13-40	72-05-37	91.4	79.4,39.4,19.4	23/05/90-03/07/90

Temperature and salinity time series

Conductivity (salinity) and temperature (C/T) data were provided to CERC by NOAA in 6-min increment time series corresponding to the five C/T Mooring Station locations (BB, F3, I2, O2, and P2) indicated on Figure 56. All data are referenced to Universal Time and are in the form of temperature (degrees C) and salinity (ppt) for an upper and lower mooring location within the water column at each station location. A summary of the data is presented in Table 3.

An example of the data is presented in Figures 57 and 58 for C/T station F3. Figure 57 represents temperature data at the 12.8-m depth, while Figure 58 is salinity at the same depth. The total depth can be seen from Table 3 to be 28.8 m. The time series begins on 6 May 1990 and extends until 17 July 1990. As shown, the temperature steadily increases from May until July, and the salinity remains relatively constant. All time series are similarly well behaved and provided a good long-term verification database for the transport modeling of salinity and temperature. Each data set contains upper and lower water column time series; therefore, the data were well-suited for the extended calibration.

Table 3
Temperature and Salinity Mooring Station Summary

Station No.	Latitude (d-m-s)	Longitude (d-m-s)	Total Depth-m	Instr Depth-m	Start-End Date d/m/yr-d/m/yr
BBU418D3 BBL419D3	40-41-26	74-00-54	12.0	5.2 8.5	14/06/90-16/07/90
BBU418D2 BBL424D2	40-41-26	74-00-46	12.0	5.0 8.0	23/05/90-13/06/90
BBU239D3 BBL424D3	40-41-26	74-00-54	12.0	5.2 8.5	14/06/90-16/07/90
BBU238D1 BBL420D1	40-42-14	73-59-48	14.7	8.1 9.9	07/05/90-13/06/90
F3U406D1 F3L421D1	41-02-47	73-08-58	28.8	12.8 24.0	06/05/90-17/07/90
I2U411D1 I2L417D1	41-08-23	72-39-34	27.5	11.5 22.7	06/05/90-18/07/90
O2U413D1 O2L422D1	41-06-43	71-42-51	36.0	31.2 16.0	08/05/90-18/07/90
P2U412D2 P2L240D2	41-15-25	71-34-28	39.0	17.1 33.7	24/05/90-18/07/90

Temperature and salinity profiles

Temperature and salinity profile (CTD) data were provided by both NOAA and SUNY. Locations of both data sets are indicated on Figure 56. The 53-profile NOAA data set provides 17-station coverage along the central axis of Long Island Sound, with several of the CTD stations coinciding with the long-term C/T time series locations. The data, referenced to Universal Time, were taken primarily during the month of July 1990 (40 profiles) with some additional data (13 profiles) taken during June 1990. A typical salinity and temperature profile is shown in Figure 59 for CTD station BB. The profile was measured on 12 June 1990 at 5:16 pm. Slight stratification in both temperature and salinity can be seen in the figure.

The SUNY data sets concentrate on the western portion of the Long Island Sound. A total of 70 profiles provide coverage during the months of May, June, July, August, and September of 1990. A typical profile is shown in Figure 60 for station E1, collected on 10 May 1990 at 10:25 am. Summaries of the profile locations and times of measurement for the NOAA and SUNY data are shown in Tables 4 and 5, respectively. Both NOAA and SUNY data sets provide an adequate coverage of Long Island Sound for specifying initial as well as verification conditions for the extended effort.

Table 4
NOAA C/T Mooring Station Summary

Station Number	Latitude N	Longitude W	Profile Dates (No. of Profiles)
A1	40-48-18	73-49-12	20 July (2)
A2	40-48-42	73-47-00	20 July (3)
A5	40-53-54	73-41-30	20 July
B3	40-55-00	73-38-12	21 July (3)
BB	40-41-10 40-41-09 40-41-12	74-00-52 74-00-50 74-00-52	12 June (2) 12 June 16 July (3)
D3	40-59-12	73-24-12	19 July (2)
F3	41-02-48	73-09-00	17 July (3)
H4	41-06-00	72-56-18	19 July (3)
I2	41-08-09 41-08-17 41-08-24 41-08-11	72-39-55 72-39-34 72-39-24 72-39-39	12 June 12 June 19 July (2) 12 June
J2	41-10-44 41-10-48	72-27-54 72-27-42	12 June 19 July (2)
K3	41-12-00	72-15-24	19 July (3)
L1	41-12-48	72-06-54	18 July (3)
M4	41-12-00	72-03-54	18 July (3)
N3	41-13-36	71-51-36	18 July (2)
O2	41-06-23 41-00-40 41-06-12 41-06-23	71-43-04 71-42-40 71-43-04 71-43-03	11 June 18 July (2) 11 June 11 June
P2	41-15-17 41-15-24 41-15-22 41-15-22	71-34-14 71-34-12 71-34-29 71-34-32	11 June 18 July (3) 11 June 11 June

Table 5
SUNY C/T Mooring Station Summary

Station Number	Latitude N	Longitude W	Profile Dates (No. of Profiles)
E1	41-1.17	73-17.47	10 May, 25 June, 23 July, 07 Aug, 25 Sept,
G1	41-0.60	73-.20	10 May, 25 June, 07 Aug 25 Sept
A2M	40-52.32 40-48.07	73-44.05 73-47.05	25 June, 23 July (2), 07 Aug (2), 25 Sept (2), 10 May, 25 June
A4	40-52.32	73-44.05	25 June (2), 23 July 92), 07 Aug (2), 25 Sept (2), 10 May
B3M	40-55.2	73-38.68	10 May, 25 June(2), 23 July (2), 07 Aug (2), 25 Sept (2)
C2	40-59.15	73-30.03	10 May, 25 June (2), 23 July (2), 07 Aug (2), 25 Sept (2)
D3M	40-59.40	73-24.00	10 May, 25 June (2), 23 July (2), 07 Aug (2), 25 Sept(2)
F3M	41-01.20 41-01.40	73-08.40 73-08.80	25 June (2), 10 May, 23 July, 07 Aug (2), 25 Sept (2)
H6M	41-01.53	72-54.55	10 May, 25 June (2), 07 Aug (2), 25 Sept (2)

Extended Validation Simulations

Introduction

A period of 72 days starting May 9, 1990 was selected for additional validation of the NY Bight hydrodynamic model in Long Island Sound because time series of field data on surface elevations, currents, salinity, and temperature as well as limited measurements of vertical profiles of salinity and temperature, were available from NOAA and SUNY for this period. This period was used by NOAA for the short-term validation of its Long Island Sound hydrodynamic model (Wei 1991). NOAA also performed long-term simulations of the Long Island Sound hydrodynamics (Schmalz 1991). In the extended validation simulations described here, 10 sigma layers and a time-step of 2.5 min were used.

One of the problems encountered in the extended validation effort was concerned with the specification of boundary and initial conditions. NOAA was primarily interested in validating a model of Long Island Sound. As a result,

data for specifying initial and boundary conditions were collected for the Long Island Sound region only. Because the NY Bight model considers the entire NY Bight, including Long Island Sound, it is necessary to specify initial conditions over the entire NY Bight and boundary conditions at the boundaries of the NY Bight model. These initial and boundary conditions had to be estimated for the NY Bight model because there were no synoptic measurements available outside of Long Island Sound for the 72-day period.

Boundary conditions

The model was forced with tide, wind, river inflow, and density gradients. Offshore and lateral surface boundary conditions were obtained as follows. Referring to Figure 25, the surface elevation signal at station 1 was obtained by computing the tidal signal at Atlantic City using the same eight tidal constituents previously described. This signal was translated without change in amplitude or phase. Similarly, the surface elevation at station 4 was obtained by computing the tidal signal at Newport for the same eight constituents and advancing the phase by 5 min. The signals at stations 2 and 3 were both obtained by multiplying the amplitude of the signal at station 1 by 0.7 and advancing the phase by 15 min. This procedure is consistent with specification of the astronomical tide during calibration and verification of the model. The low-frequency (non-astronomical) component of the signal was not considered because it was impossible to estimate.

While information on winds was available at the JFK and LaGuardia Airports, it was not representative of wind conditions over the ocean. Fortunately, winds over water were available for the period under consideration from the U.S. Navy's Fleet Numerical Oceanographic Center. These data are specified at the 19.5-m elevation at a 2.5-deg spacing of latitude and longitude. These winds were in turn interpolated by the WIS to a 0.25-deg spacing for use in connection with wave hindcasting. In the present study, the WIS winds were obtained at 6-hr intervals for several representative locations around the NY Bight, including locations closest to stations 1 through 4 of Figure 25. They were examined, along with winds measured at the two airports, to understand the behavior of the winds over the region. On the basis of the examination, it was decided to average the WIS winds at stations 1 through 4 and use the average as a spatially uniform but time-varying input to the model. Stick plots of the average wind vectors are shown in Figure 61.

River flows play an important role in terms of circulation in Long Island Sound. Therefore, in addition to the Hudson River flow, the daily average discharges for the Norwalk, Housatonic, Quinnipiac, Connecticut, and Thames Rivers were obtained from the NOS and input to the model. These rivers represent over 90 percent of the freshwater flow into Long Island Sound. Because no field data were available for furnishing salinity conditions for May-July 1990 at the offshore and lateral boundaries of the model grid, salinity boundary conditions were obtained from the boundary conditions used for the May-August 1976 long-term simulation. Equilibrium temperature and heat

exchange coefficient values were obtained as before from meteorological data collected at the JFK Airport. They are shown in Figures 62-63. River temperature boundary values were obtained from "Water Resources Data for Connecticut for Water Year 1990" (U.S. Geological Survey 1991).

Initial conditions

Conditions outside Long Island Sound corresponding to May 9, 1976, were obtained from the long-term simulation and used for May 9, 1990. Conditions inside Long Island Sound were obtained from 1990 salinity and temperature gauge and profile measurements for May 9 or the time closest to that date following a procedure similar to that used for the long-term simulation. All values were first interpolated to specified horizontal planes, smoothed, then interpolated to sigma layers at individual grid cells. Care was taken to avoid sudden jumps in values near boundaries and between cells located on the periphery of Long Island Sound.

Discussion of Results

Surface elevations

NOAA gauge locations where comparisons are made are shown in Figure 52. Figures 64-67 show comparisons of computed and observed surface elevations at gauges exterior to Long Island Sound such as the Battery, New London, Fishers Island, and Point Judith, and Figures 68-70 show comparisons at gauges interior to Long Island Sound, such as Willets Point, Bridgeport, and Port Jefferson. It is important to note that the observed elevations represent the total measured signal, including all tidal constituents and low-frequency energy, whereas the computed elevations represent contributions due to the eight major tidal constituents only. Therefore, a source of difference between computed and observed elevations is the fact that the observed elevations contain the effect of low-frequency forcing.

Additional differences are due to a lack of adequate resolution in the computational grid. For example, standing waves are known to be present in the Sound; however, because of the coarse spatial discretization, the model may not have reproduced this hydrodynamic feature correctly. Overall, the agreement is excellent both with respect to range and phase. Because some of the gauges, such as Willets Point and New London, are located in the interior shallow areas, better agreement could not be obtained without an increase in resolution.

Currents

The locations of the RADS stations where current measurements were obtained are shown in Figure 56. At each station, measurements were taken at three vertical bins corresponding approximately to the upper, middle, and low-

er third of the water column. For convenience, the lower, middle, and upper bins were designated as layers 1, 2, and 3, respectively. To make computed and observed values comparable, both time series were filtered with a low-frequency filter with a cut-off period of 36 hr. In other words, contributions to the series from periods greater than 36 hr were removed. This retained most of the tidal contribution in the signal but removed contributions from low-frequency sources such as pressure fluctuations, shelf oscillations, etc. Because of the nonrecursive filtering process, 3 days (72 hours) of data at the beginning and end of the time series are eliminated from the final signal. In general, currents are more difficult to match than elevations. In this case, because of the complex shoreline geometry, as well as bathymetry of the Sound, the task of matching computed to observed currents was made more difficult and challenging.

Figures 71-76 show the velocity magnitudes and directions at RADS stations 1 and 10. Comparisons at stations 7 and 12 were not presented because the depths for these locations in the model were less than half those at the corresponding prototype measurement stations. This was partly due to the coarse grid used and partly due to the rapidly varying bathymetry at the gauge, e.g. station 12. The comparisons shown indicate that magnitudes are well-reproduced at both gauges and the directions agree well at station 10. The deviation in direction at station 1 is attributable to the fact that the computed direction is constrained by the model grid at this location. Agreement can be improved by using a finer grid.

Temperature time series

Locations of CT mooring stations are shown in Figure 56. At each CT mooring station, observations of temperature were collected at two levels. Comparisons between model results and observations were made at stations F3, I2, and P2. At station O2, model depth differed considerably from the prototype station depth, so comparisons are not presented for O2. To conserve space, comparisons for stations F3 and I2 only are presented in Figures 77-80. Note that prototype data for temperature and salinity were collected every 6 min but were plotted every hour, whereas model results were saved and plotted every 6 hr. This difference in sampling rate is evidenced as larger amplitude oscillations in the field data.

Model layers 2 and 6 corresponded to the lower and upper sensor locations, respectively. Following start-up transients, model results follow the trend of observations very well for the entire simulation at layer 2 of F3. At layer 6, they follow the same trend, with model temperatures being within 1-2 deg of observed. At I2, model results match observations well until approximately day 48, after which there is a deviation in the trend. The maximum deviation does not exceed 3 deg. At P2 (Appendix E), the observations exhibit large oscillations and are different in trend from computed results. Model temperatures are less than observed but within 2 to 4 deg. This underprediction may

be due to the highly dynamic nature of the flow at station P2. Overall, model results match prototype trends very well.

Salinity time series

Time series of salinity at stations I2 and P2 are shown in Figures 81-84. At both gauges, model results follow the trend of observations but are higher in value by 1-2 ppt. The agreement is better at station P2. At station F3 also (Appendix E), computed salinities match the trend of observations but are higher by 2-3 ppt. For all three gauges, the agreement is better at the higher level. The deviation of model results may be due to the following reason:

The river boundary condition in the model was originally designed to be taken at the head of tide (the farthest point up the river influenced by ocean tides and salinity). At this point, the salinity at the boundary is set to zero (implying freshwater inflow) during computation. However, in the case of the NY Bight application, it was impractical to specify the river boundary condition in this manner, because the head of tide is generally tens of miles upstream of the river mouth and therefore beyond the limits of the present computational grid. At the locations on the grid where the river boundary conditions were actually applied, the salinity was far from zero. During initial testing for the NY Bight application, the model tended to become unstable near river boundaries where salinities were specified as zero. To overcome the problem, the boundary condition was modified as follows. At each time-step, the salinity in the cell exterior to a river boundary cell was made equal to the salinity computed by the model for the river boundary cell. It is believed this may not have been completely realistic and may have resulted in computed salinities that were too high.

Ideally, the river boundary condition should reflect freshwater inflow, which produces lower salinity water flowing continuously into the model region. However, because of tidal influence near the river boundary, salinity is transported up the river during flood tide and lower salinity water is brought into the model region during ebb tide. Both of these effects will tend to decrease salinities in the model, especially in the region close to river boundaries. Because of time limitations in the present study, it was not possible to implement a more realistic river boundary condition. This improvement to the boundary condition should be considered in future modeling work.

Temperature profiles

Computed vertical profiles of temperature and salinity at the end of the simulation period were compared at a few locations with corresponding observed profiles. Figures 85-89 show the comparisons at stations B3M, E1, F3M, I2, and P2 (locations shown in Figure 56). These stations are distributed over the entire Long Island Sound. In the figures, squares correspond to observations and solid curves represent model results. The observed profiles at

the first three stations were profiles taken by SUNY and the profiles at the last two stations were taken by NOS. Where there was a choice, as in the case of the SUNY profiles, downcast profiles were selected for comparison, because they are more representative of actual conditions at the sensor depth[1]. In the case of the first three stations, model results at the end of the simulation (July 20) are presented whereas for the last two stations, model results corresponding to observation dates were used.

Generally, the computed profiles follow the shape of the measured profiles except near the free surface. Overall, model temperatures are lower than observed and the deviation is within 3 deg C. The agreement is considered good and the deviation is within acceptable limits for the following reasons. Model results are representative of daily-averaged values over a grid cell whereas field profiles represent values at a specific location at the particular time they were taken, usually during the daylight hours. In the month of July, diurnal variation in temperature may be on the order of 3 to 5 deg C, as indicated by the time series measurements.

Salinity profiles

At all the gauges, computed and measured profiles are similar in shape. The agreement is excellent at P2. The similarity in trends is well reproduced at stations B3M, F3M, and I2. Model salinities are generally higher than observed and the deviation is within 2-3 ppt. As before, the deviation may be explained in terms of the river boundary condition.

East River net flow

The East River forms a vital hydrodynamic connection between the Long Island Sound and the Outer Bight/NY Harbor. As a part of the extended verification of the NY Bight model, it was considered essential to examine the long-term average net flow in the East River connection. Estimates of the net flow were available from a study conducted by HydroQual (HydroQual 1991). Over a 100-day period (May 15-August 24, 1989), field data taken at the South Clason section (Figure 90) indicated a net flux of -380 m^3/sec whereas HydroQual's 3-D hydrodynamic model of the East River[2] estimated about -320 m^3/sec, with the negative sign indicating the net flow is directed from the Long Island Sound toward the NY Harbor.

---

[1]Personal Communication, 24 November 1991, D.W. Pritchard, Professor Emeritus, State University of New York at Stony Brook, Severna Park, MD.

[2]Personal Communication, 14 September 1993, A.F. Blumberg, Senior Scientist, HydroQual, Inc., Mahwah, NJ.

Over the short term, the net flow exhibits much variability. According to Pritchard[1], these long-term estimates can not be in error by more than a factor of two. In the present study, as a part of the extended validation effort, the net flux through the East River, averaged over 72 days, was computed. The magnitude of the net flux was about 717 m^3/sec, directed toward the NY Harbor. Thus the model predicts the direction of the net flux correctly. Even though the computed magnitude appears to be on the high side, it is still within a factor of two from the estimate from the 100-day field data. In summary, the NY Bight hydrodynamic model has been shown to represent the East River hydrodynamic connection correctly, in regards to both the magnitude and direction of the net flow.

Conclusions from the Long Island Sound Validation

The NY Bight model reproduced observed surface elevations and currents in Long Island Sound reasonably well. Deviations are attributable to coarseness of model grid resolution in the Long Island Sound and uncertainty in the boundary conditions imposed on the model. Computed time series and profiles of temperature and salinity also matched prototype trends and values to reasonable degree. The salinity comparison may be improved by modifying the river boundary condition. Computed magnitude and direction of net flow in the East River agree with reported values. In summary, the NY Bight hydrodynamic model has been shown to be capable of acceptably reproducing the hydrodynamics of Long Island Sound and the East River connection to the NY Harbor.

[1]Personal Communication, 24 November 1991, D.W. Pritchard, Professor Emeritus, State University of New York, at Stony Brook, Severna Park, MD.

7 Hydrodynamic Monitoring Program

Purpose of Monitoring

The NY Bight is a highly complex hydrodynamic system. Although the flow regime is influenced by surface wind forcing and river inflow, it is primarily controlled by the changing water surface elevation and vertical distribution of temperature, and salinity at the boundaries as well as the initial vertical distribution of temperature and salinity throughout the domain. In order to numerically reproduce the hydrodynamics of the NY Bight, Long Island Sound, and the regions within the NY Harbor, these boundary forcings and initial conditions must be known.

The modeling effort described in this report utilized available prototype data as the basis for specifying initial and boundary conditions. However, there were no time periods during which all necessary data were available. In the tidal calibration and verification phases described in Chapter 4, density effects resulting from salinity or temperature were not considered. Even in this simple case, the water surface elevation time series at the outer computational boundary were not known but had to be deduced from measured gauge data on shore stations, i.e., Atlantic City, NJ, and Newport, RI.

Results of the data analysis showed the presence of low-frequency energy with a period on the order of several days. This non-astronomical component was included in the simulations by specifying it as a boundary condition on the outer computational boundary. The procedure used to define the low-frequency component of the elevation time series at the outer boundary was detailed in the "Boundary Condition Selection" section of Chapter 4. This approach was successful in achieving verification to water surface elevations at shore stations; however, it was only marginally successful for verification of current measurements. In some cases, model-to-prototype data comparisons of the low-frequency events were well matched, in other cases they were not. This apparent inconsistency was due to the fact that the phasing of the low-frequency component was not known, i.e., from what direction is the low-frequency component propagating? If low-frequency modulation of the tidal

signal has residual effects which may impact long-term water quality or particle tracking studies, then the low-frequency component at the model boundary must be known. This lack of data represented one shortcoming of the present study. Prototype data corresponding to the model offshore boundary locations would help to improve model-to-prototype comparisons.

When the flow regime becomes more complex and density effects have to be considered, the lack of proper boundary conditions becomes even more acute. In the long-term simulations described in Chapter 5, it was necessary to model both temperature and salinity because these two variables define the water density via an equation of state (Equations 7 and 8). The calculation of temperature and salinity also requires specification of an initial condition over the entire computational domain. A vertical distribution time series of temperature and salinity on the outer computational boundary is then used to compute temporal variations in temperature, salinity, density, and velocity throughout the modeled domain. If these initial and boundary conditions are not estimated properly, incorrect densities are computed, which result in the computations of unrealistic density-driven currents. The proper simulation of these currents can be seen to be critical to computing accurate seasonal water quality effects.

This study made use of the MESA cruise data consisting of periodic measurements of vertical temperature and salinity profiles at many locations throughout the NY Bight. Although these data were somewhat sparse, they were used to develop initial conditions and estimates of depth versus temperature/salinity relationships at the boundary for each month of April through October 1976. These monthly estimated conditions were used to develop input boundary conditions required to run the HM and reproduce hydrodynamics and associated temperature, salinity, and density for the April through October 1976 time period. The computed flow field was then input to the water quality model, resulting in a reasonable verification of the summer 1976 hypoxia event.

Because this hypoxia simulation was the primary goal of the water quality demonstration effort, a considerable amount of time was expended in developing a proper hydrodynamic flow field. For example, many sensitivity studies were required to develop realistic initial and boundary conditions such that acceptable long-term current, temperature, and salinity comparisons could be made (see "Discussion of Results" in Chapter 5).

If real-time predictions of future events are to be made or impending impacts to the NY Bight are to be modeled, then existing conditions must be known to a higher degree of certainty than was available to this study. If these initial and boundary conditions are not known, reliable estimates of certain types of long-term or residual impact may not be possible. This fact can be amply demonstrated by the calibration/verification and long-term simulation efforts documented in this report. Therefore, based on experience gained through the present numerical investigation of the hydrodynamic response of the NY Bight system, it is recommended that a prototype data monitoring program be initiated.

Several levels of prototype data monitoring can be used in a comprehensive program, each with options as to the number and location of gauges. Some of these choices are critical to a well-planned monitoring program and others are not. The following section describes the types of monitoring, and associated degrees of commitment, which can be used to provide input to the combined hydrodynamic/water quality modeling effort in the NY Bight.

Prototype Measurement Deployment Options

Three levels of prototype measurement are recommended to support a maximum usage of the hydrodynamic/environmental models of the NY Bight. These levels include long-term (on the order of years) continuous operation of gauges, short-term (weeks to months) continuous recording, and long-term spot measurement (with a period on the order of 20 days for a year(s)). The following sections discuss each monitoring option.

Long-term continuous monitoring

The highest priority measurements, and the most costly to install and maintain in terms of equipment, are those needed to quantify the time change in water surface elevation, temperature, surface wind speed, barometric pressure, and vertical profiles of currents, temperature, and salinity at prototype locations approximating the offshore computational boundary. Data should be measured every 1- 2 hr. These prototype monitoring stations should be long-term, continuous recording stations. Their primary use would be to document seasonal changes and to provide a historical record of offshore hydrodynamics and atmospheric data for use in either reproducing past events as a means of investigating the effects of proposed containment islands, disposal sites, etc.; or to furnish initial and boundary conditions for the model to forecast the effect of proposed near-term environmental scenarios on the NY Bight system.

In reference to the grid shown on Figure 91, long-term stations should be positioned at locations M1, M2, M3, and M4. Meteorological data would only be necessary at locations M1 and M2. The offshore gauges M1 and M2 are of the highest priority because they represent conditions on the outer computational boundary, i.e., the continental shelf. The stations are selected to coincide with the boundary control points shown in Figure 25. If gauges at these locations are not feasible due to the extreme depths, they could be located in shallower water at alternate locations M1A and M2A.

As was noted in the previous section, the lack of data at these offshore locations resulted in a lack of ability to achieve consistent model-to-prototype velocity comparisons for the low-frequency phenomena as well as an inability to reproduce temperature and salinity magnitudes at all monitoring gauges

(however, temperature and salinity trends were well-reproduced). Data at locations M1 (M1A) and M2 (M2A) would eliminate many of these difficulties.

It was noted in Chapter 4 (Hopkins and Dieterle 1987) that a typical summer (August 1978) steady-state head differential of 2 cm exists between the northeast and southwest nearshore boundaries of the NY Bight with a corresponding zero elevation difference along the shelf break. This gradient leads to a conclusion that circulation is generally parallel to the contours of the continental shelf and directed from northeast to southwest. However, it has been noted that velocities within the Hudson Canyon are, on the average, directed toward the apex of the NY Bight and nearshore current reversals along the New Jersey shore north of the entrance to Delaware Bay, and easterly flows along Long Island have been observed to generate large-scale circulation cells.

The above generalizations represent long-term average circulation patterns. Variations about these averages can be substantial. Actual circulation is a (partial) function of wind forcing and surface gradients (of which the low-frequency surface elevation variations can be a significant contributor). As was shown in the hydrodynamic/water quality model verification to the summer 1976 hypoxia event, the circulation was generally from southwest to northeast, opposite to what is assumed normal. This flow was forced in part by persistent winds from the southwest.

The placement of long-term gauges at locations M3 and M4 would quantify the on-off shelf and along-shelf surface slope and the resulting large-scale circulation pattern. Gauges at these locations would be considerably less expensive to install and maintain than would gauges at M1 and M2. Additionally, they would complement the M1 and M2 gauges to provide a comprehensive data set that would quantify boundary conditions in the NY Bight and provide a complete base condition for numerical studies.

Finally, long-term gauges placed at M5 and M6 would provide verification of proper flow through the NY Bight transect and East River connection between the NY Harbor and Long Island Sound. Because these gauges are primarily for verification purposes, they are of somewhat lower priority. As such, they could be included under short-term gauges in the following section.

In addition to providing boundary conditions at exterior boundaries (M1 - M4), it is necessary to document the hydrodynamics at interior boundaries. A minimum gauge deployment for the present model would include flow and elevation data in the Hudson River and in the Kills. If a high resolution grid is developed for future studies, stream gauges must be located on all major tributaries. Because many streamflow and tidal data are routinely collected by various agencies, a concerted level of coordination will be made to gain maximum use of existing data.

Short-term continuous monitoring

The second hierarchy of gauges are short-term continuously recording gauges installed to support site-specific studies requiring a high resolution inset computational grid. These monitoring stations would provide short-term hydrodynamic data for developing and verifying the linkages of the present NY Bight model to a high-resolution NY Harbor/Apex model. Monitoring stations are required at locations common to both grids to assure that boundary conditions generated by the NY Bight model are proper. Other locations are required to provide model validation data at strategic locations. Key positions would be in areas such as the transect of the apex, East River, the Battery, the Hudson River, Arthur Kill, Newark Bay, and Kill Van Kull and the western portion of Long Island Sound. A total of 7-10 measurement stations would be required for this effort. Some of the initial verifications deployments could be relocated to support site-specific studies.

The short-term gauges would be deployed for periods of time on the order of several weeks to several months with a sampling rate on the order of 0.5-2 hr. In addition to hydrodynamic data (surface elevations, velocities, salinity, and temperature), environmental data to support the water quality model should be collected in conjunction with the hydrodynamic data.

Long-term spot monitoring

Long-term spot measurement stations should be placed to provide key location information on long-term changes in environmental-related parameters. For example, the seasonal variations in salinity and temperature profiles over a yearly cycle could be documented as a part of a continuous monitoring program. These data should include the transect of the NY Bight, axis of Long Island Sound, the East and Hudson Rivers, Raritan Bay, and locations in the NY Bight. Long-term spot measurement stations should be located to coincide with long-term continuous stations M3, M4, M5, and M6 in order to provide continuity between the two time-scale measurement sampling locations. Because the long-term spot monitoring program is primarily aimed at long-term changes in environmental parameters, details are included in the environmental modeling report.

Sample monitoring program

In this section, a sample long-term and short-term continuous monitoring program is described. Included in the examples are the expected number of gauges at each location.

The minimum long-term continuous monitoring configuration would be the placement of a vertical array of gauges at locations M1 and M2 (placement of instruments at M3 and M4 would be highly desirable) shown in Figure 91.

Each array should be attached to a buoy, which measures surface conditions such as temperature, wind velocity, barometric pressure, and water surface elevation (at tidal frequencies). The vertical array of instruments should include a minimum of three instrument packages corresponding to near surface, mid-depth, and near bottom. Required measurements include velocity and direction, salinity, and water temperature. It would be advisable to establish two verification stations at M5 and M6. These data would provide a confidence check on model results. Table 6 presents a summary of long-term gauge components and associated costs for a 2-year deployment. In the table, *El* is surface elevation (at tidal frequencies), *Ts* is surface temperature, *P* is barometric pressure, *W* is surface wind speed, *V* is water velocity and direction, *S* is salinity (conductivity), and *T* is water temperature. Planning of this proposed monitoring program will require approximately 6 months. The approximate cost range for deployment is $1-1.5 million and includes planning, equipment purchases, instrument installation and retrieval, periodic maintenance, data processing, and preparation of a data report.

Table 6
Summary of Long-term Gauge Deployment

Station Location	Surface	Surface, Mid-depth, Bottom
M1	El, Ts, P, W	V, S, T
M2	El, Ts, P, W	V, S, T
M3	El, Ts, P, W	V, S, T
M4	El, Ts, P, W	V, S, T,
M5	El, Ts, P, W	V, S, T,
M6	El, Ts, P, W	V, S, T,

In order to present an example short-term continuous monitoring program, it is necessary to assume some specific project which the monitoring effort is intended to support. Assume that the area of interest is circulation in Kill Van Kull. A study of this nature would require multiple gauge string locations across the waterway, to include the shallow areas as well as the dredged channel. This type of study would require application of a high-resolution grid. Therefore, in order to verify the inset grid, data would be required at the east and west end of Kill Van Kull, Newark Bay, and Arthur Kill.

In addition to high-resolution grid monitoring stations, locations common to both grids are required to assure that the bight model-generated boundary conditions are correct. Because the high resolution grid contains river input, additional interior gauge locations will be necessary to quantify initial and boundary conditions. Many of these data are available and can be obtained at a nominal cost. Table 7 presents a summary of short-term gauge components and associated costs for a 2-month deployment.

Table 7
Summary of Short-term Gauge Deployment

Station	Surface	Measurement	No. Across/Vert Location
Kill Van Kull - East	El	V, S, T	1/3(sur,mid,bot)
Kill Van Kull - West	El	V, S, T	1/3(sur,mid,bot)
Newark Bay (central)	El	V, S, T	1/3(sur,mid,bot)
Arthur Kill - North	El	V, S, T	1/3(sur,mid,bot)
Raritan Bay/ Arthur Kill	El	V, S, T	1/3(sur,mid,bot)
Bight Apex	El	V, S, T	3/3(sur,mid,bot)
Hackensack River	El	V, S	1/1(mid)
Passaic River	El	V, S	1/1(mid)
Hudson River	El	V, S	1/3(sur,mid,bot)
The Narrows	El	V, S	1/3(sur,mid,bot)

The cost of the above monitoring plan would be on the order of $1 million and would require approximately 6 to 12 months to formulate and finalize.

8 Conclusions and Recommendations

Conclusions

It is concluded on the basis of this study that the hydrodynamic model CH3D-WES does an excellent job of reproducing the hydrodynamics of the coupled NY Bight, NY Harbor, and Long Island Sound system. This conclusion is based on the following:

a. The model was demonstrated to satisfactorily reproduce quantitative as well as qualitative circulation patterns over the entire NY Bight. Known areas of recirculation southwest of the apex were predicted by the model. These steady-state patterns were due to imposed steady-state surface gradients, wind forcing, and river inflow.

b. The model was shown to successfully reproduce tidal propagation as well as tidally induced circulation. Excellent reproduction of surface elevations was achieved at all comparison stations and very acceptable reproduction of currents was achieved. It was noted that low-frequency energy, observable as oscillations (on the order of days) in elevation and current time series, was present in the system. This energy is not of astronomical origin. This low-frequency phenomenon is common to all systems along the east coast of the United States. Because the precise origins of these fluctuations are unknown, the boundary conditions necessary to reproduce them are unknown.

c. Long-term simulations for the period of 1 April to 1 October 1976 were made in order to generate hydrodynamic forcing data for the environmental model. During this long-term verification, the model was shown to be capable of acceptably reproducing not only surface elevations and currents, but also salinities and temperatures. Although initial and boundary conditions for salinity and temperature had to be based on extrapolations and interpolations of existing data, spatial and temporal trends as well as magnitudes were acceptably reproduced by the model.

d. An extended validation of the model was made to the Long Island Sound. This extended effort was intended to demonstrate that the model is capable of reproducing flow and circulation in the Long Island Sound as well as the East River hydrodynamic connection between NY Harbor and the NY Bight and Long Island Sound. Although it was recognized at the outset that the model did not have adequate spatial resolution in the Long Island Sound to reproduce small-scale circulation features, results did demonstrate a quantitative reproduction of hydrodynamics and temperature/salinity. These results were obtained with incomplete boundary/initial conditions. The acceptable reproduction of these quantities, in spite of the lack of complete boundary and initial conditions, demonstrated the accuracy and versatility of the model.

In view of the above comparisons, it was concluded that the model is capable of reproducing all major hydrodynamic features of the NY Bight, NY Harbor, East River, and Long Island Sound flow regime. Problem areas in which a less than acceptable match of model-to-prototype data was achieved are generally explainable in terms of improperly posed boundary/initial conditions and/or lack of resolution in the computational grid to capture small-scale flow features. These two sources of error can, to some degree, be improved upon. The following describes actions that will produce a more accurate and flexible numerical modeling capability.

Recommendations

The sources of error introduced into model results are due to: (a) lack of grid resolution in some modeled areas, and (b) lack of prototype data for comparison with model results and for specification of initial and boundary conditions. Recommendations for future studies therefore address these two issues. The following are recommended:

a. Development of a fine-resolution grid. This would include the areas of the Long Island Sound and East River as in the present model, but would substantially increase the spatial resolution. In addition to the areas presently modeled, the high-resolution model would include Jamaica Bay, Raritan Bay, Arthur Kill, Newark Bay, Kill Van Kull, and the Hackensack, Passaic, and Hudson Rivers to the head of tide.

b. Extension of the existing HM grid to the head of tide of the Hackensack, Passaic, and Hudson rivers. This feature is necessary to provide proper river boundary conditions for the high resolution model because many water quality parameters are strongly influenced by temperature and salinity. The only acceptable approach to accurately simulating temperature and salinity is to model the tributaries to a point beyond the effect of the tide, i.e., beyond the head of tide.

c. Developmeant and implementation of a data collection and monitoring program. The program would collect three types of data: long-term continuous, short-term continuous, and long-term spot measurements. The long-term continuous data would provide hydrodynamic boundary conditions for the outer boundaries of the computational grid, i.e., on the continental shelf and lateral model boundaries. Parameters of interest include all necessary hydrodynamic data, temperature and salinity data, and wind and pressure data. Short-term continuous data would support coupling/verification of the NY Bight model and the recommended fine-resolution grid. Finally, a long-term spot measurement program aimed at documenting multi-year and seasonal variations in environmentally related parameters such as temperature and salinity is recommended for long-term modeling efforts.

The above recommendations, when implemented, would provide the New York District with a modeling capability for highly accurate hydrodynamic and environmental simulations of the NY Bight.

References

Beardsley, R. C., and Boicourt, W. C. (1981). "On estuarine and continental-shelf circulation in the Middle Atlantic Bight." *Evolution of physical oceanography*. B.A. Warren and C. Wunsch, eds., MIT Press, Cambridge, MA, 198-233.

Blumberg, A. F., and Mellor, G. L. (1987). "A description of a three-dimensional coastal ocean circulation model." *Three-dimensional coastal models, coastal and estuarine sciences 4*. N. S. Heaps, ed., American Geophysical Union, 1-16.

Blumberg, A. F., Galperin, B., Oey, L.-Y., Wu, K. B., Grehl, B. J., and Dodge, L. J. (1988). "Analysis of circulation in New York Bight." *Assessment of pollutant fate in New York Bight*. Technical Report by HydroQual, Inc. to Dynamic Corp. and EPA Region II, New York Bight Restoration Study, Mahwah, NJ.

Bumpus, D. F. (1973). "A description of the circulation on the continental shelf of the east coast of the United States," *Prog. Oceanography* 6, 111-157.

Cialone, M. A. (1991). "Coastal Modeling System (CMS) user's manual," Instruction Report CERC-91-1, U.S. Army Engineer Waterways Experiment Station, Vicksburg, MS, B-2 - B-10.

Donaldson, C. (1973). "Atmospheric turbulence and the dispersal of atmospheric pollutants." *AMS workshop on micrometeorology*. D. A. Haugen, ed., Science Press, Boston, 313-90.

Earwaker, K. L., ed. (1990). "Long Island Sound oceanography project: 1988 - 1990," NOS Oceanographic Circulation Survey Report No. 10, National Oceanic and Atmospheric Administration, U.S. Department of Commerce.

Edinger, J. E., Brady, D. K., and Geyer, J. C. (1974). "Heat exchange and transport in the environment," Report 14, EPRI Publication No. 74-049-00-3, prepared for Electric Power Research Institute, Palo Alto, CA.

Garratt, J. R. (1977). "Review of drag coefficients over oceans and continents," *Monthly Weather Review* 105, 915-29.

Hopkins, T. S., and Dieterle, D. A. (1983). "An externally forced barotropic circulation model for the New York Bight," *Continental Shelf Research* 2, 49-73.

_____. (1987). "Analysis of the baroclinic circulation of the New York Bight with a 3D diagnostic model," *Continental Shelf Research*, 237-65.

HydroQual, Inc. (1991). "The transport through the East River from data and three dimensional hydrodynamic modeling," Report NENG0013, prepared for the Management Committee of the Long Island Sound Study and New England Interstate Water Pollution Control Commission.

Johnson, B. H. (1980). "VAHM - a vertically averaged hydrodynamic model using boundary-fitted coordinates," Miscellaneous Paper HL-80-3, U.S. Army Engineer Waterways Experiment Station, Vicksburg, MS.

Johnson, B. H., Kim, K. W., Heath, R. E., and Butler, H. L. (1991). "Verification of a three-dimensional numerical hydrodynamic model of Chesapeake Bay," Technical Report HL-91-7, U.S. Army Engineer Waterways Experiment Station, Vicksburg, MS.

Leendertse, J. J., Alexander, R. C., and Liu, S.-K., (1973). "A three-dimensional model for estuaries and coastal seas," *Principles of computation*, Vol 1, R-1417-OWRR, Rand Corporation, Santa Monica, CA.

Leonard, B. P. (1979). "A stable and accurate convective modeling procedure based on upstream interpolation," *Computer Methods in Applied Mechanics and Engineering* 19, 59-98.

Lewellen, W.S., (1977). "Use of invariant modeling." *Handbook of turbulence.* W. Frost, ed., Plenum Publishing Corp., 1, 237-80.

Mayer, D.A., Hansen, D.V., and Minton, S.M. (1979) "Chapter 7, water movement on the New Jersey Shelf, 1975 and 1976, " Oxygen depletion and associated benthic mortalities in New York Bight, 1976. R.L. Swanson and C.J. Sindermann, eds. NOAA Professional Paper 11, National Oceanic Atmospheric Administration, U.S. Department of Commerce.

Moody, J. A., Beardsley, R. C., Brown, W. S., Daifuku, P., Irish, J. D., Mayer, D. A., Mofjeld, H. O., Petrie, B., Ramp, S., Smith, P., and Wright, W. P. (1984). "Atlas of tidal elevation and current observations on the northeast American continental shelf and slope," Bulletin 1611, U.S. Geological Survey.

Oey, L.-Y., Mellor, G. L., and Hires, R. I. (1985a). "Tidal modeling of the Hudson-Raritan Estuary," *Estuarine, Coastal, and Shelf Science* 20, 511-27.

_____. (1985b). "A three-dimensional simulation of the Hudson-Raritan Estuary; Part I, Description of the model and model simulation," *Journal of Physical Oceanography* 15, 1676-92.

Oey, L.-Y., Mellor, G. L., and Hires, R. I. (1985c). "A three-dimensional simulation of the Hudson-Raritan Estuary; Part II, Comparison with observations" *Journal of Physical Oceanography* 15, 1693-1707.

_____. 1985d. "A three-dimensional simulation of the Hudson-Raritan Estuary; Part III, Salt flux analysis," *Journal of Physical Oceanography* 15, 1711-20.

Saunders, P. M. (1977). "Wind stress on the ocean over the eastern continental shelf of North America," *Journal of Physical Oceanography* 7, 555-66.

Schmalz, R. A., Jr. (1991). "Simulation of three-dimensional hydrodynamics in Long Island Sound : Annual timescales." *Proceedings of the Second International Conference on Estuarine and Coastal Modeling*. American Society of Civil Engineers Tampa, FL, 441-52.

Schwiderski, E. W., (1979). "Global ocean tides; Part II: The semidiurnal principal lunar tide (M2), atlas of tidal charts and maps," NSWC TR 79-414, Naval Surface Weapons Center, Dahlgren, VA.

Schwiderski, E. W., and Szeto, L. T. (1981). "The NSWC global ocean tide data tape (GDTD), its features and application, random-point tide program," NSWC TR 81-254, Naval Surface Weapons Center, Dahlgren, VA.

Sheng, Y. P. (1982). "Hydraulic applications of a second-order closure model of turbulent transport." *Applying research to hydraulic practice*. P. Smith, ed., American Society of Civil Engineering, 106-19.

_____. (1986). "A three-dimensional mathematical model of coastal, estuarine and lake currents using boundary fitted grid," Report No. 585, A.R.A.P. Group of Titan Systems, Princeton, NJ, 22.

_____. (1990). "A simplified second order closure model of turbulent transport," unpublished paper prepared for the U.S. Army Engineer Waterways Experiment Station, Vicksburg, MS.

Stoddard, A., and Han, G.C. (1990). "Hydrodynamic and water quality data compilation for the New York Bight: Phase II," draft report prepared for Evans-Hamilton, Inc, Houston, TX.

U.S. Geological Survey (1991). "Water resources data Connecticut Water Year 1990," U.S. Geological Survey Water-Data Report CT-90-1 (prepared in cooperation with State of Connecticut and with other agencies).

Wei, E. J. (1991). "Simulation of three-dimensional hydrodynamics in Long Island Sound : Seasonal timescale." *Proceedings of the Second International Conference on Estuarine and Coastal Modeling*. American Society of Civil Engineers, Tampa, FL, 430-40.

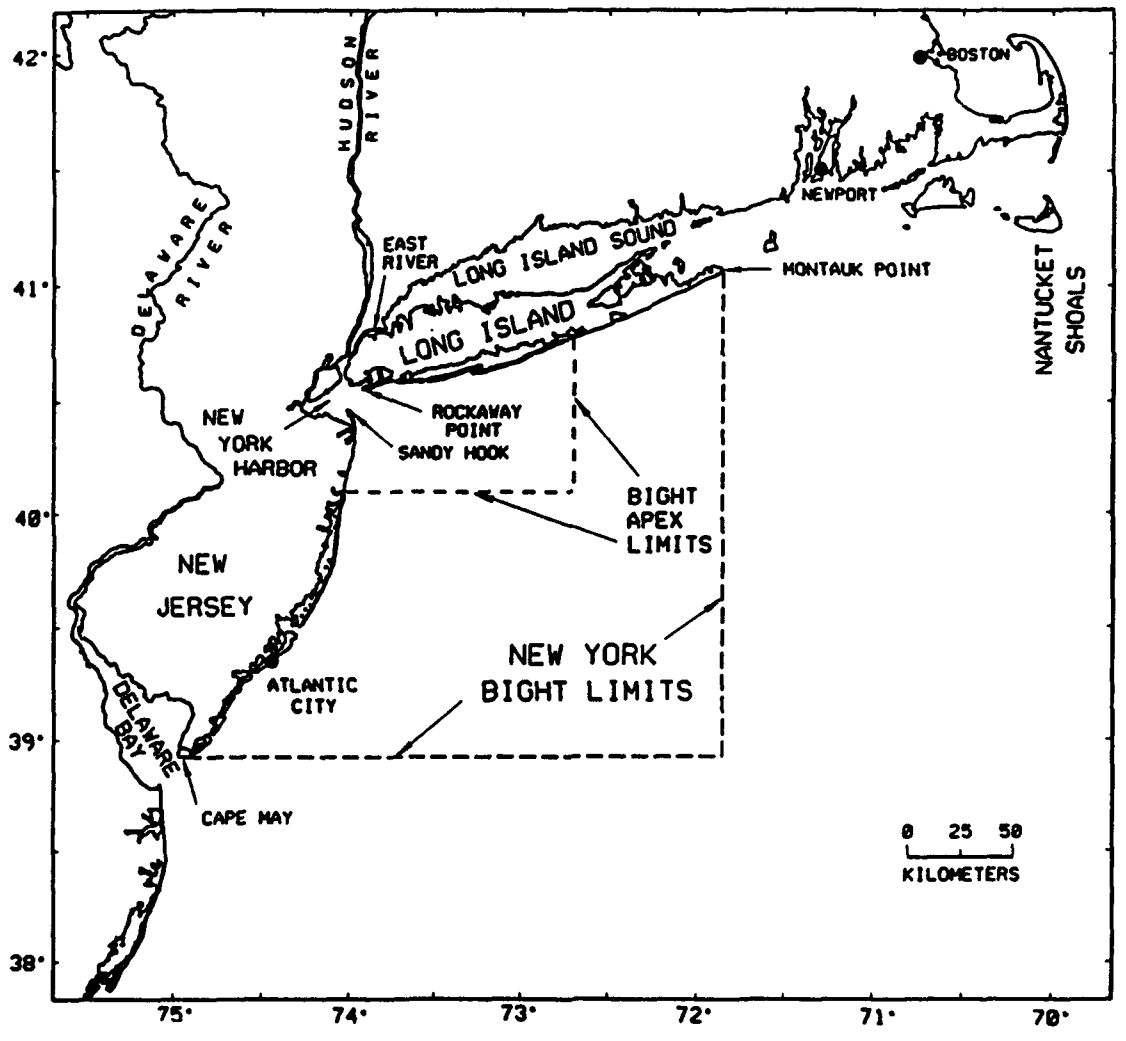

Figure 1. The New York Bight

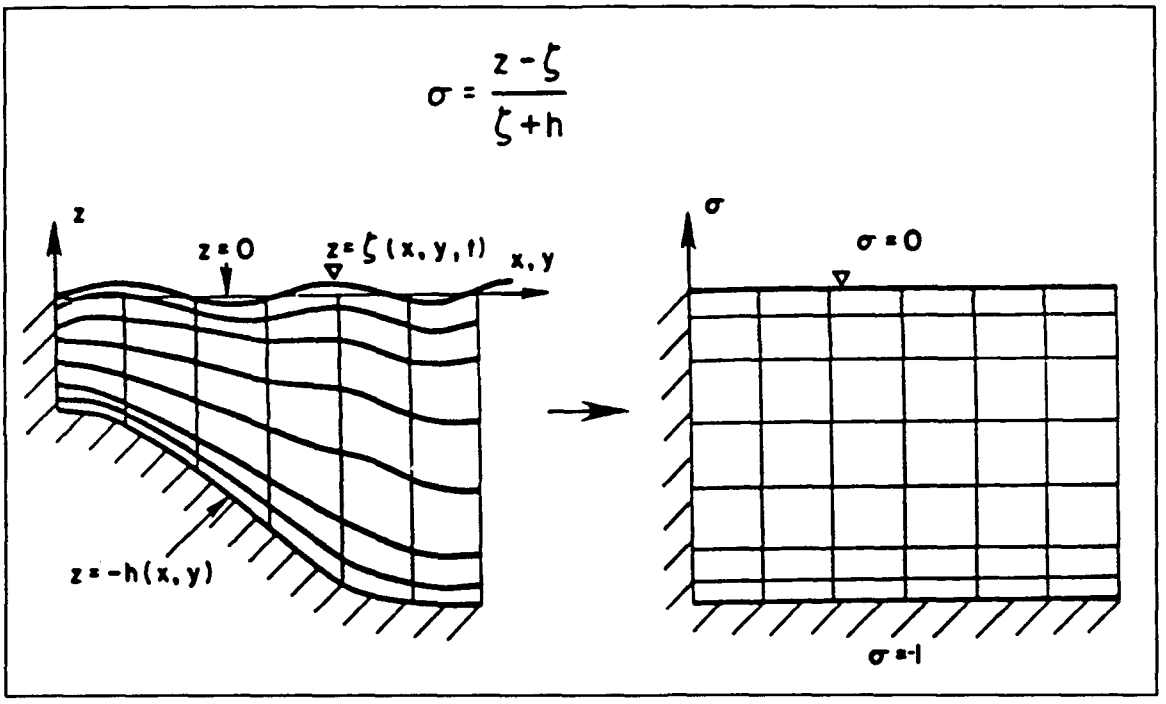

Figure 2. Sigma-stretched grid

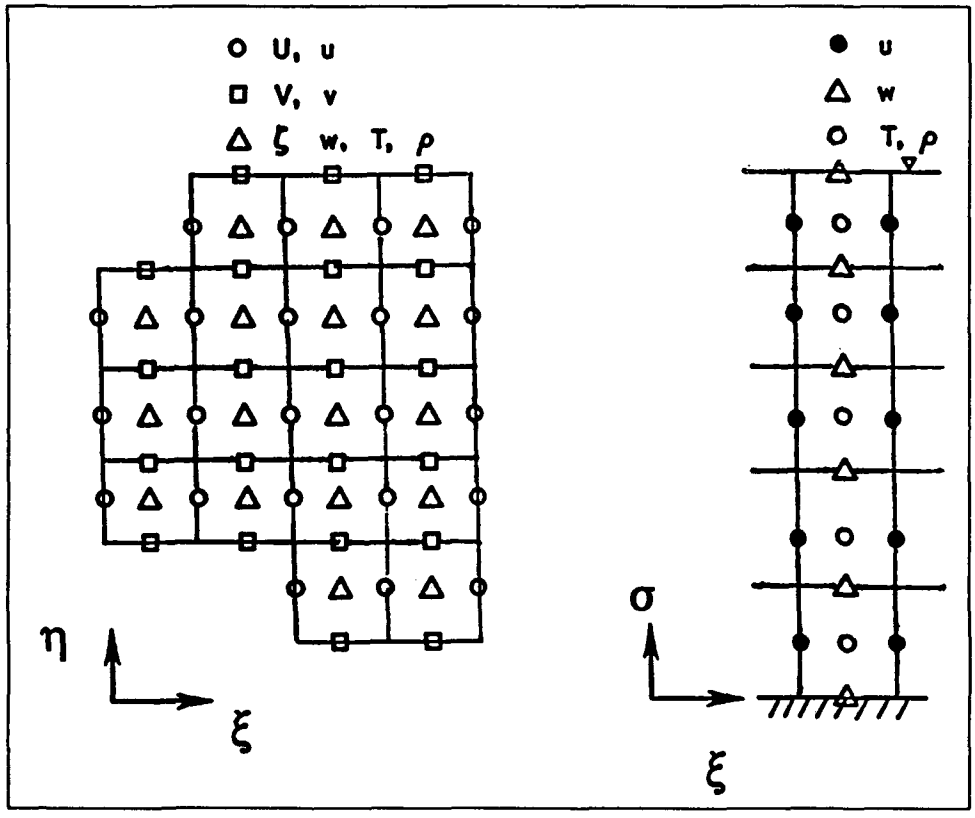

Figure 3. Staggered numerical grid

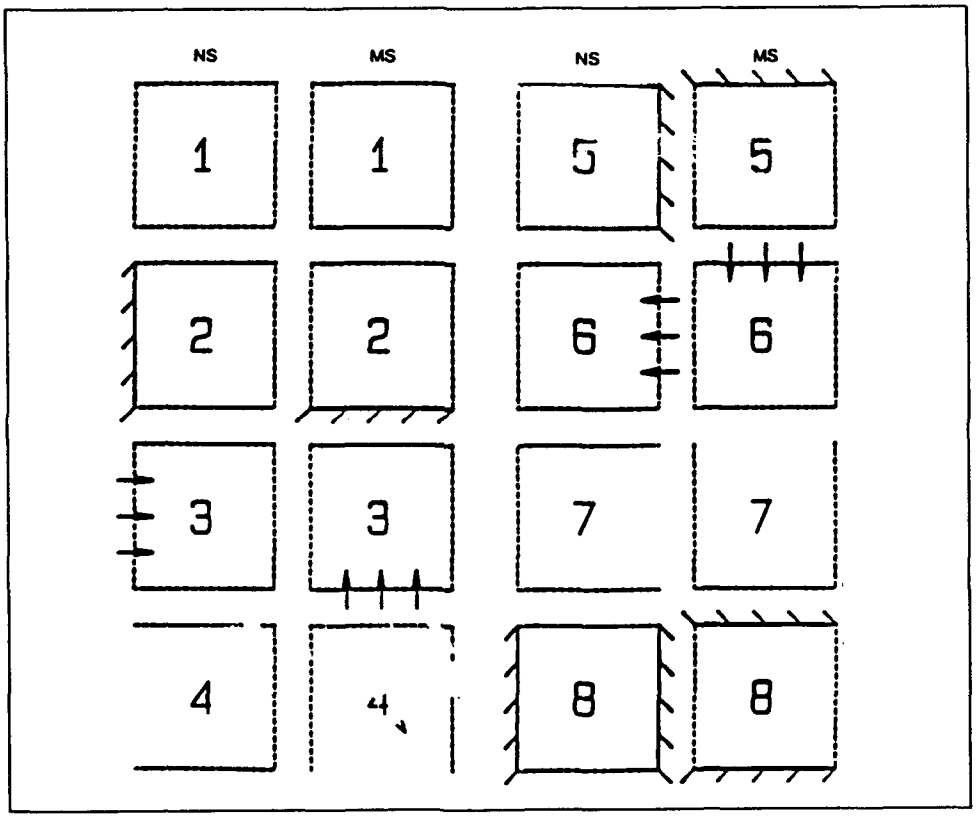

Figure 4. Computational arrays

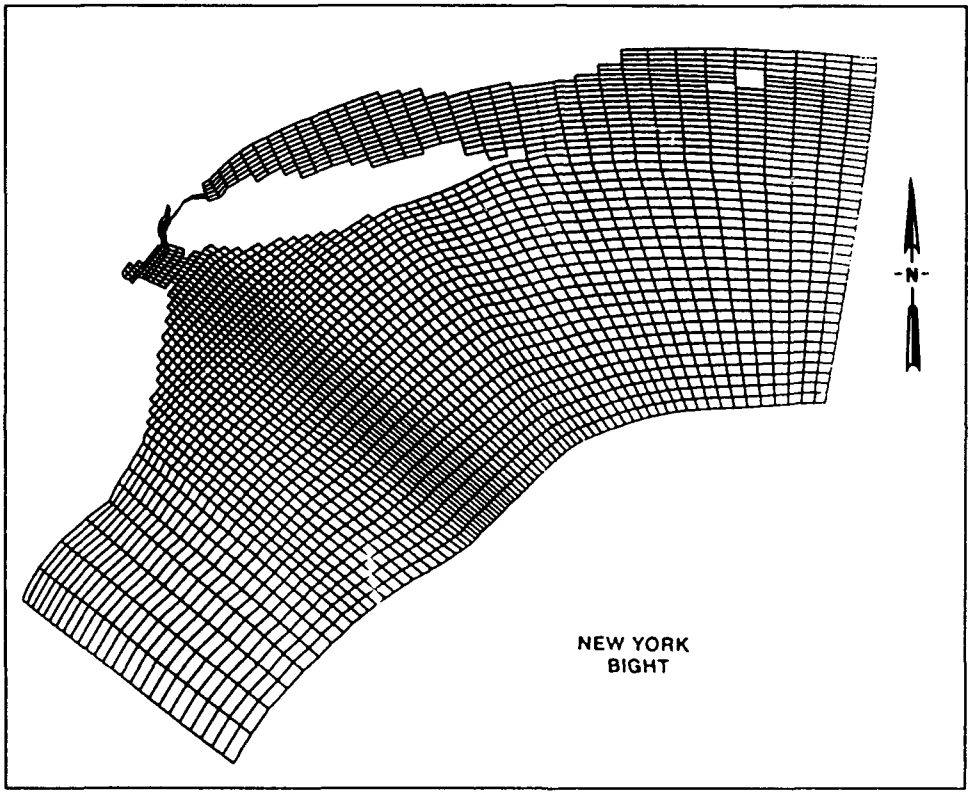

Figure 5. New York Bight computation grid

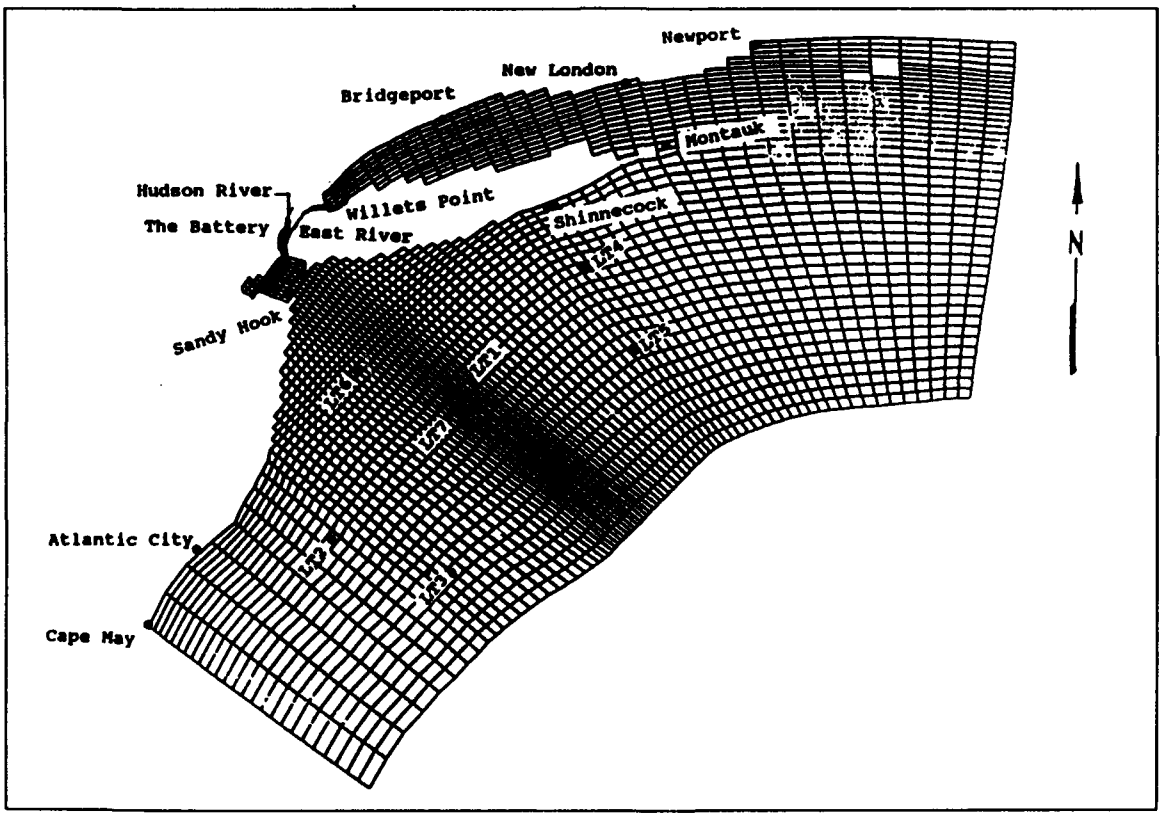

Figure 6. Prototype data locations

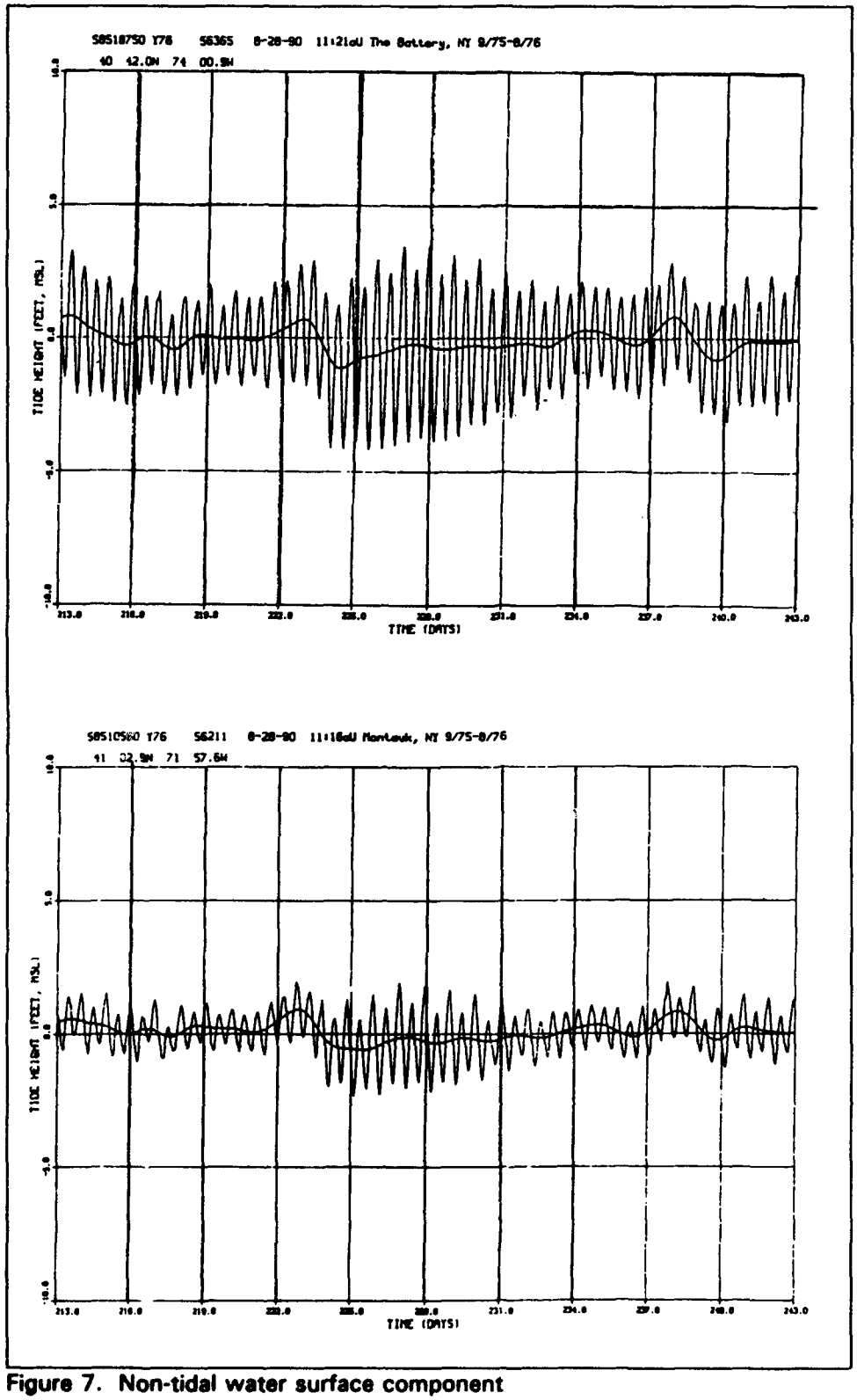

Figure 7. Non-tidal water surface component

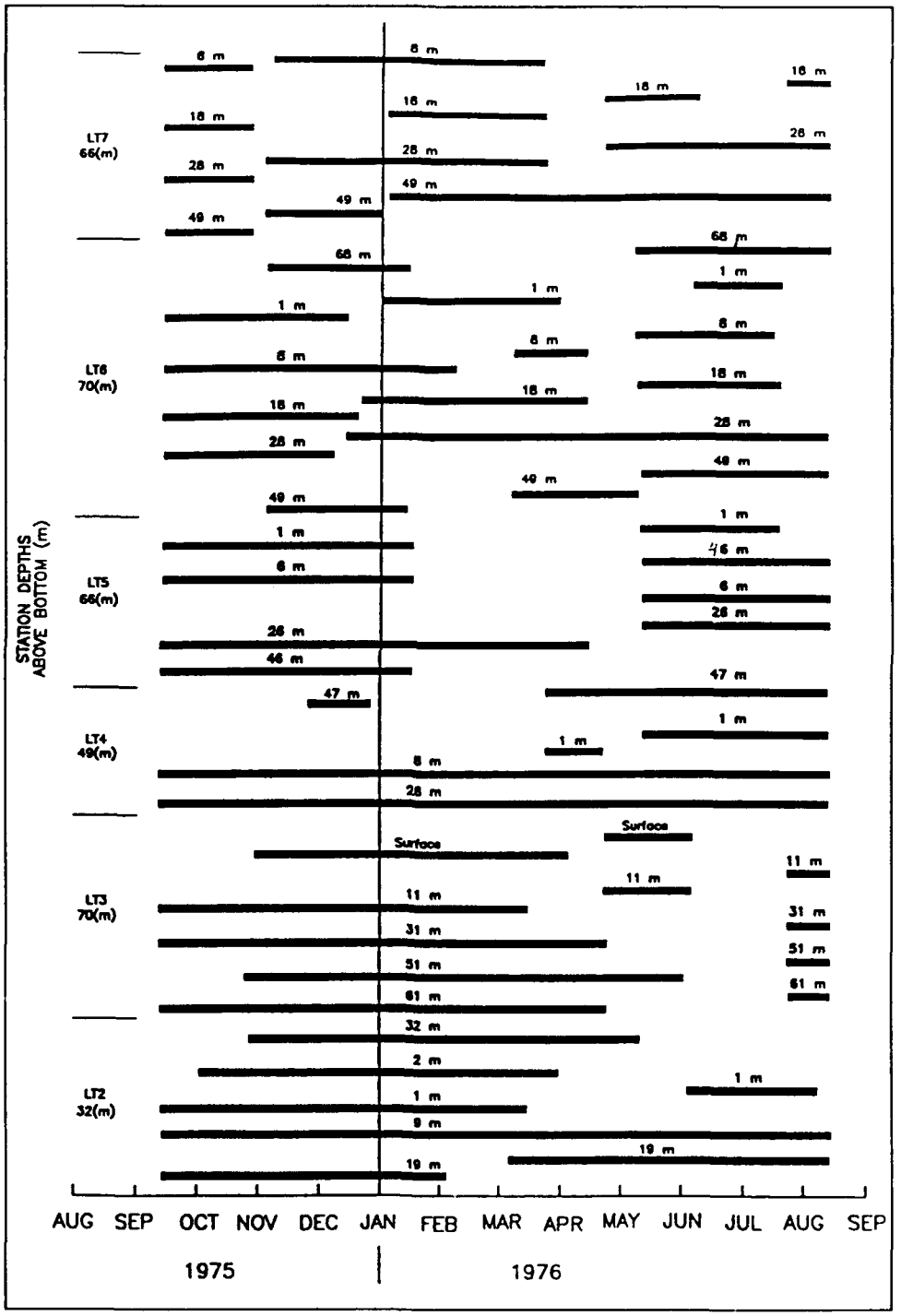

Figure 8. Temporal distribution of current and temperature data

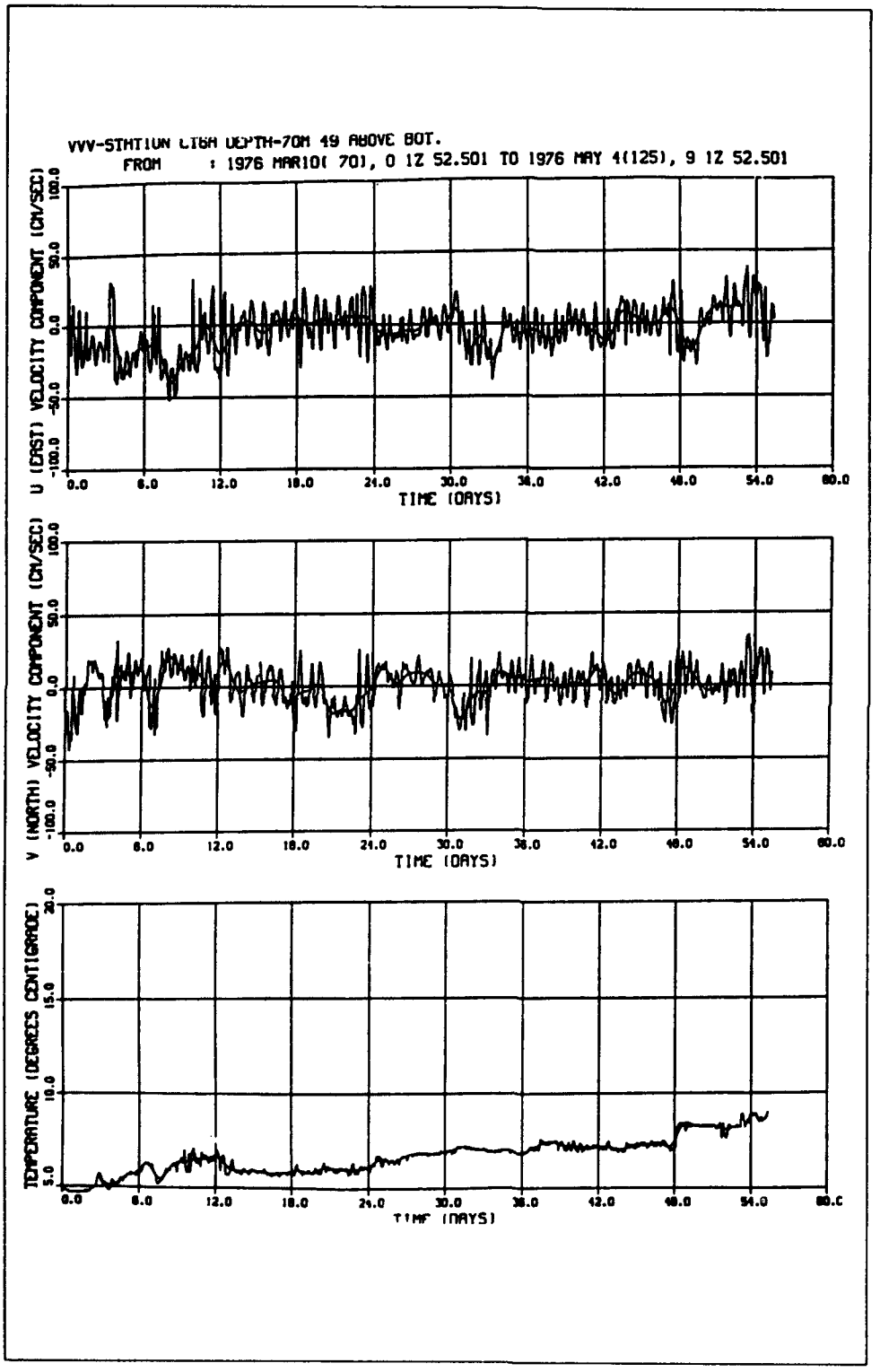

Figure 9. Current and temperature data

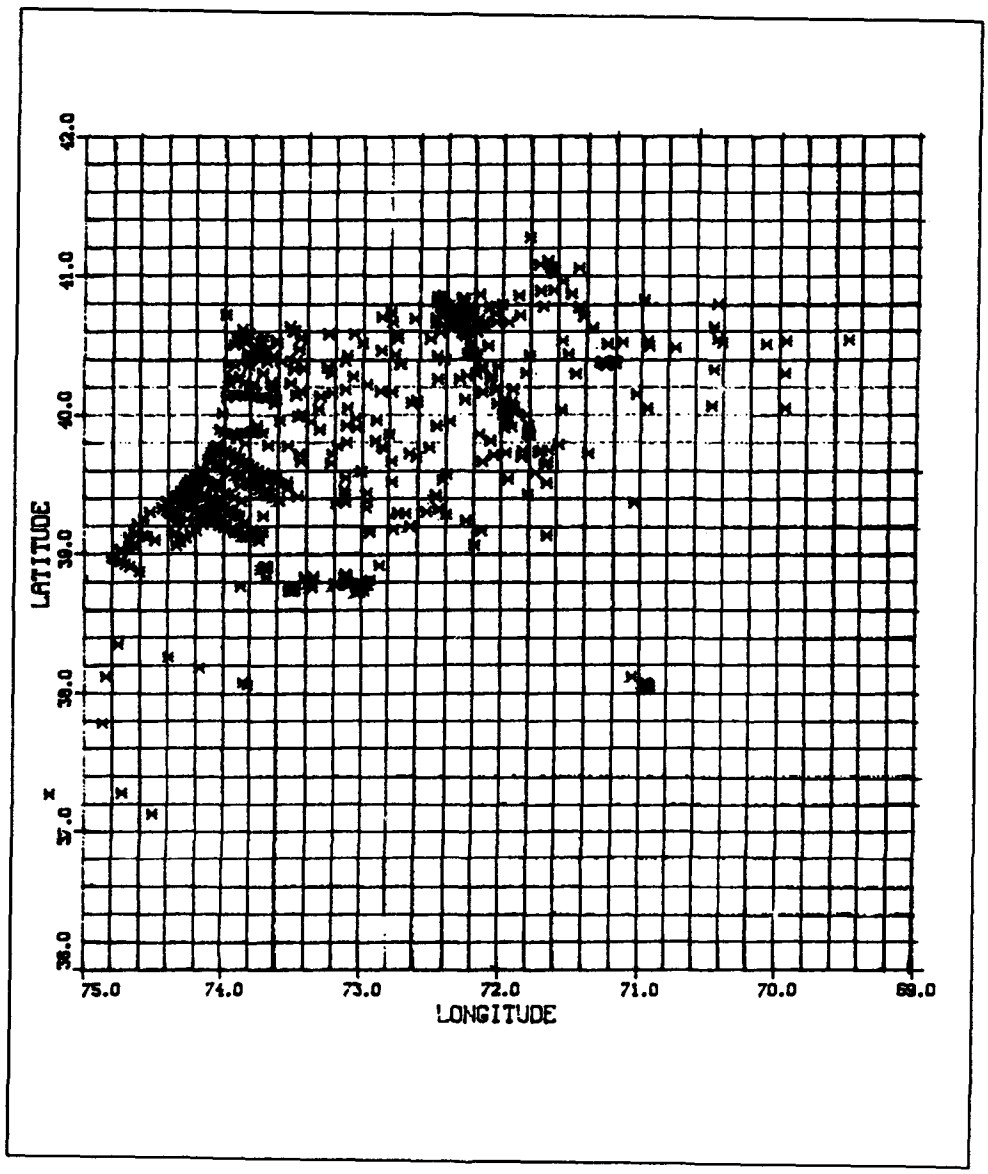

Figure 10. Ship measurements locations for April-September 1976

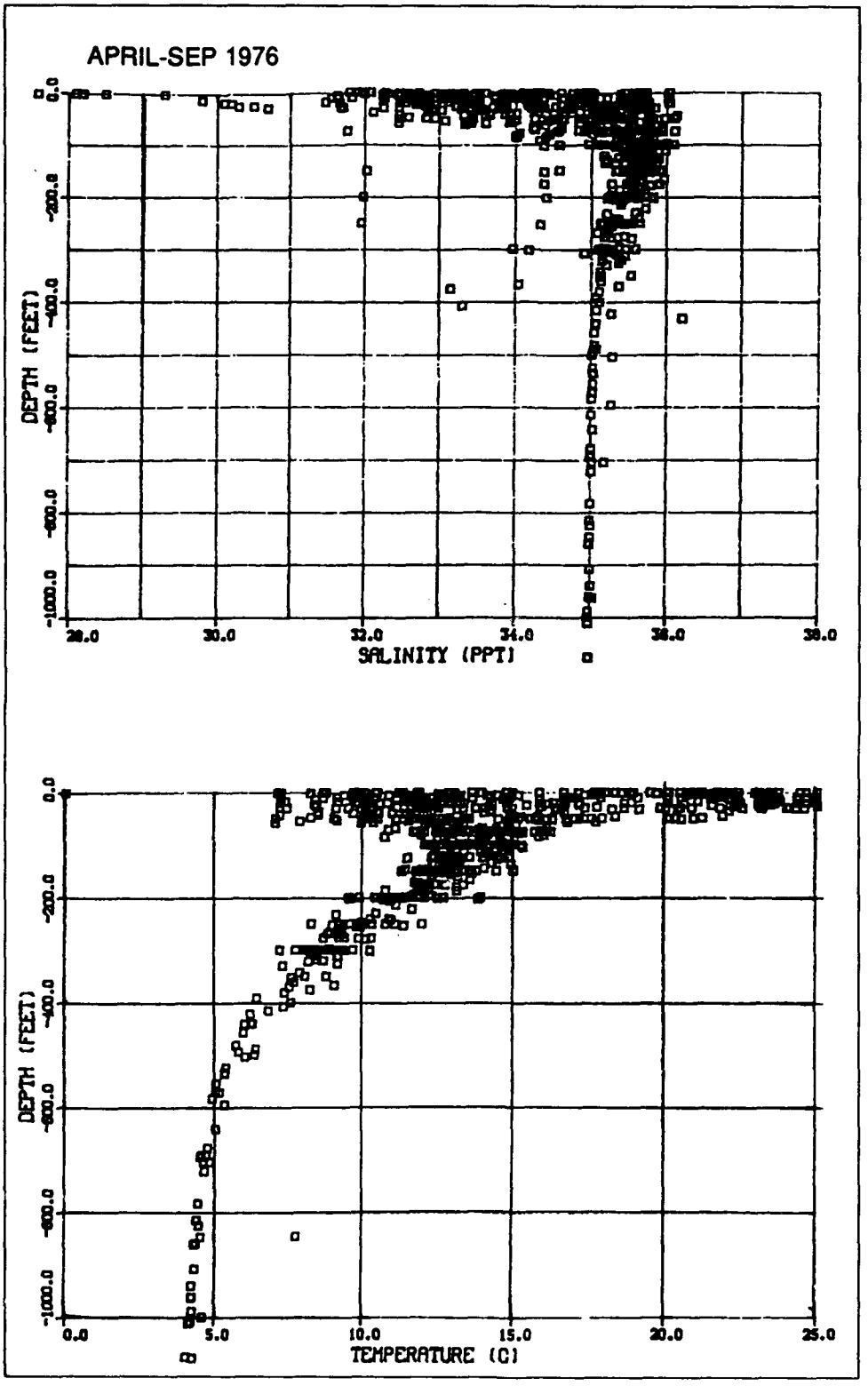

Figure 11. Temperature/salinity data for April-September 1976

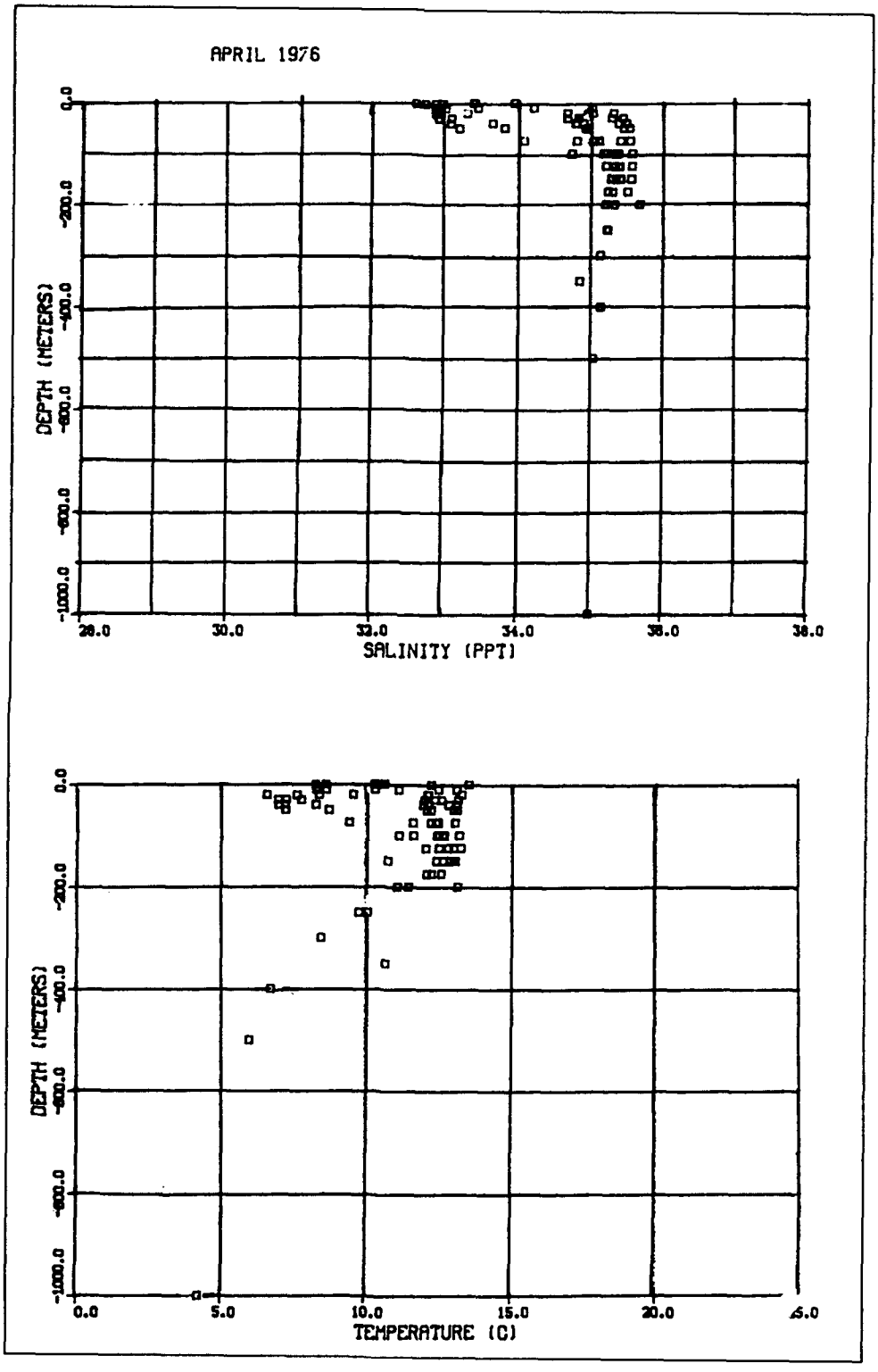

Figure 12. Temperature/salinity data for April 1976

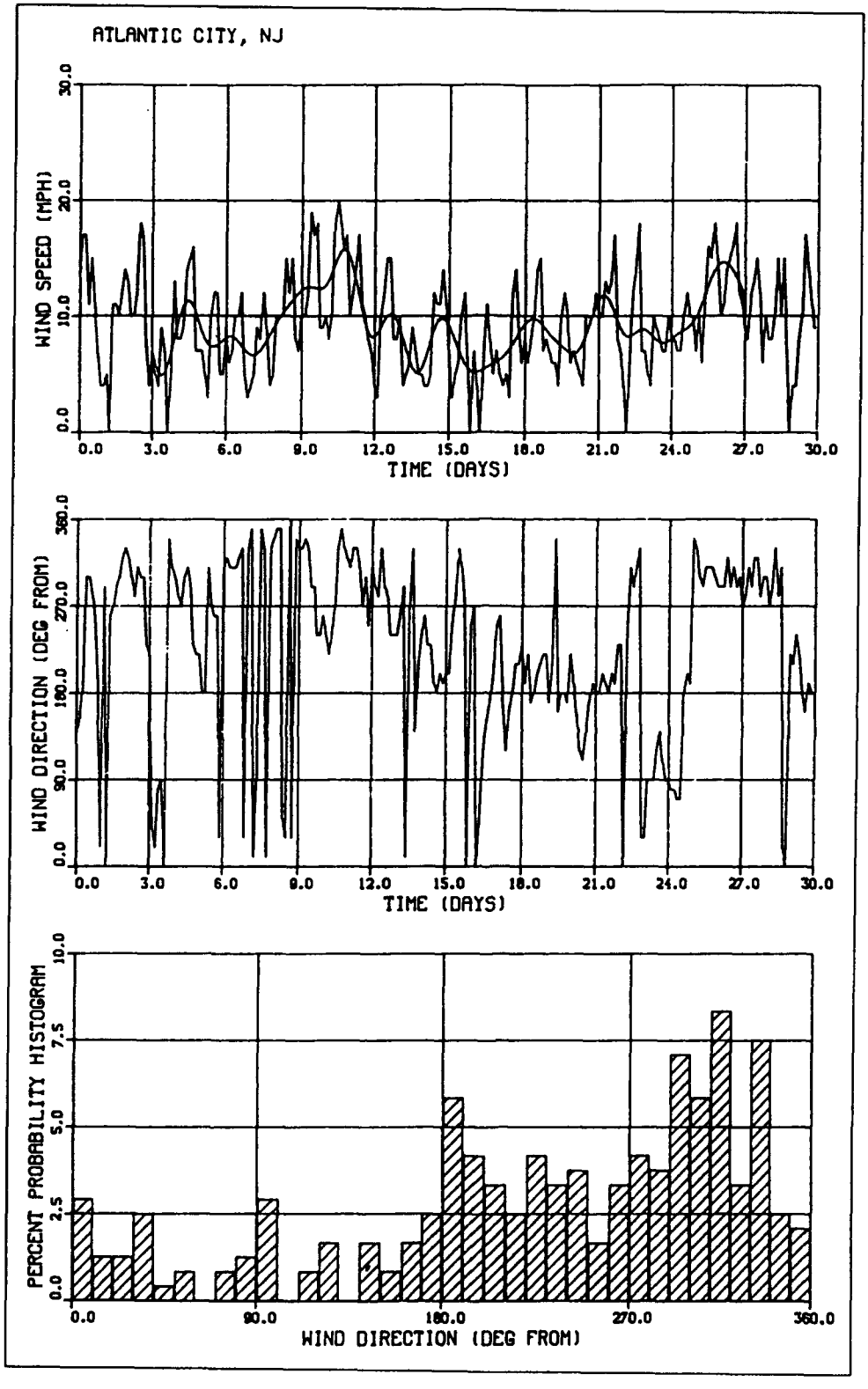

Figure 13. April 1976 wind data for Atlantic City, NJ

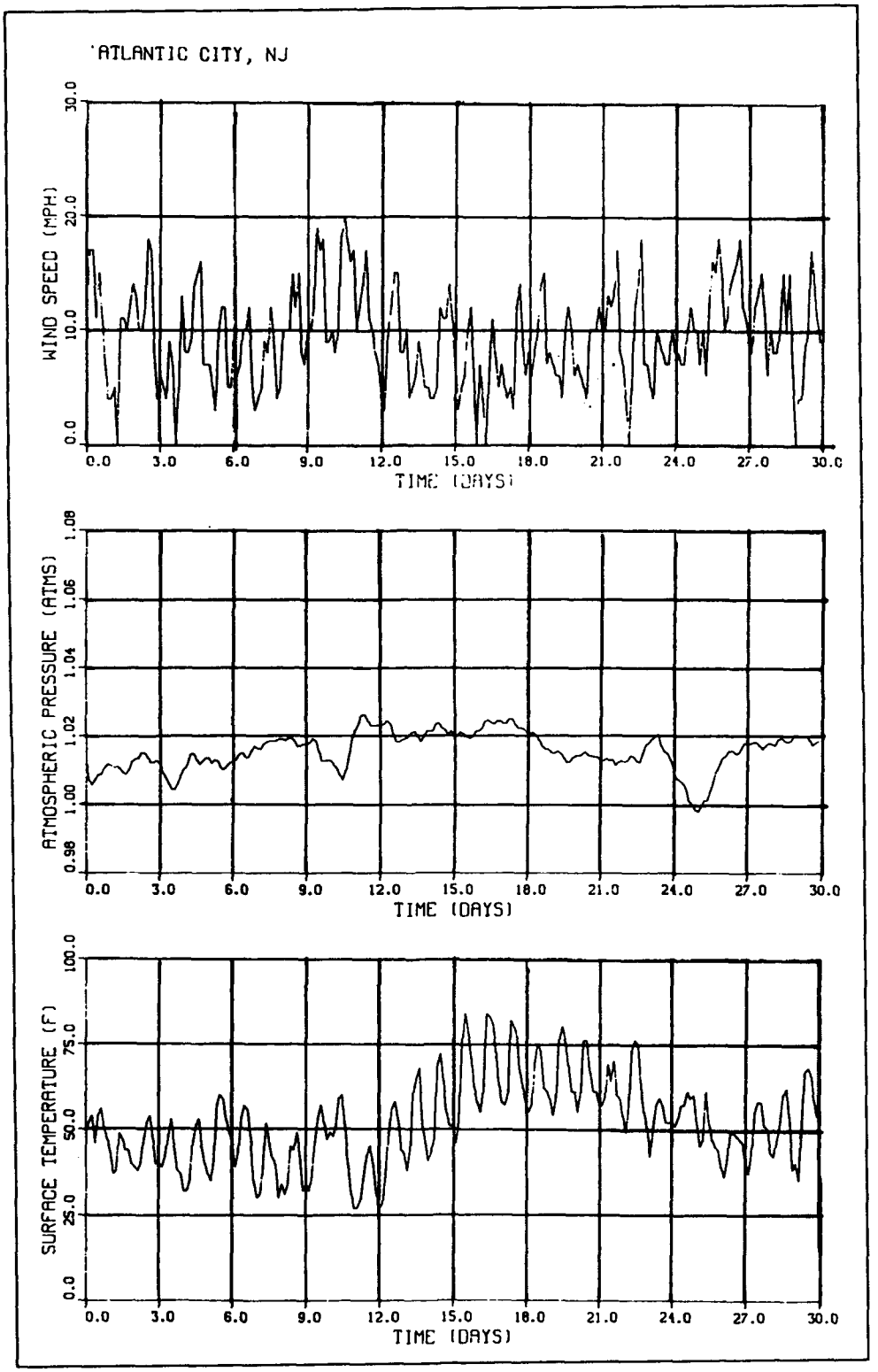

Figure 14. April 1976 wind, pressure, and temperature data for Atlantic City, NJ

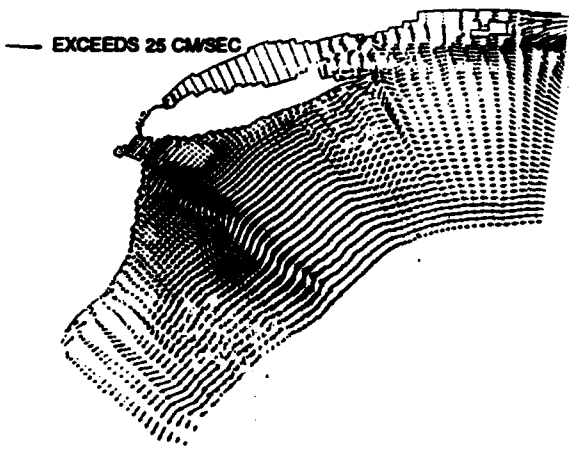

a. Surface current with no wind and no river flow

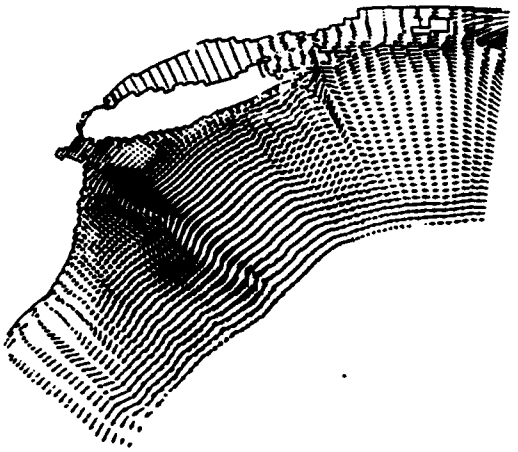

b. Mid-layer current with no wind and no river flow

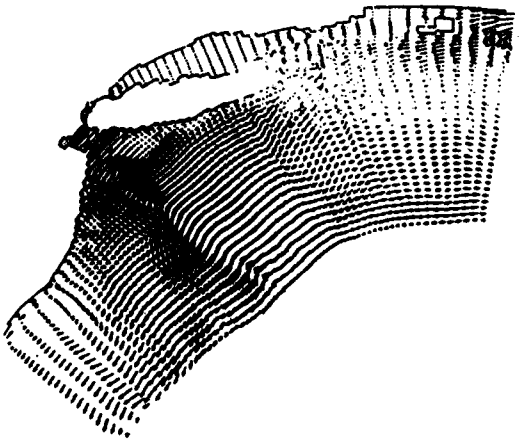

c. Bottom current with no wind and no river inflow

Figure 15. Circulation with zero wind field

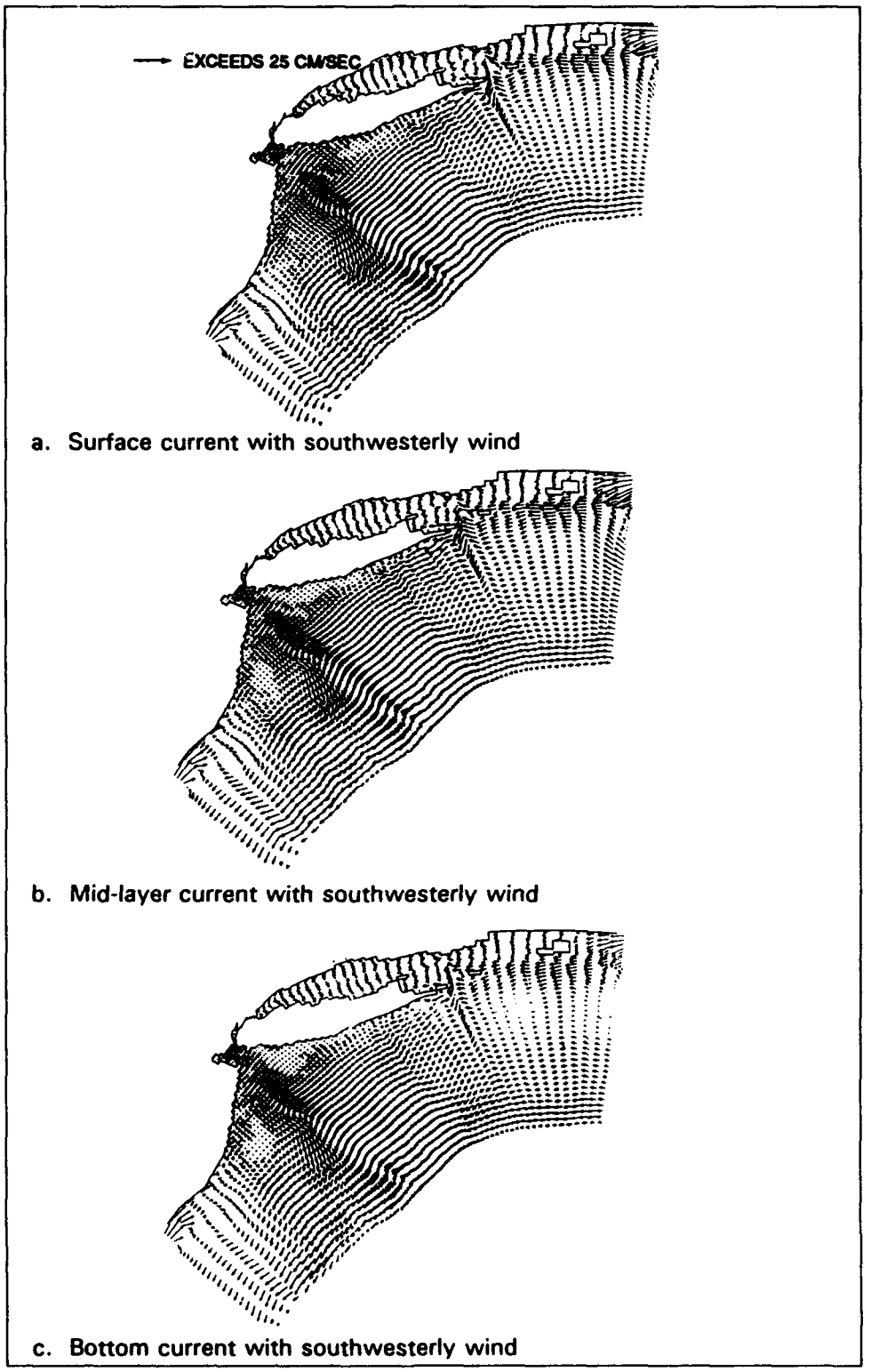

a. Surface current with southwesterly wind

b. Mid-layer current with southwesterly wind

c. Bottom current with southwesterly wind

Figure 16. Case 1: Circulation with southwest wind field

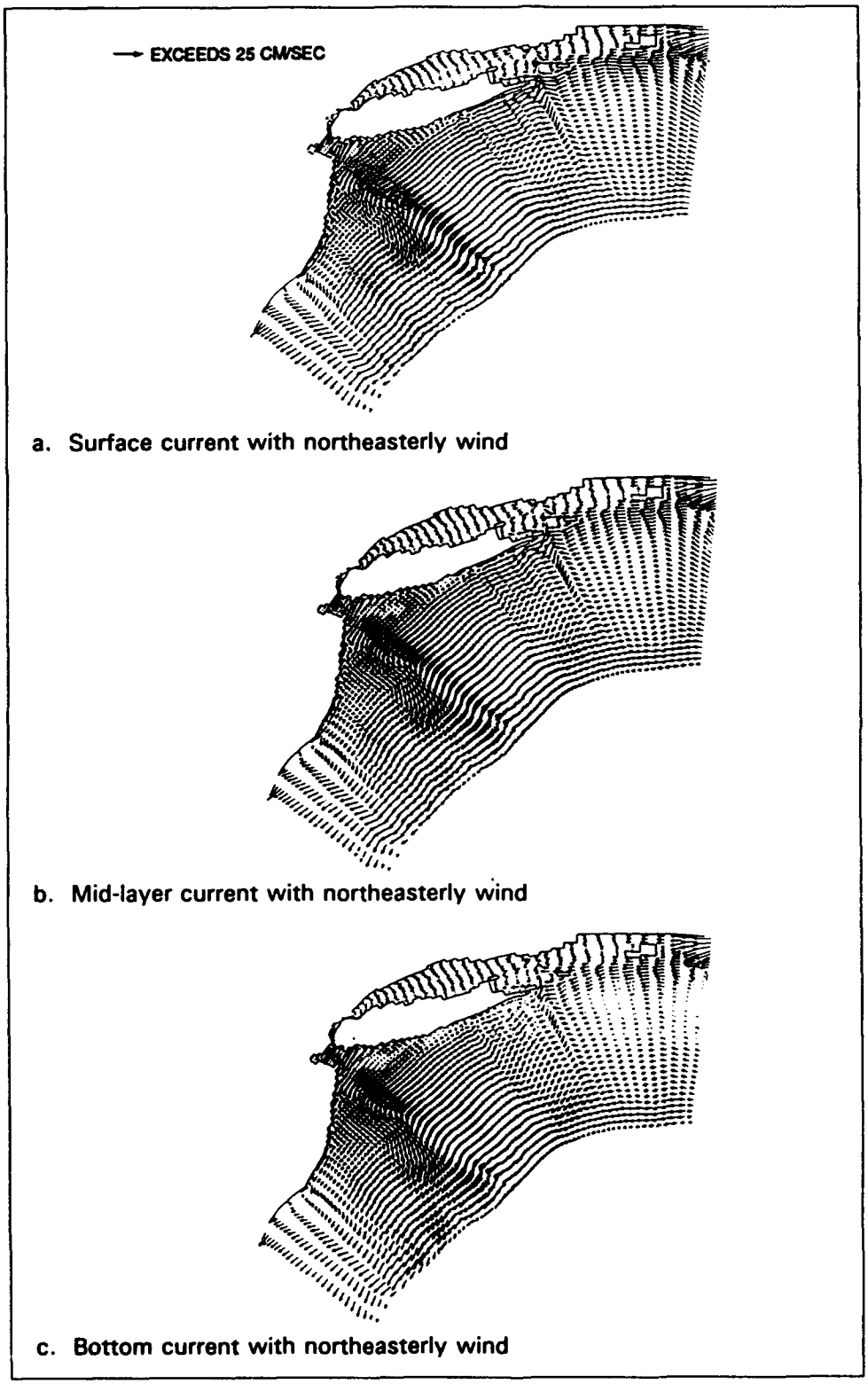

a. Surface current with northeasterly wind

b. Mid-layer current with northeasterly wind

c. Bottom current with northeasterly wind

Figure 17. Case 2: Circulation with northeast wind field

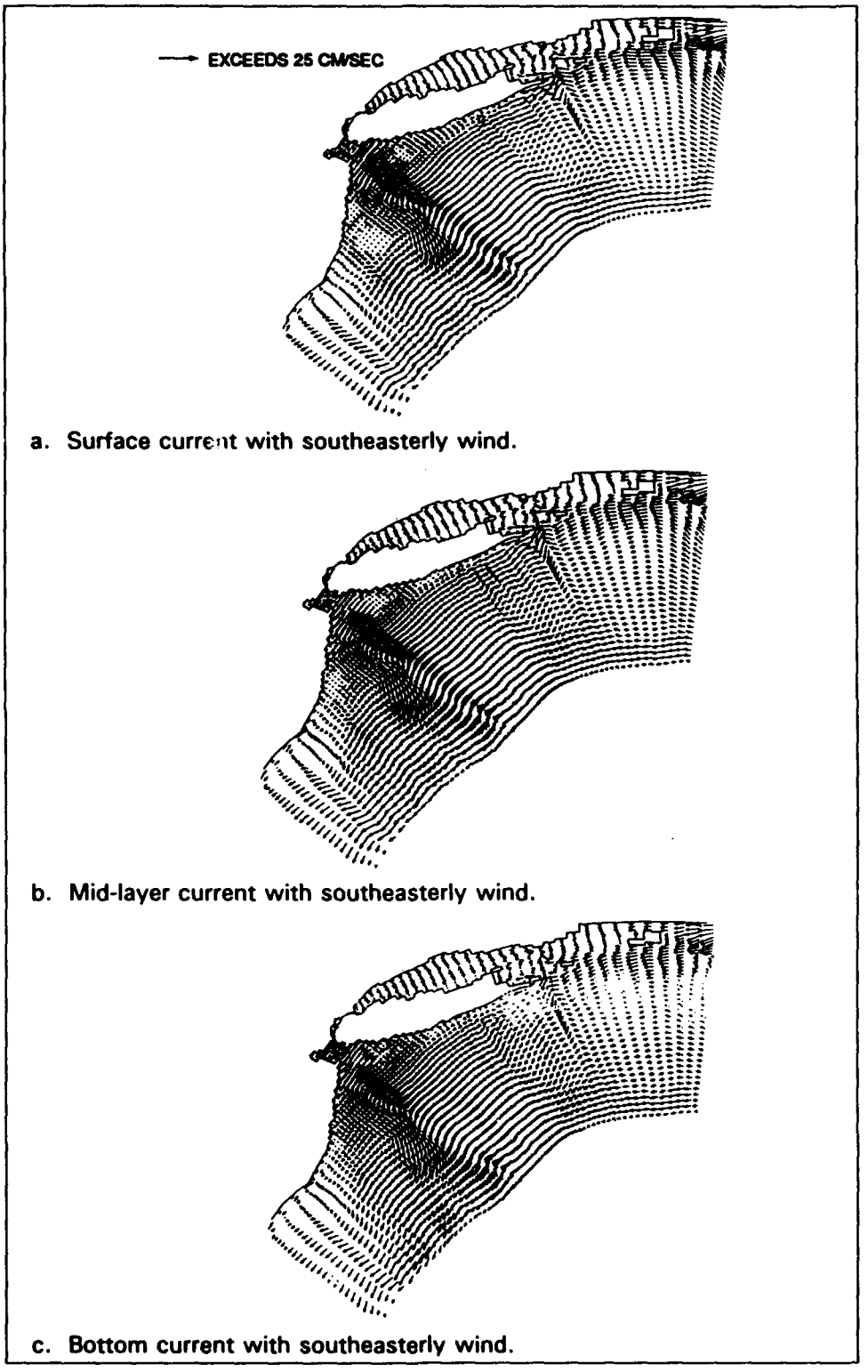

a. Surface current with southeasterly wind.

b. Mid-layer current with southeasterly wind.

c. Bottom current with southeasterly wind.

Figure 18. Case 3: Circulation with southeast wind field

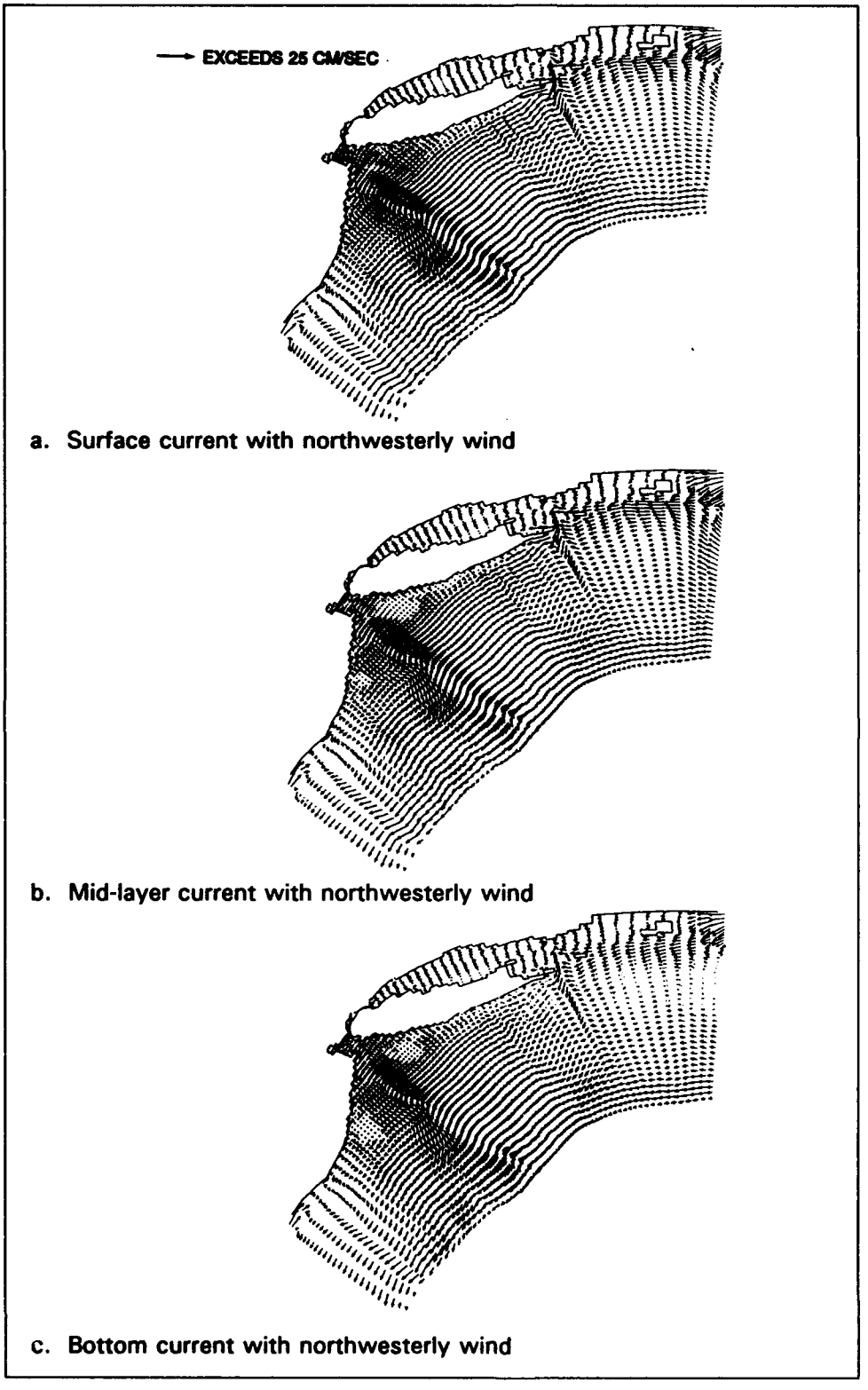

a. Surface current with northwesterly wind

b. Mid-layer current with northwesterly wind

c. Bottom current with northwesterly wind

Figure 19. Case 4: Circulation with northwest wind field

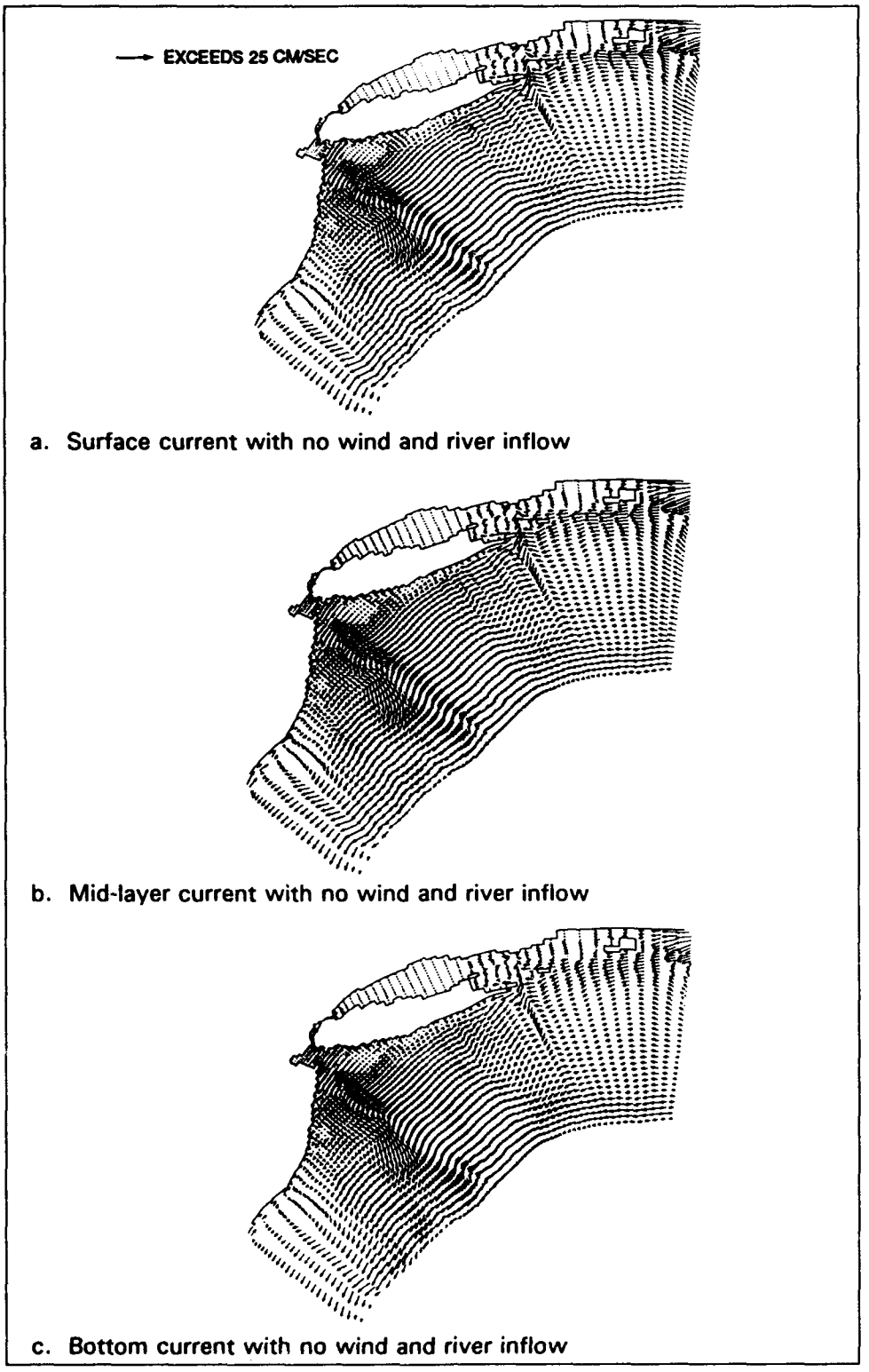

a. Surface current with no wind and river inflow

b. Mid-layer current with no wind and river inflow

c. Bottom current with no wind and river inflow

Figure 20. Case 5: Circulation with no wind and Hudson River inflow

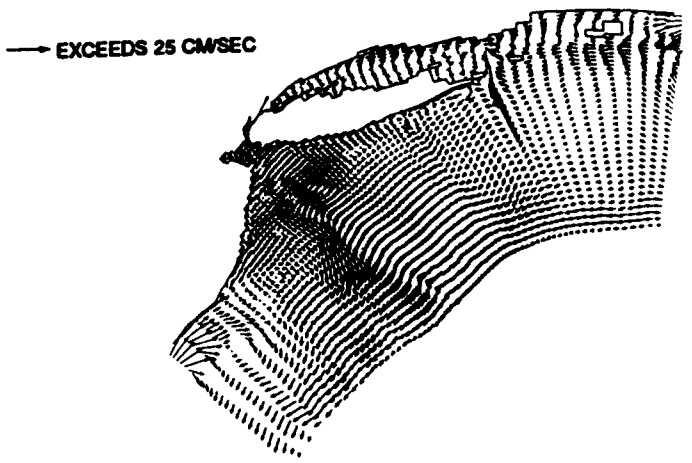

a. Surface current with doubled southwesterly wind and river inflow

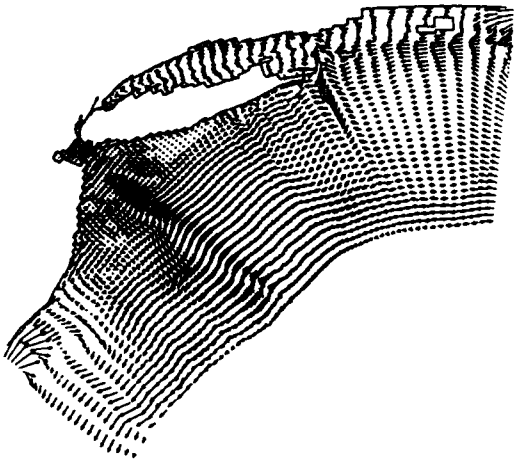

b. Mid-layer current with doubled southwesterly wind and river inflow

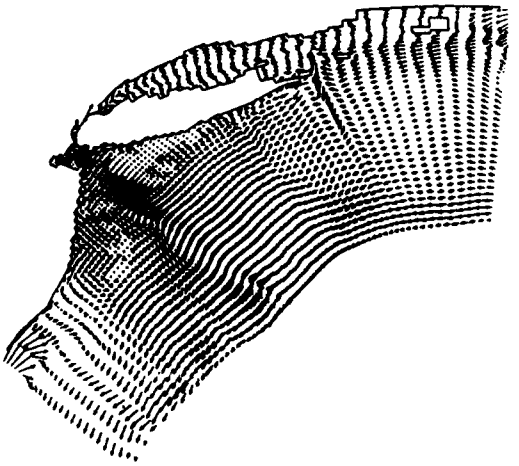

c. Bottom current with doubled southwesterly wind and river inflow

Figure 21. Case 6: Circulation with doubled southwest wind and river inflow

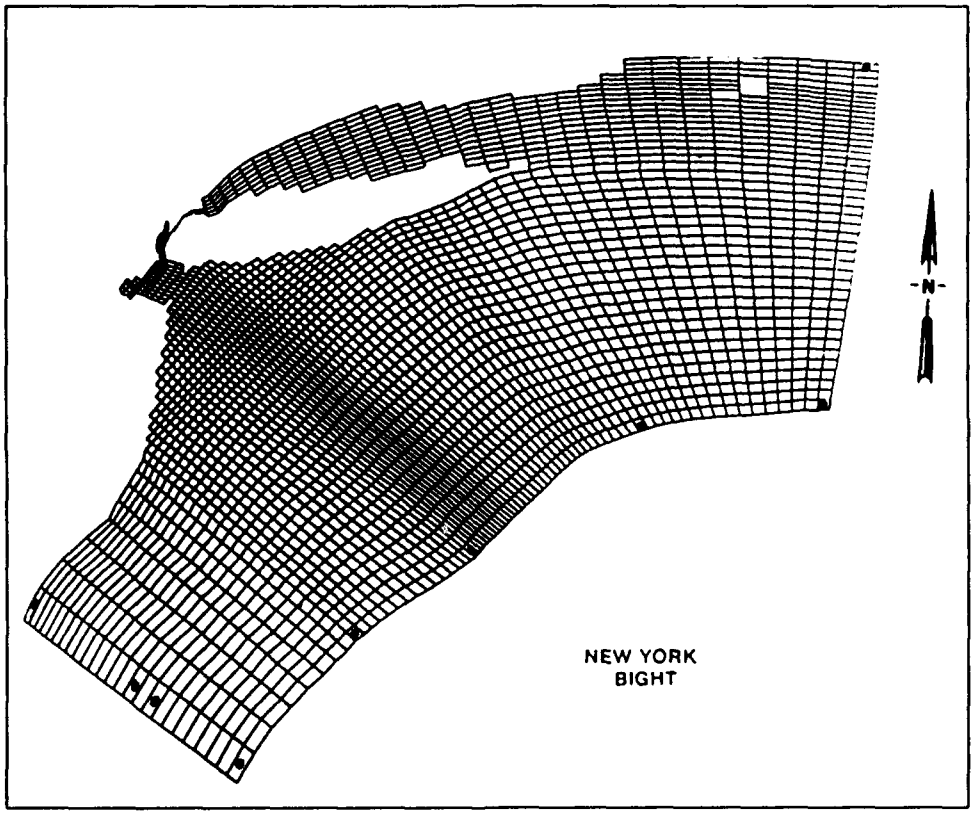

Figure 22. Tidal Boundary Control Points

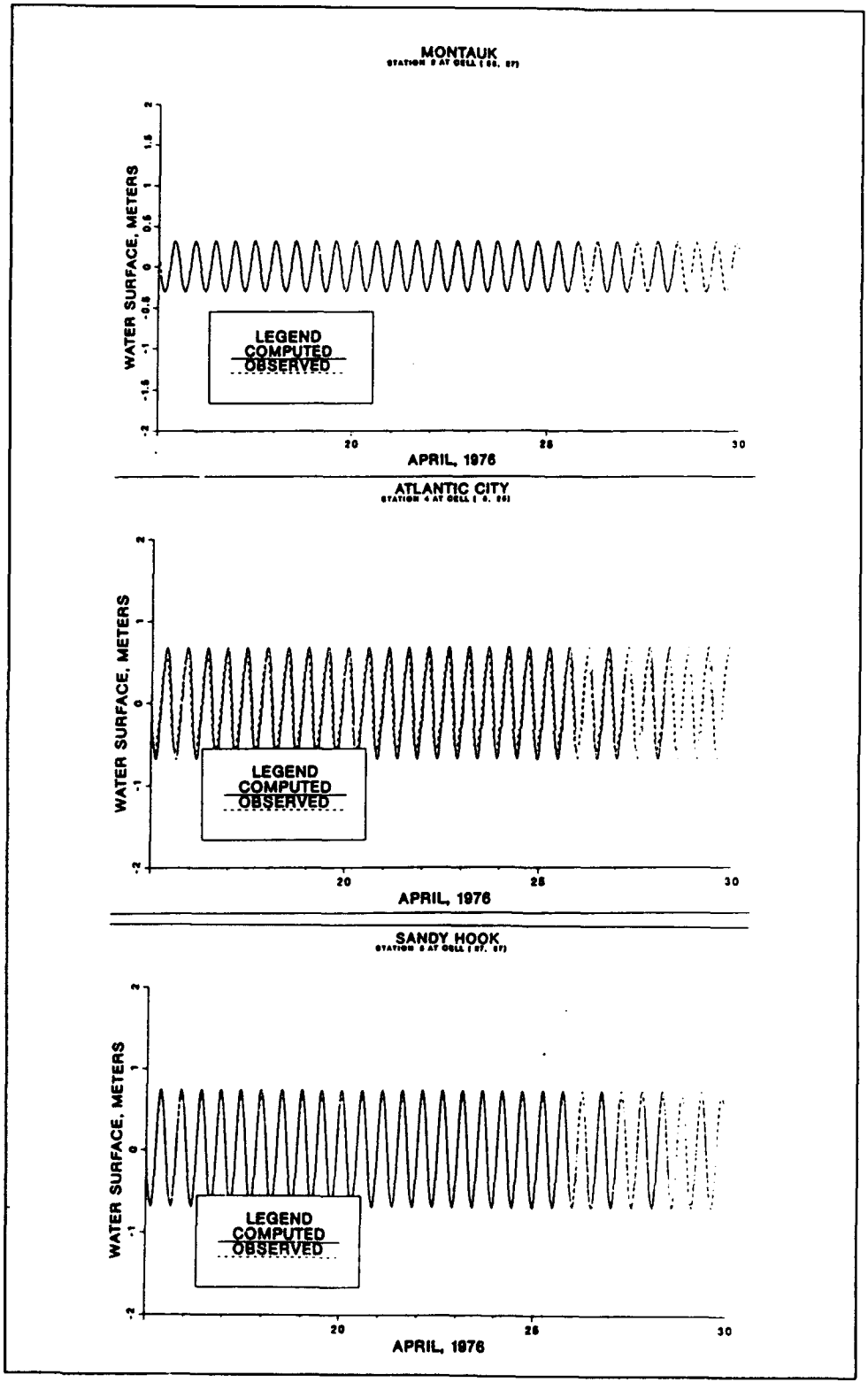

Figure 23. M_2 tide component comparisons (Sheet 1 of 3)

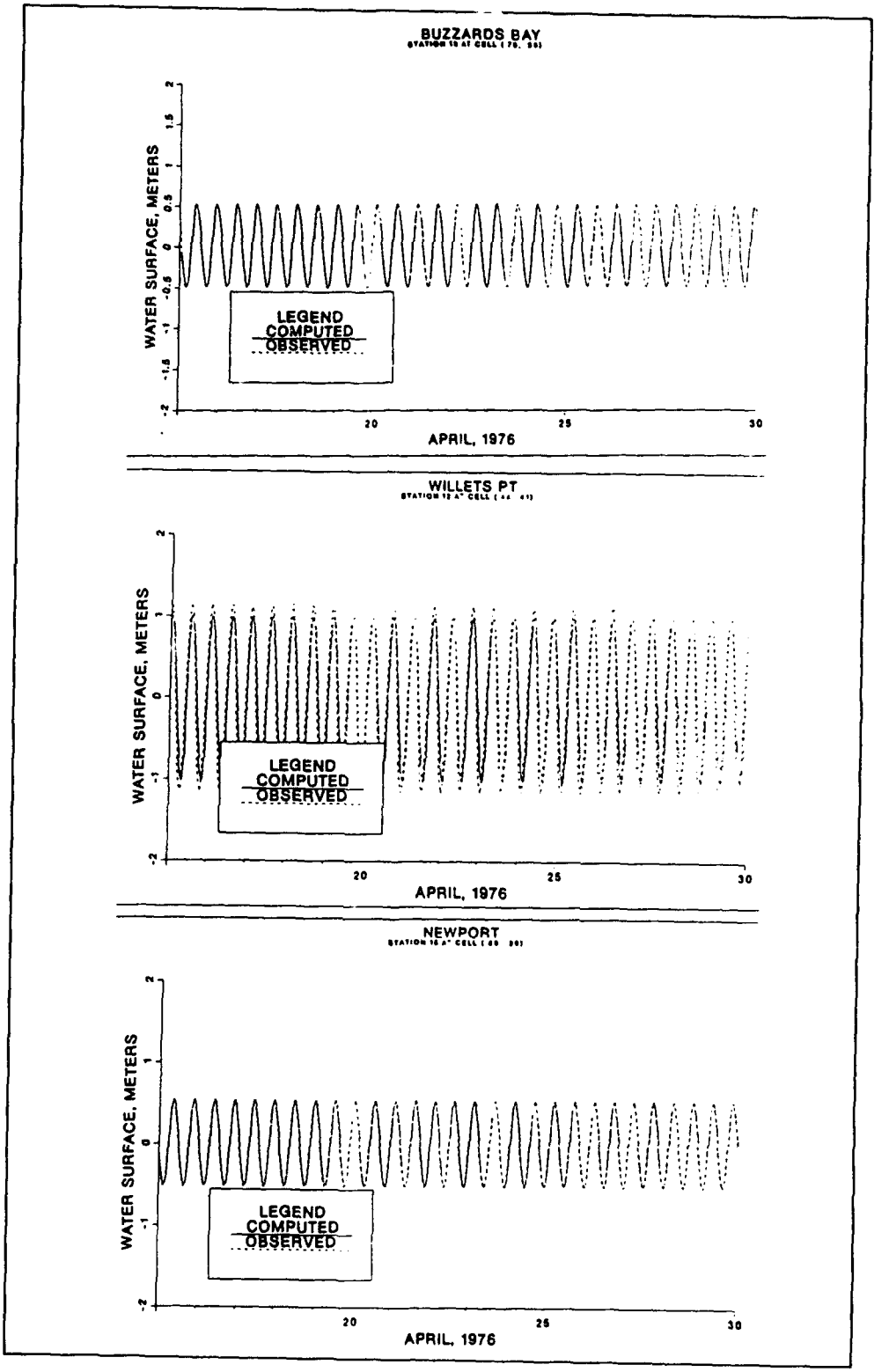

Figure 23. (Sheet 2 of 3)

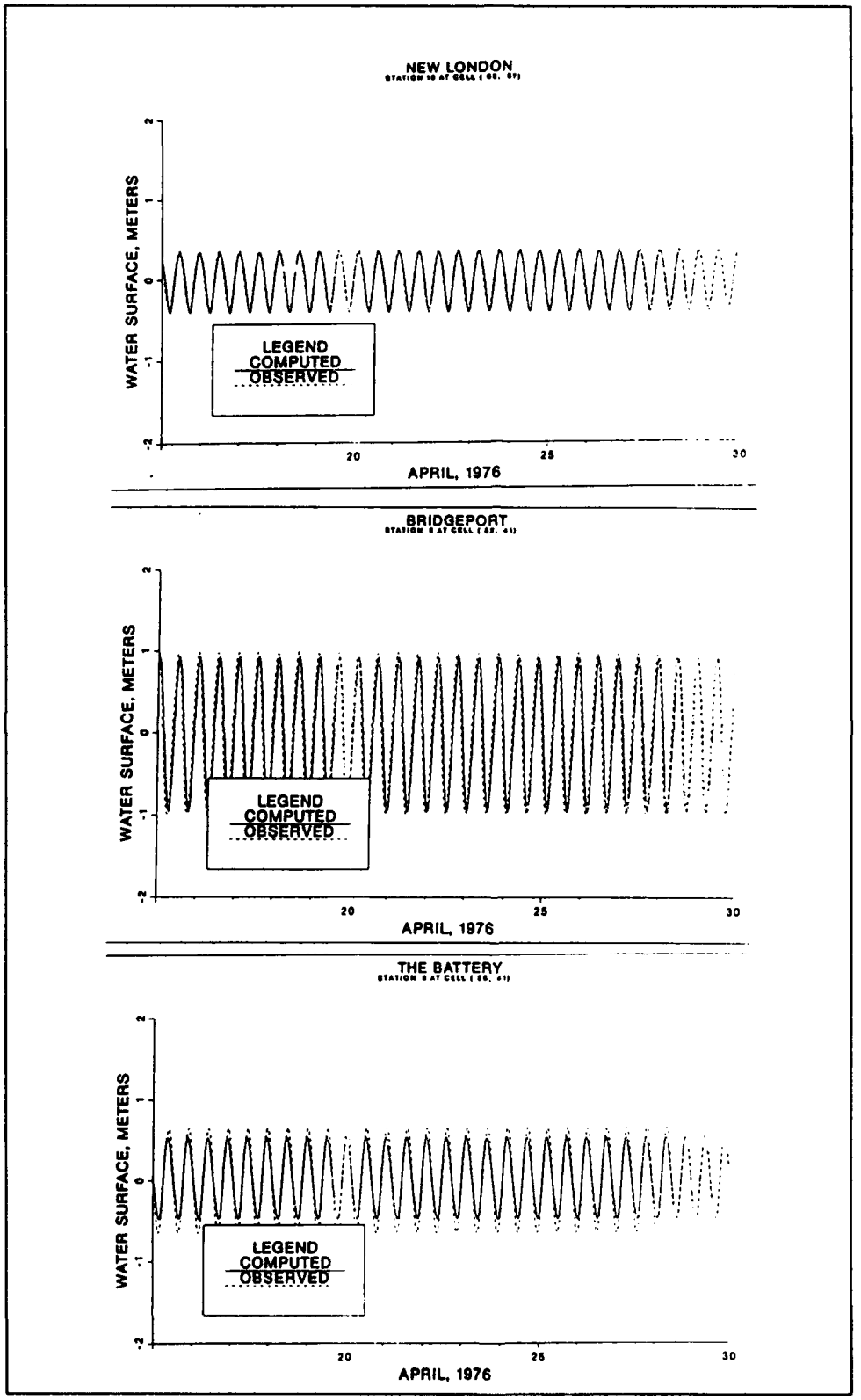

Figure 23. (Sheet 3 of 3)

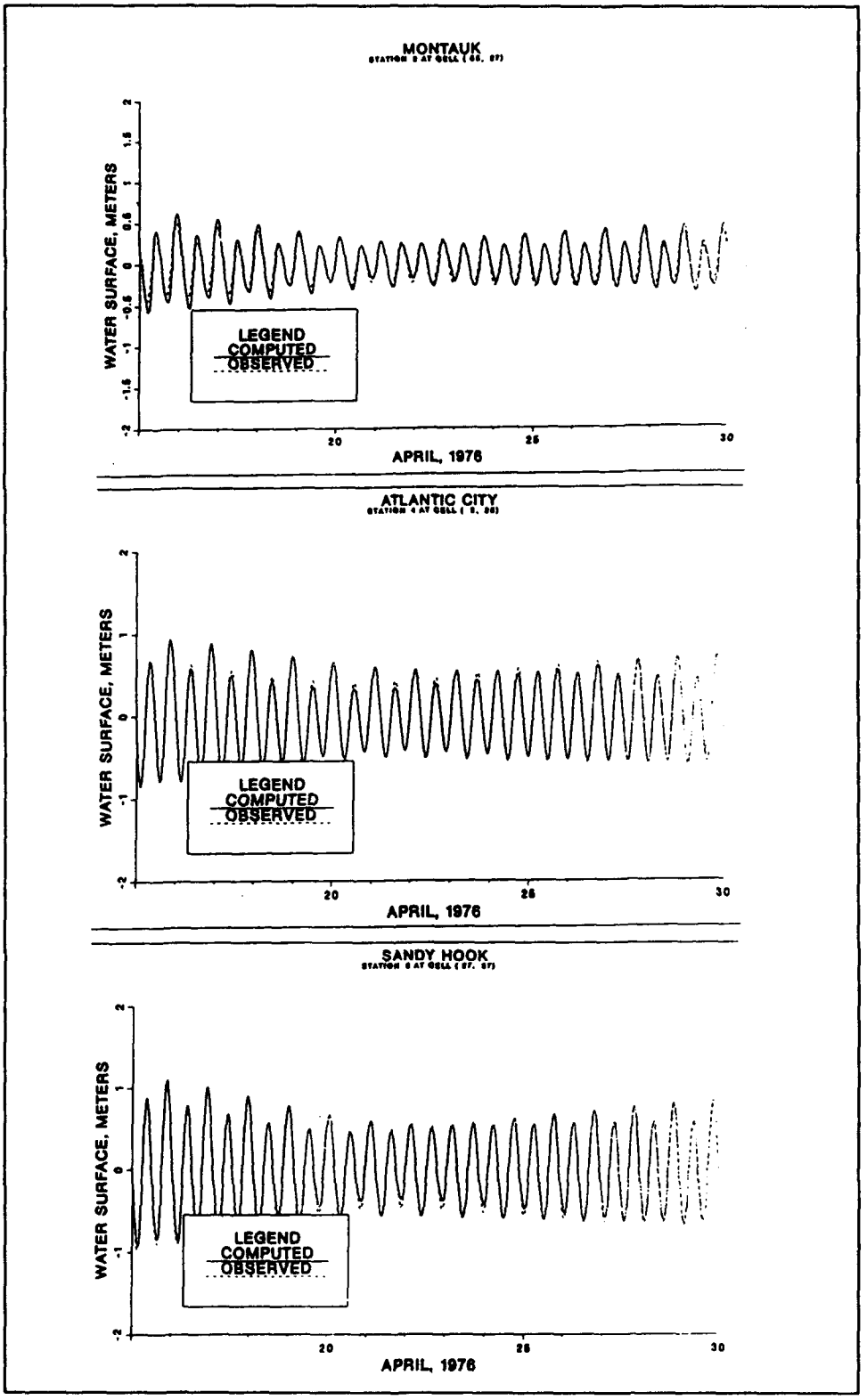

Figure 24. Mixed tide component comparison (Sheet 1 of 3)

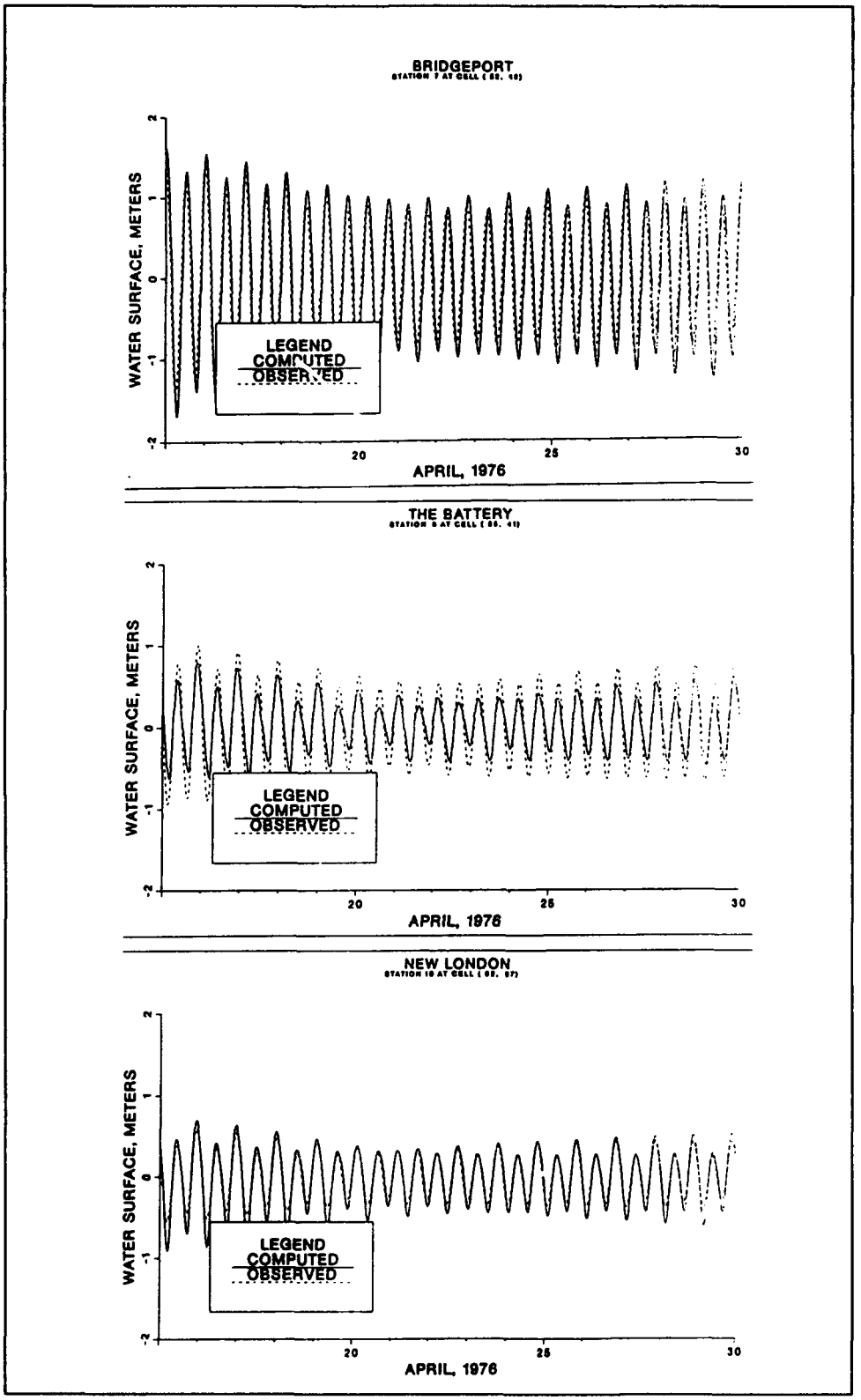

Figure 24 (Sheet 2 of 3)

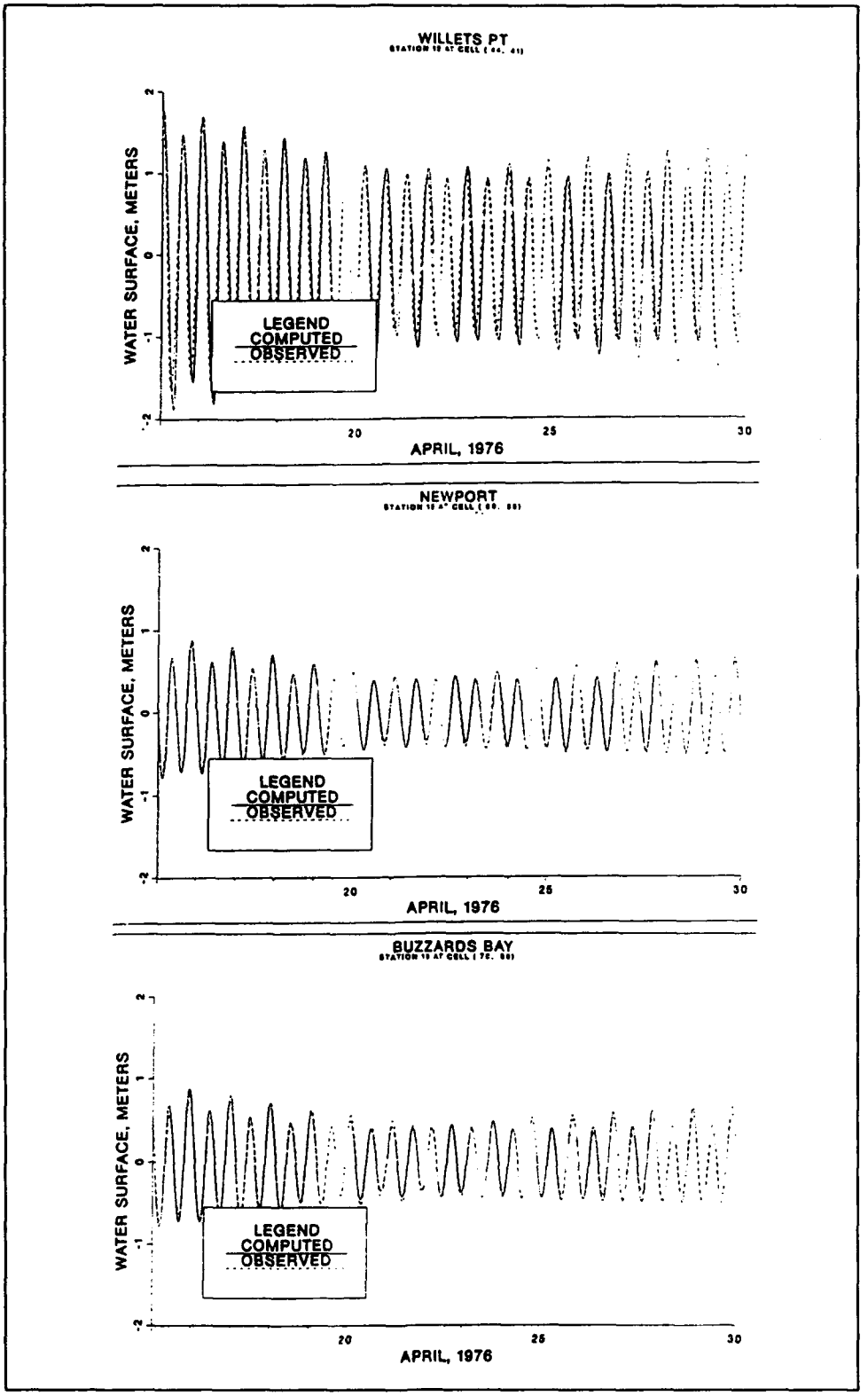

Figure 24. (Sheet 3 of 3)

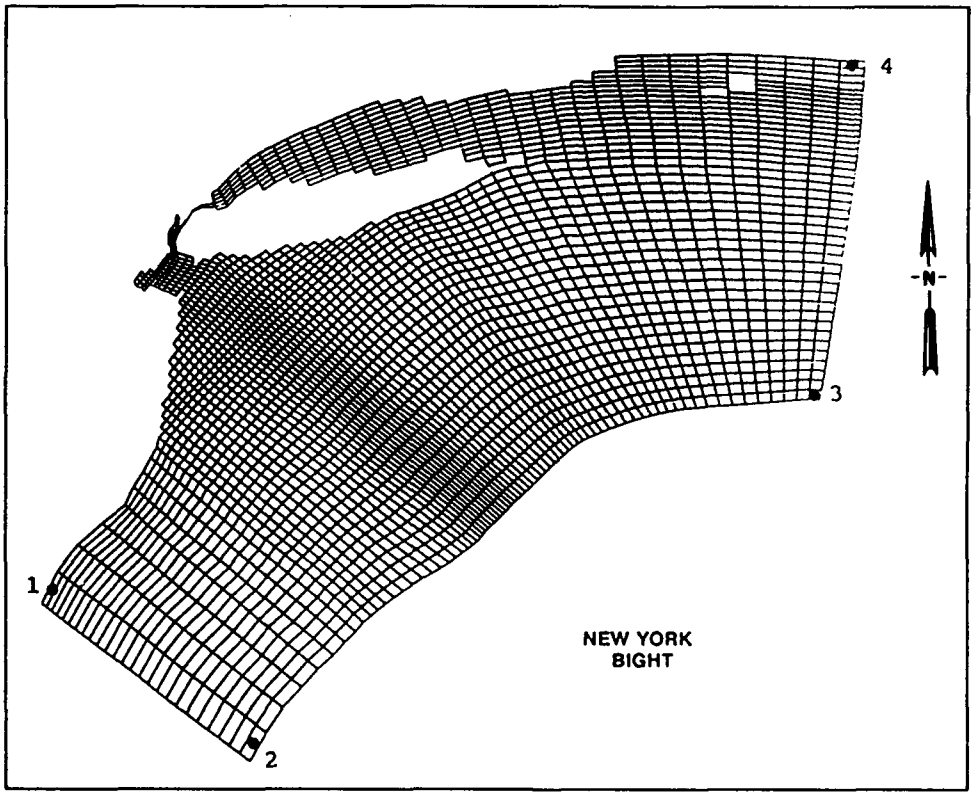

Figure 25. Calibration/verification tidal control points

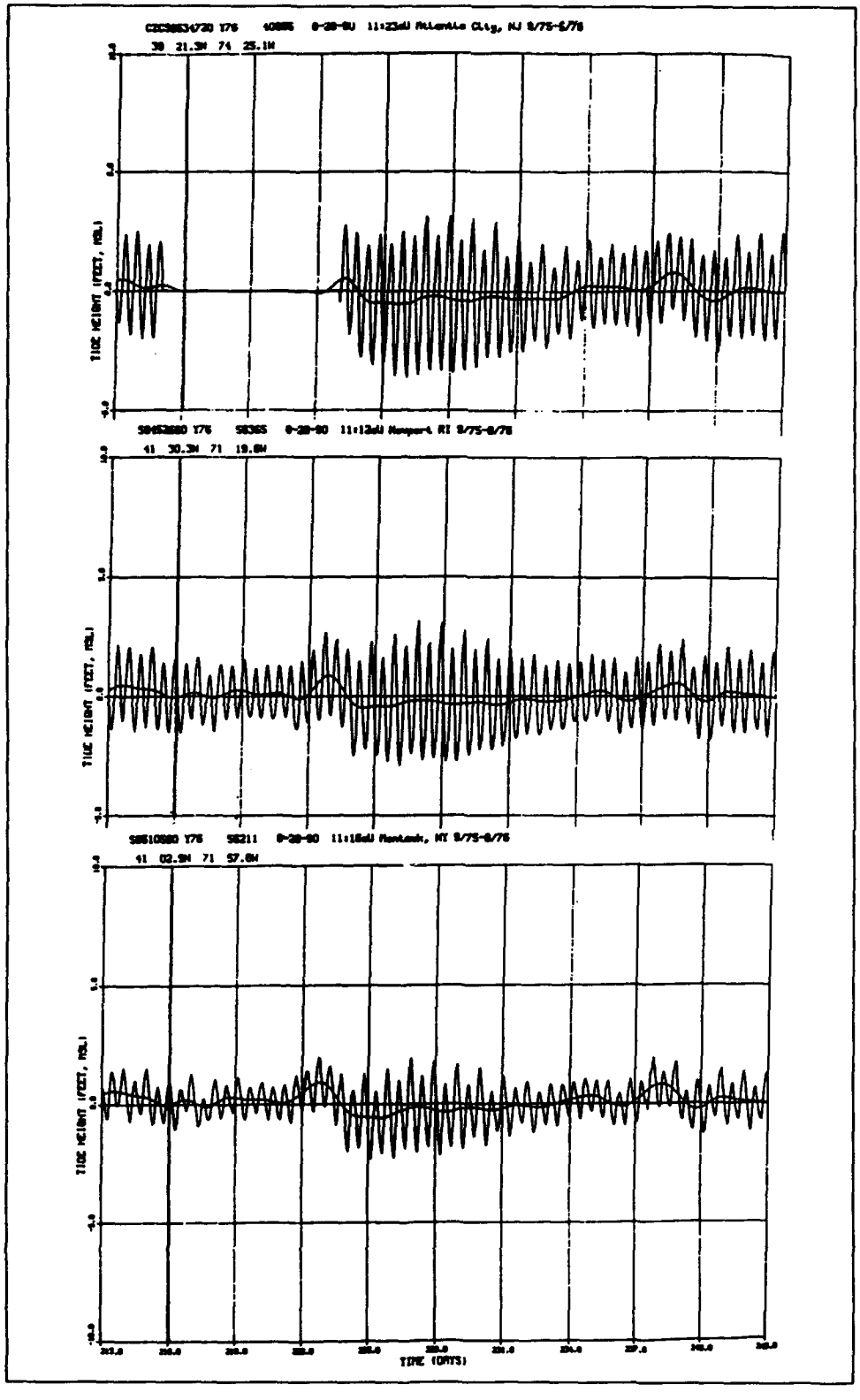

Figure 26. Prototype tide elevations for April 1976

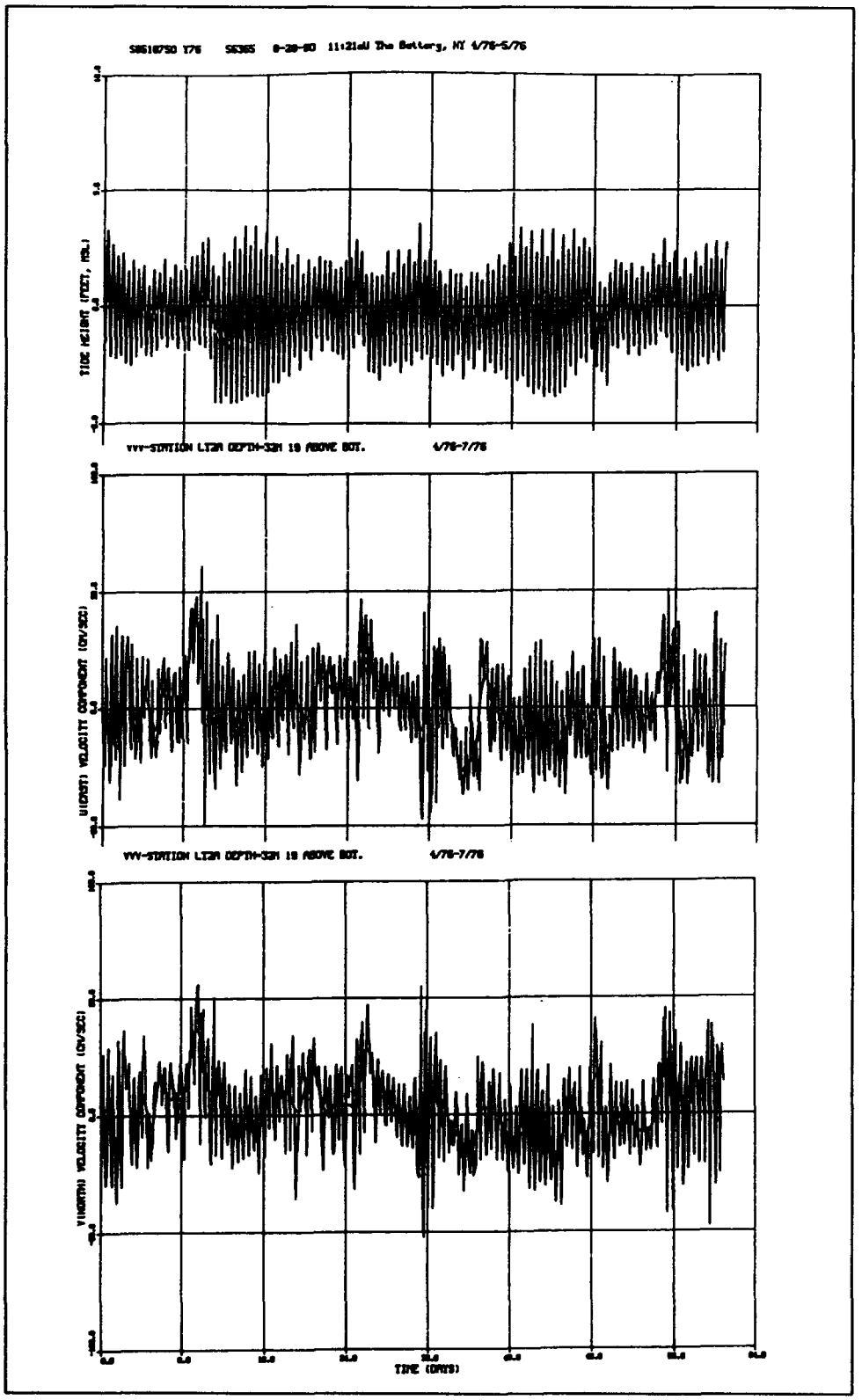

Figure 27. Low-frequency correlation of height and current data

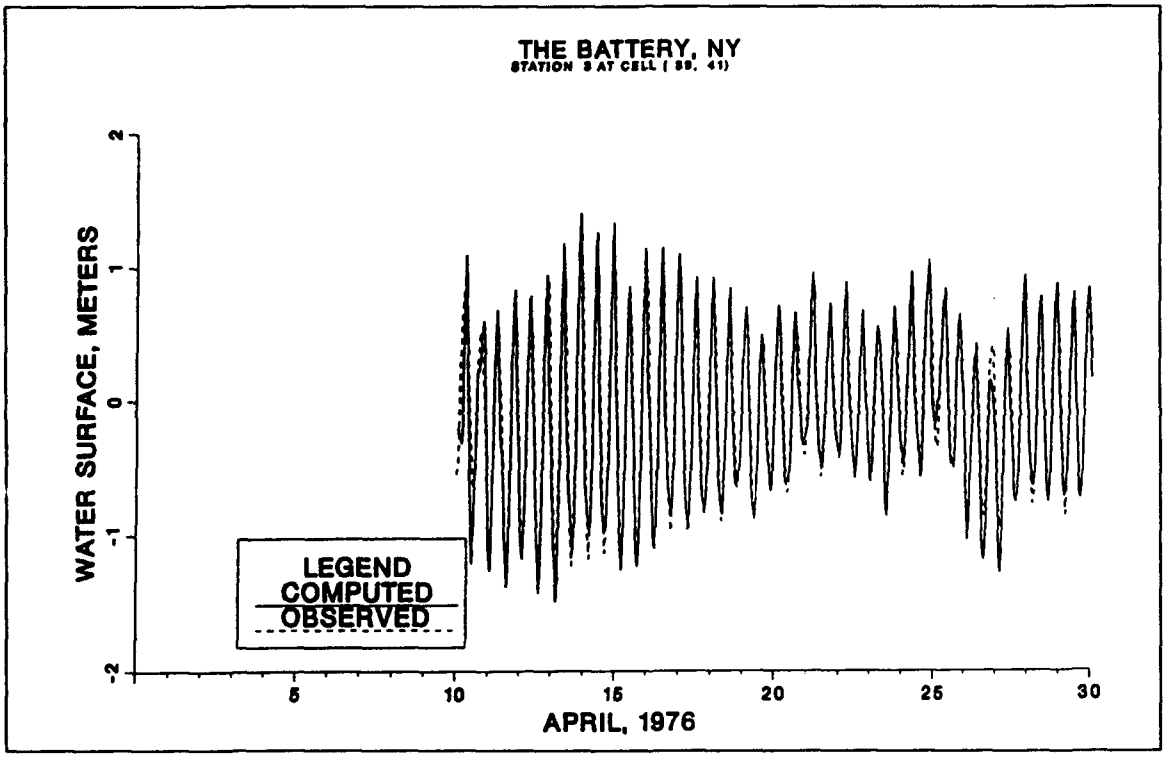

Figure 28. April 1976 water surface comparison for the Battery

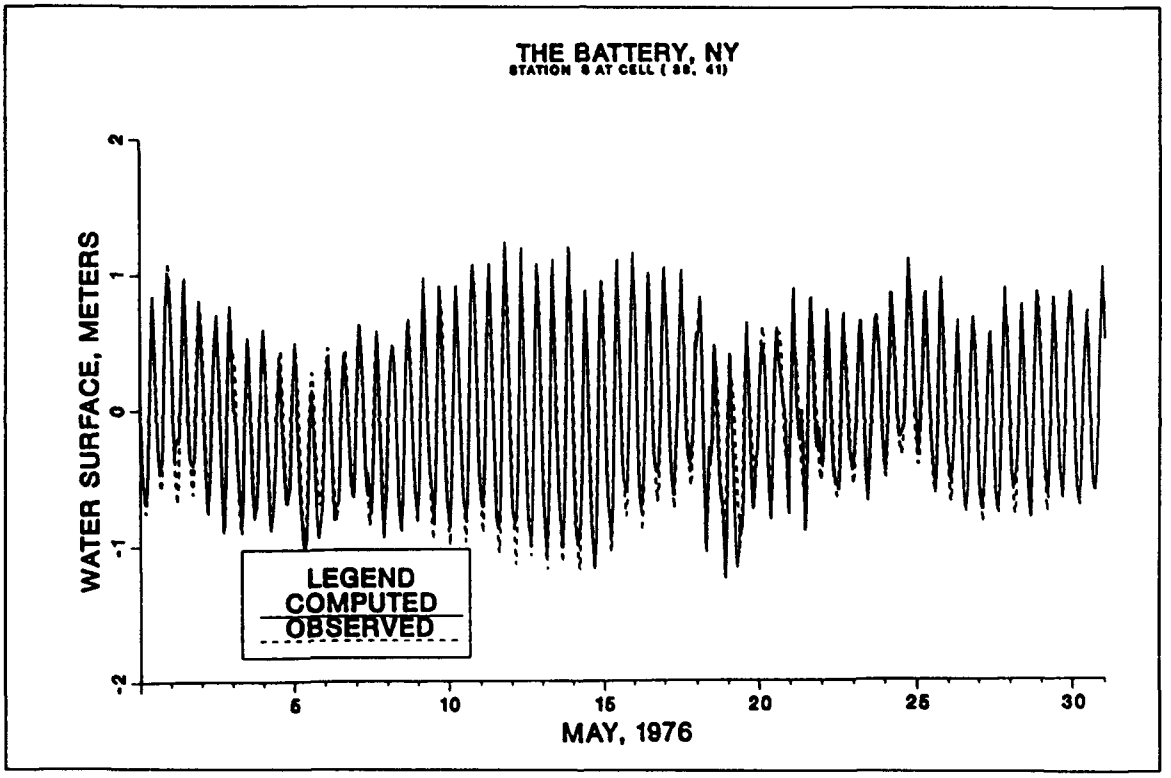

Figure 29. May 1976 water surface comparison for the Battery

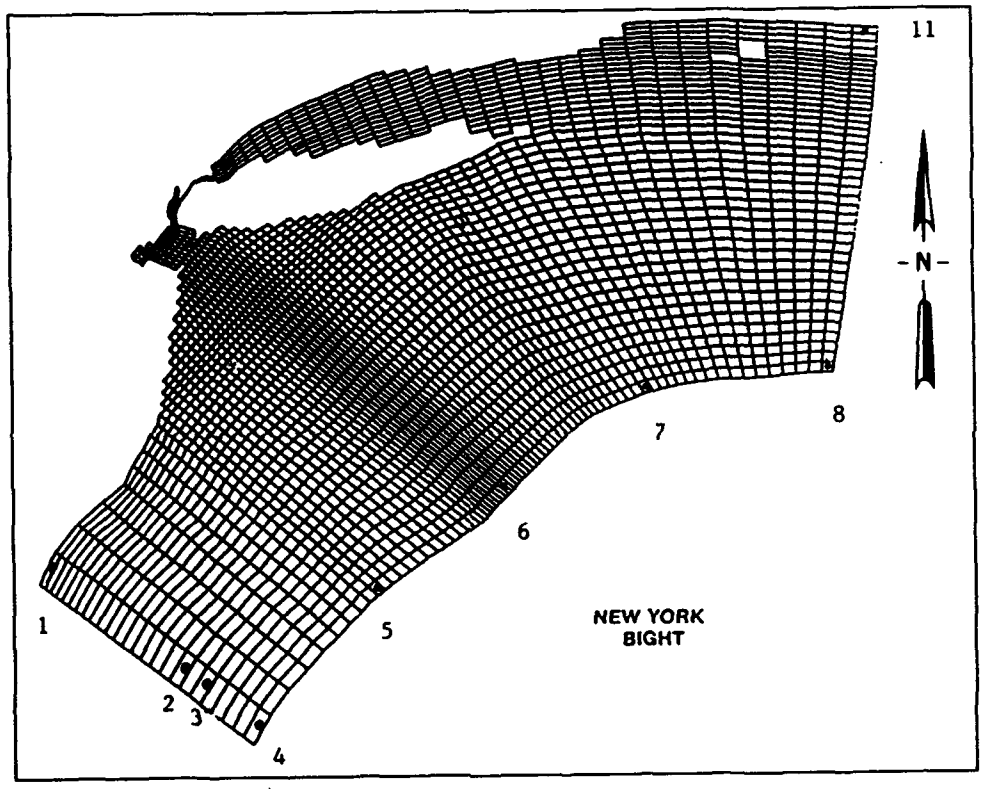

Figure 30. Tidal control points for long-term verification

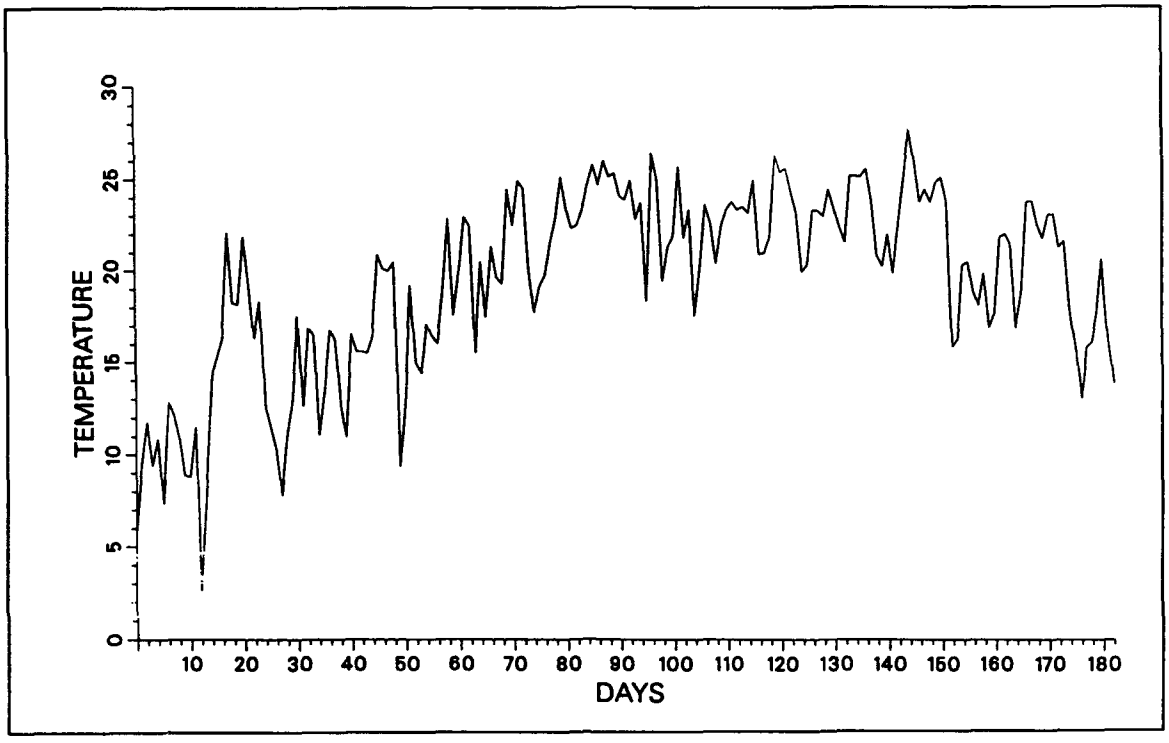

Figure 31. Variation of daily equilibrium temperature

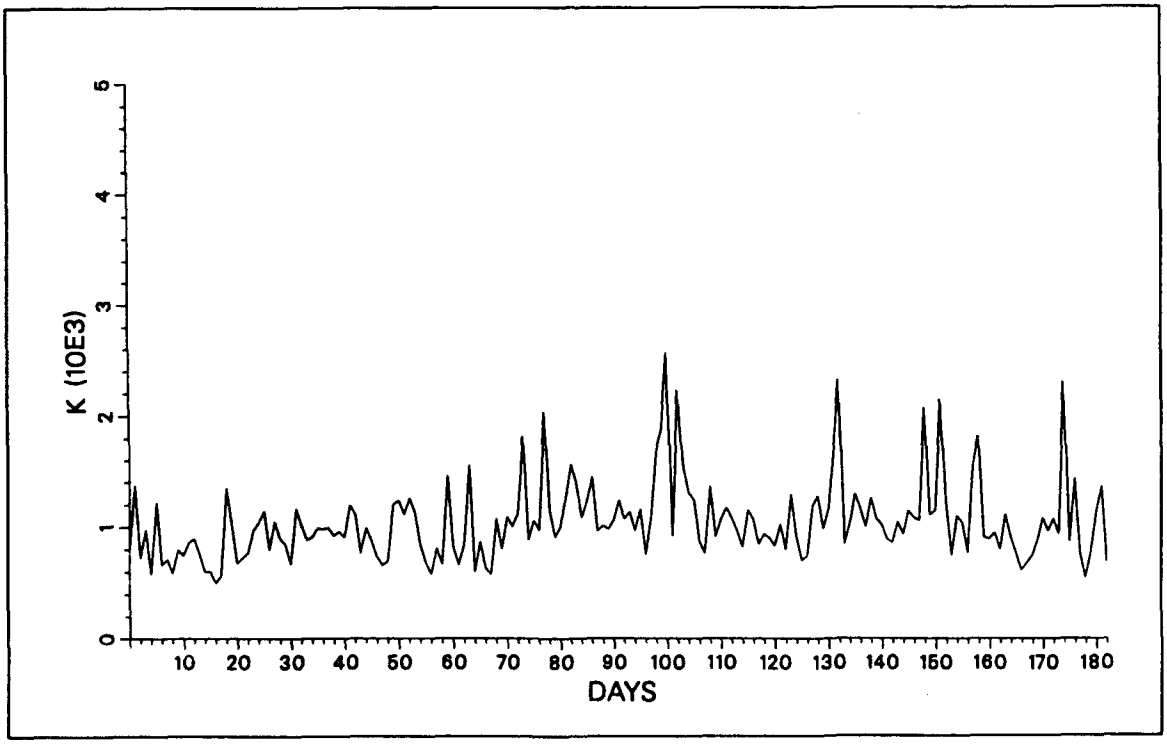

Figure 32. Variation of surface heat exchange coefficient

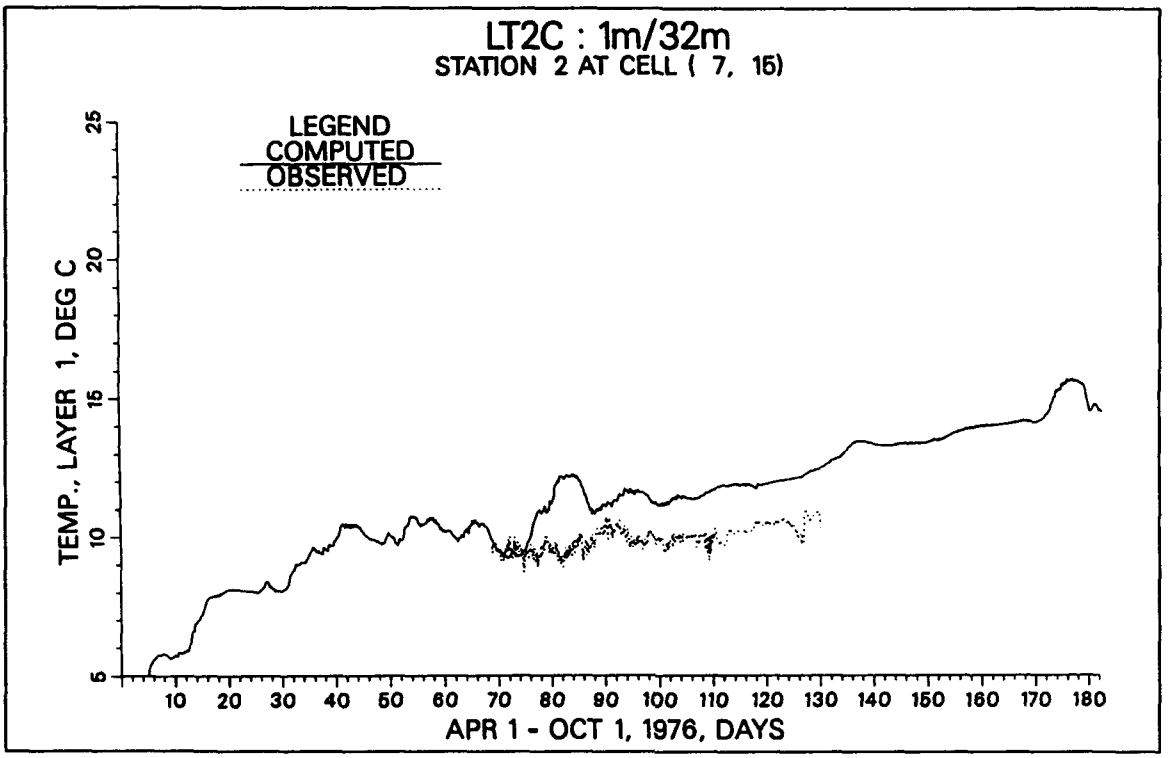

Figure 33. Temperature comparison at LT2C

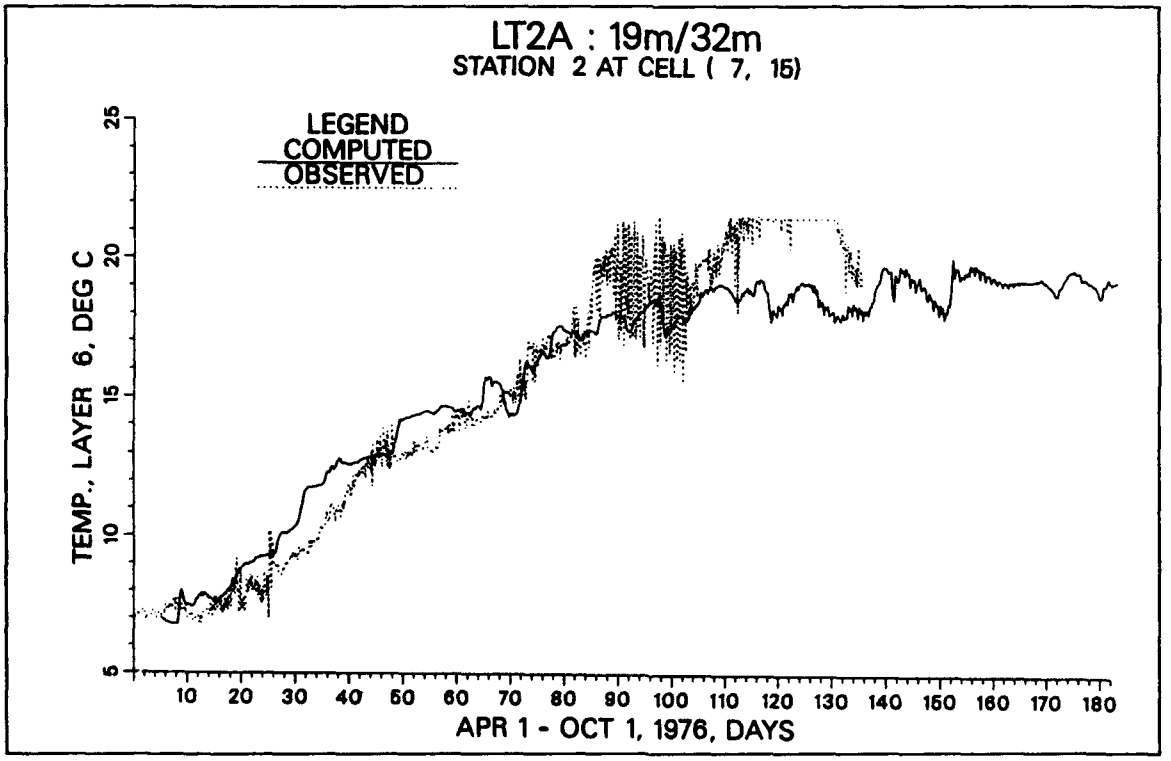

Figure 34. Temperature comparison at LT2A

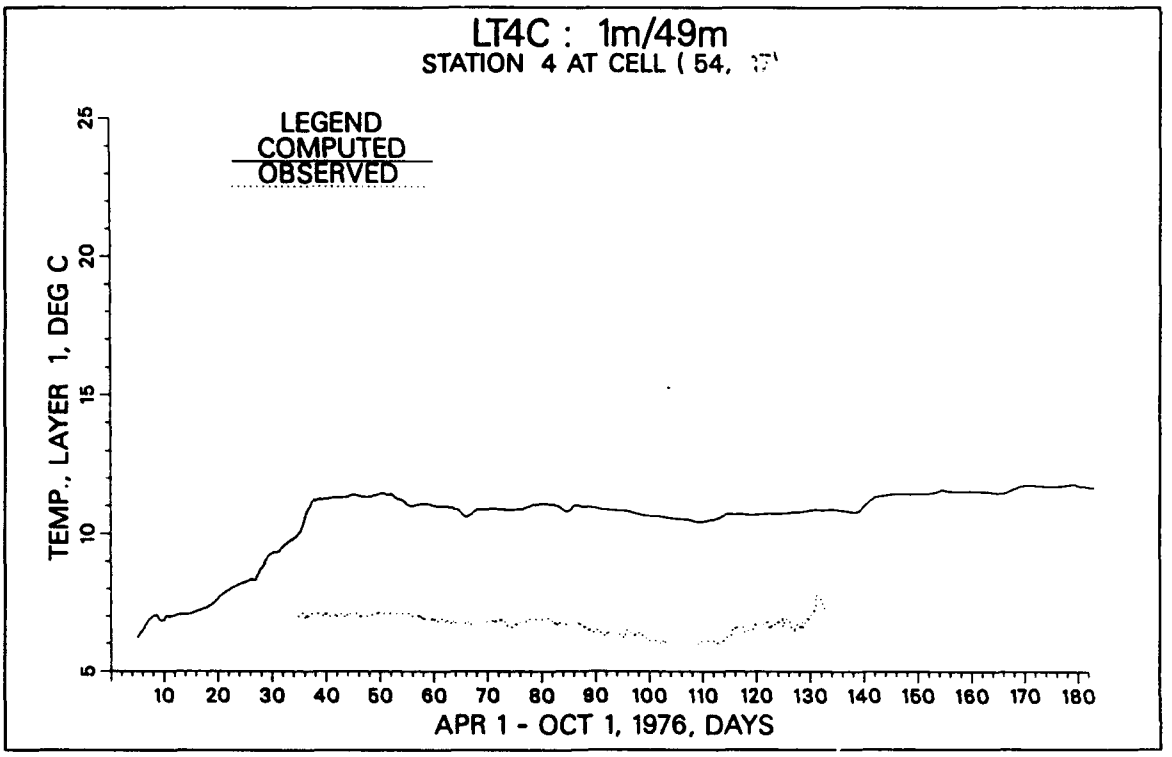

Figure 35. Temperature comparison at LT4C

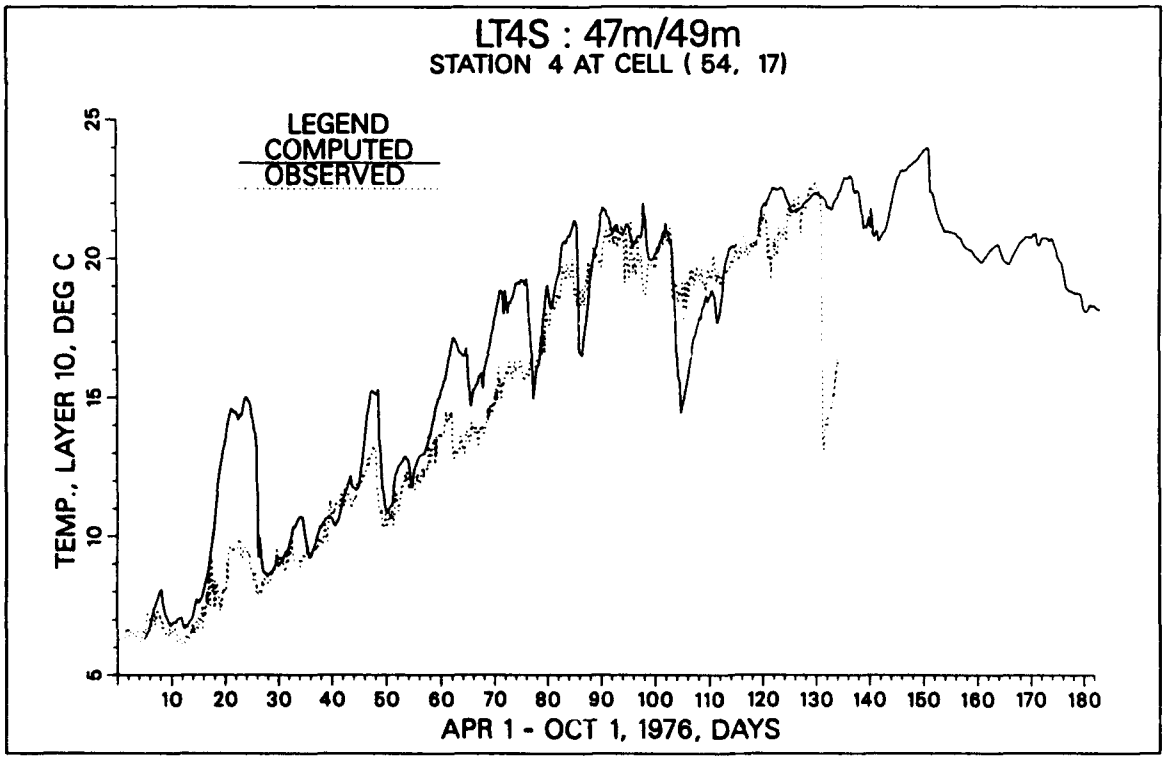

Figure 36. Temperature comparison at LT4S

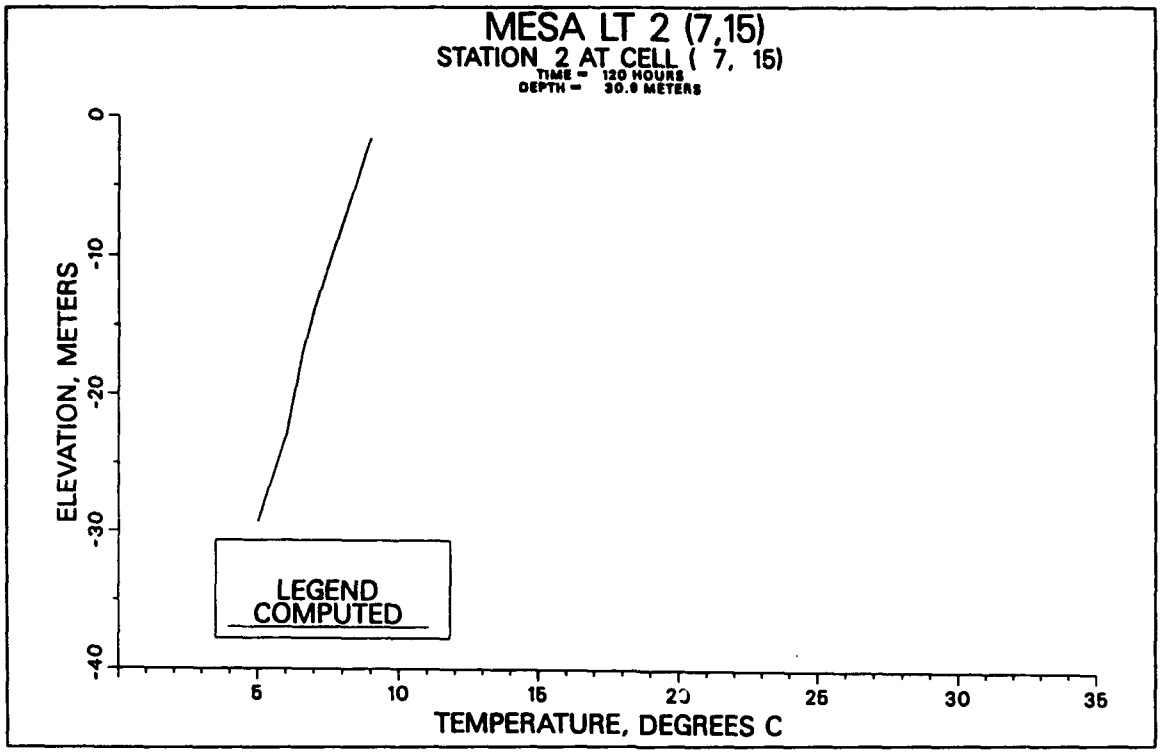

Figure 37. Temperature profile at LT2, 120 hr

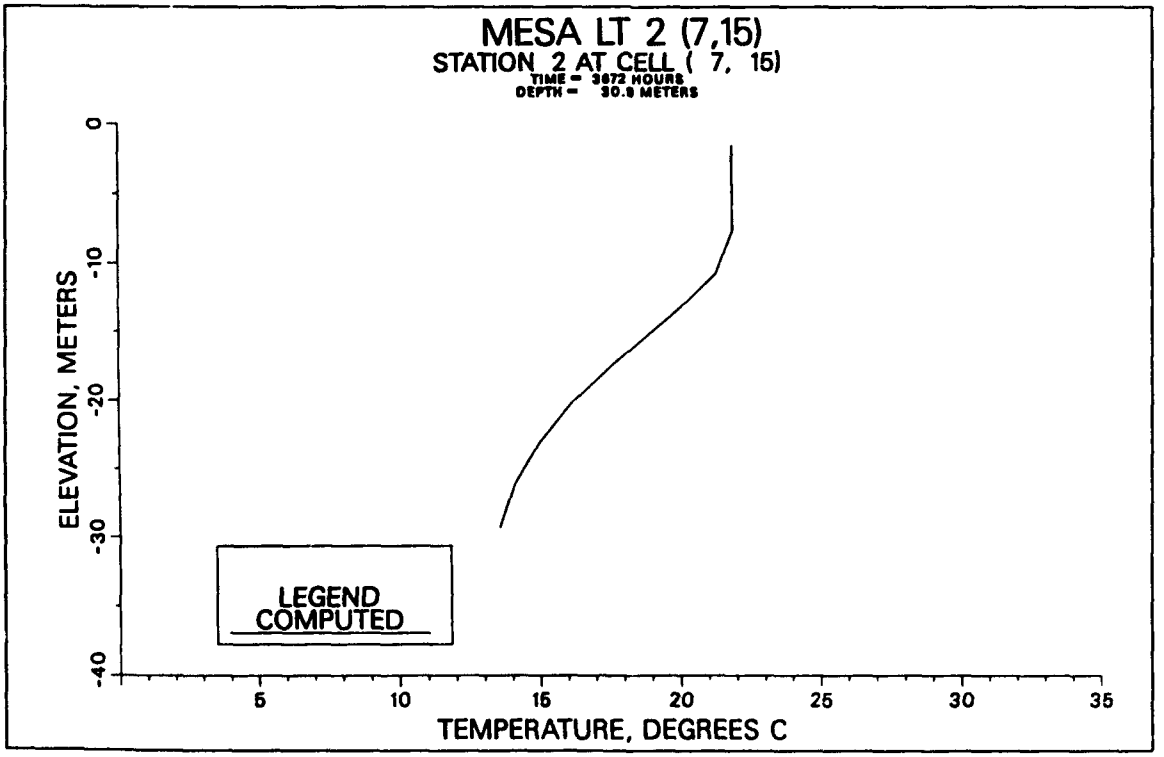

Figure 38. Temperature profile at LT2, 3672 hr

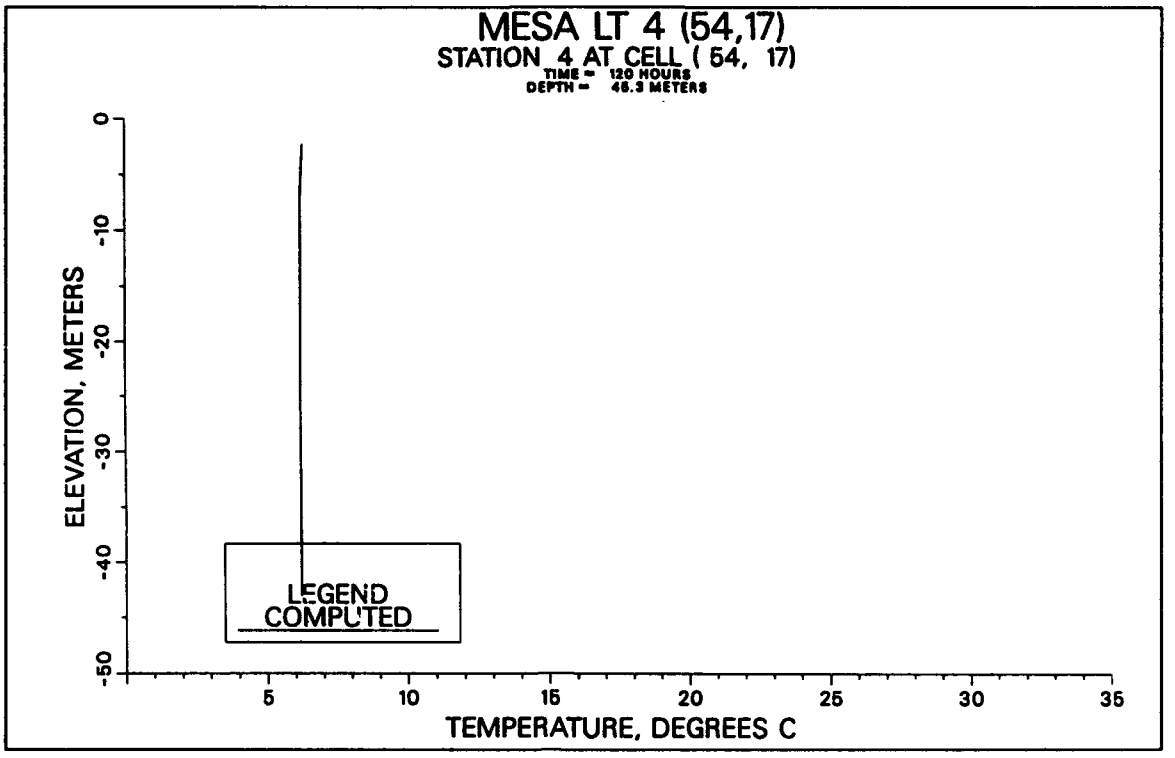

Figure 39. Temperature profile at LT4, 120 hr

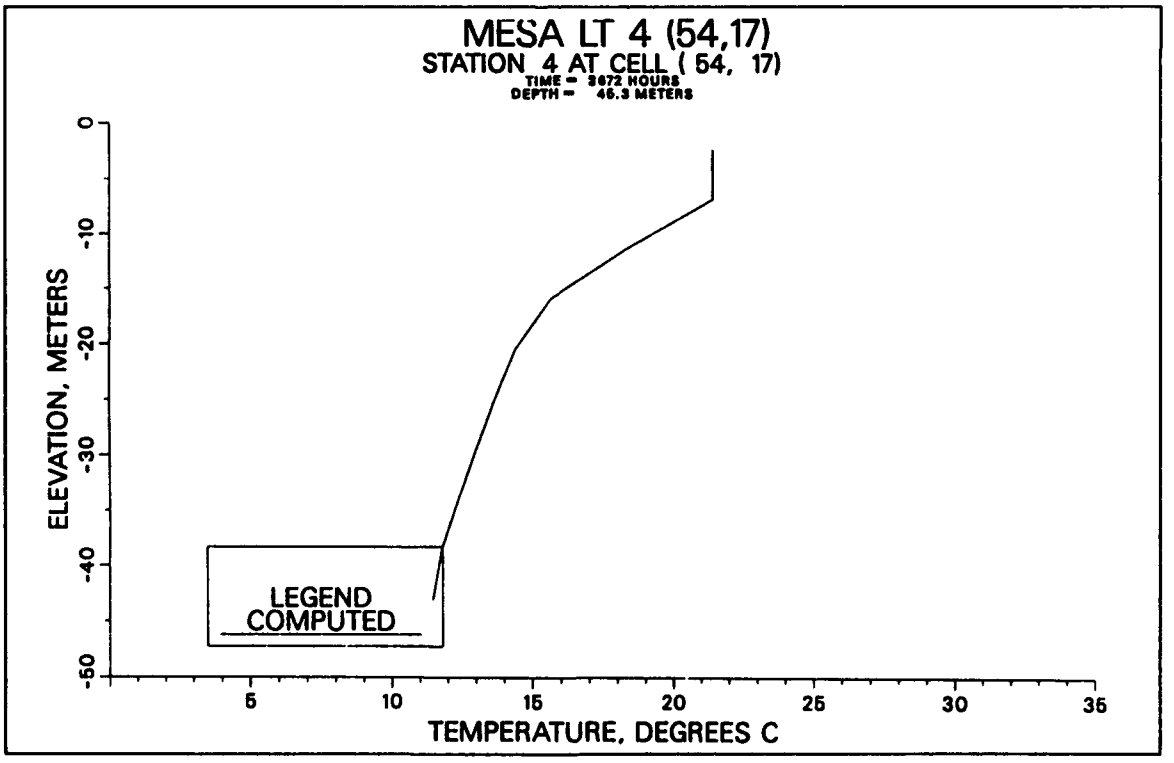

Figure 40. Temperature profile at LT4, 3672 hr

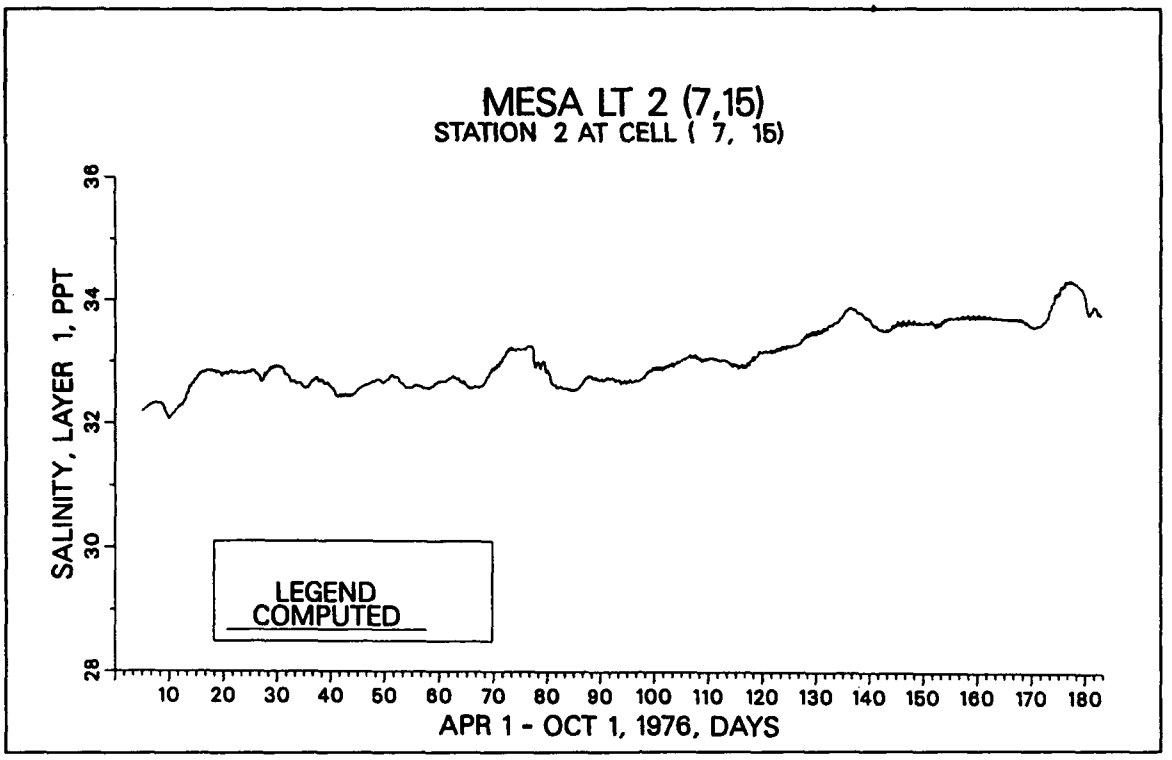

Figure 41. Variation of computed salinity at LT2, layer 1

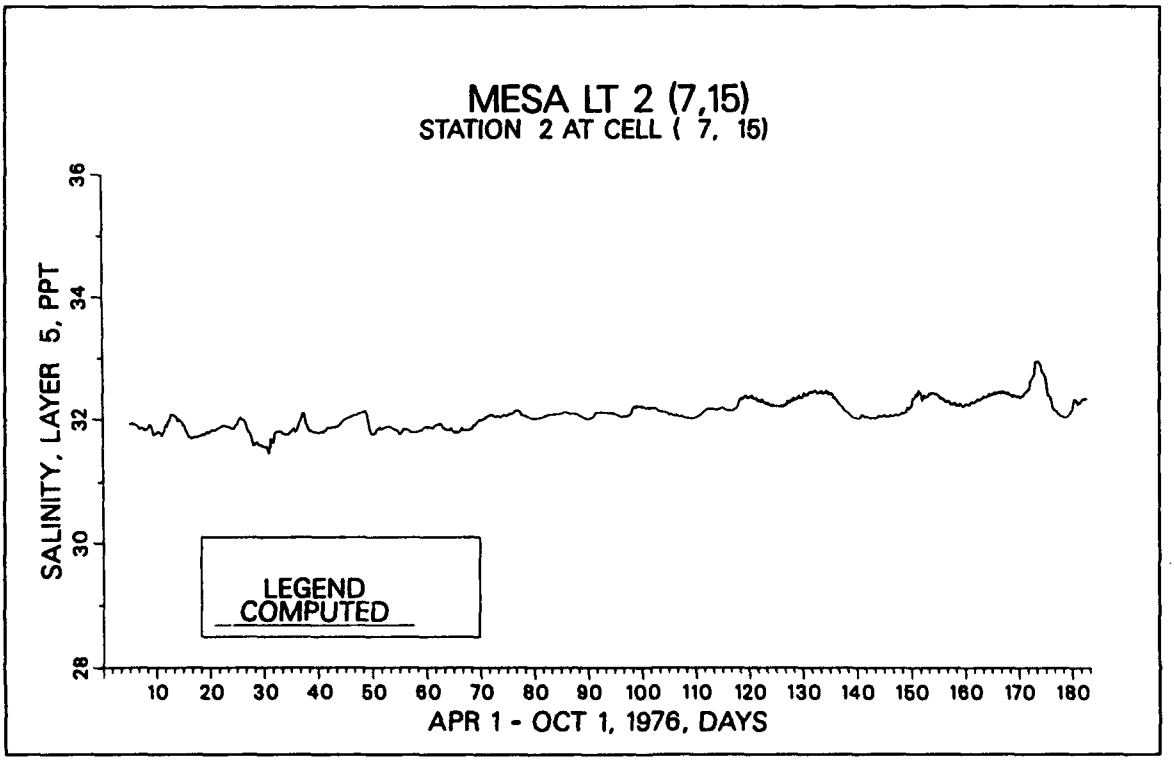

Figure 42. Variation of computed salinity at LT2, layer 5

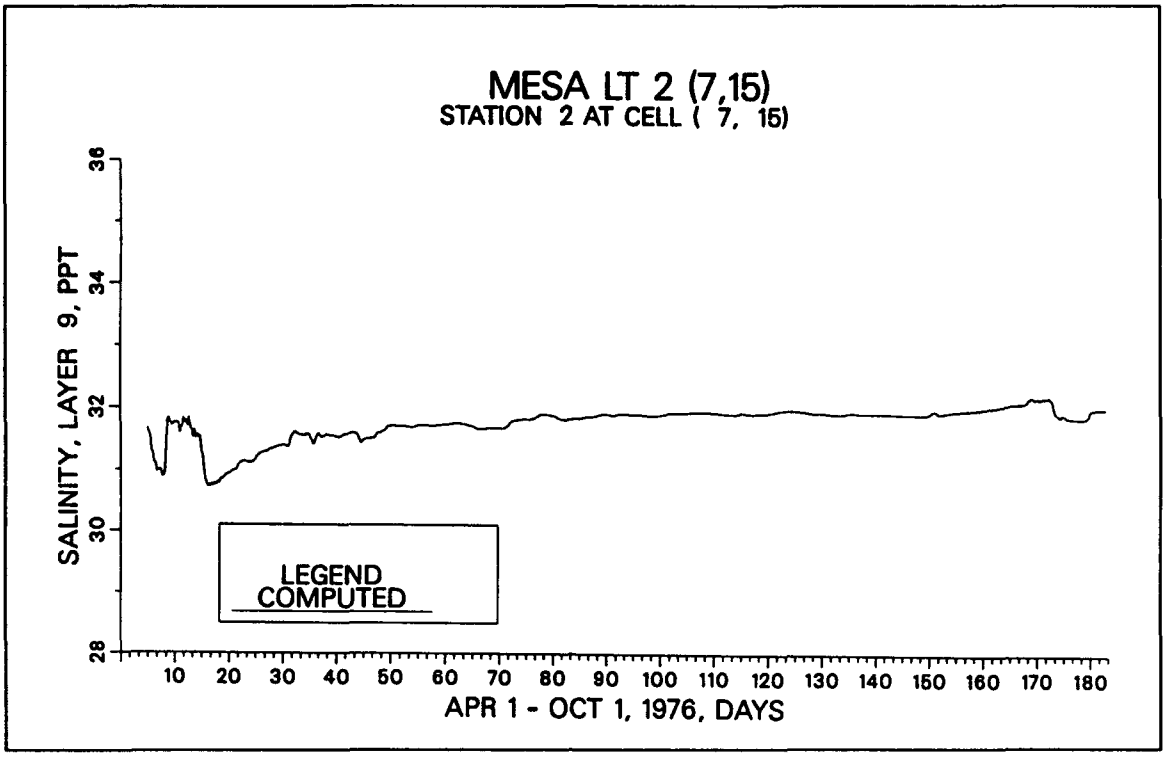

Figure 43. Variation of computed salinity at LT2, layer 9

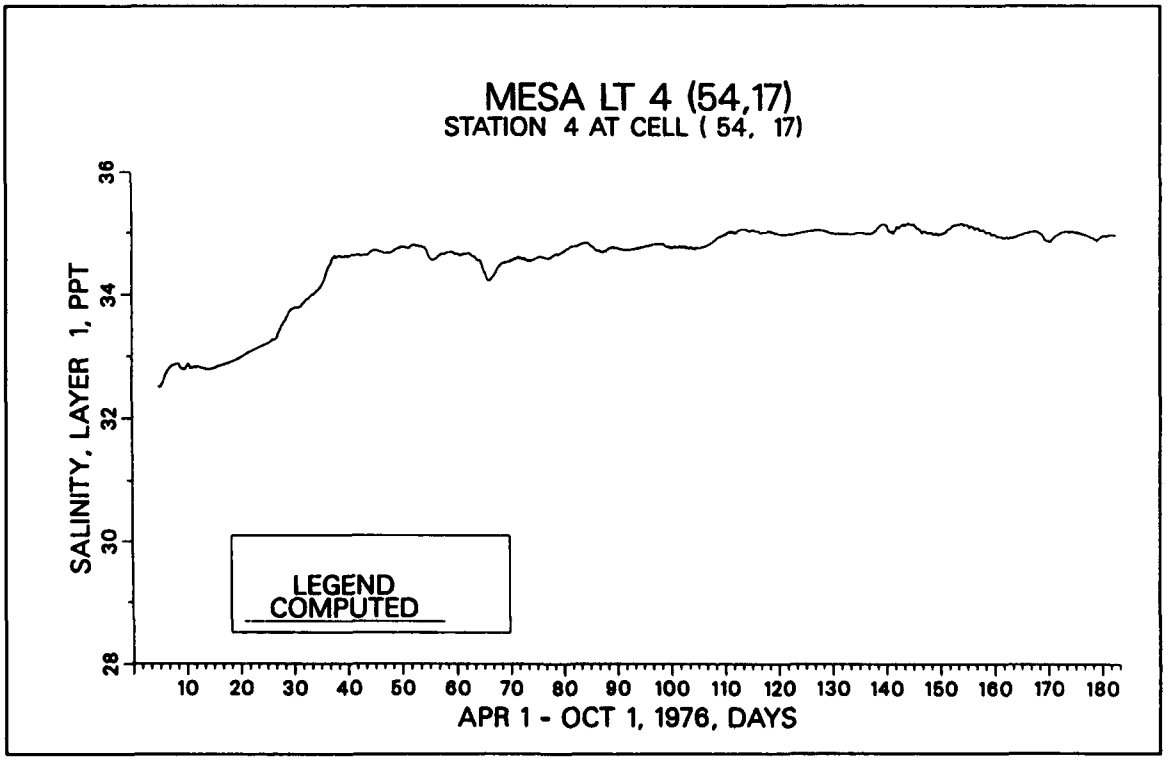

Figure 44. Variation of computed salinity at LT4, layer 1

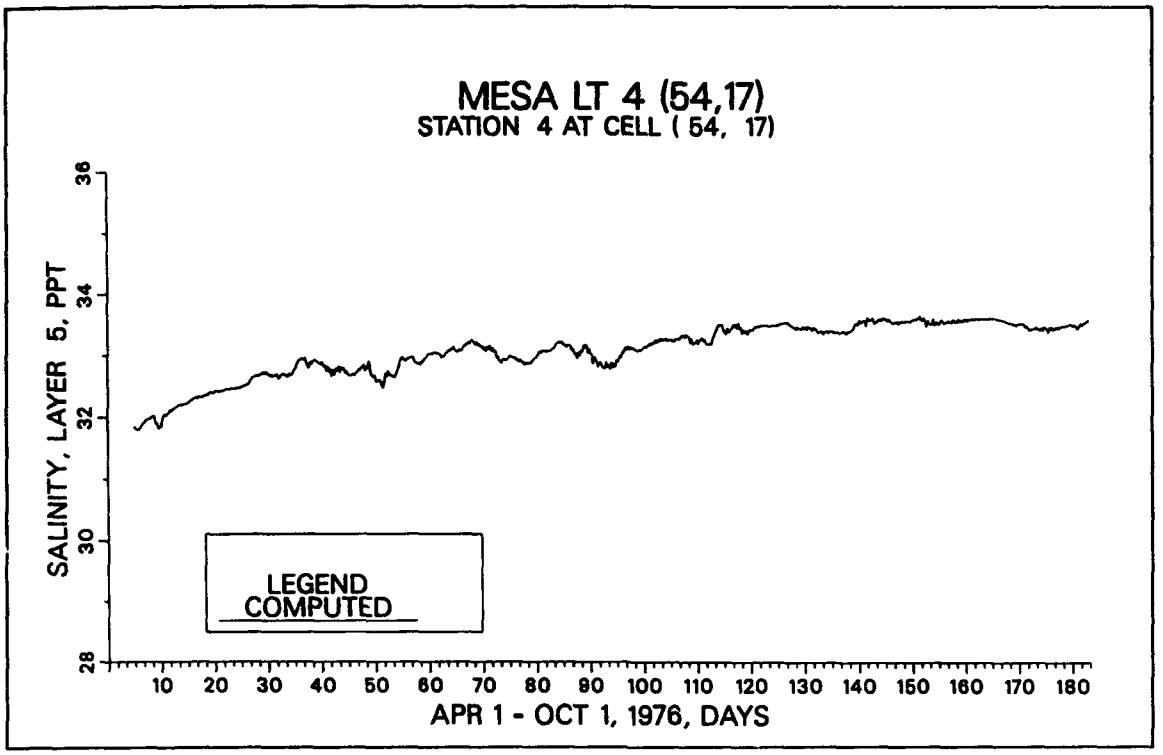

Figure 45. Variation of computed salinity at LT4, layer 5

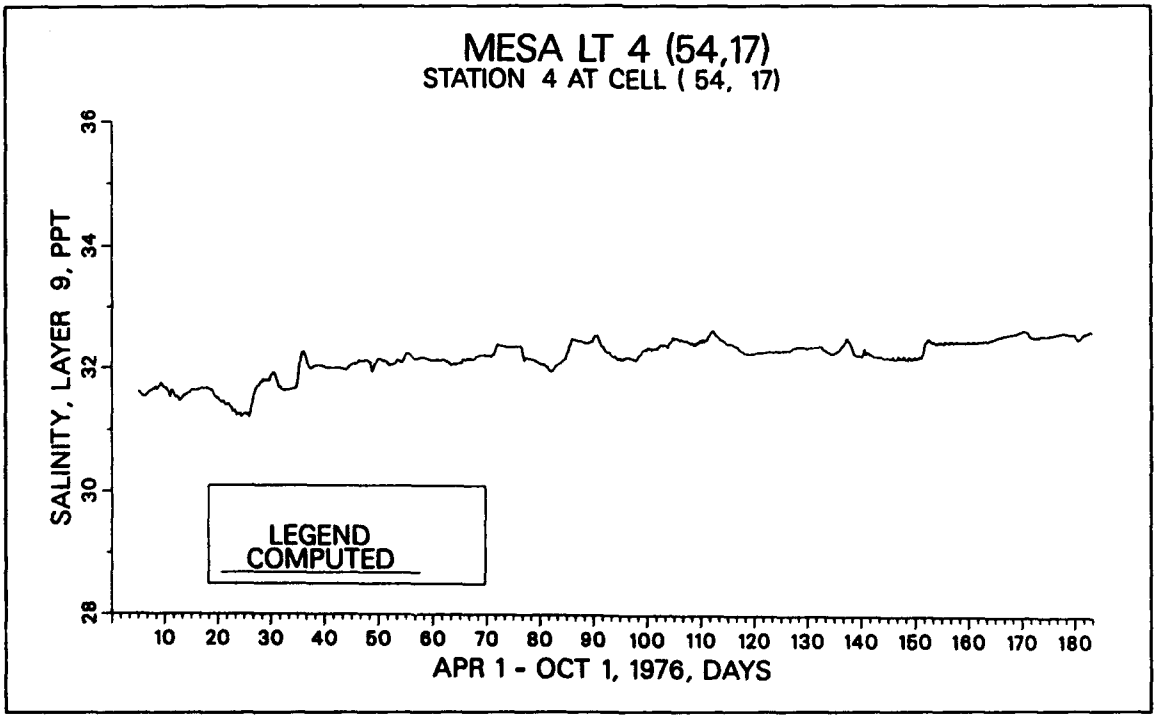

Figure 46. Variation of computed salinity at LT4, layer 9

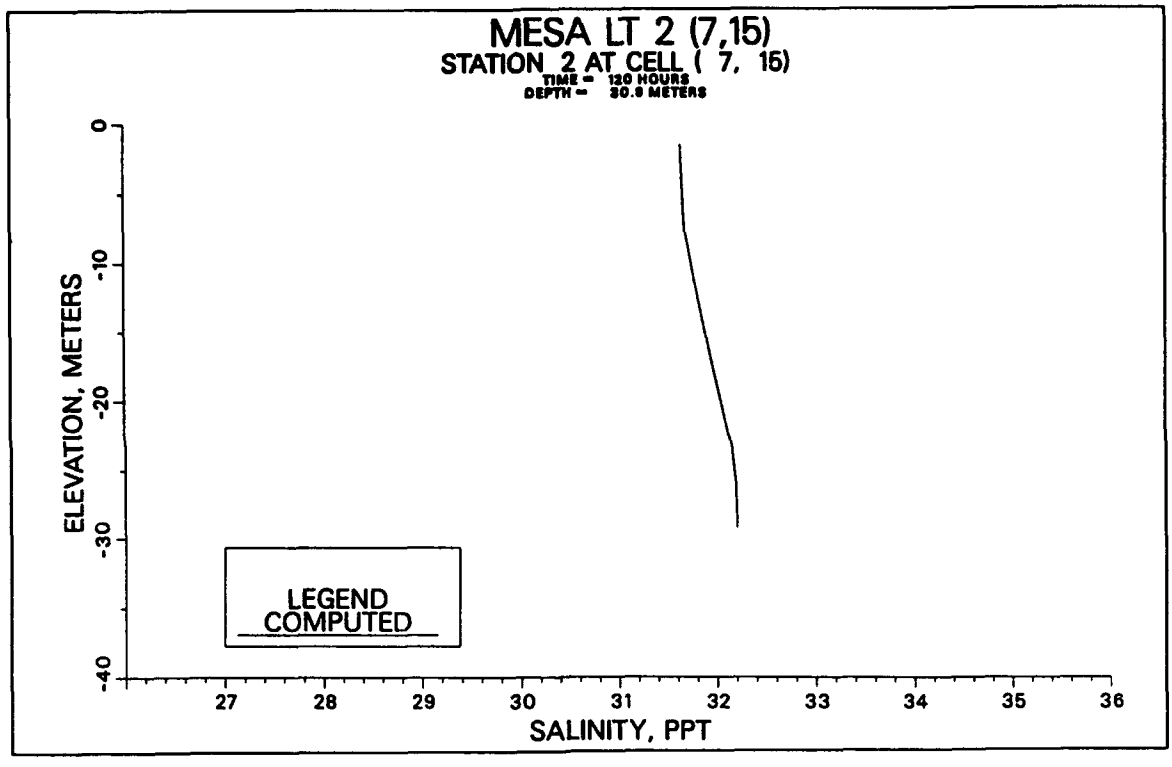

Figure 47. Salinity profile at LT2 at 120 hr

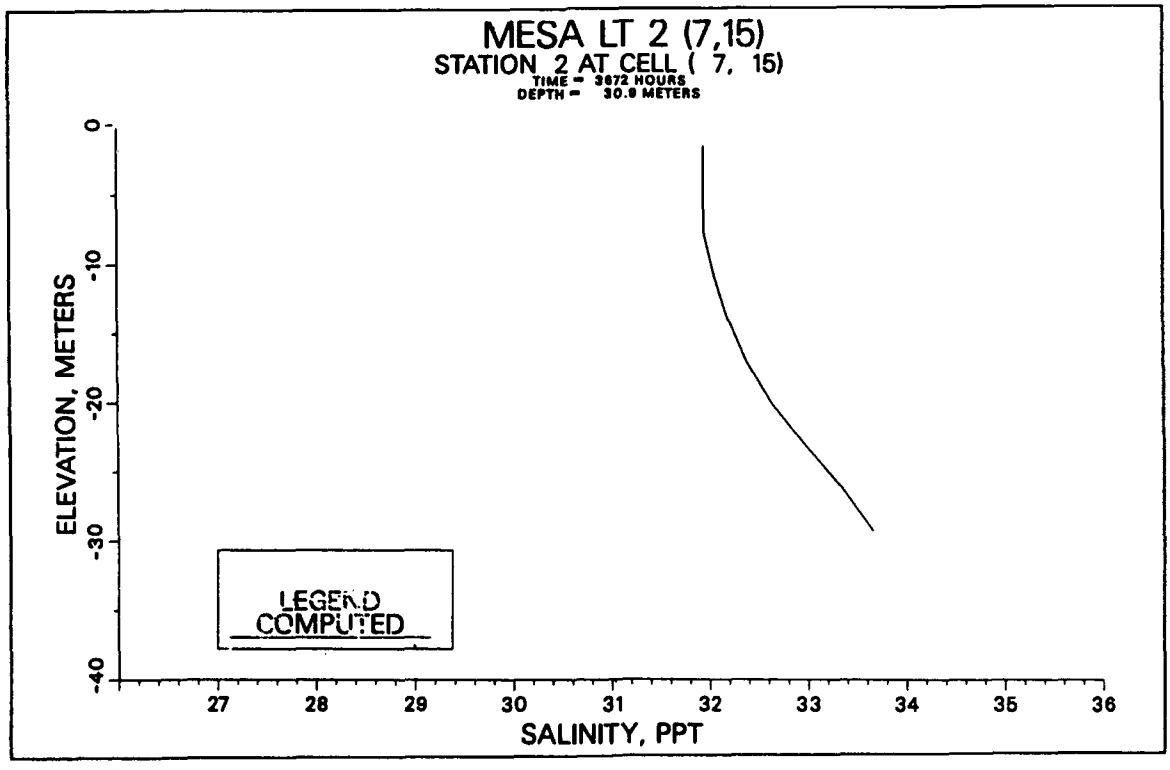

Figure 48. Salinity profile at LT2 at 3672 hr

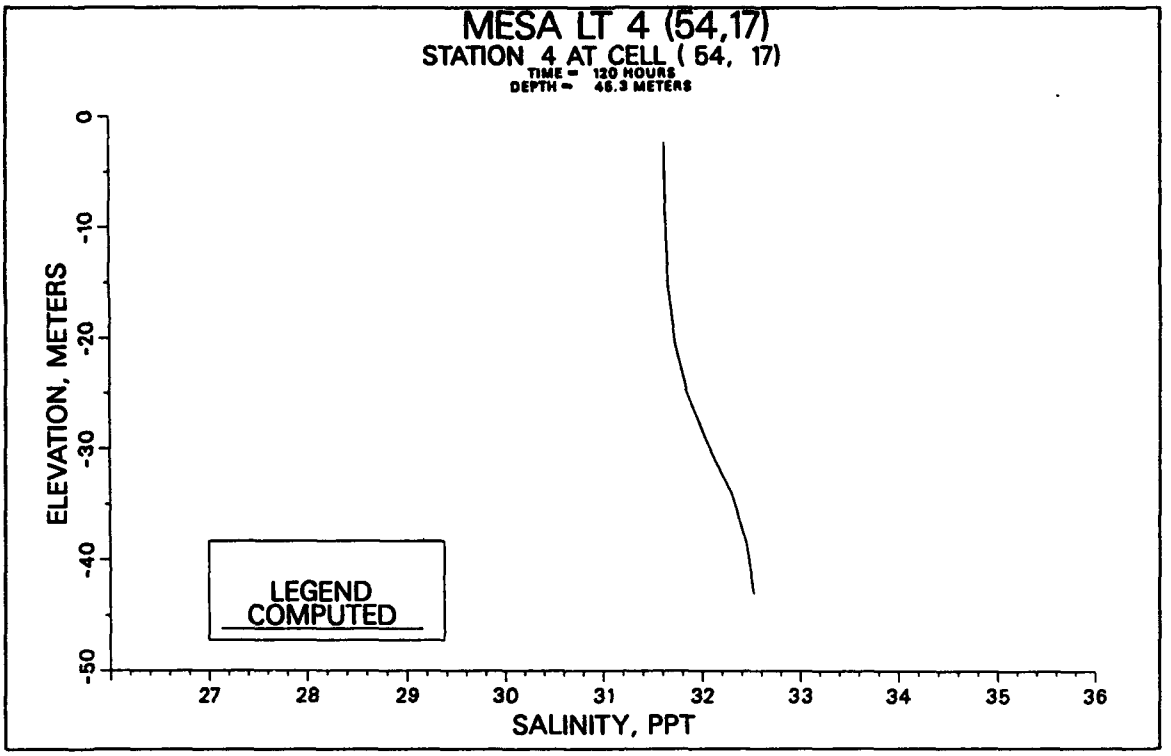

Figure 49. Salinity profile at LT4 at 120 hr

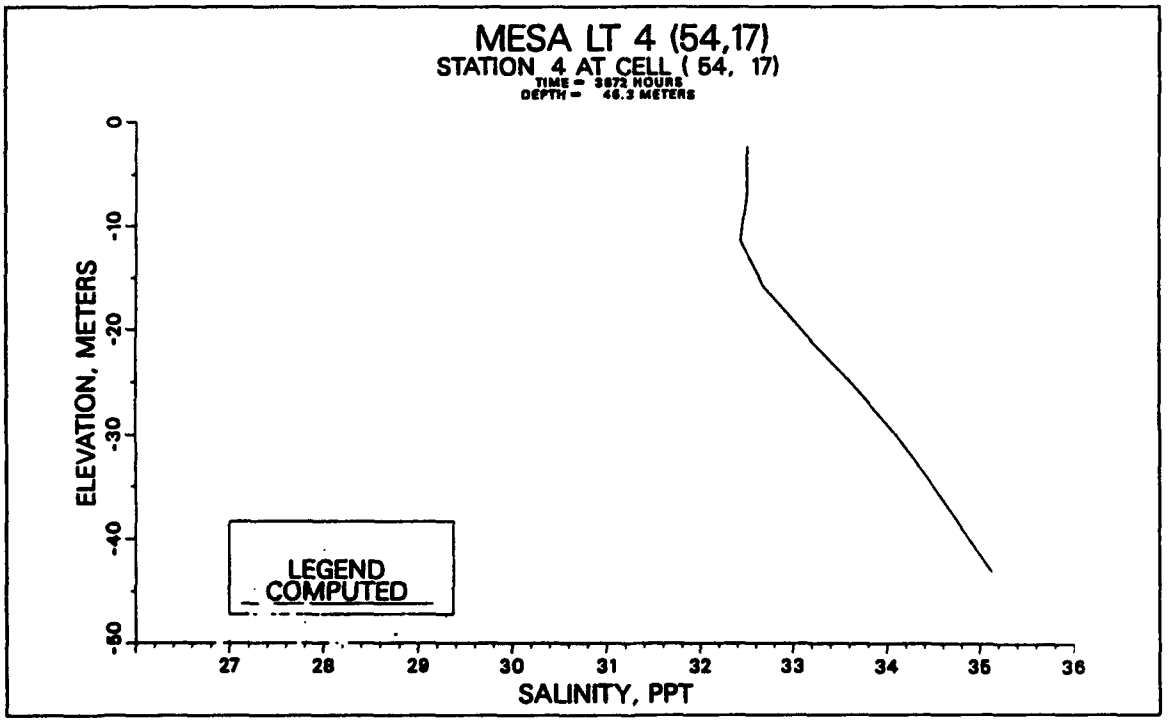

Figure 50. Salinity profile at LT4 at 3672 hr

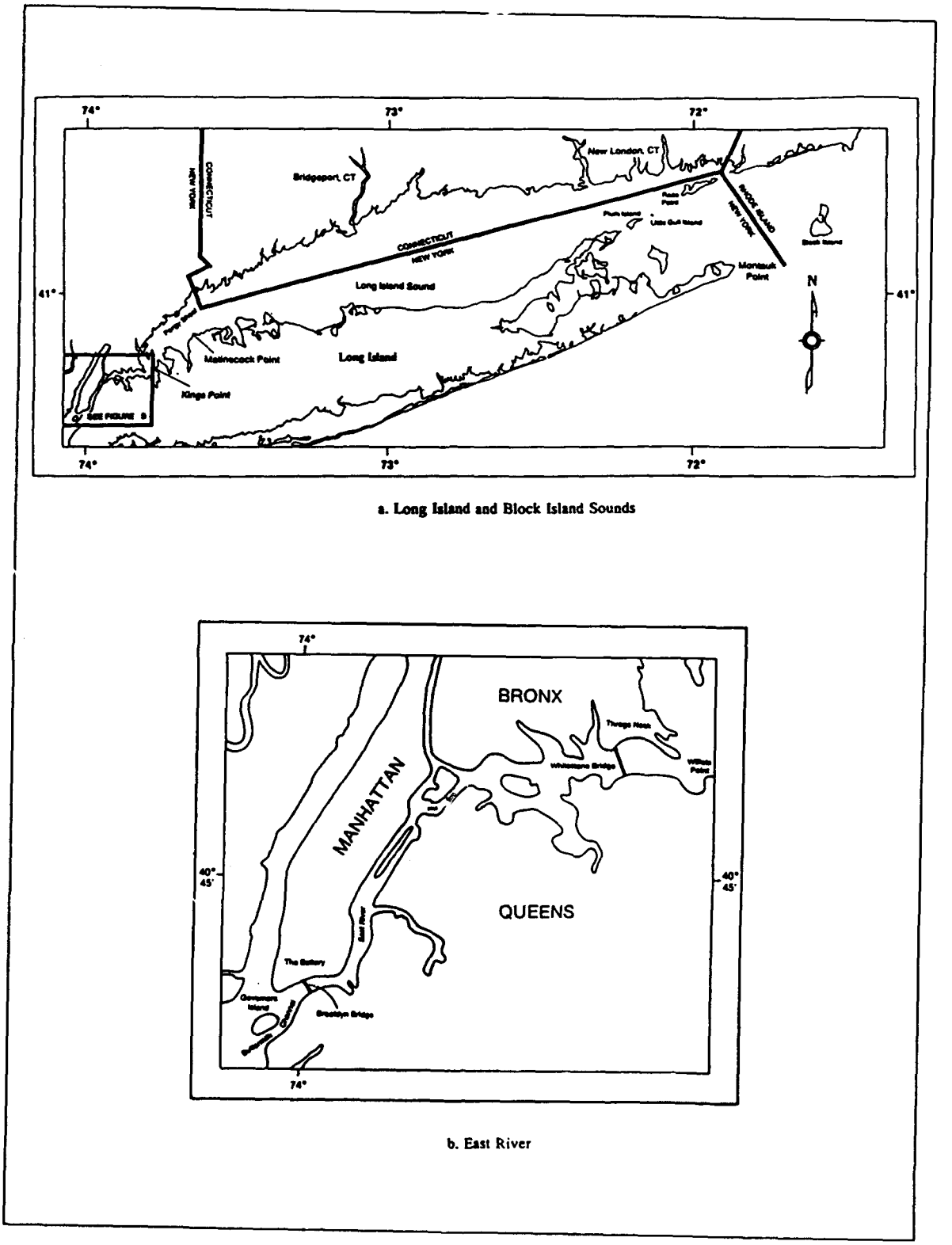

a. Long Island and Block Island Sounds

b. East River

Figure 51. Long Island Sound and vicinity (Earwaker 1990)

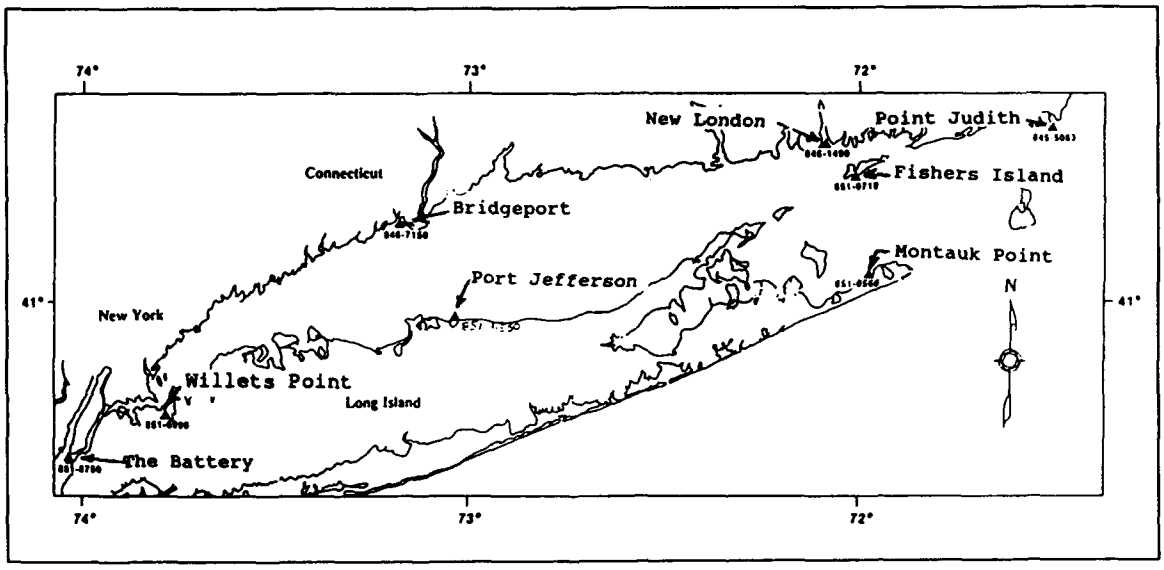

Figure 52. Extended verification water level station locations

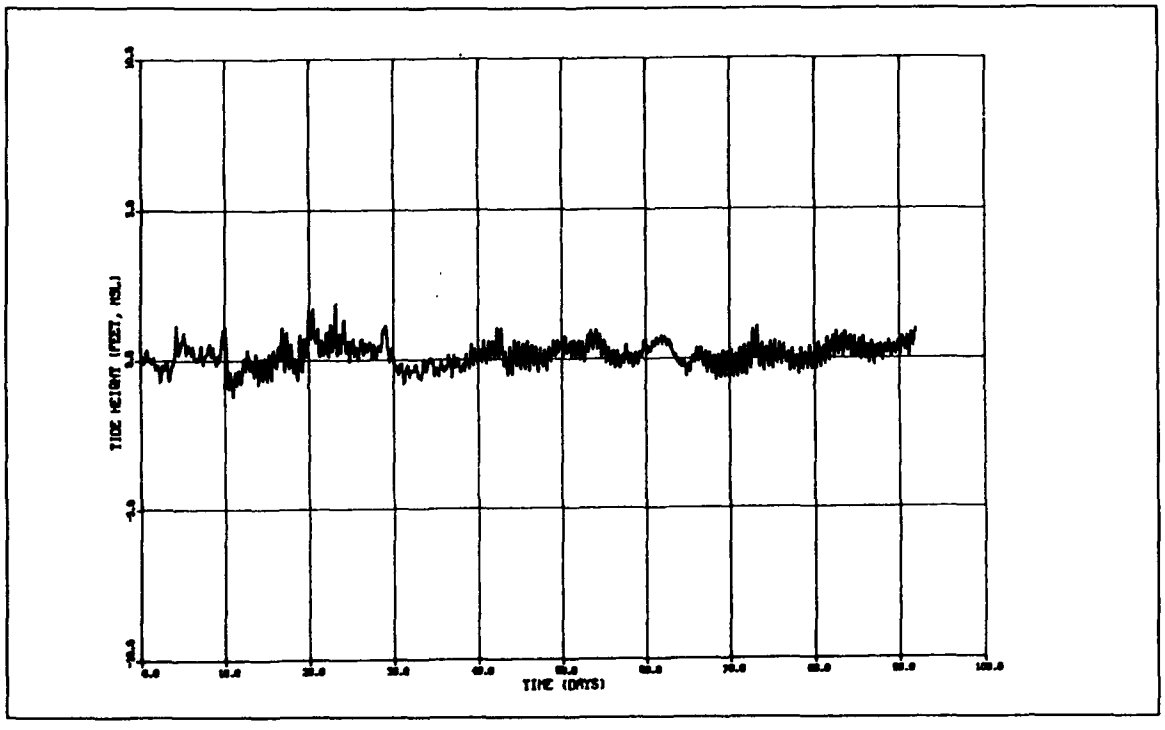

Figure 53. Residual water surface elevation for Bridgeport

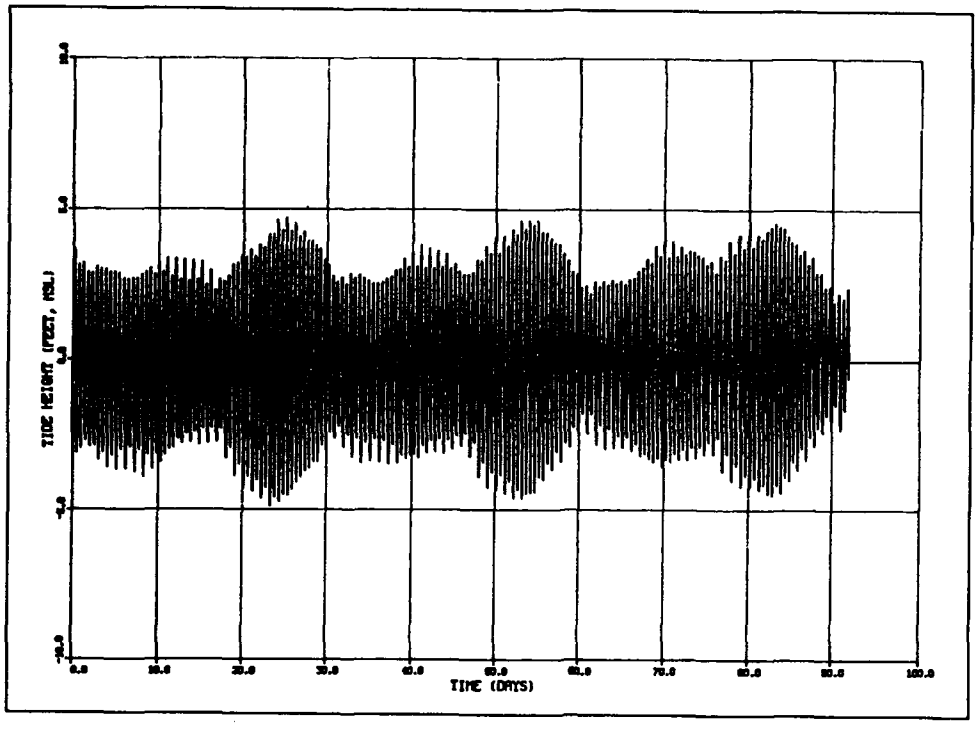

Figure 54. Tidal constituent-based tide for Bridgeport

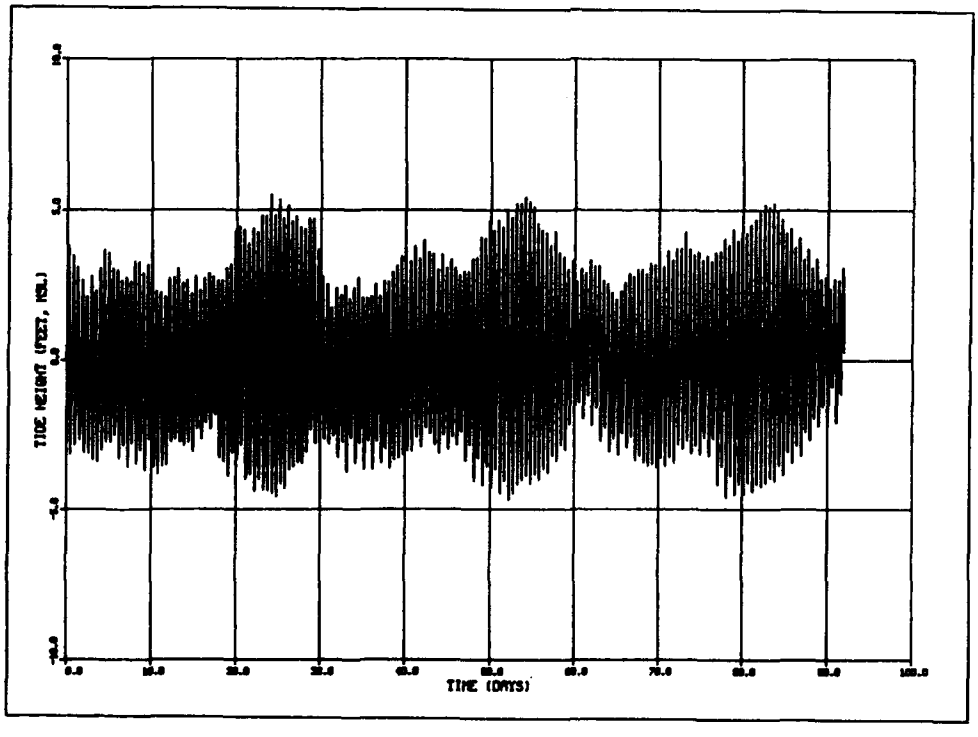

Figure 55. Harmonic-plus-residual reconstructed water surface elevation for Bridgeport

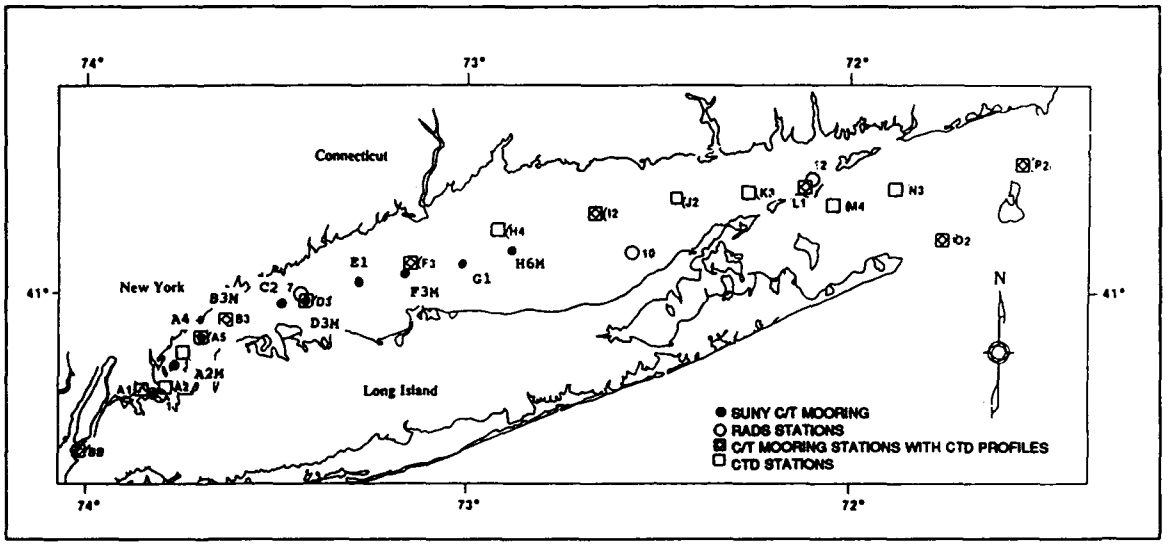

Figure 56. Program monitoring station locations

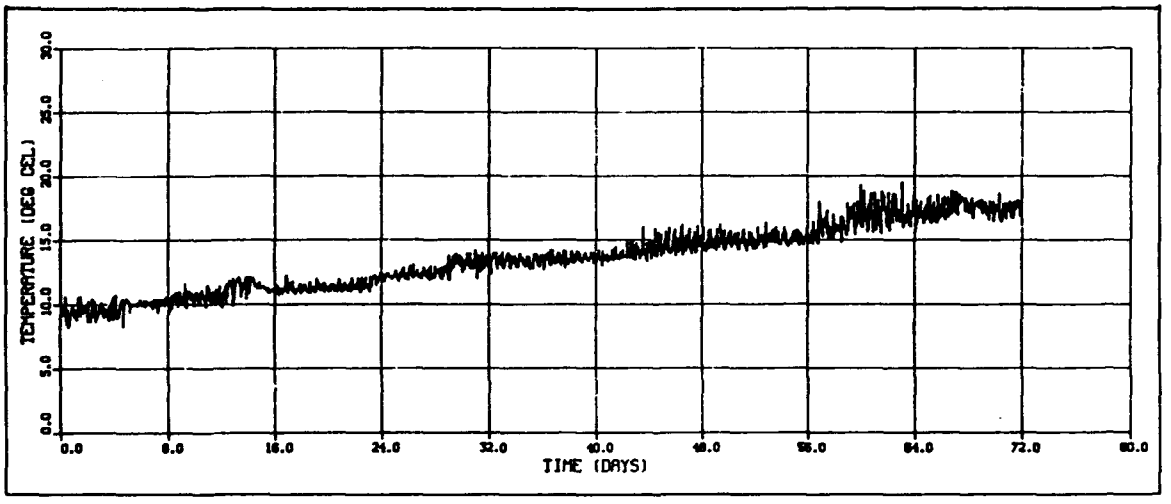

Figure 57. Temperature time series for C/T station F3U406D1

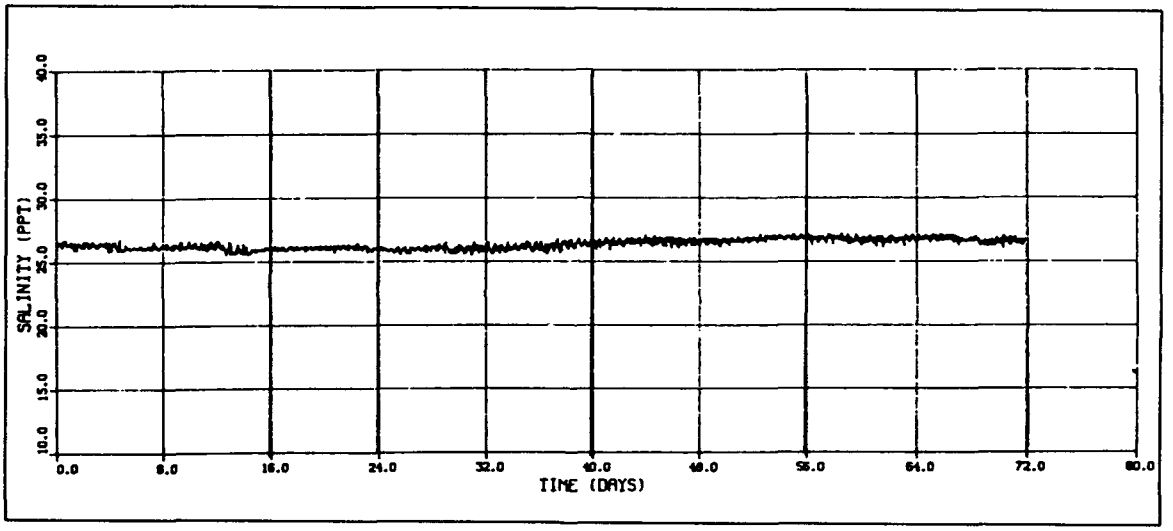

Figure 58. Salinity time series for C/T Station F3L421D1

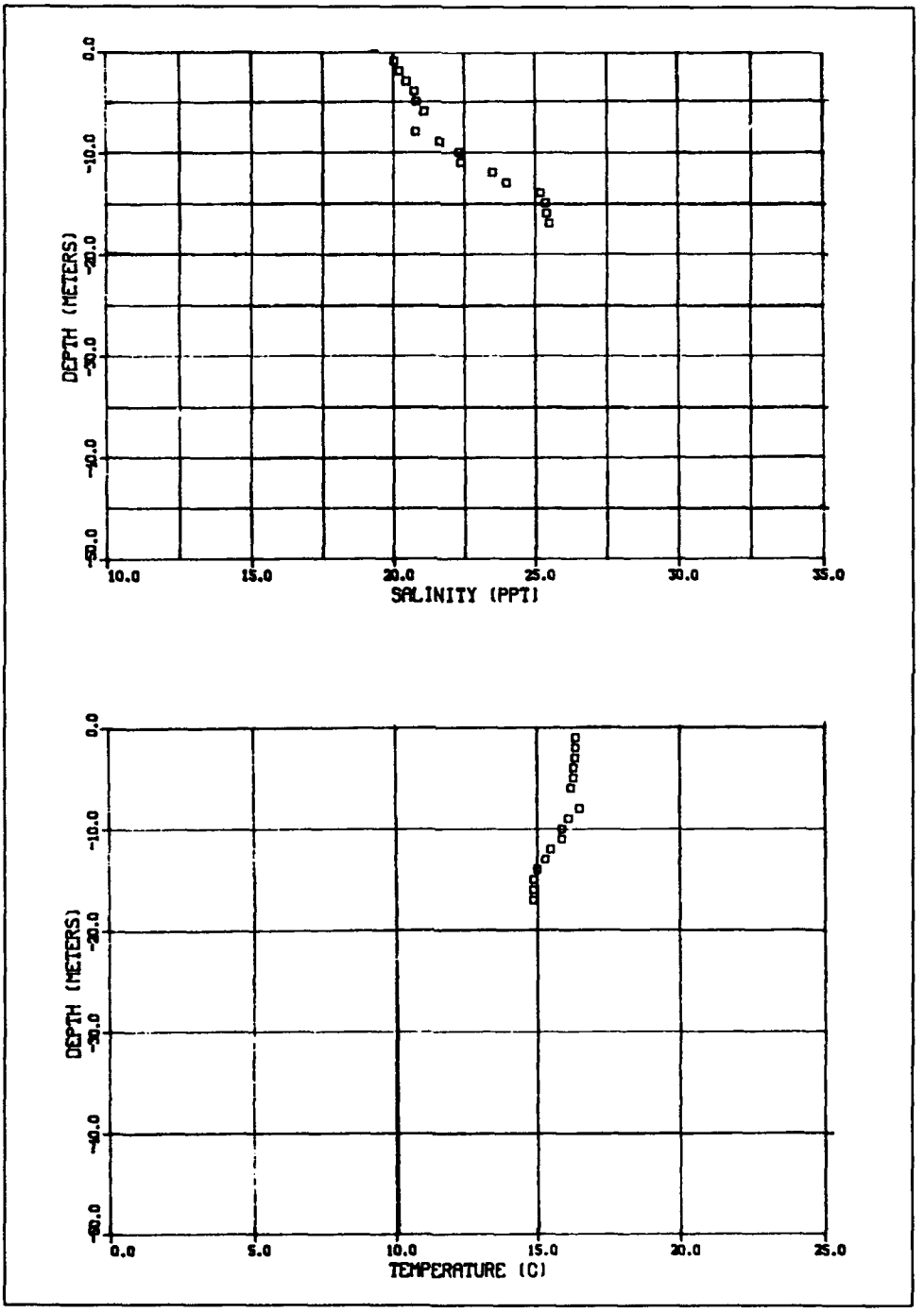

Figure 59. NOAA CTD station BB profile data

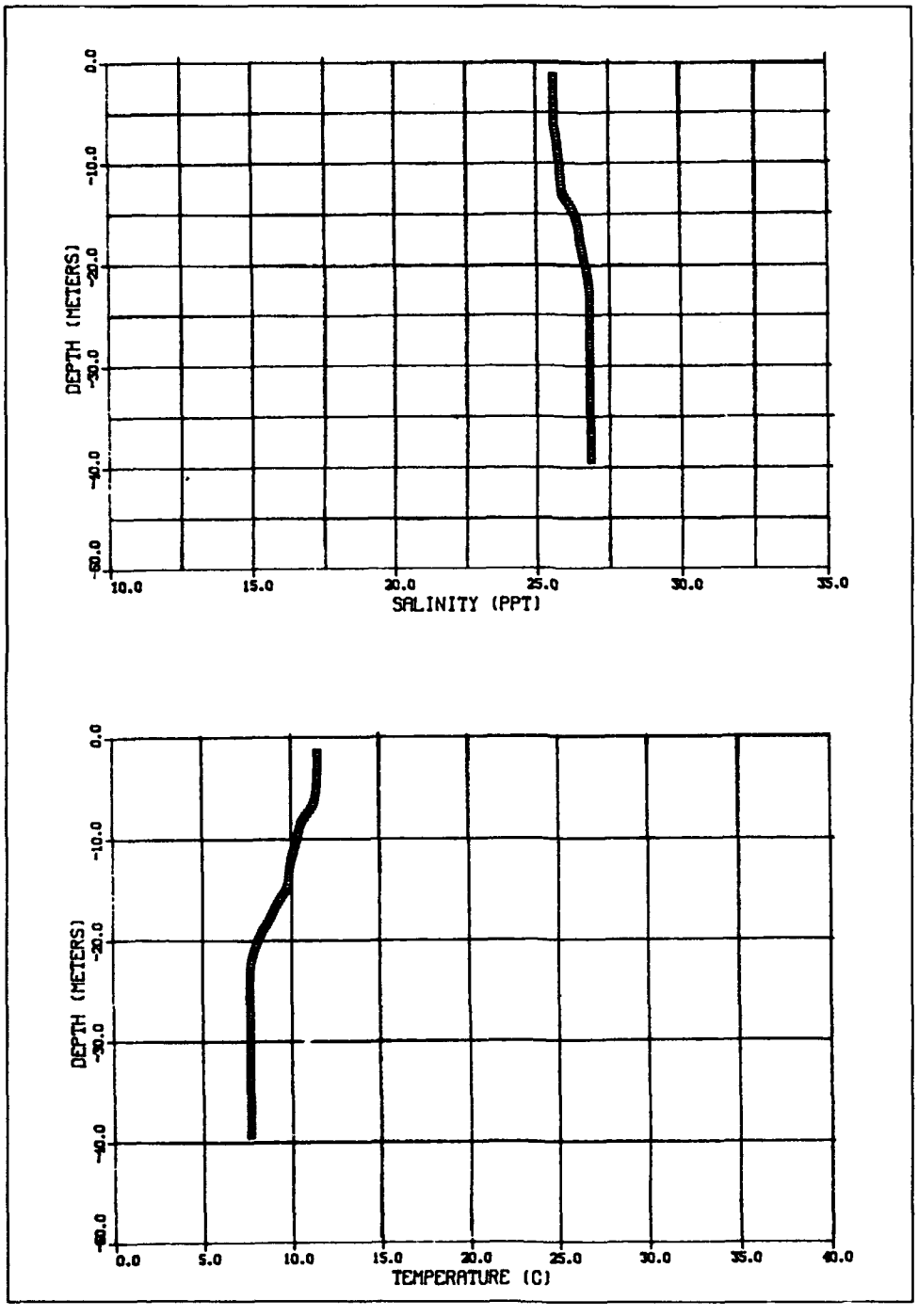

Figure 60. Suny CTD station E1 profile data

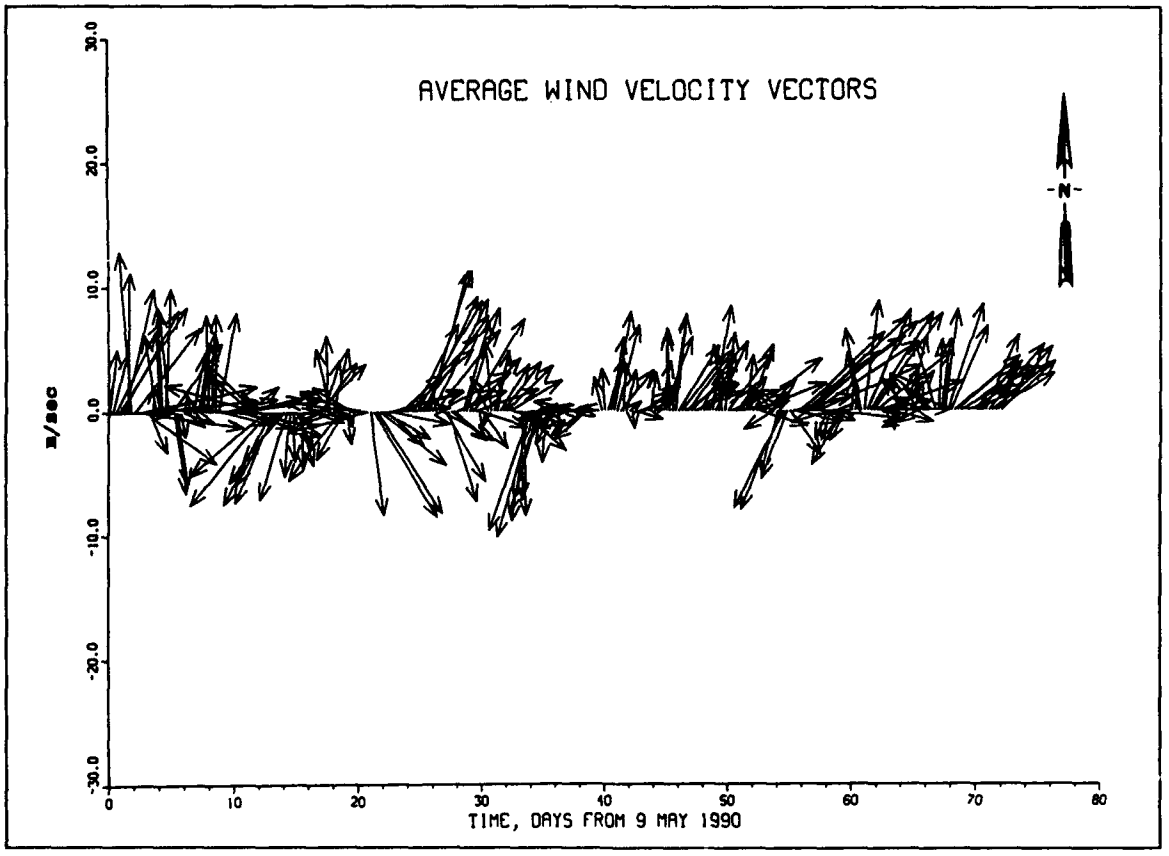

Figure 61. Average WIS winds used for Long Island Sound validation

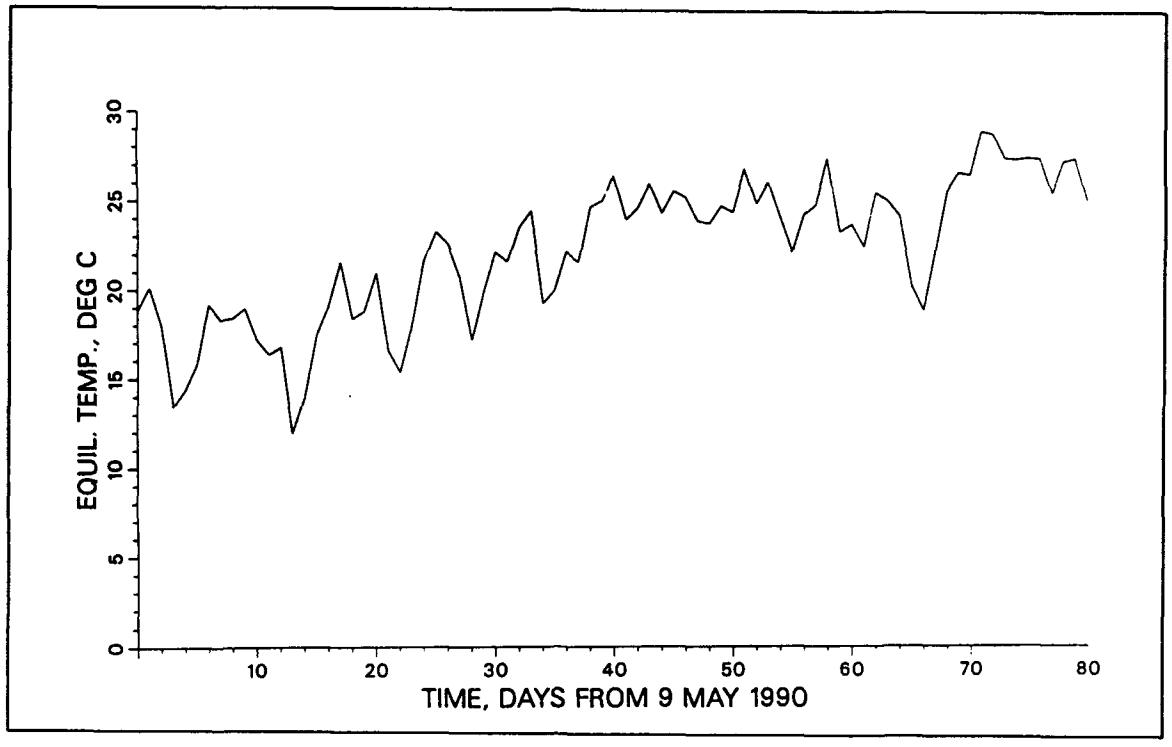

Figure 62. Variation of equilibrium temperature, May-July 1990

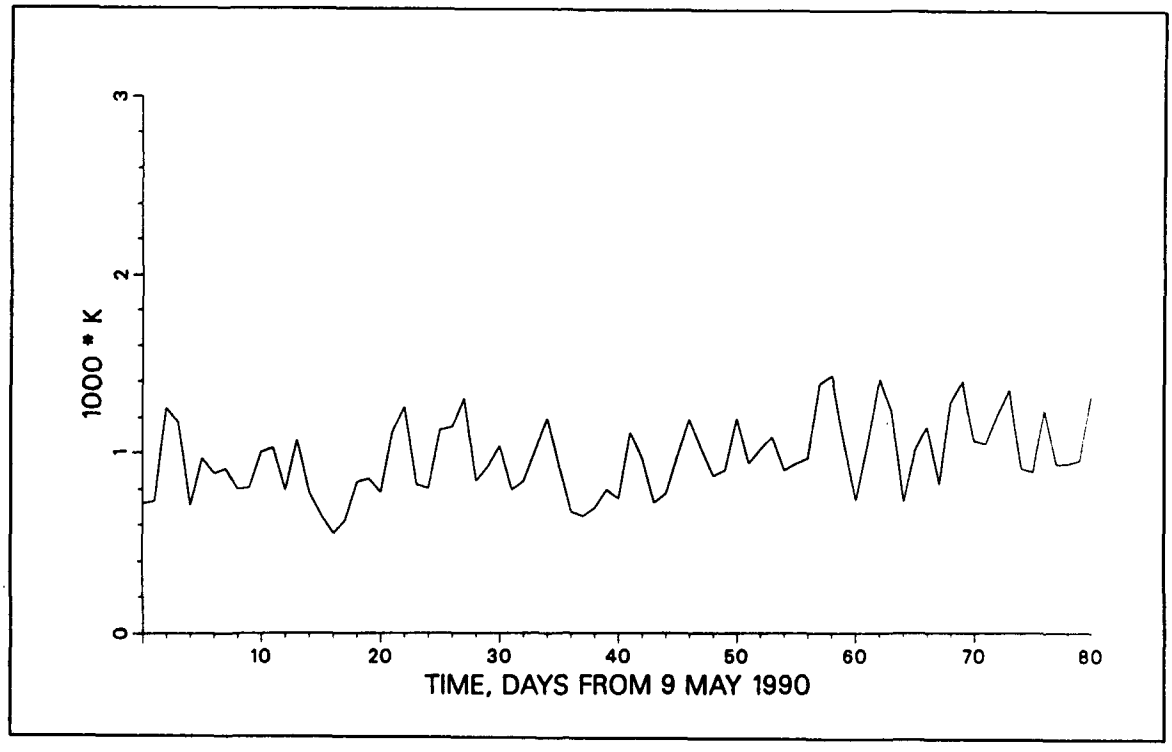

Figure 63. Variation of heat exchange coefficient, May-July 1990

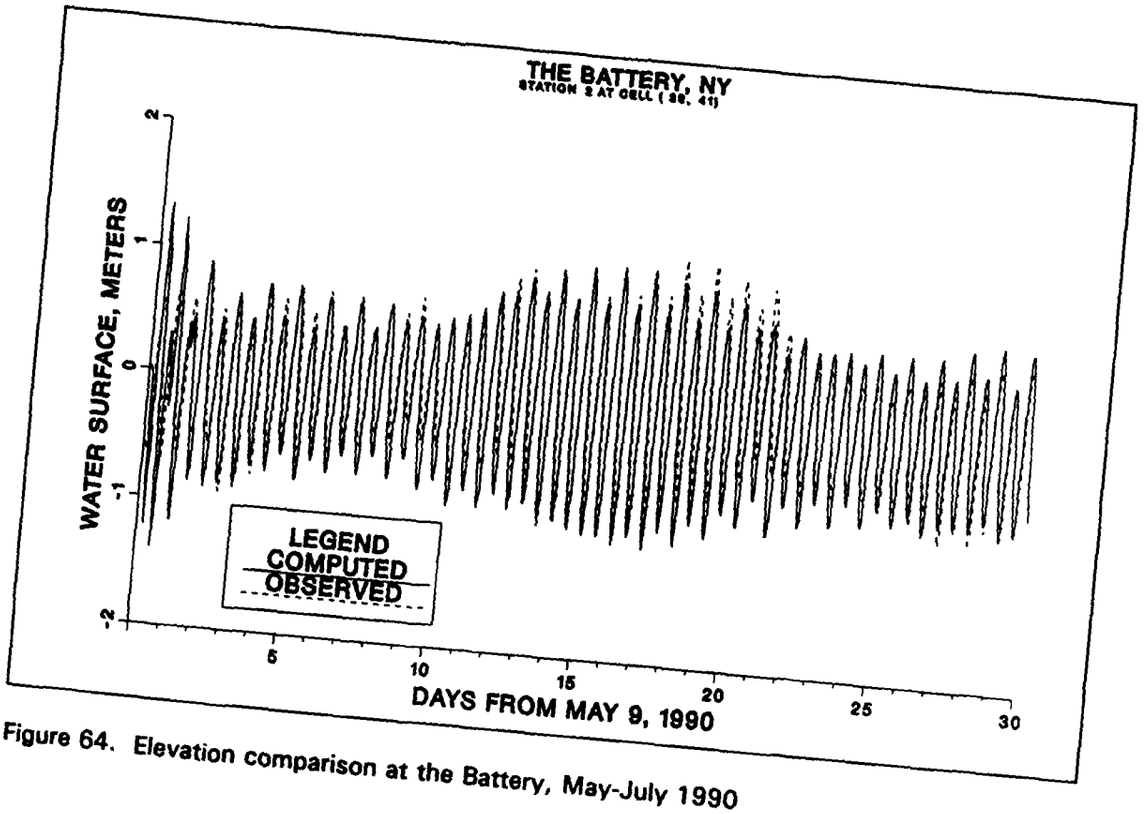

Figure 64. Elevation comparison at the Battery, May-July 1990

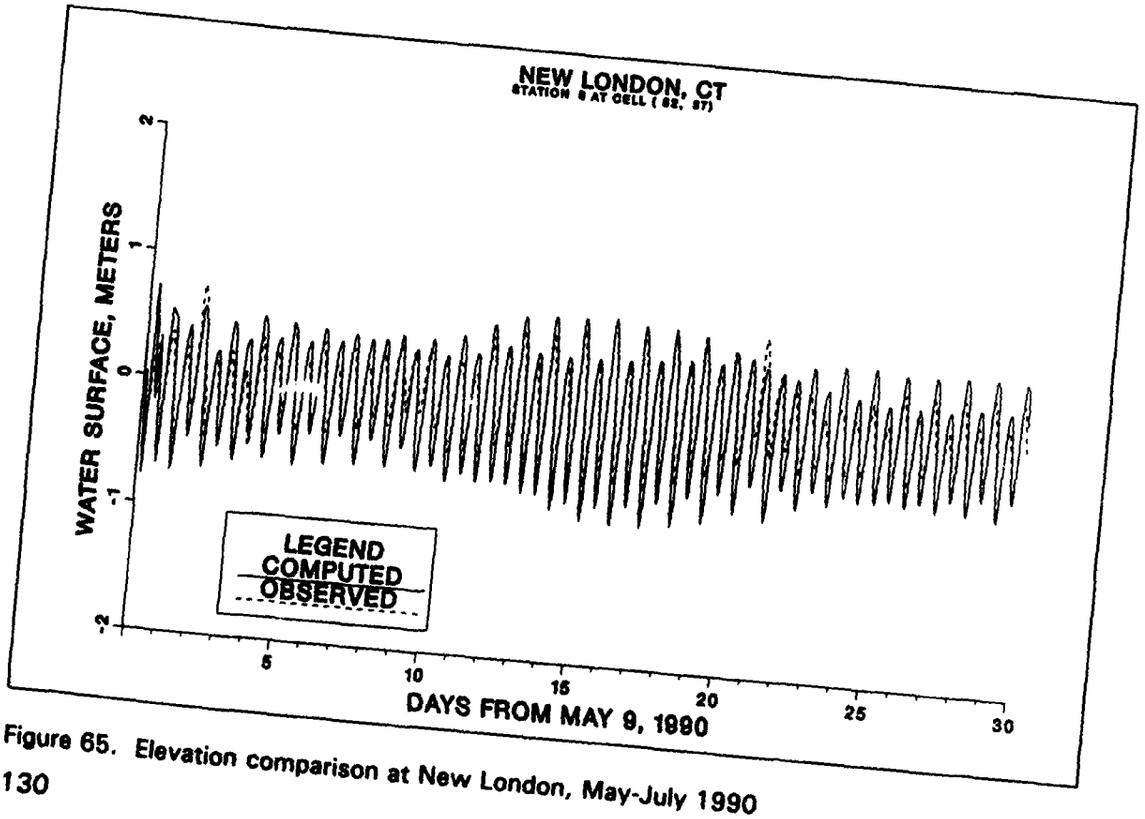

Figure 65. Elevation comparison at New London, May-July 1990

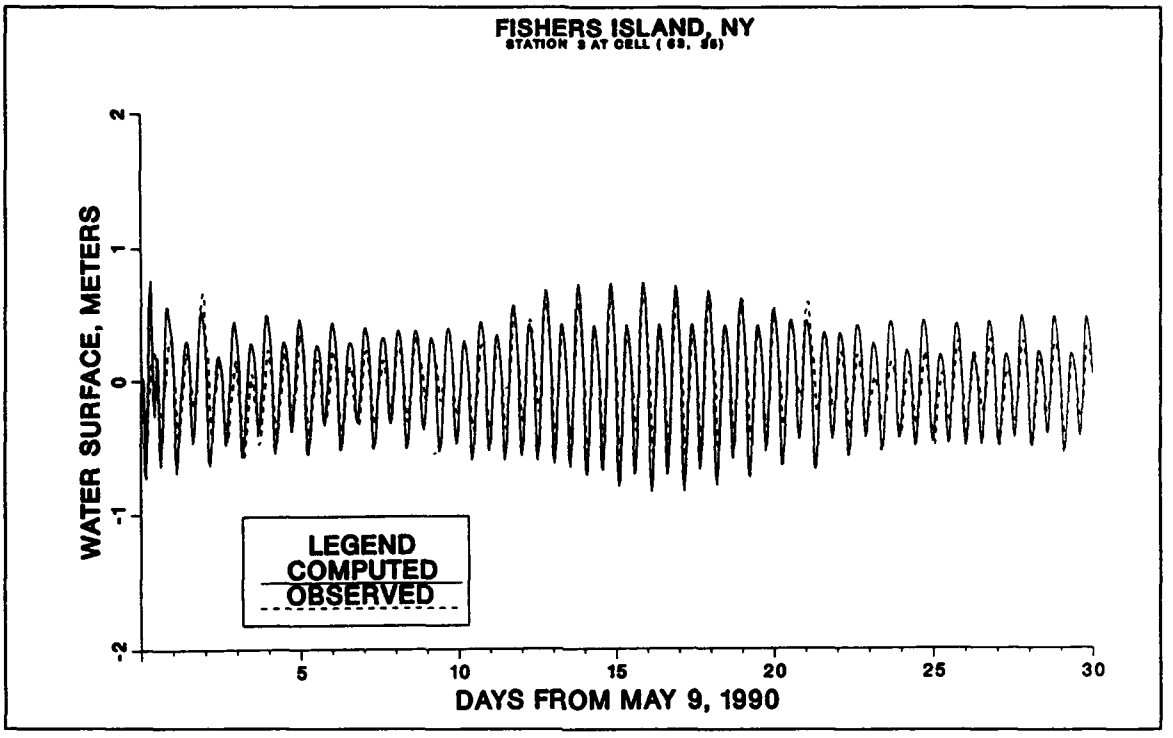

Figure 66. Elevation comparison at Fishers Island, May-July 1990

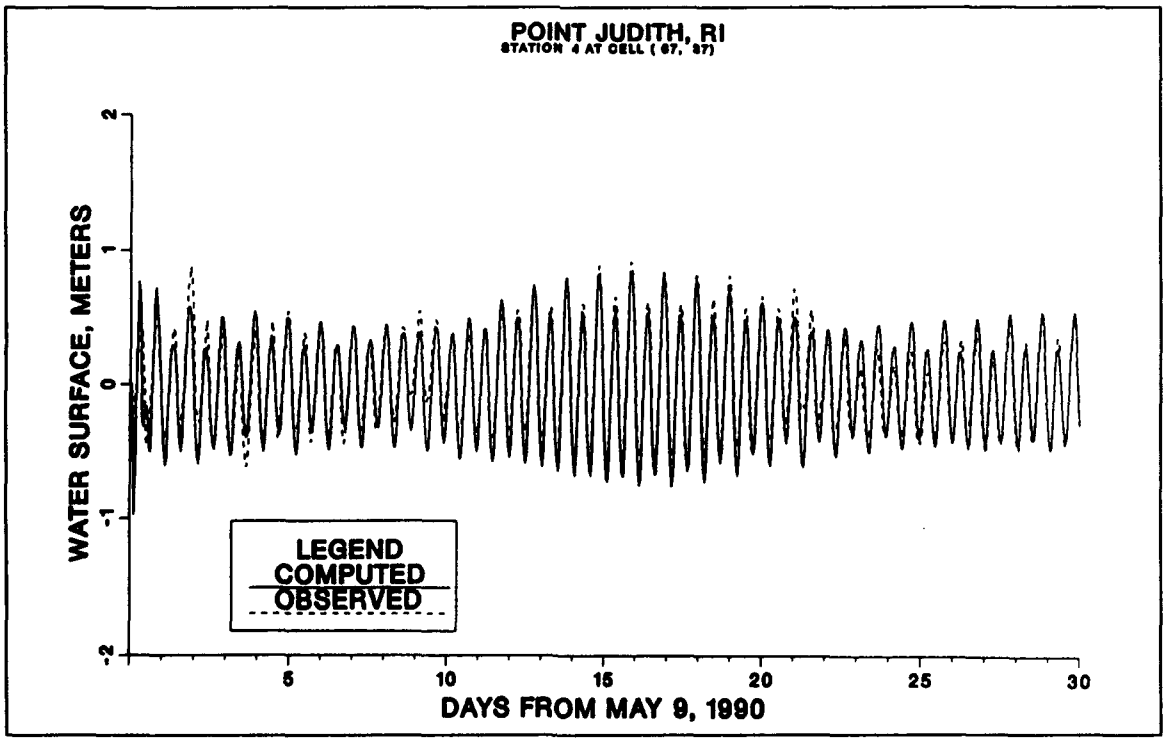

Figure 67. Elevation comparison at Point Judith, May-July 1990

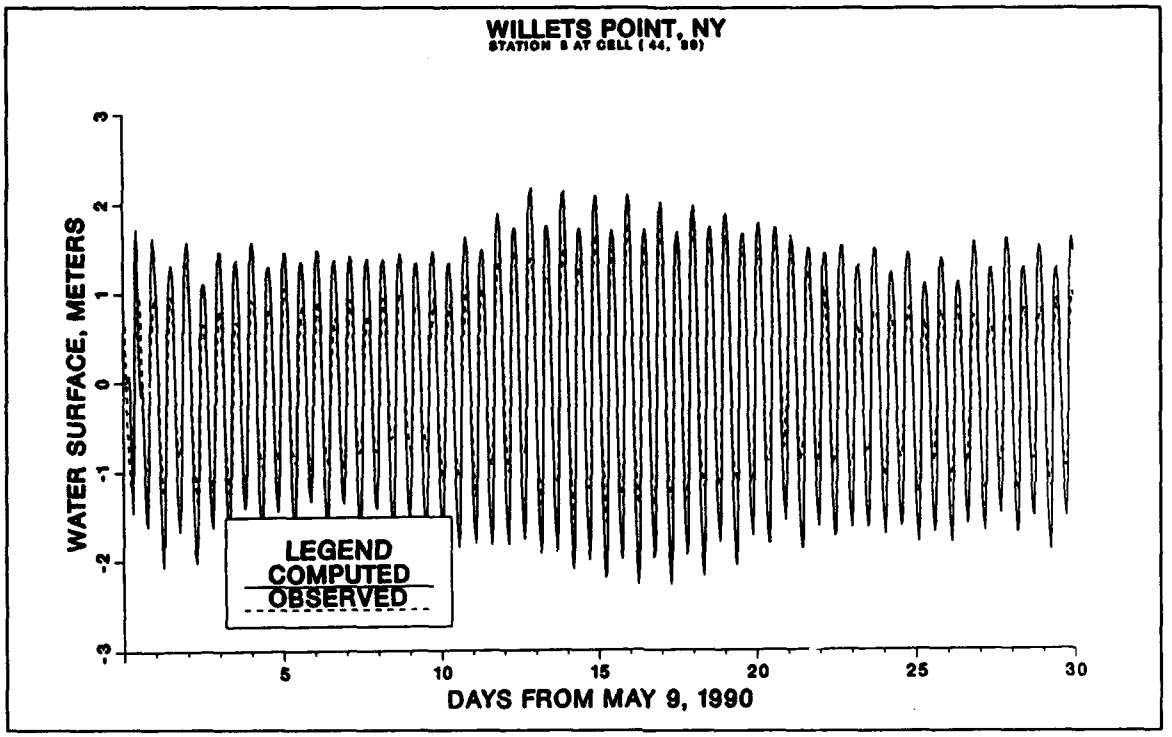

Figure 68. Elevation comparison at Willets Point, May-July 1990

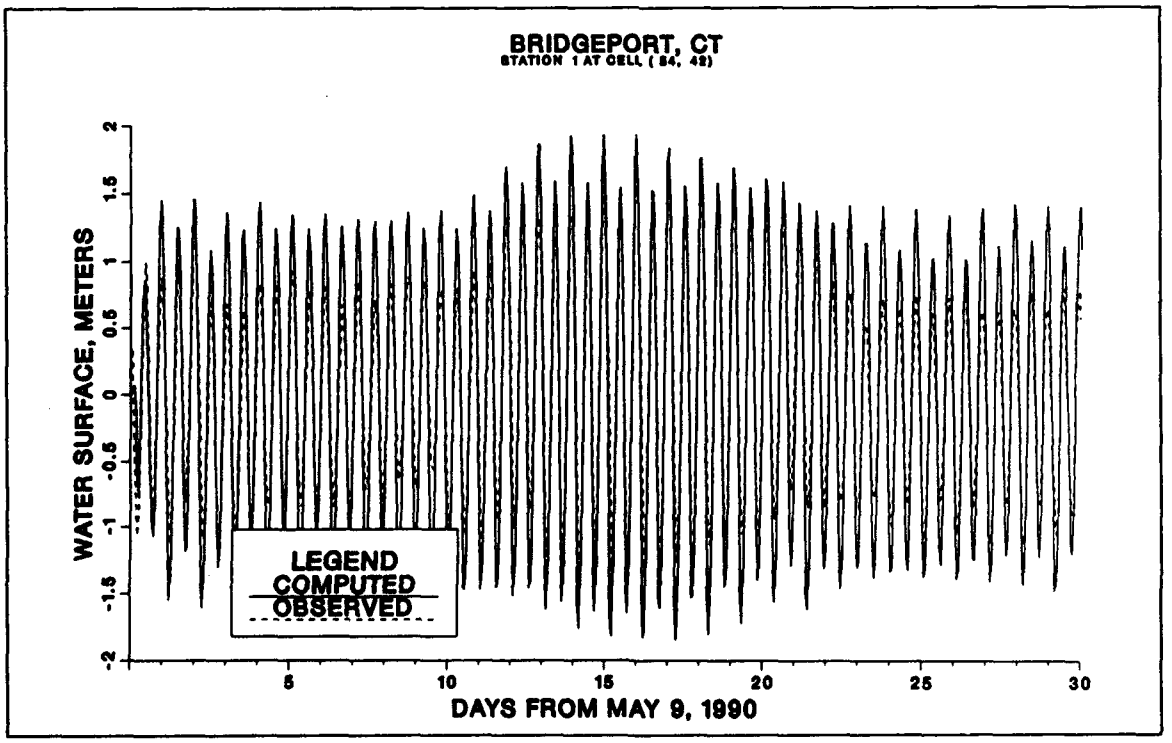

Figure 69. Elevation comparison at Bridgeport, May-June 1990

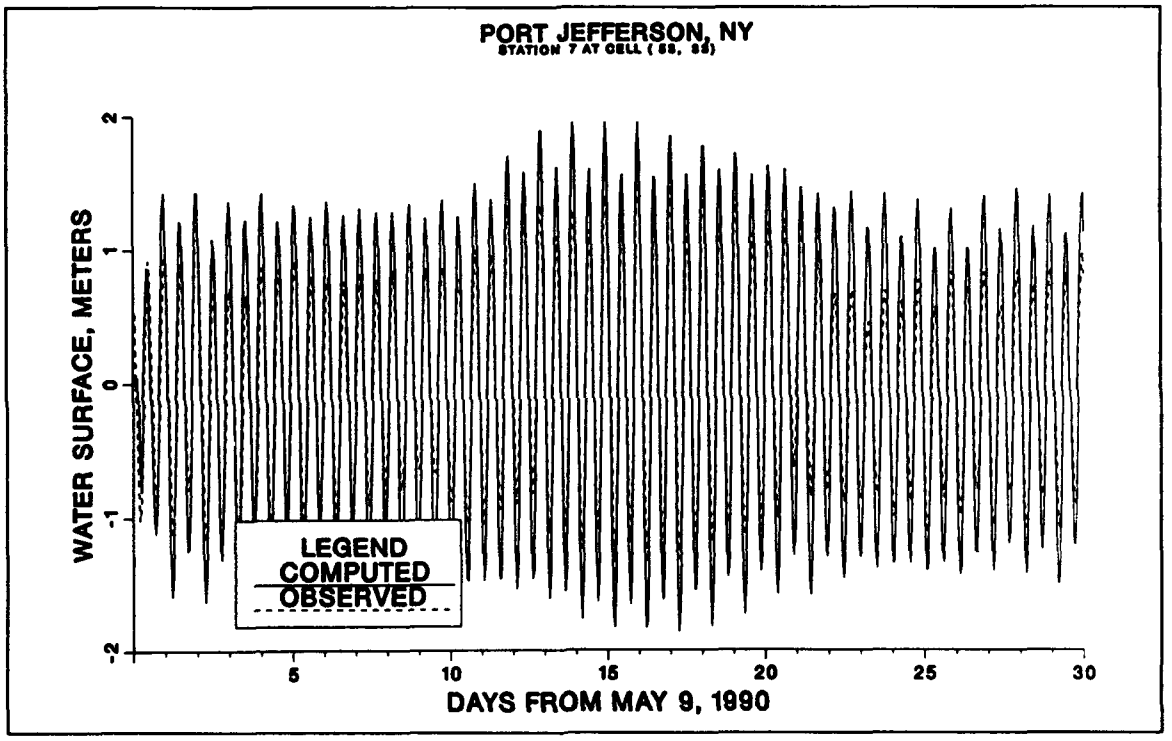

Figure 70. Elevation comparison at Port Jefferson, May-July 1990

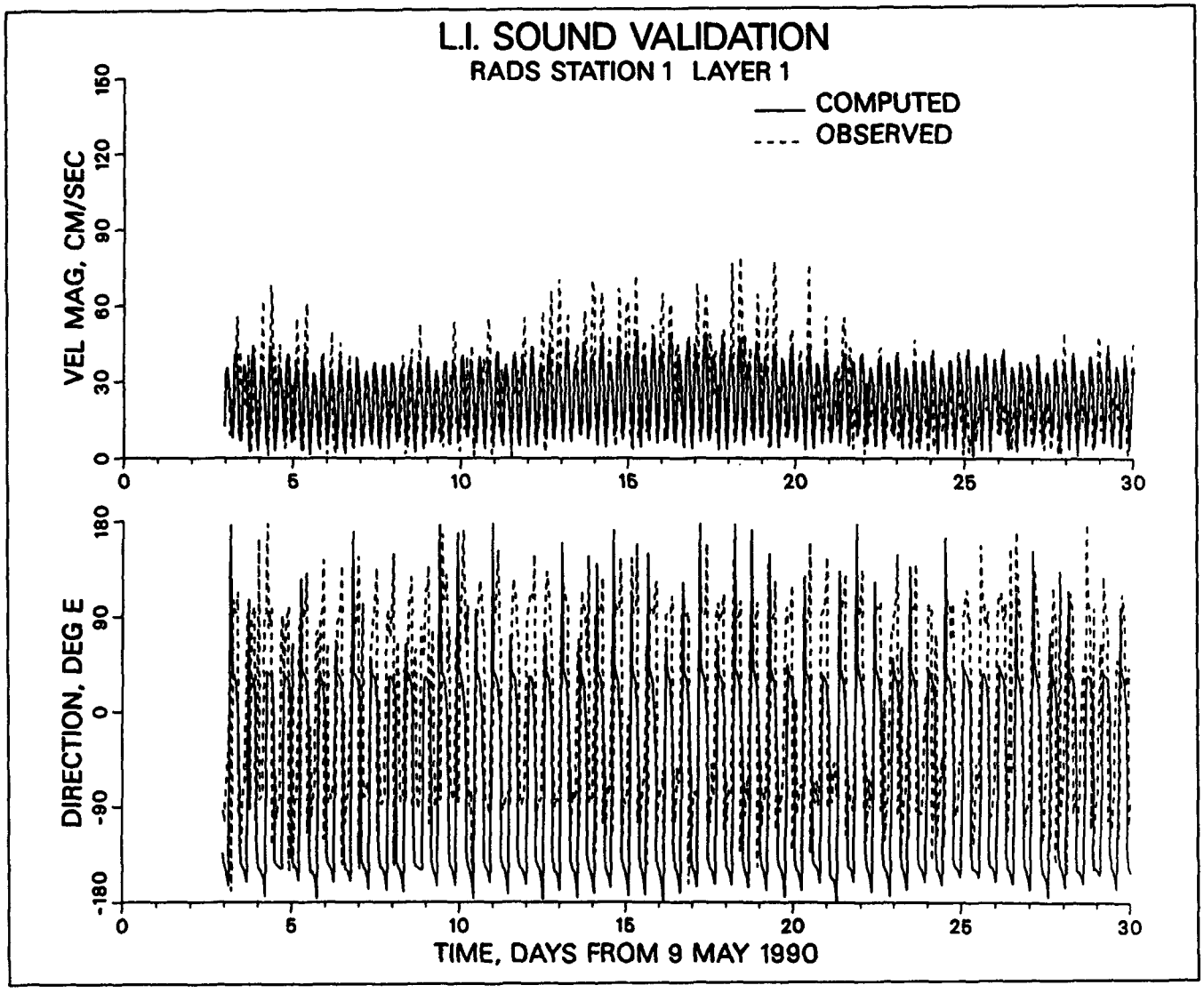

Figure 71. Velocity comparison at RADS station 1, level 1

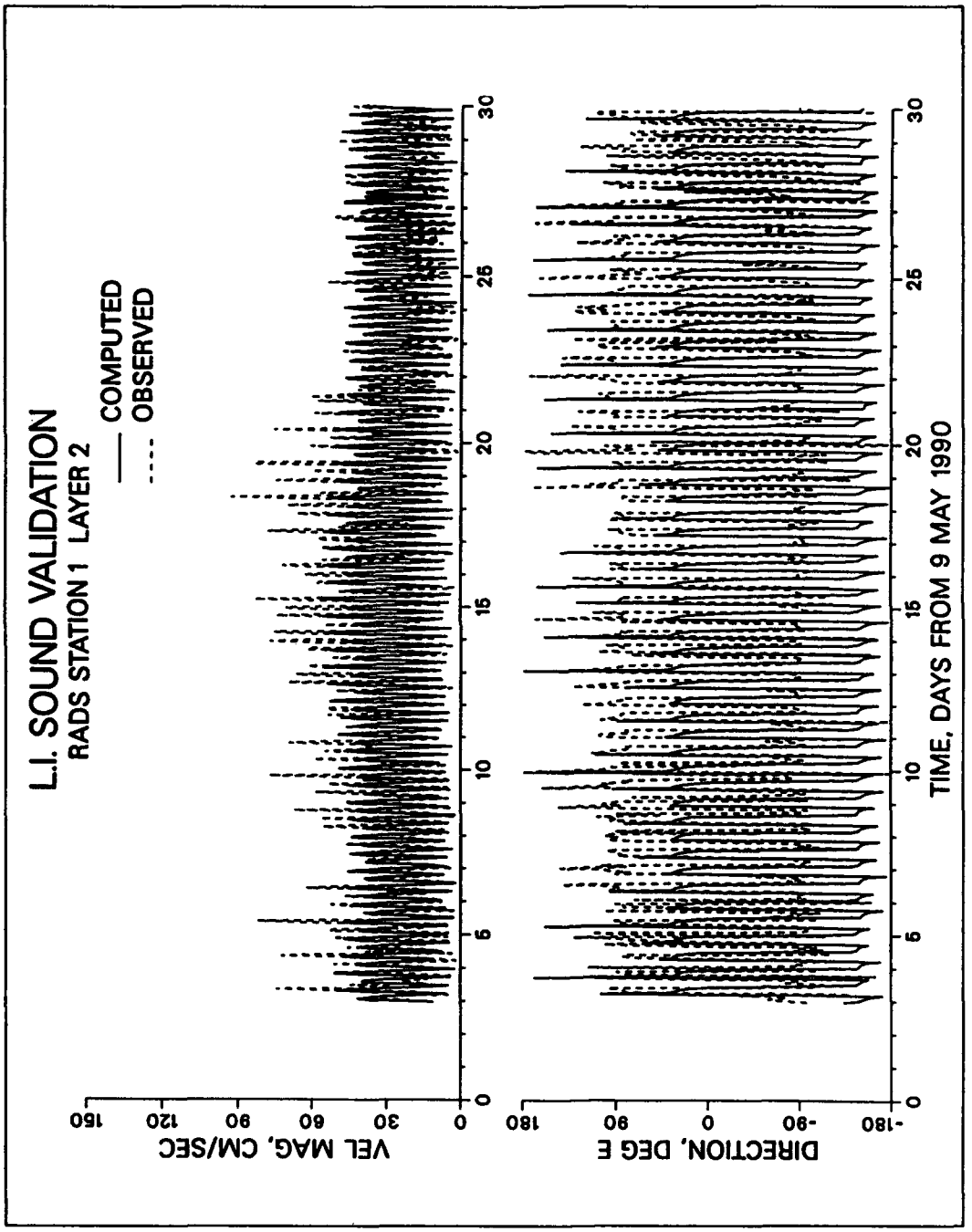

Figure 72. Velocity comparison at RADS station 1, level 2

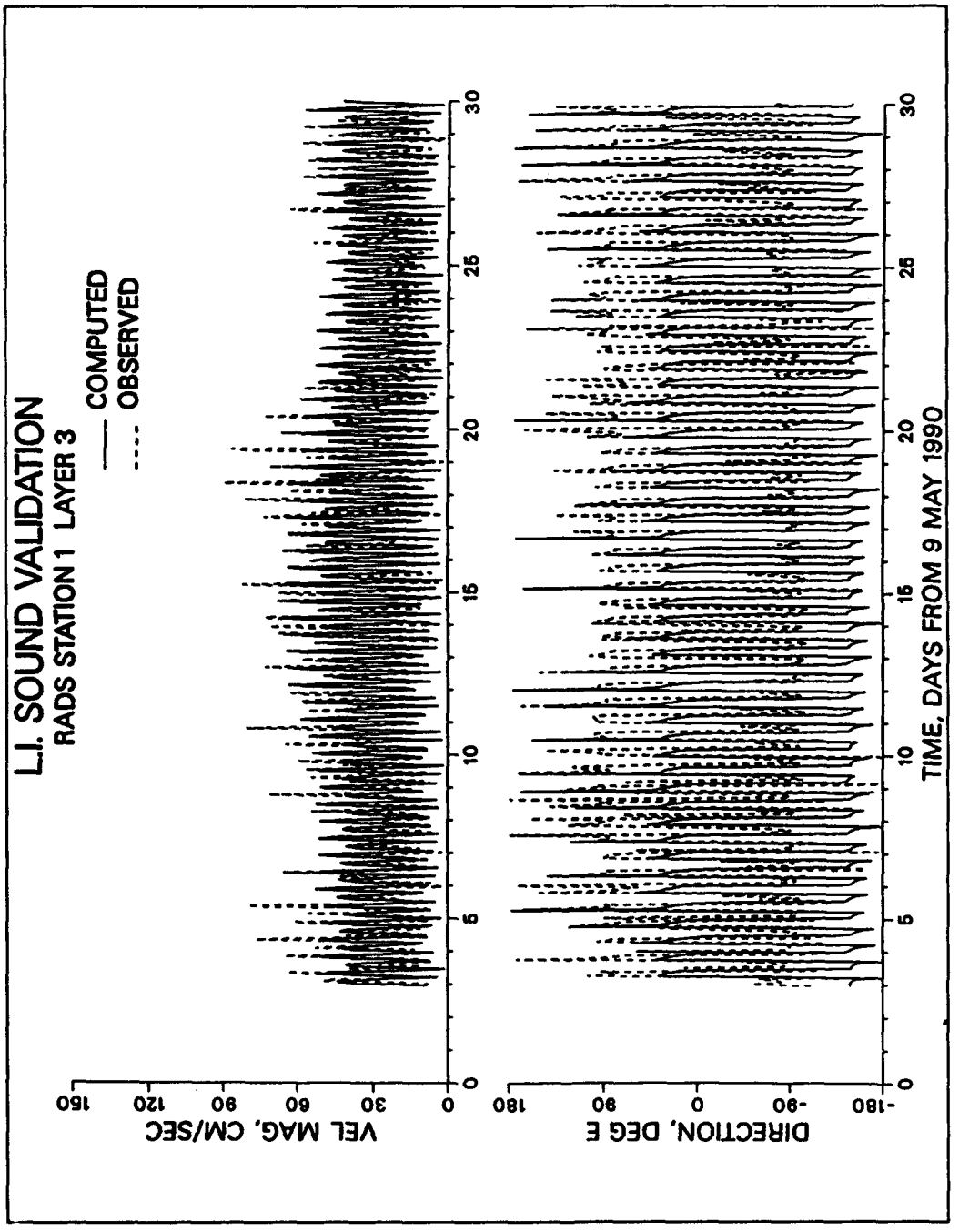

Figure 73. Velocity comparison at RADS station 1, level 3

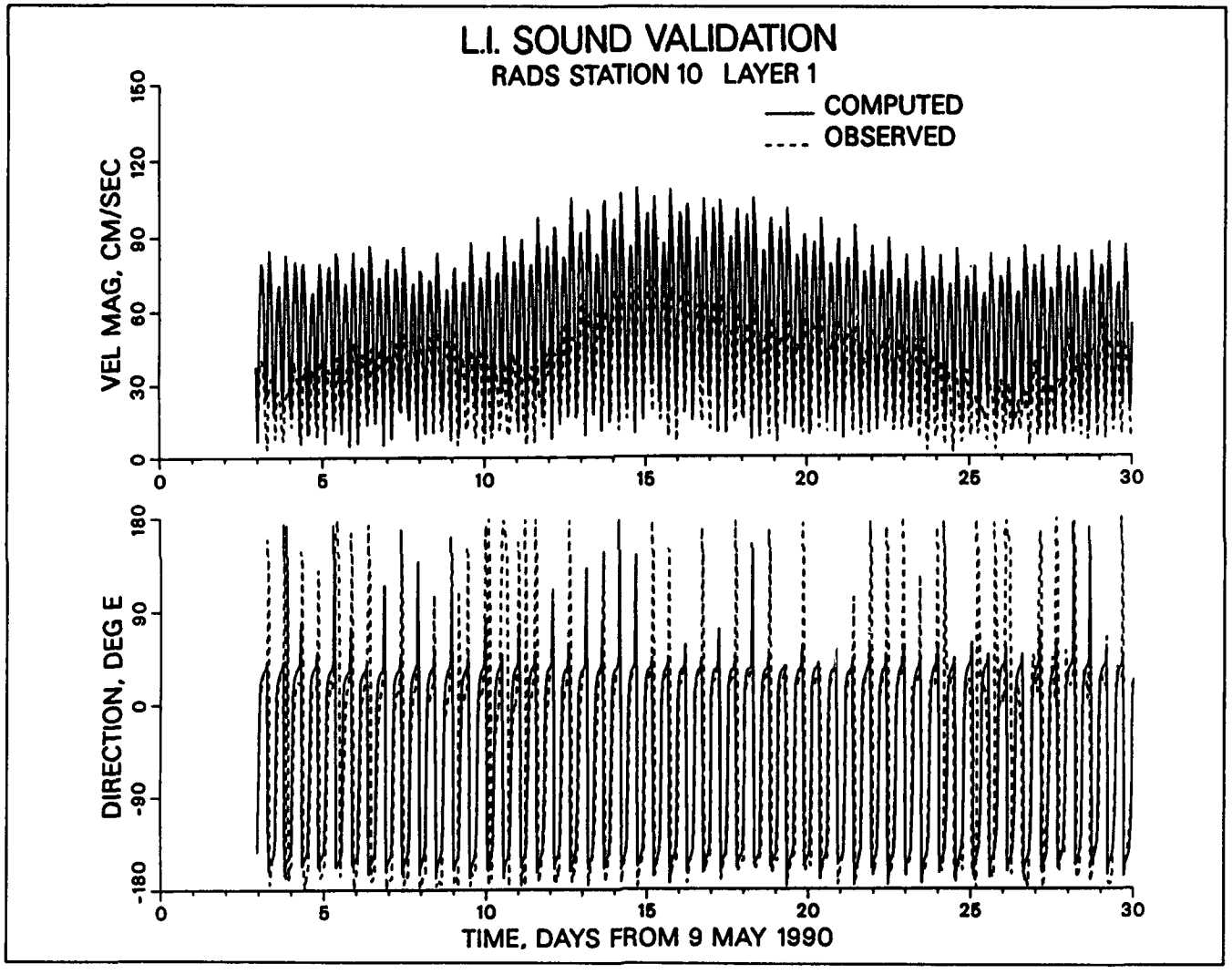

Figure 74. Velocity comparison at RADS station 10, level 1

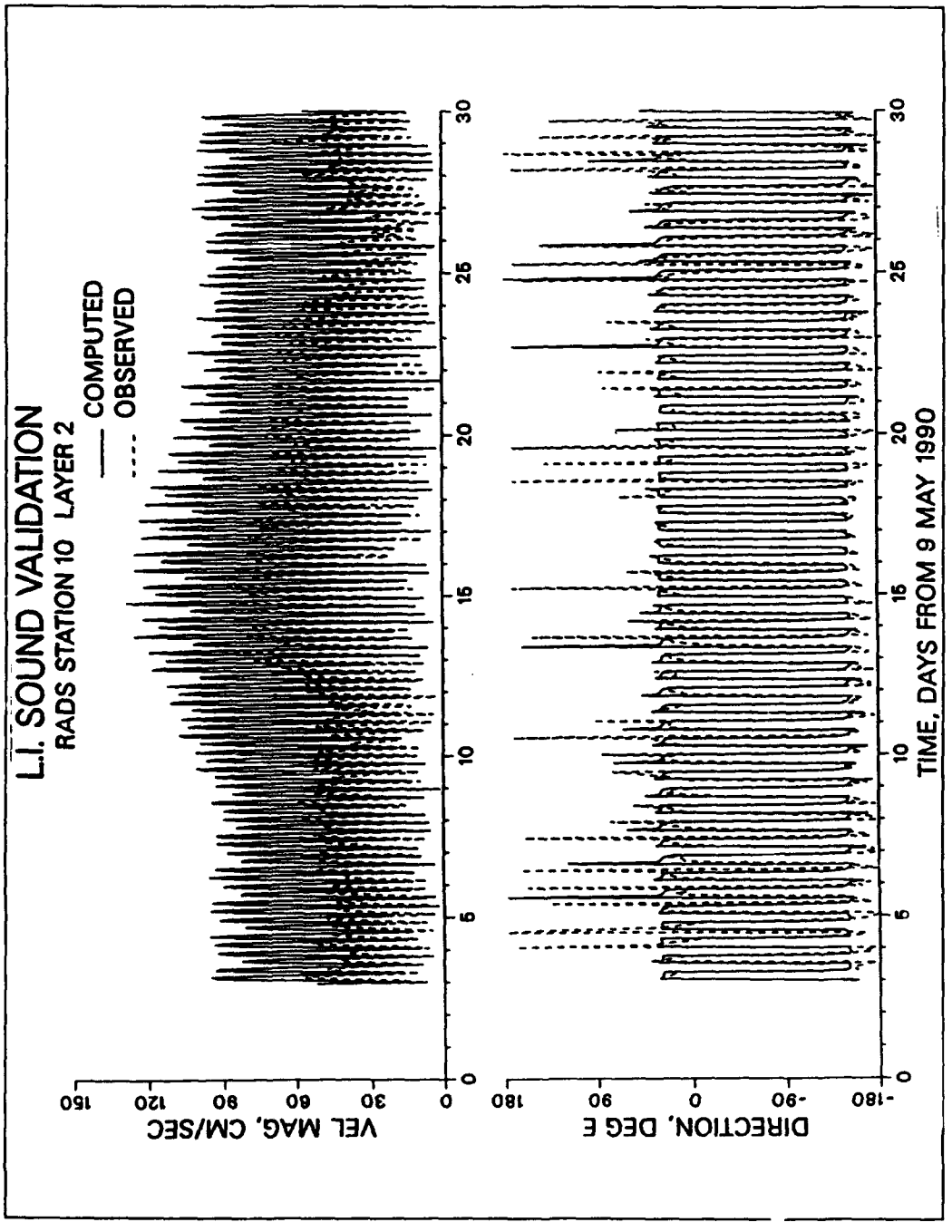

Figure 75. Velocity comparison at RADS station 10, level 2

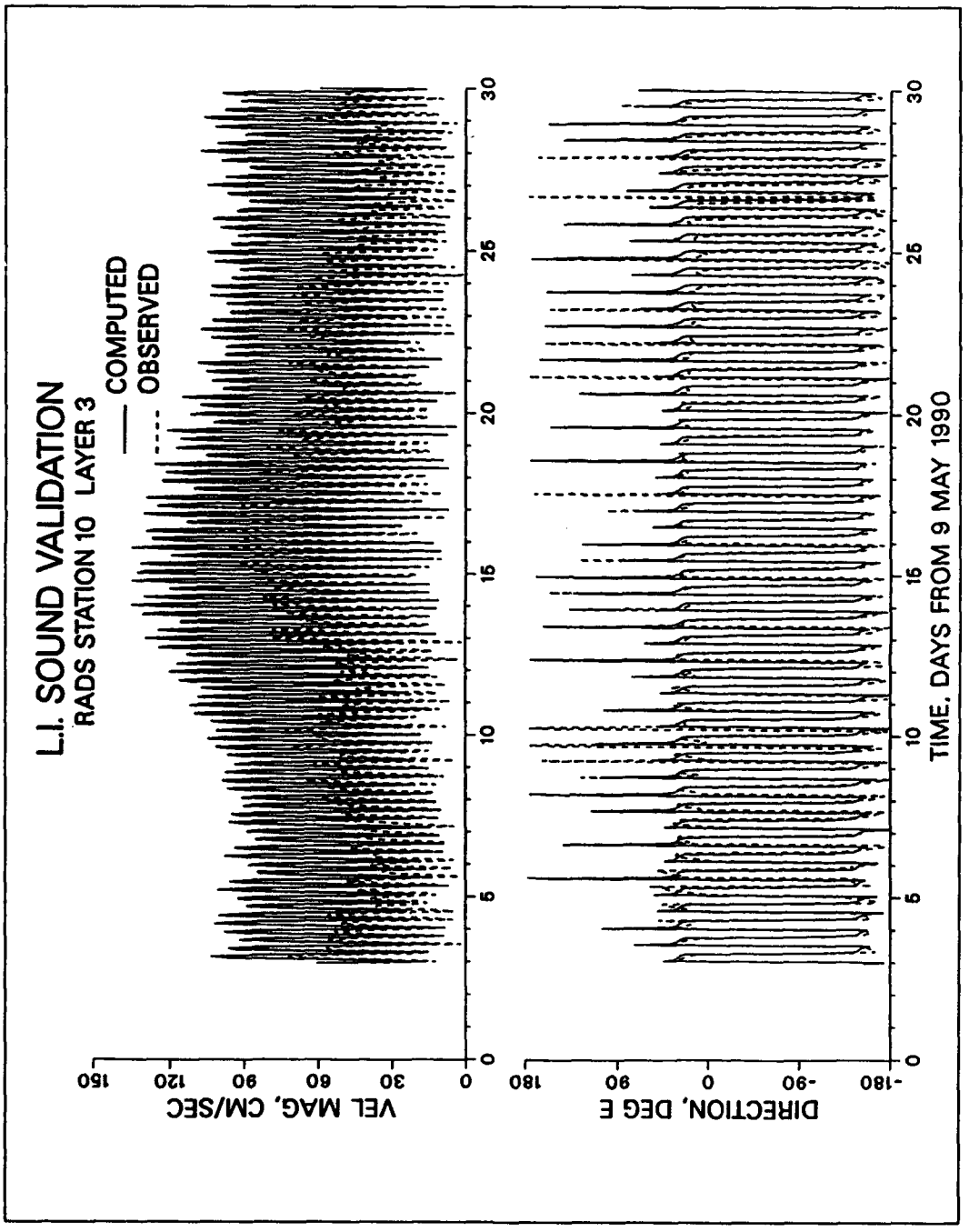

Figure 76. Velocity comparison at RADS station 10, level 3

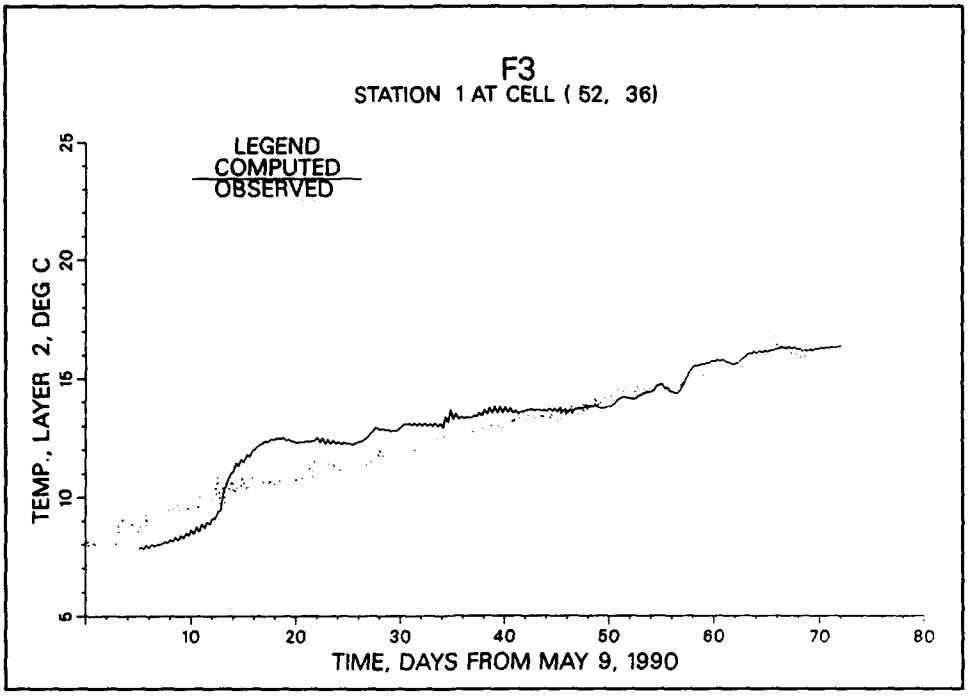

Figure 77. Temperature comparison at F3, lower level

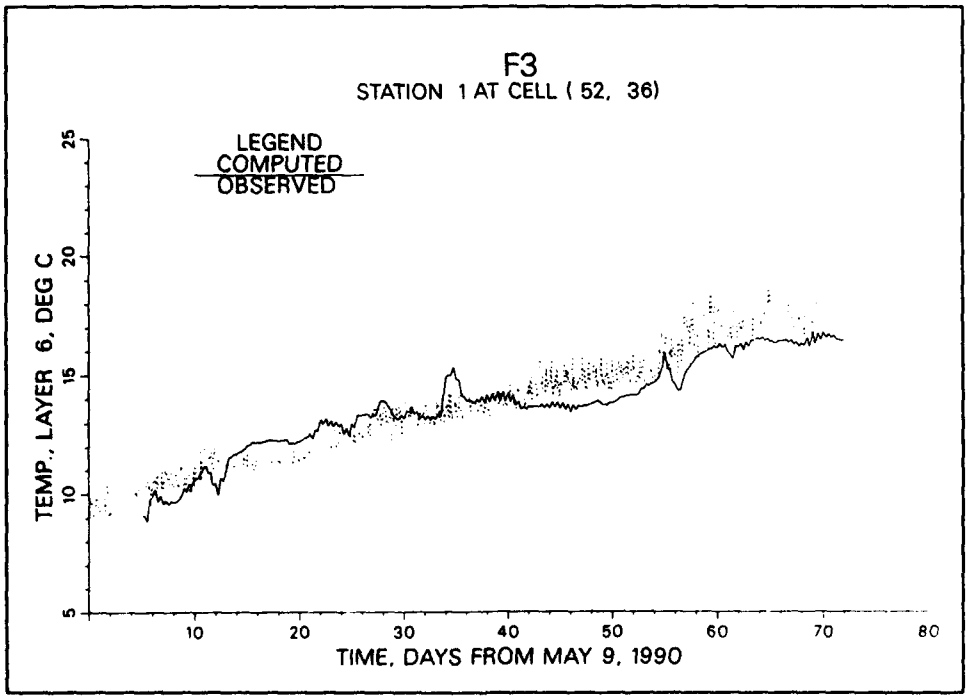

Figure 78. Temperature comparison at F3, upper level

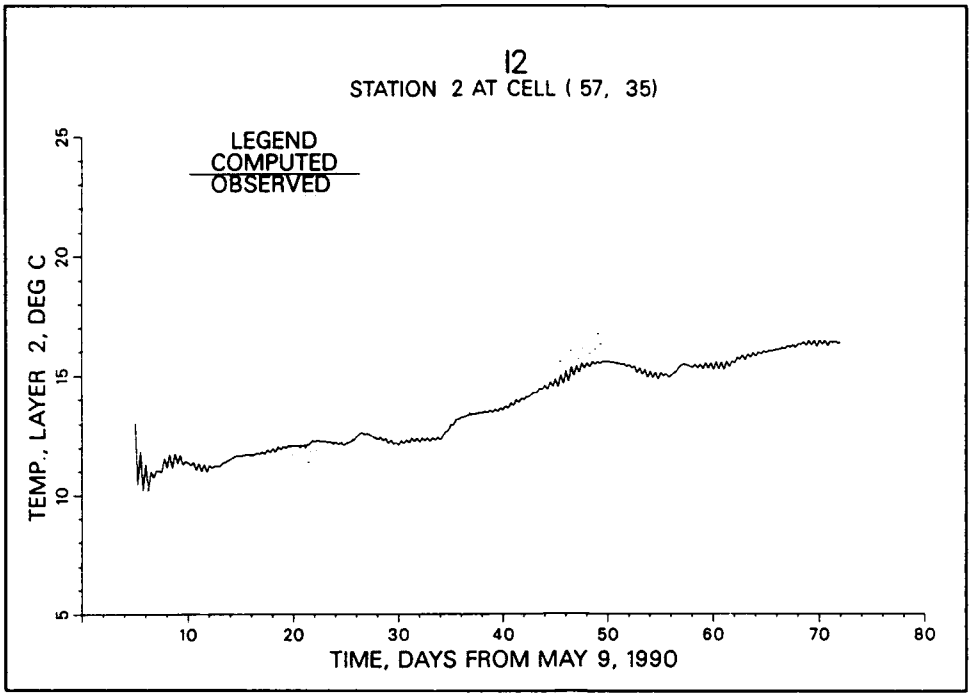

Figure 79. Temperature comparison I2, lower level

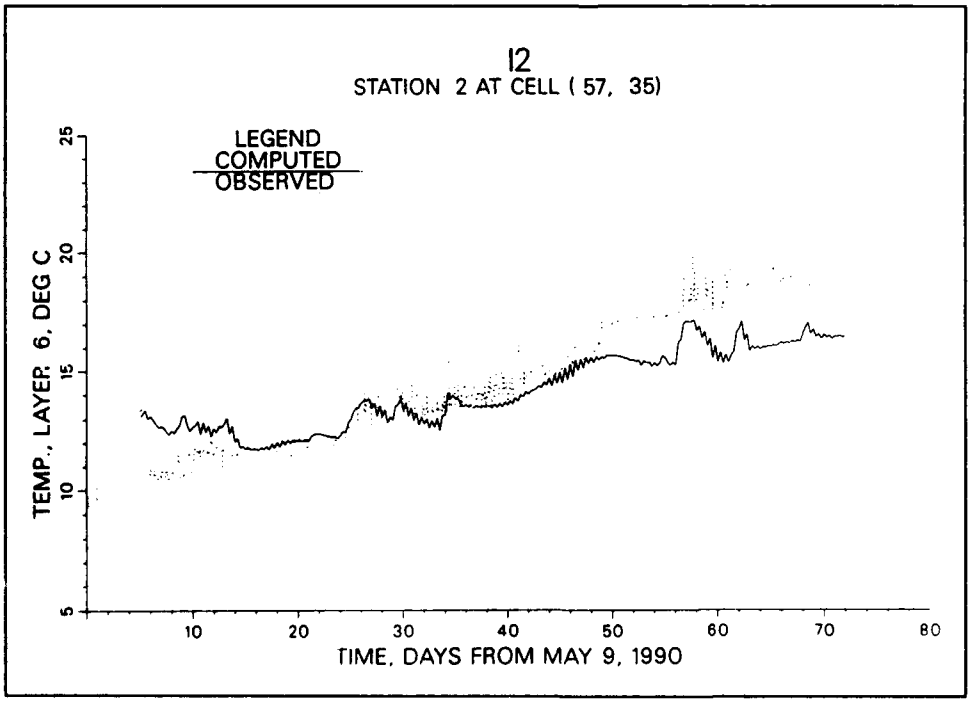

Figure 80. Temperature comparison I2, upper level

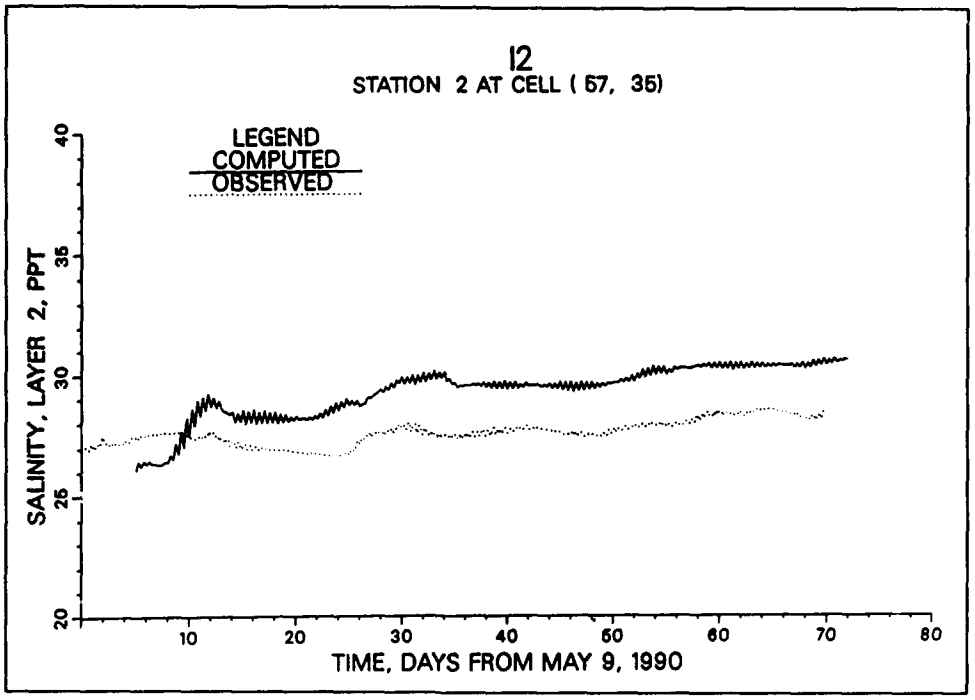

Figure 81. Salinity comparison at I2, lower level

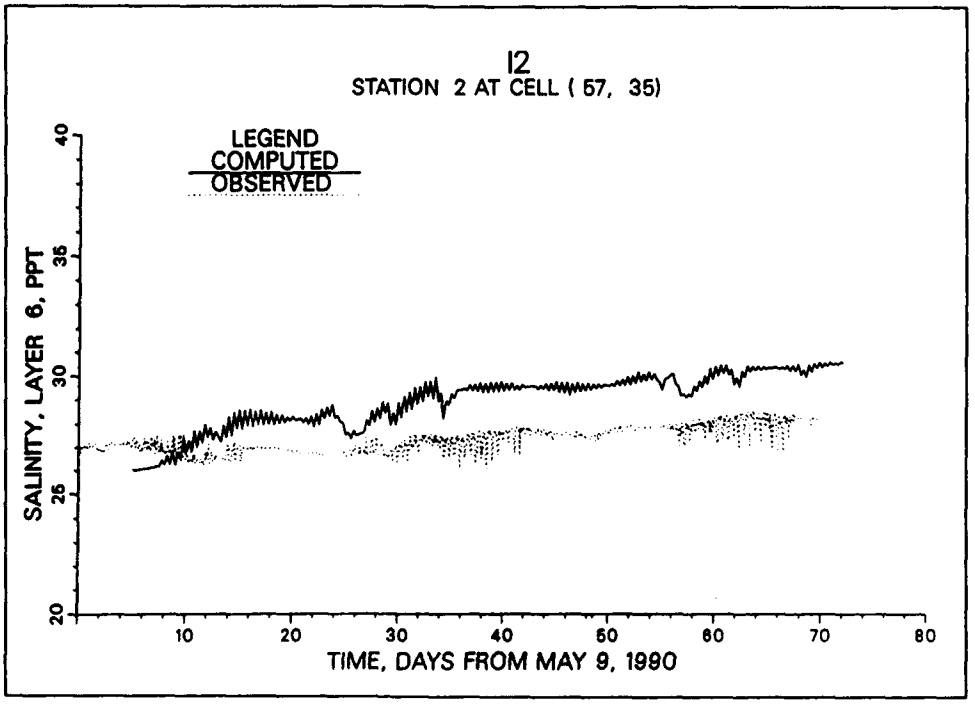

Figure 82. Salinity comparison at I2, upper level

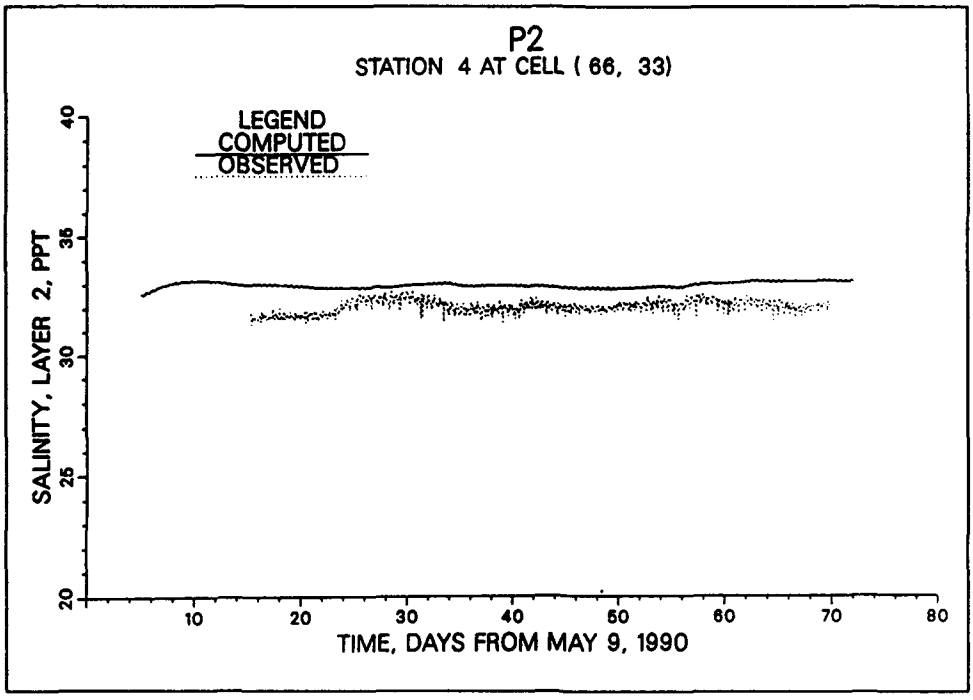

Figure 83. Salinity comparison at P2, lower level

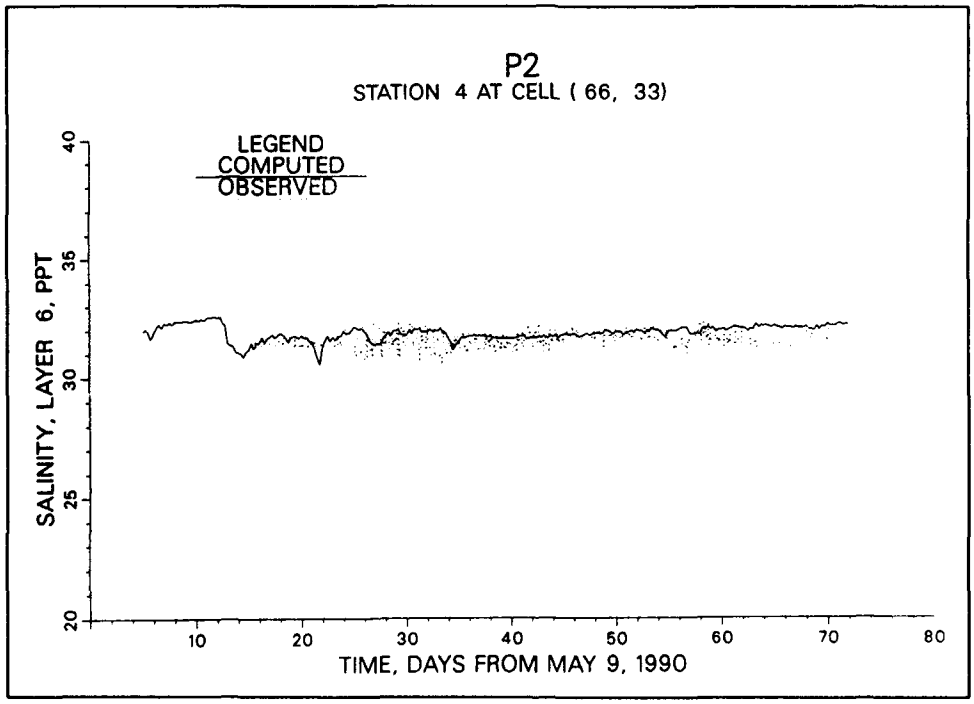

Figure 84. Salinity comparison at P2, upper level

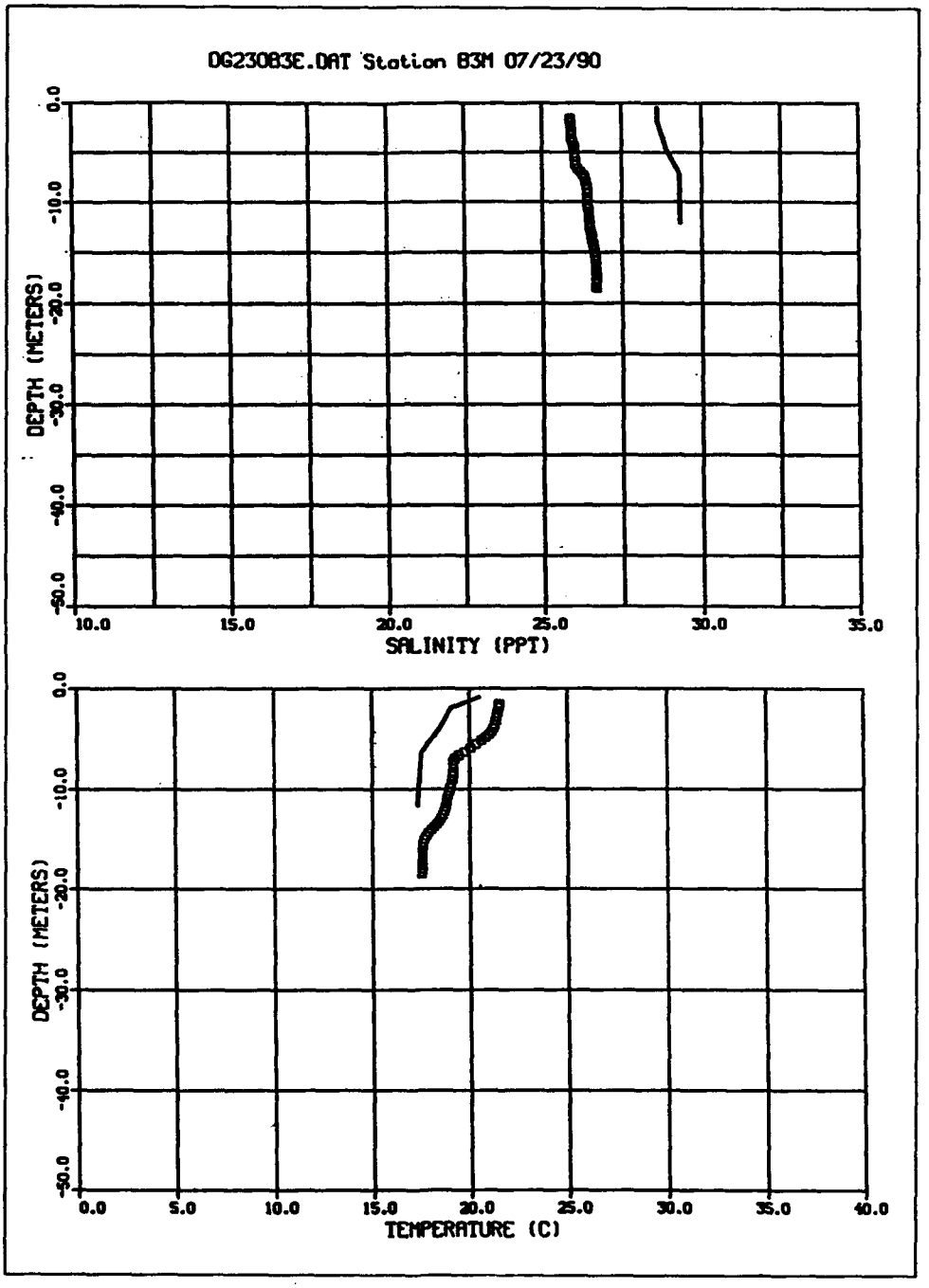

Figure 85. Temperature and salinity profile comparison at B3M

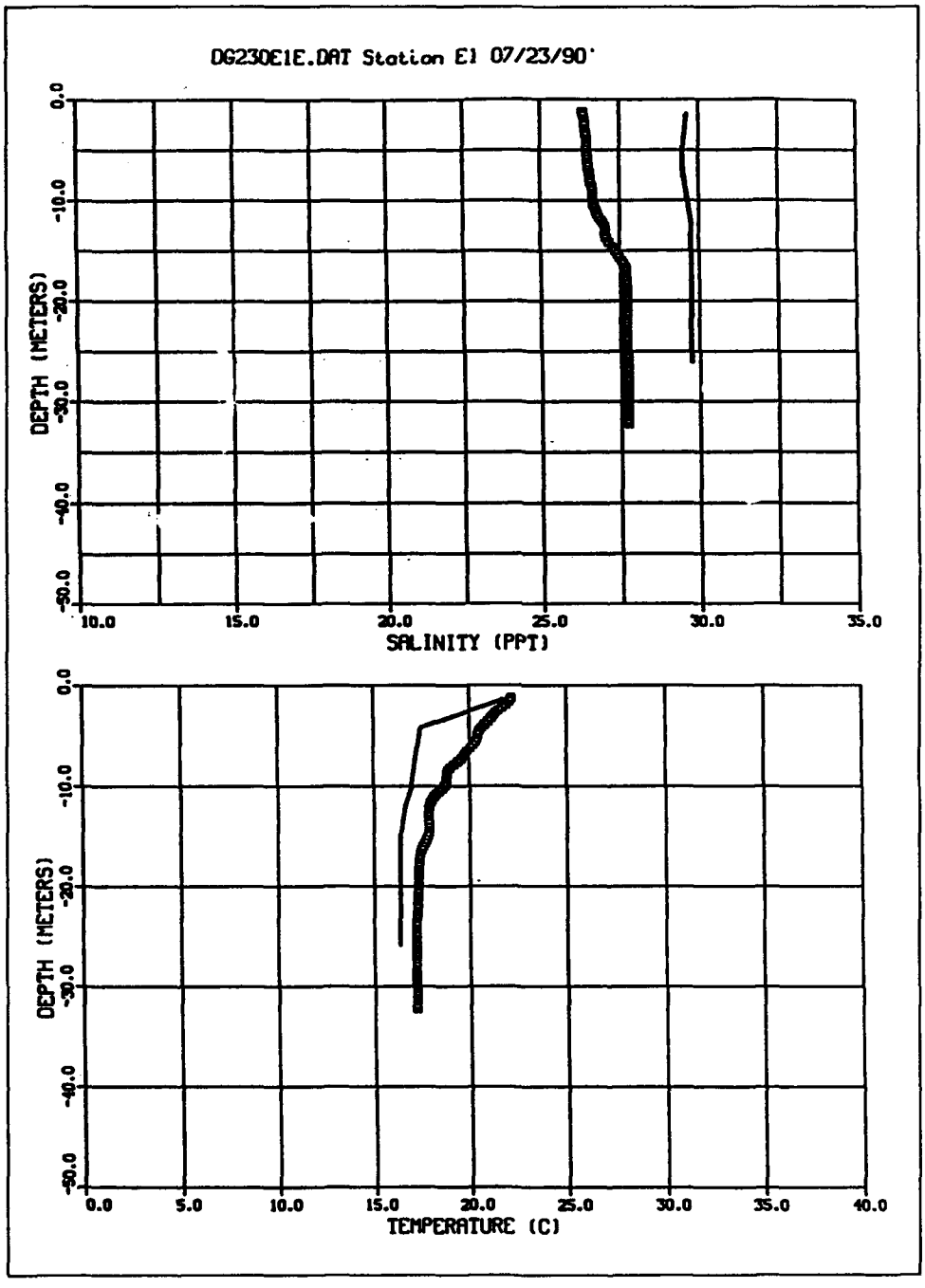

Figure 86. Temperature and salinity profile comparison at E1

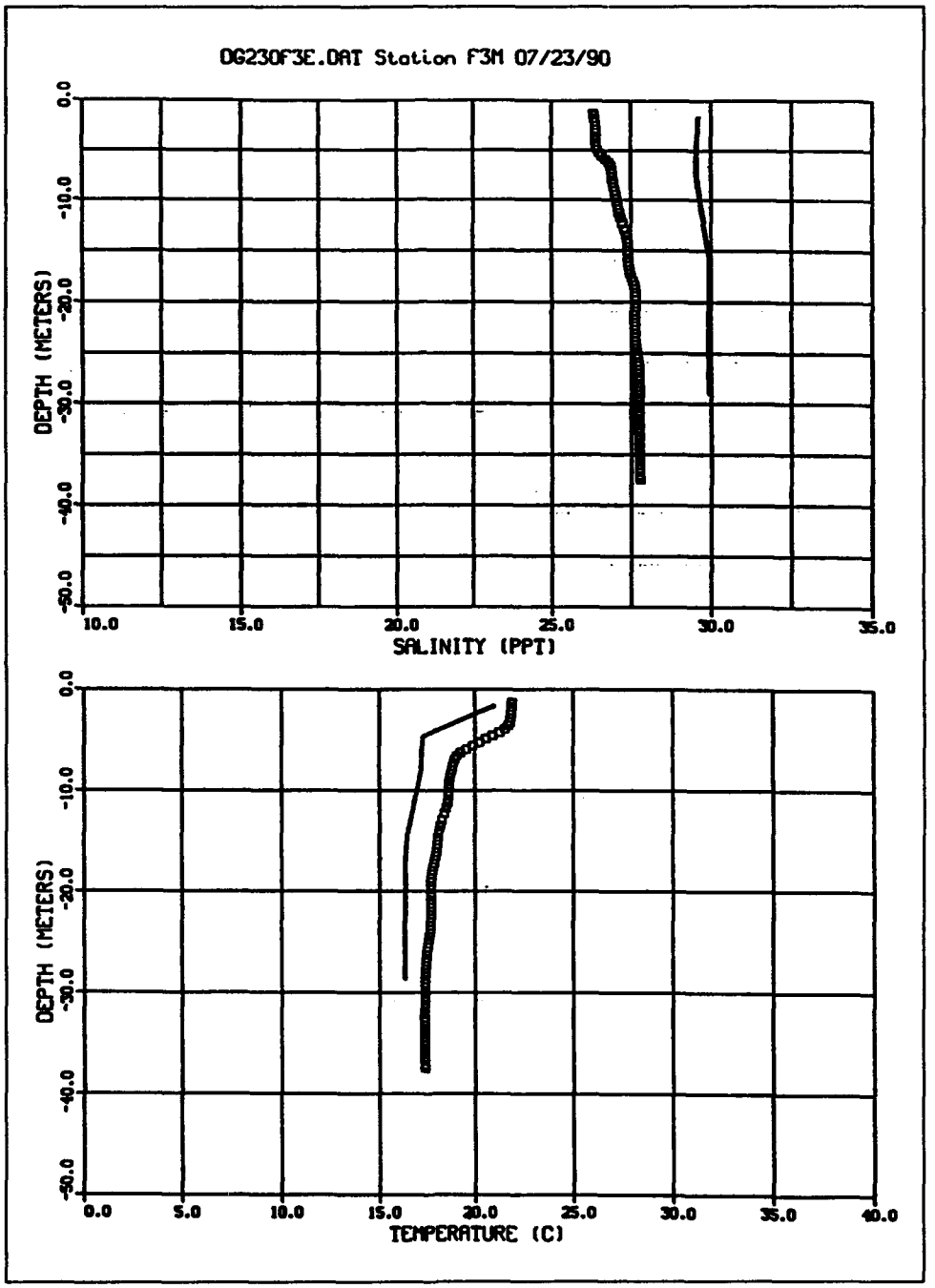

Figure 87. Temperature and salinity profile comparison at F3M

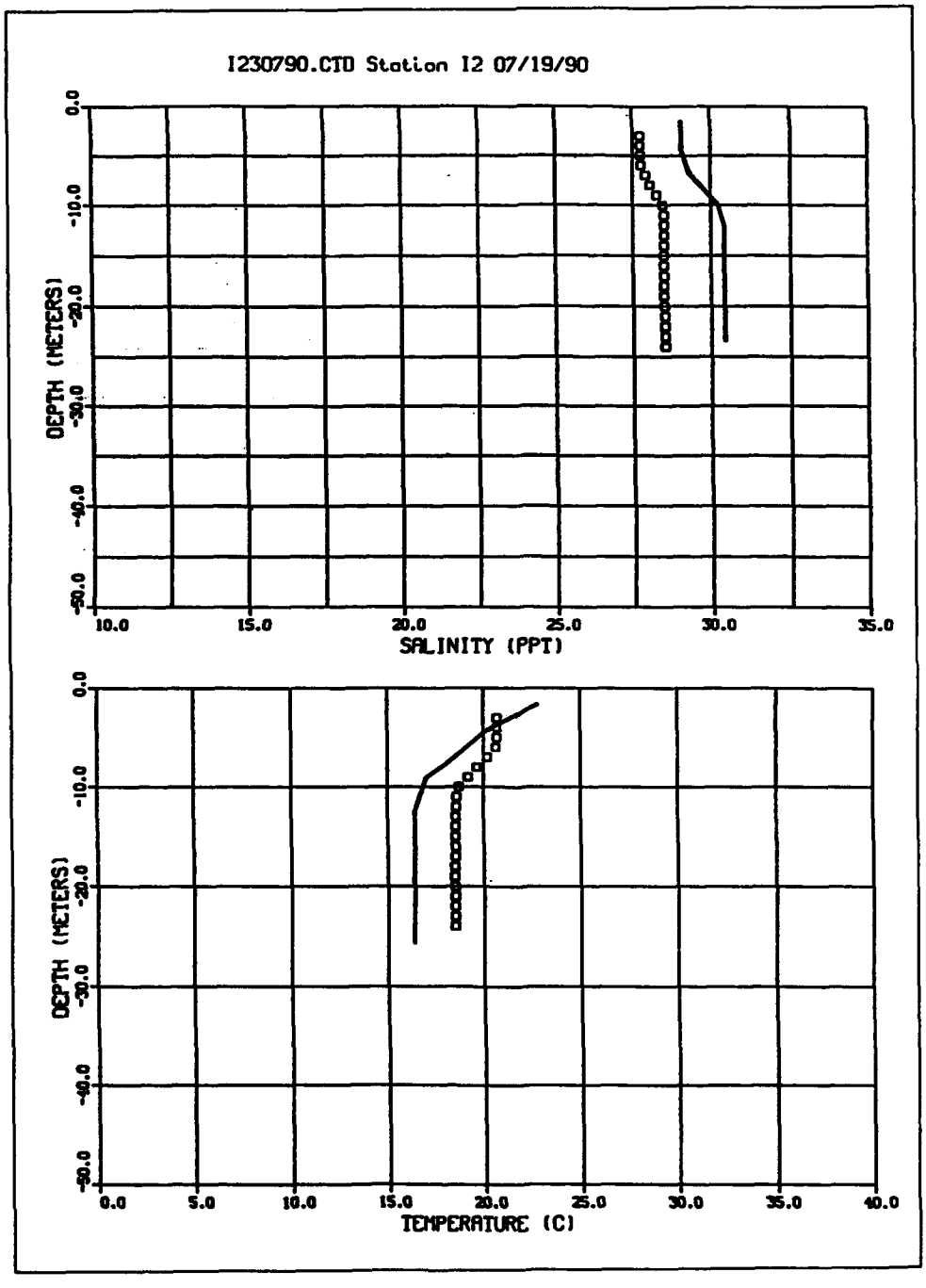

Figure 88. Temperature and salinity profile comparison at I2

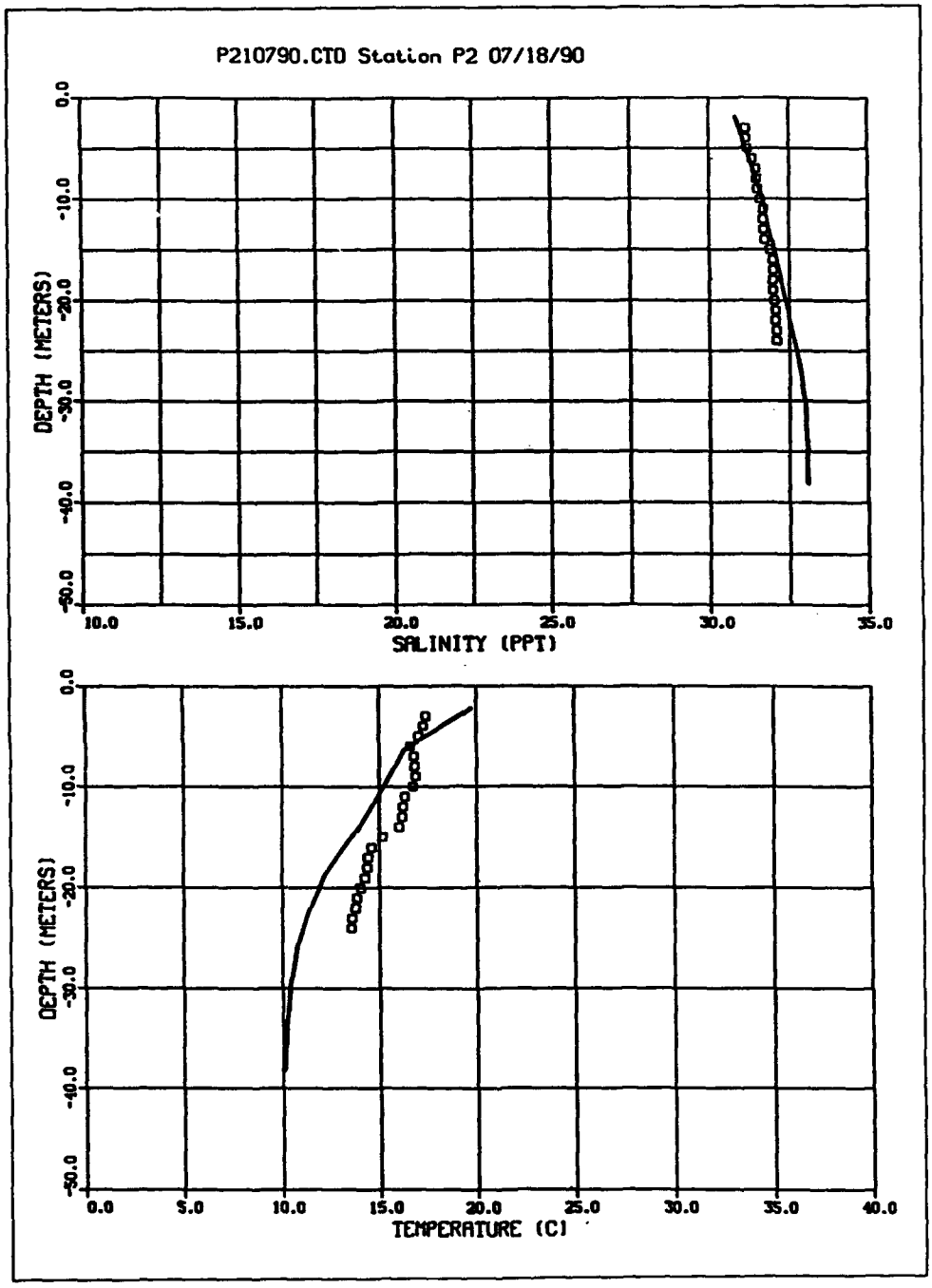

Figure 89. Temperature and salinity profile comparison at P2

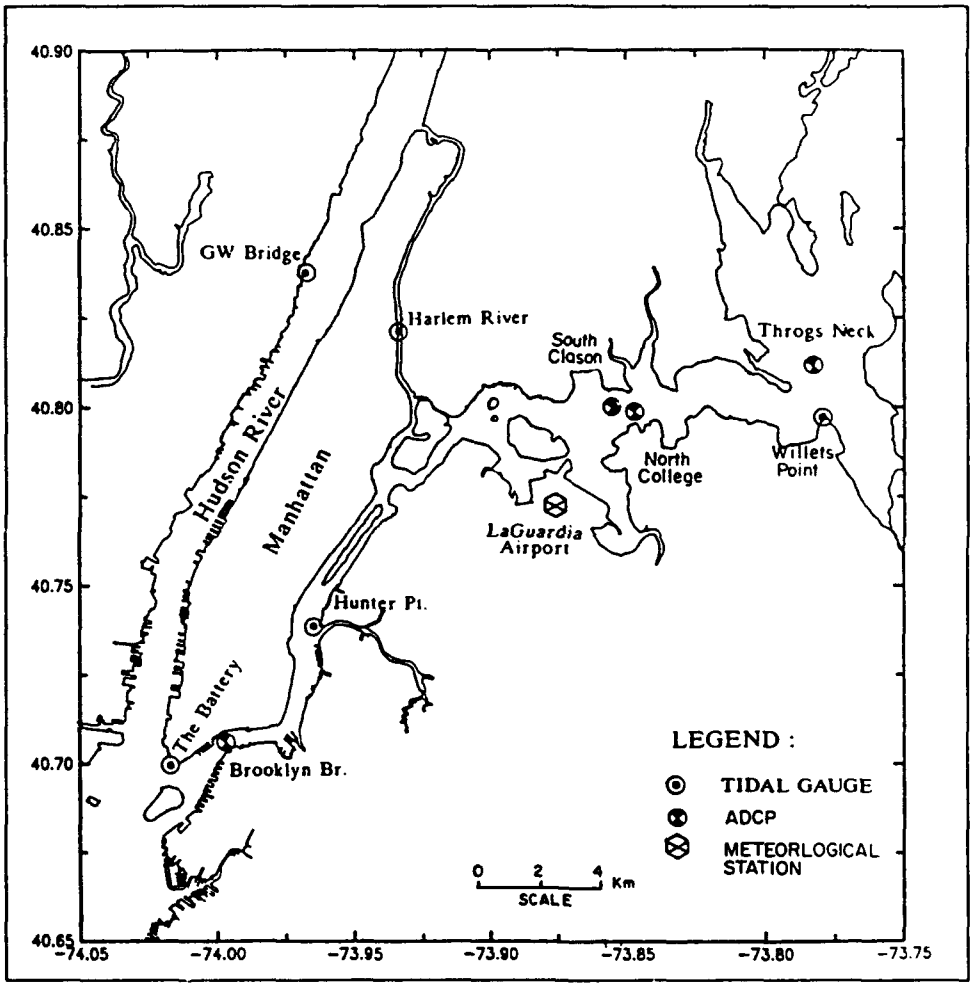

Figure 90. East River hydrodynamic sample stations, from HydroQual

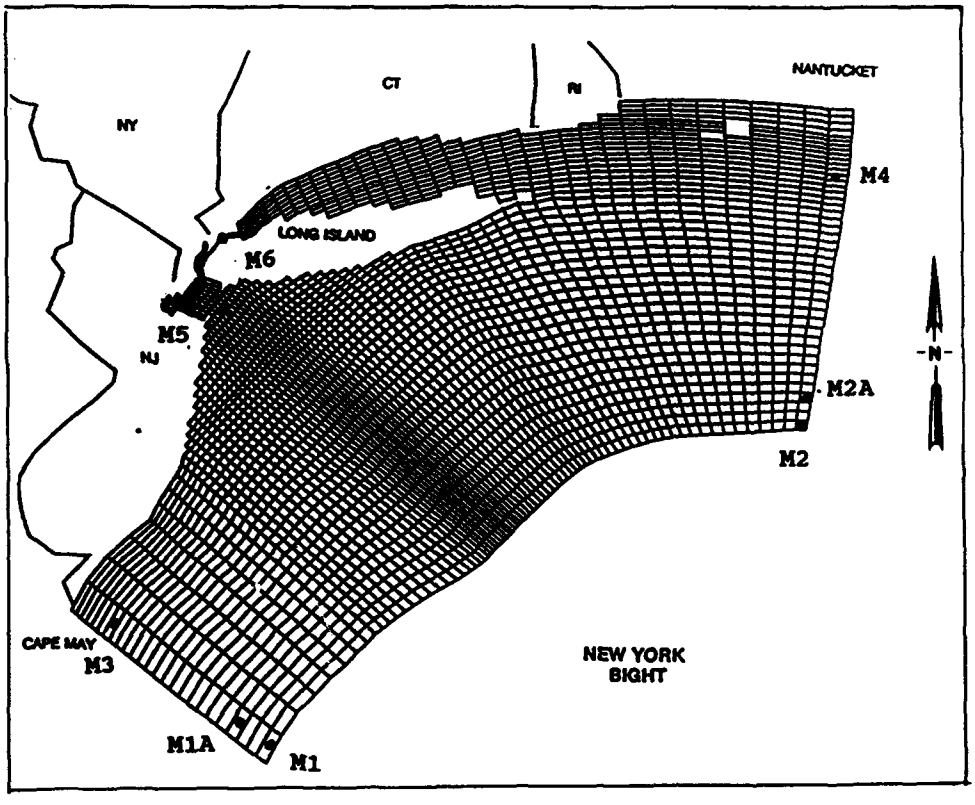

Figure 91. Recommended long-term monitoring station locations

Appendix A
Boundary/Initial Conditions

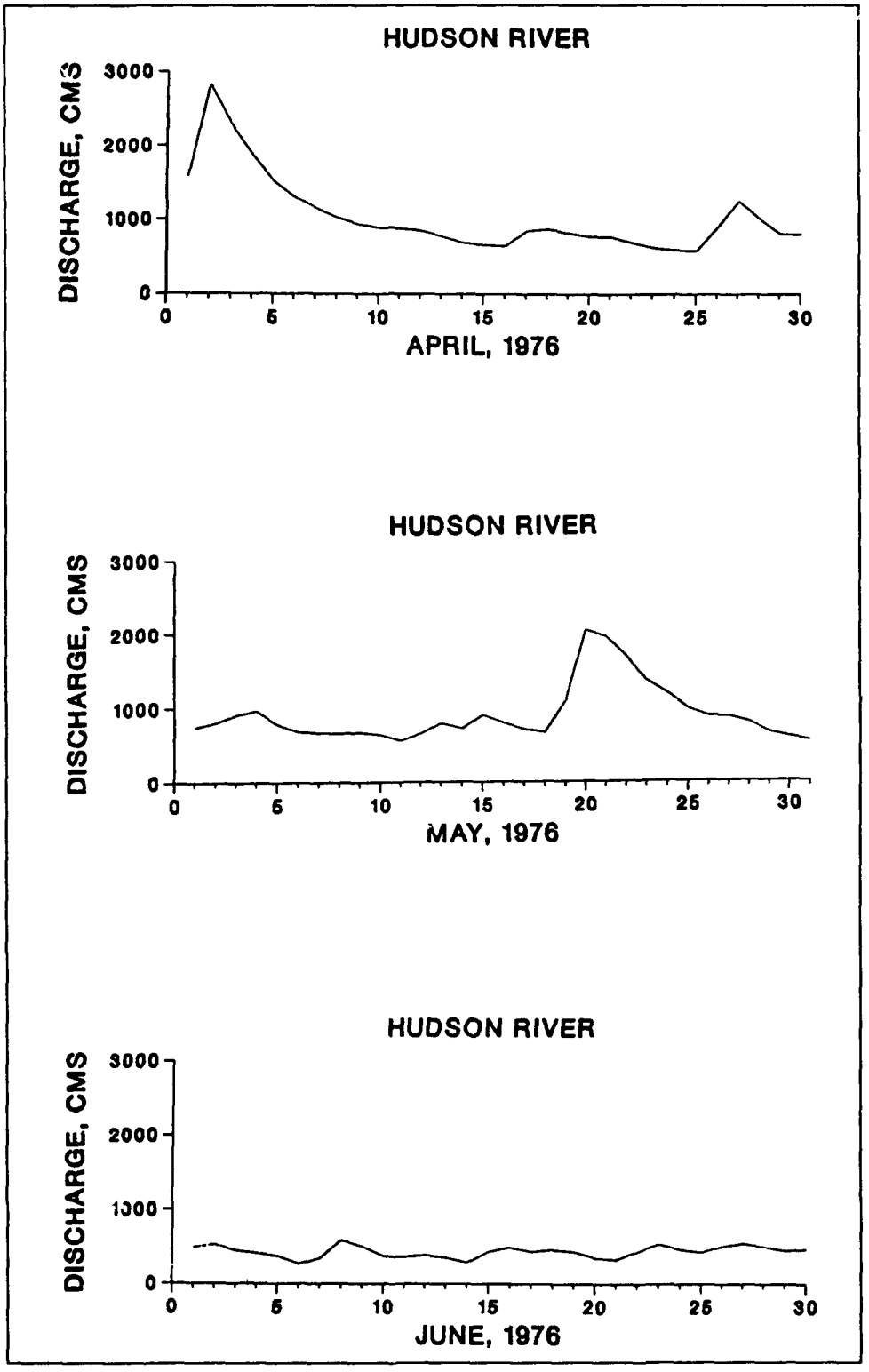

Figure A1. Hudson river inflow, April - October 1976 (Sheet 1 of 3)

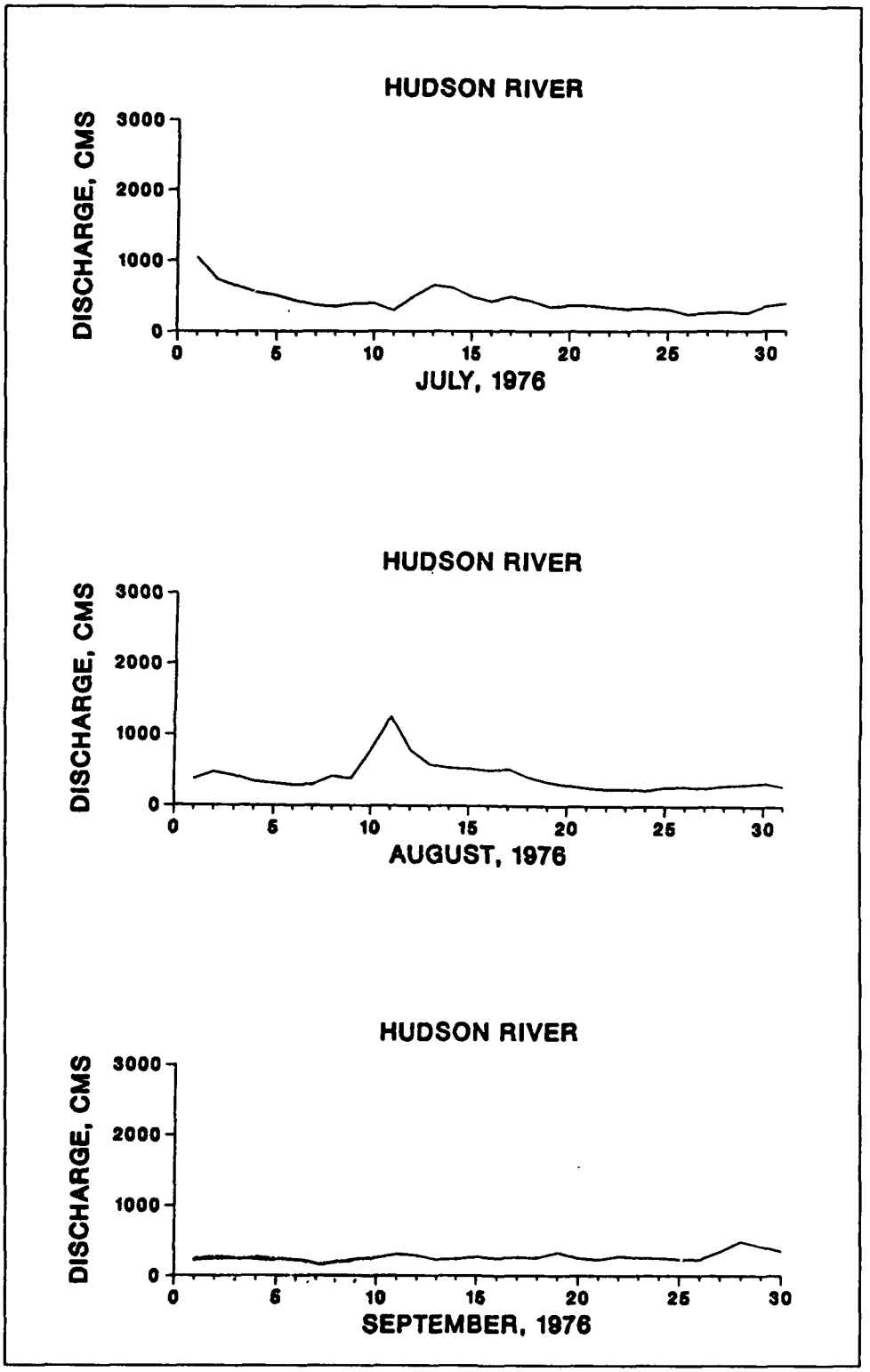

Figure A1. (Sheet 2 of 3)

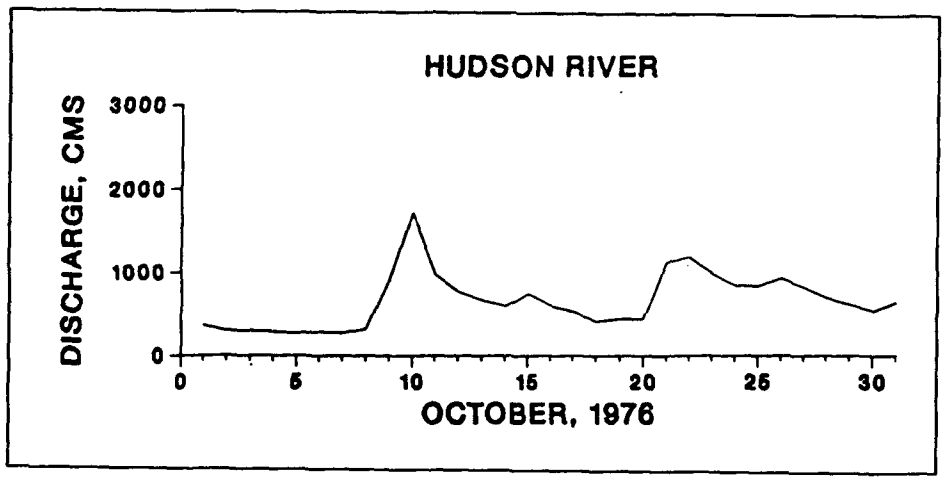

Figure A1. (Sheet 3 of 3)

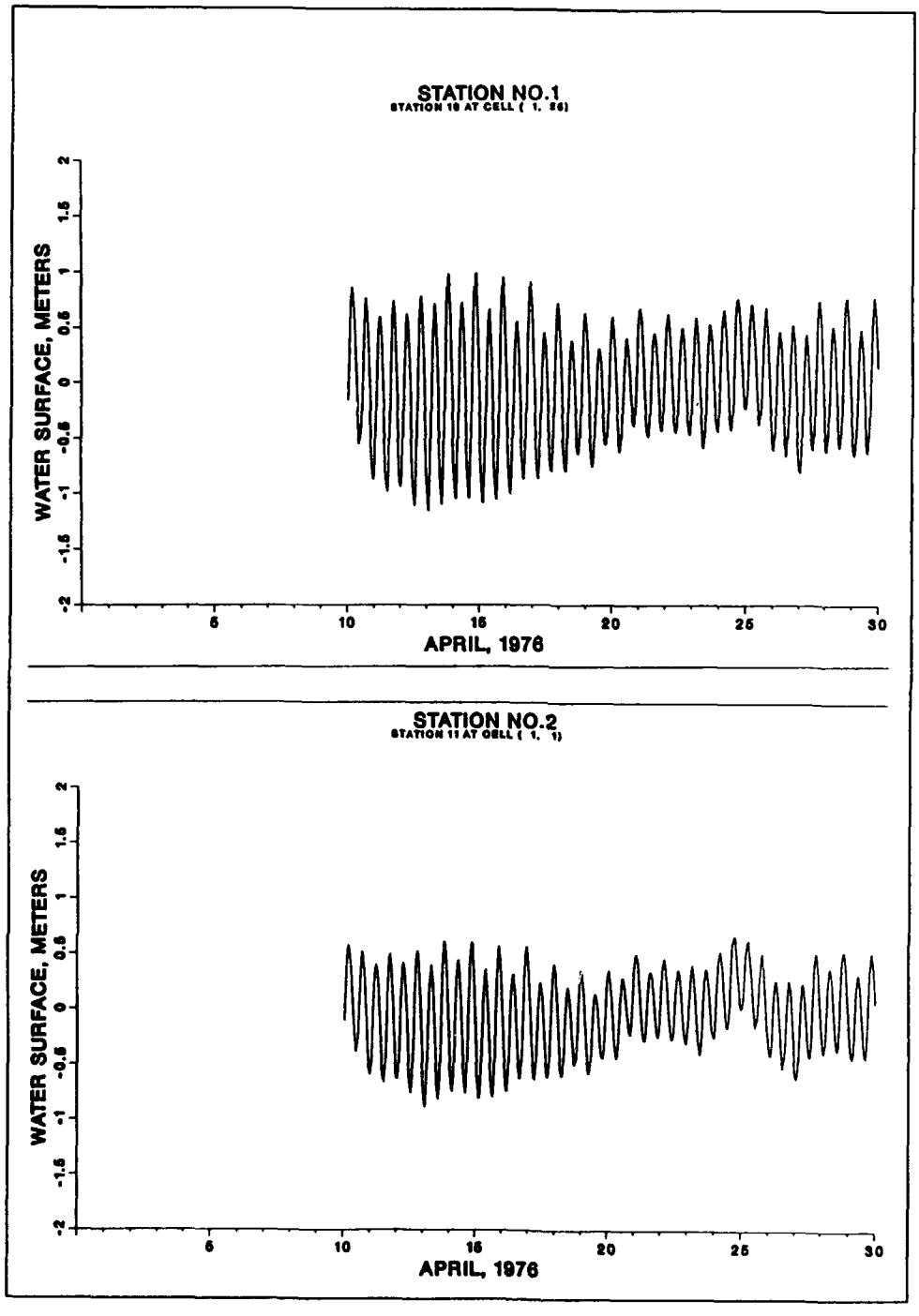

Figure A2. Tidal boundary stations 1 and 2 - April 1976

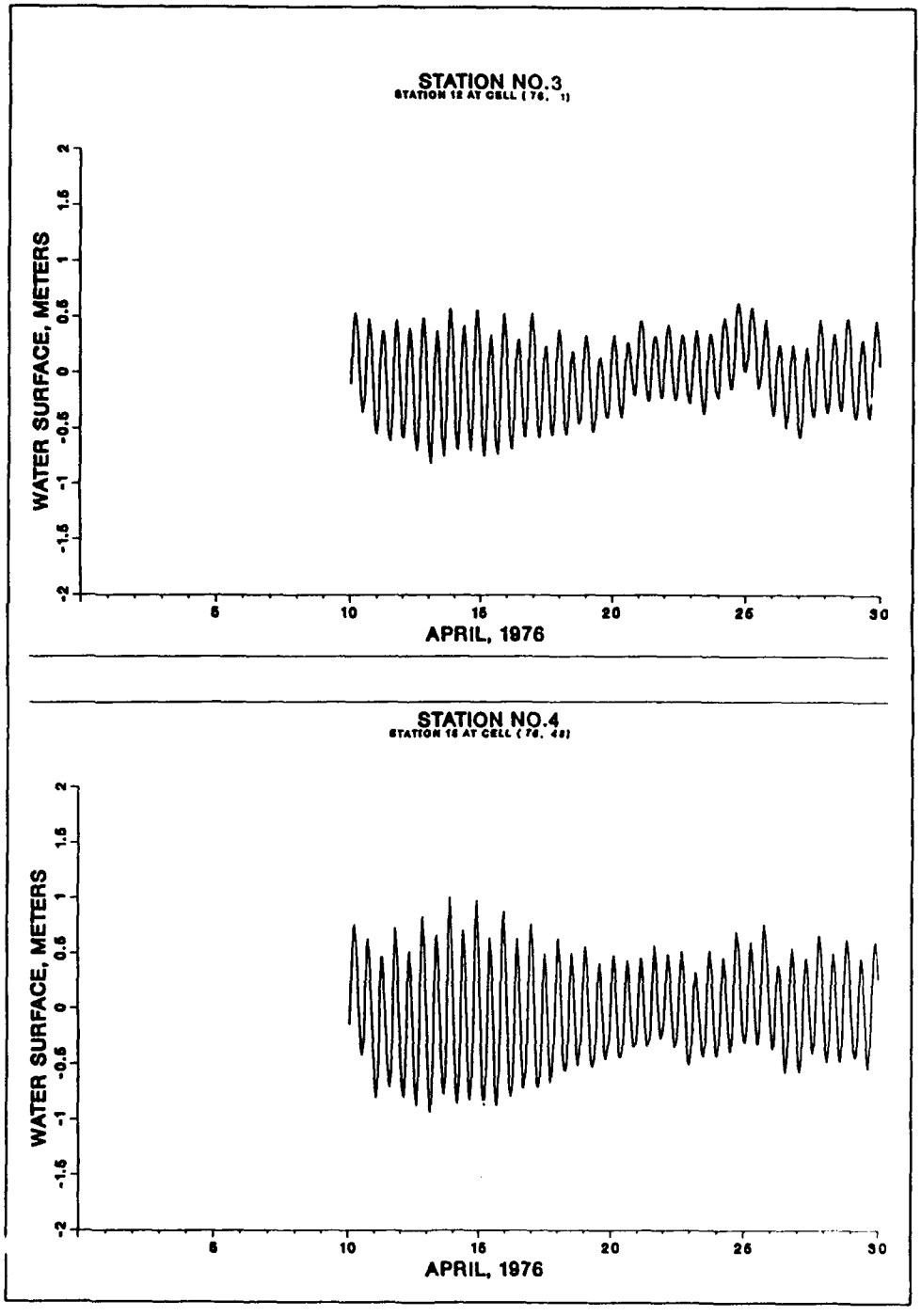

Figure A3. Tidal boundary stations 3 and 4 - April 1976

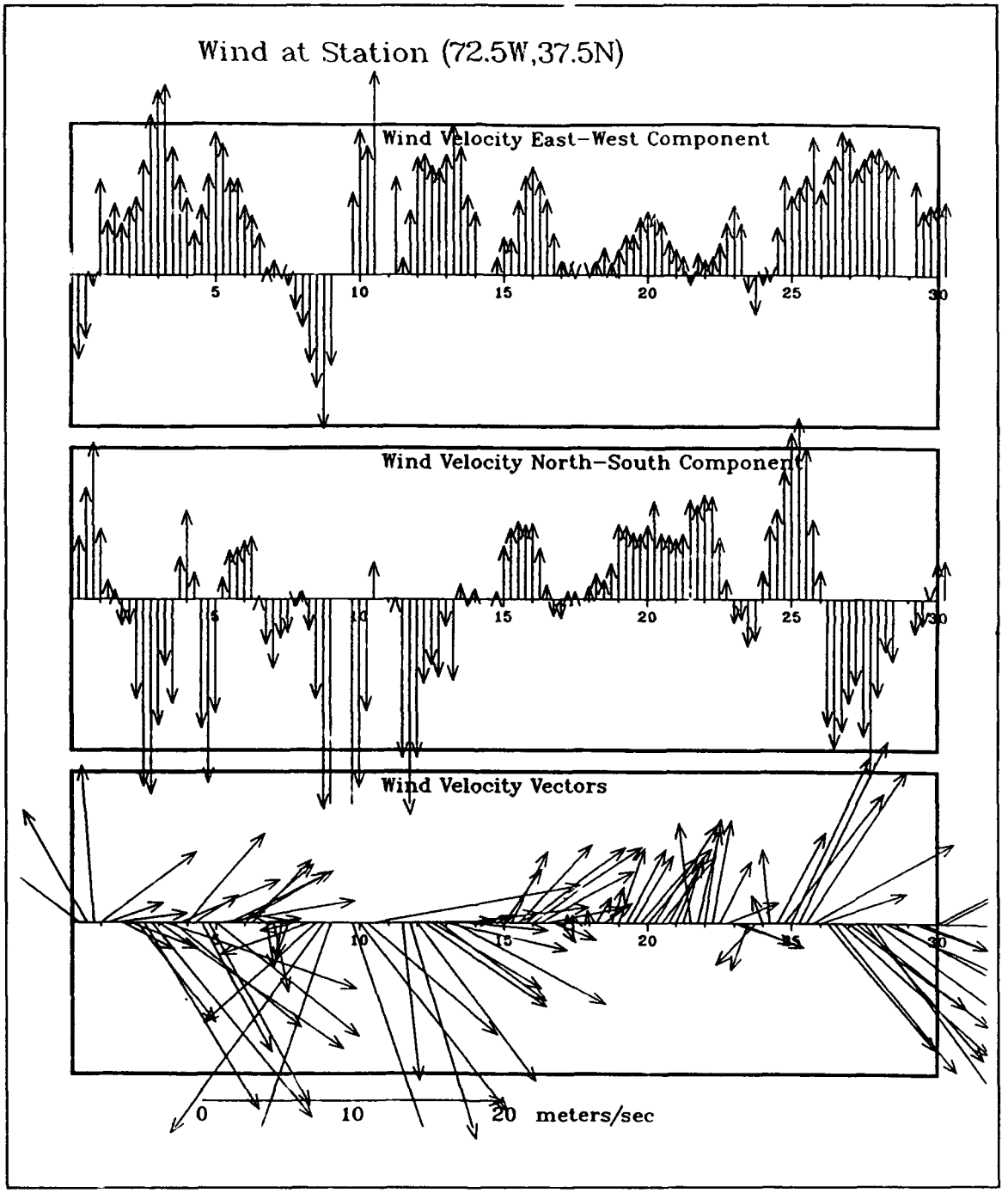

Figure A4. Wind data at station (72.5W,37.5N) during April 1976

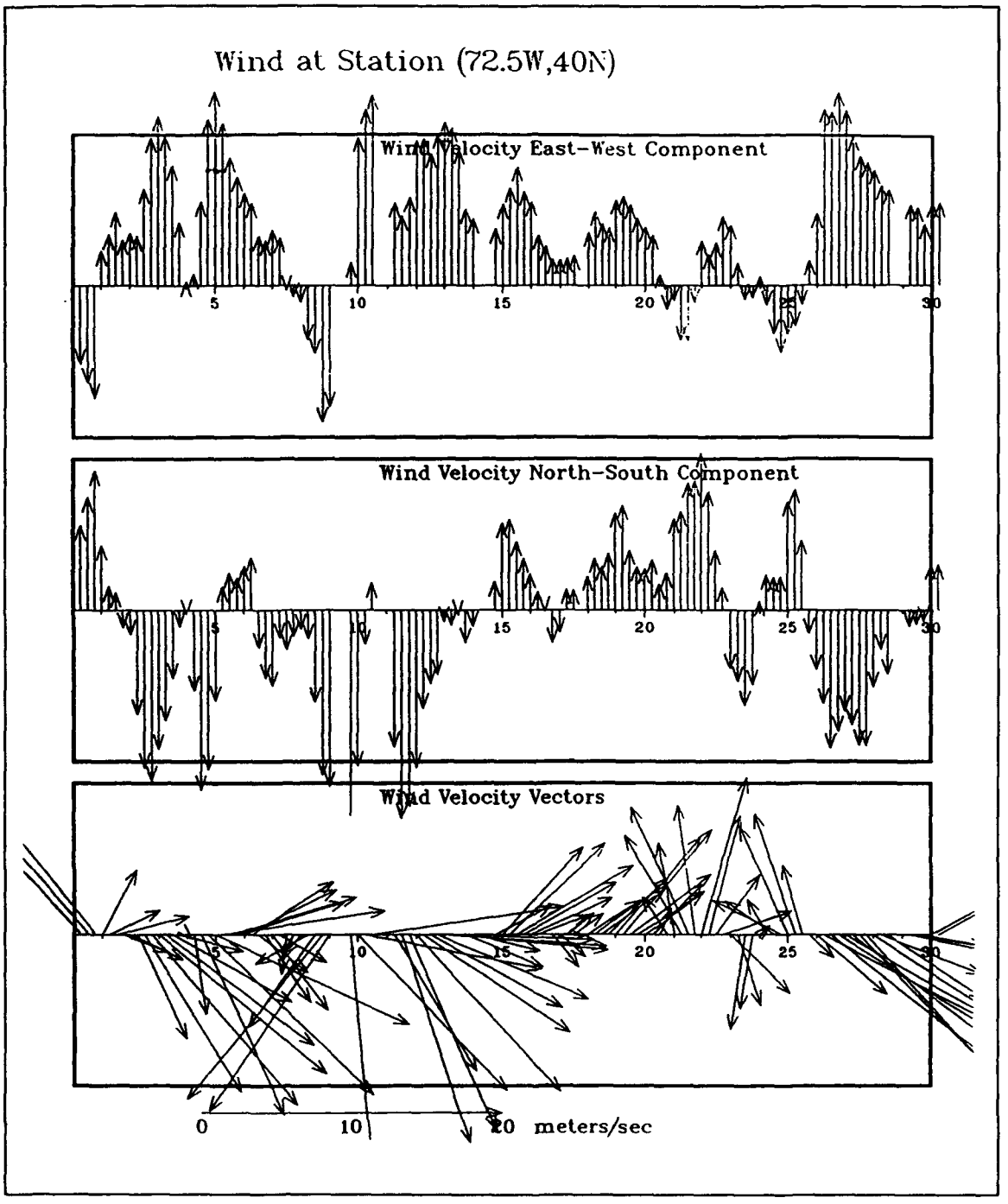

Figure A5. Wind data at station (72.5W,40N) during April 1976

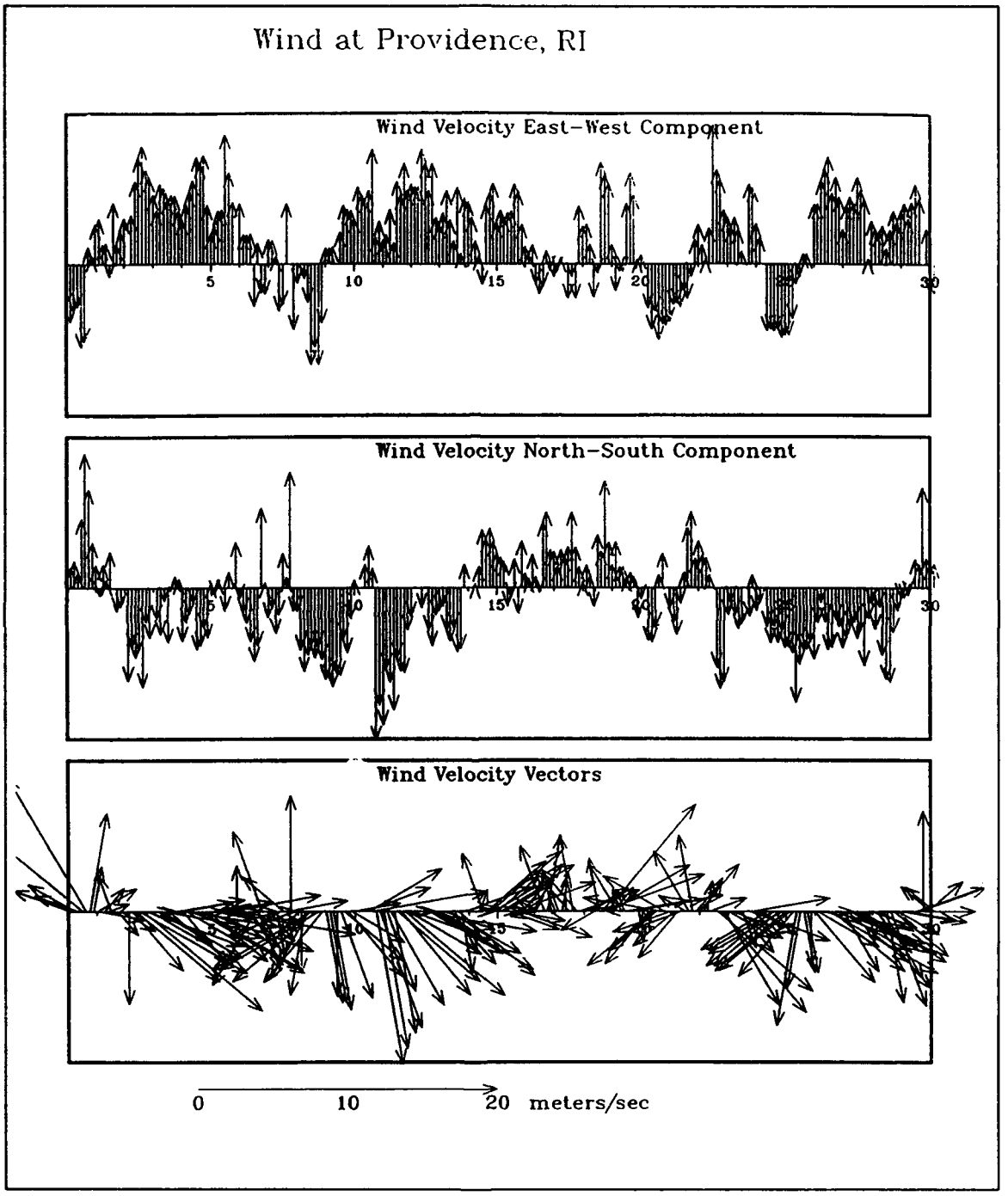

Figure A6. Wind data at Providence, RI during April 1976

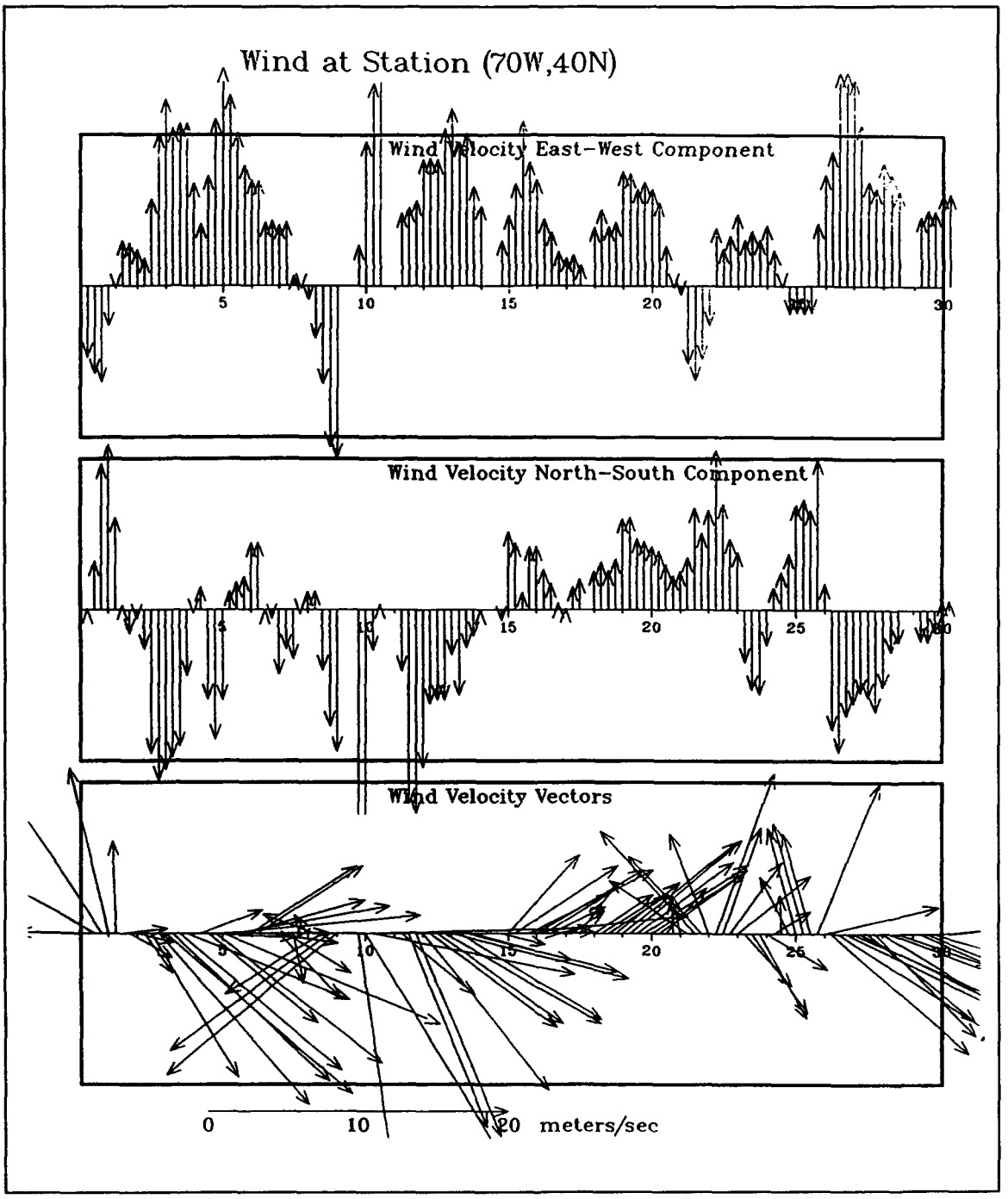

Figure A7. Wind data at station (70W,40N) during April 1976

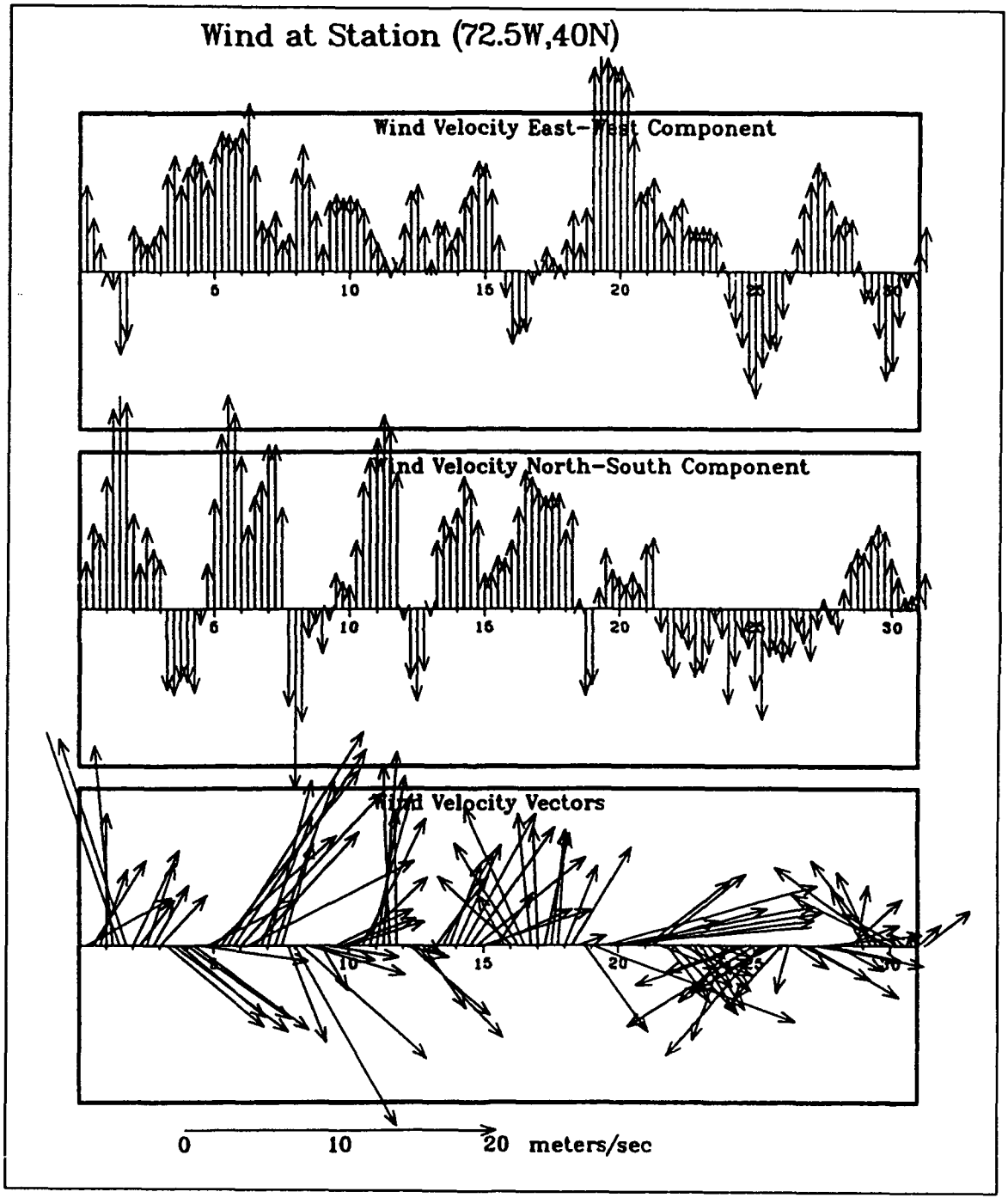

Figure A8. Wind data at station (72.5W,40N) during May 1976

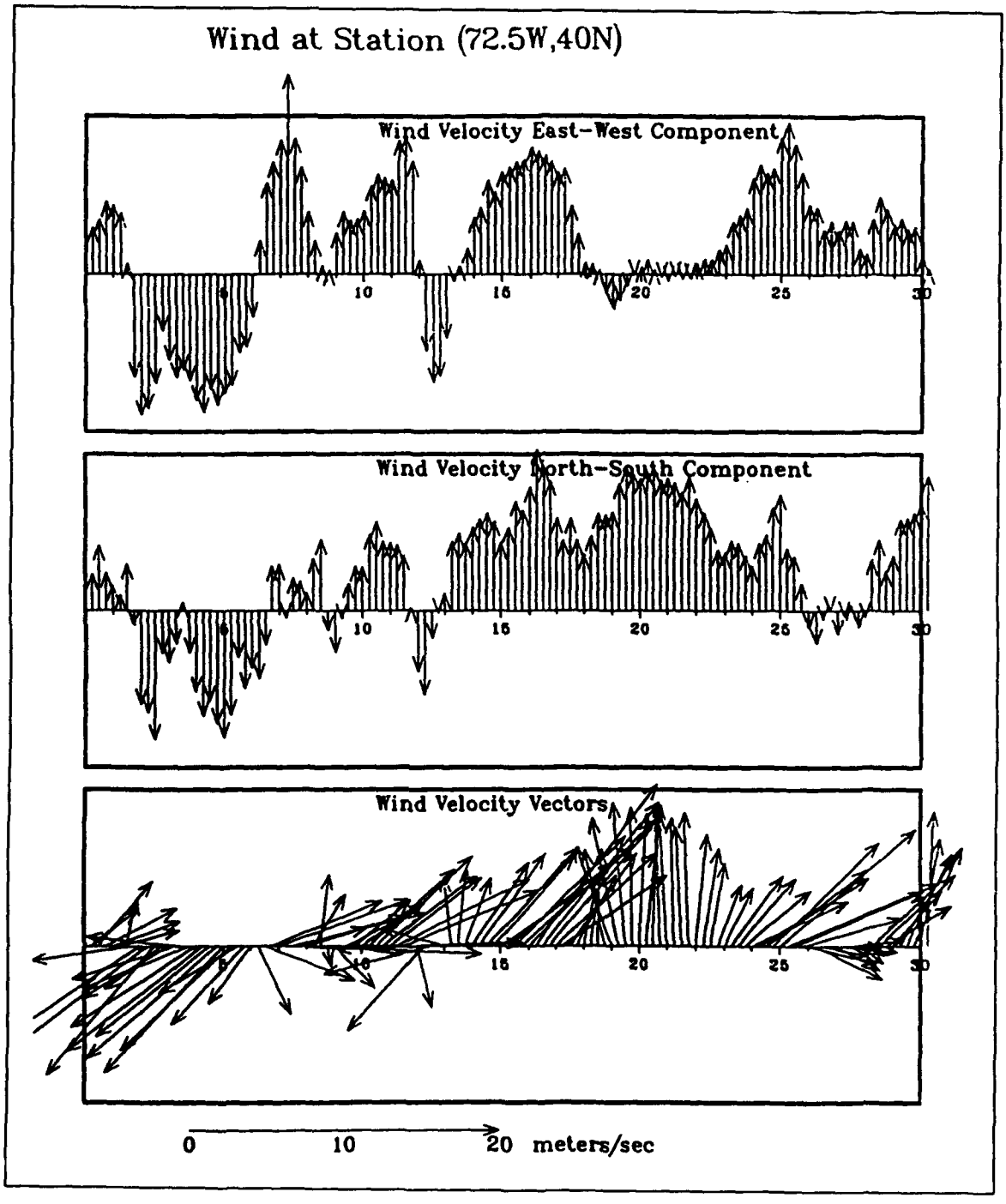

Figure A9. Wind data at station (72.5W,40N) during June 1976

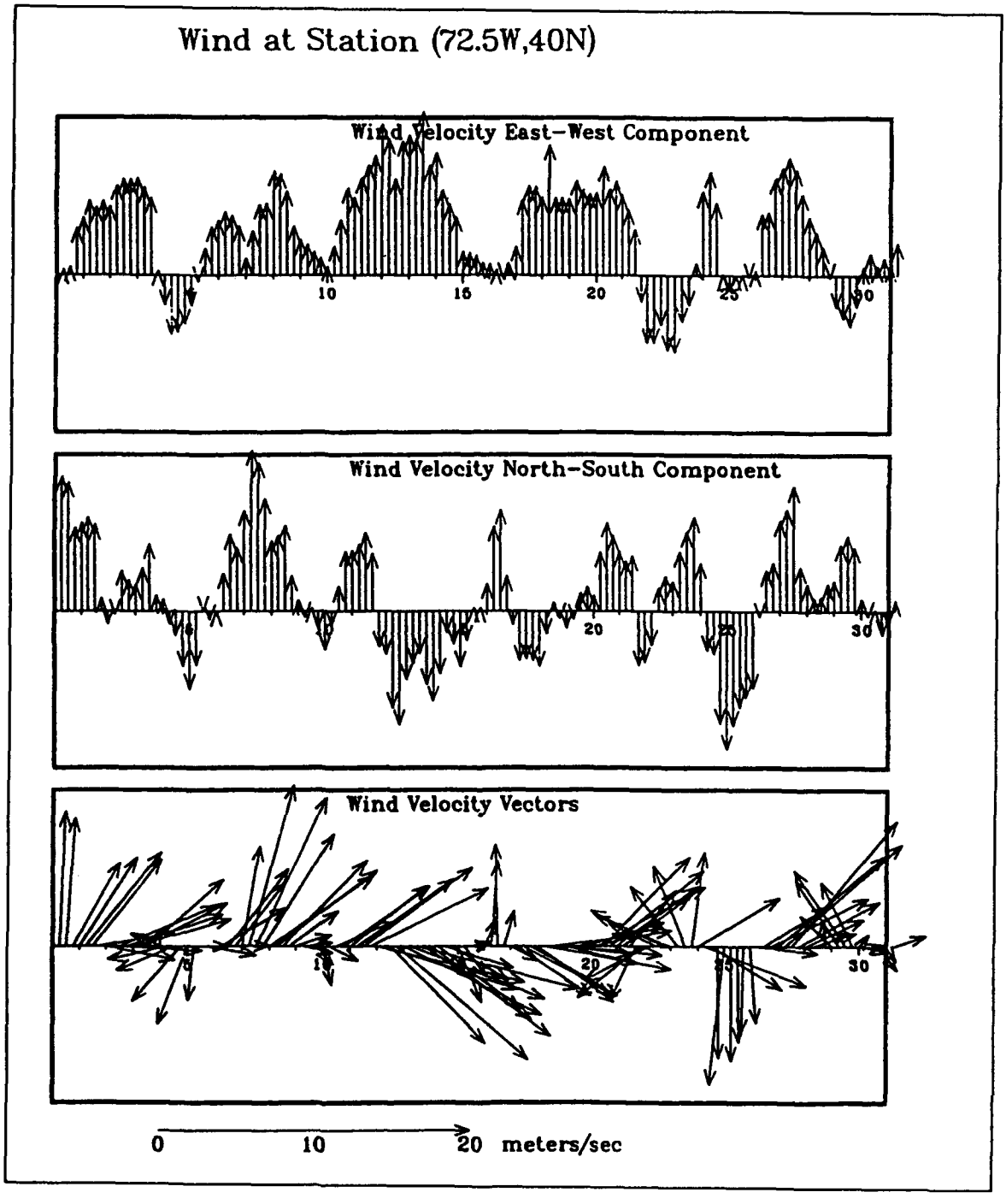

Figure A10. Wind data at station (72.5W,40N) during July 1976

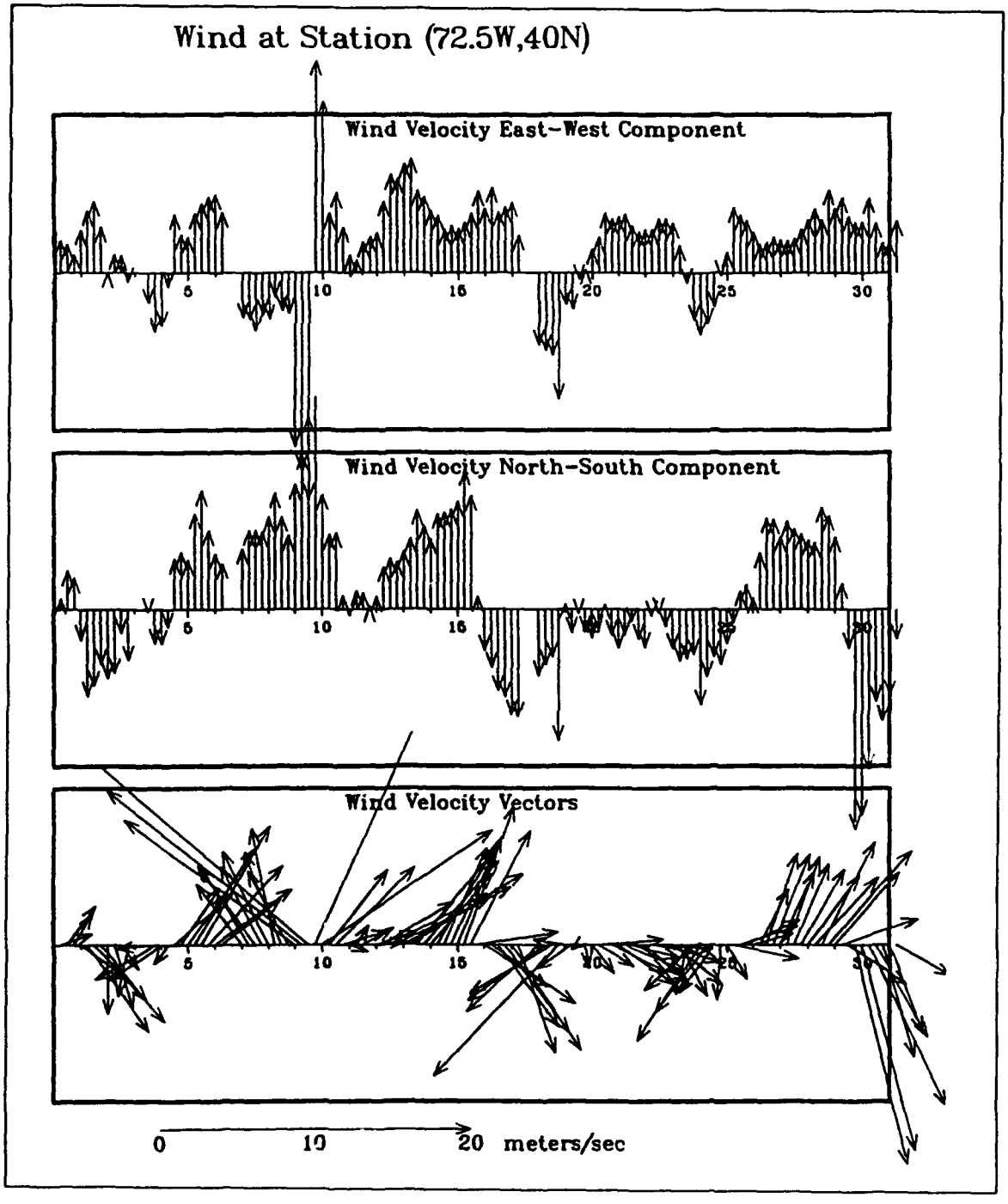

Figure A11. Wind data at station (72.5W,40N) during August 1976

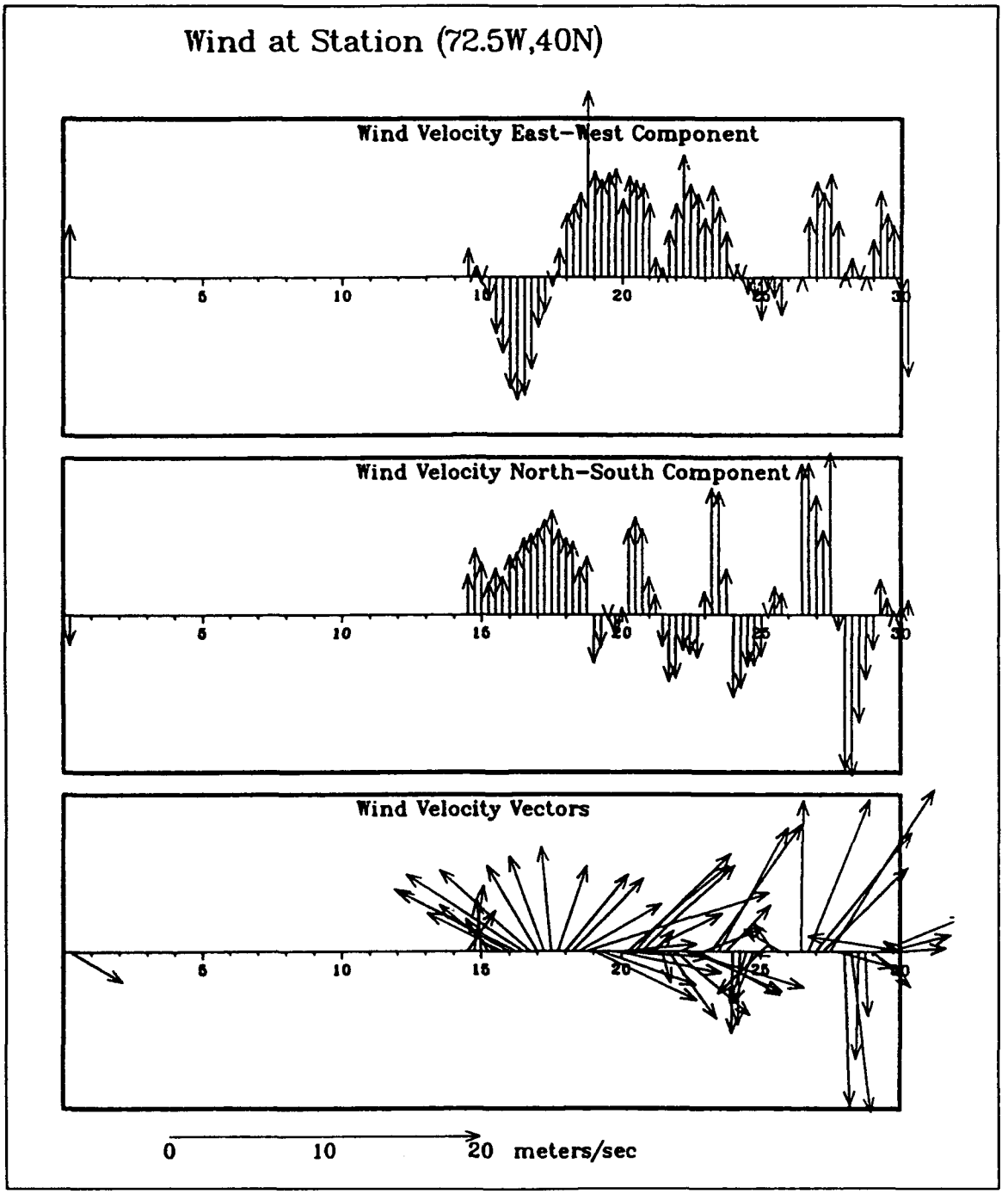

Figure A12. Wind data at station (72.5W,40N) during September 1976

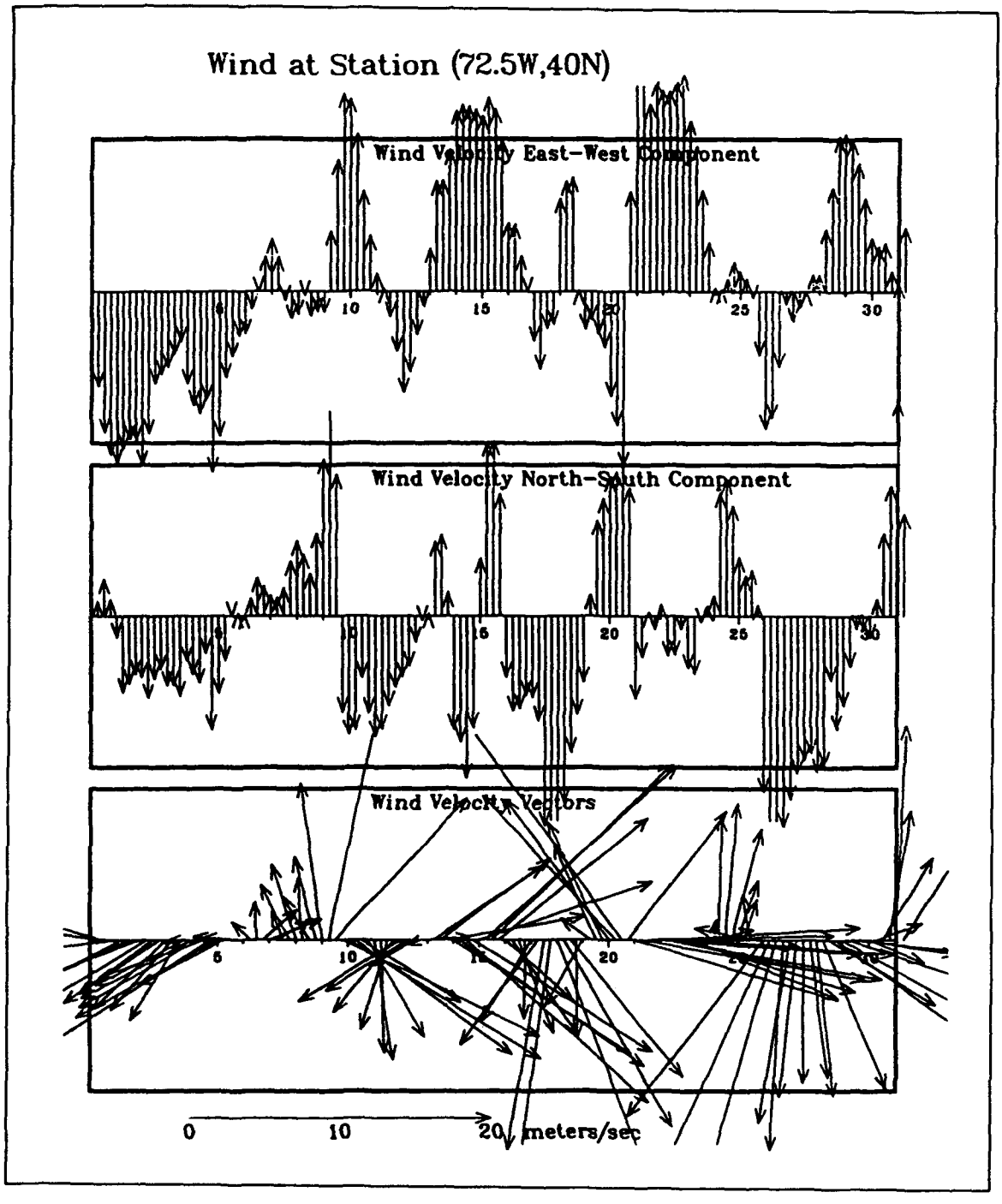

Figure A13. Wind data at station (72.5W,40N) during October 1976

Appendix B
Calibration Comparisons

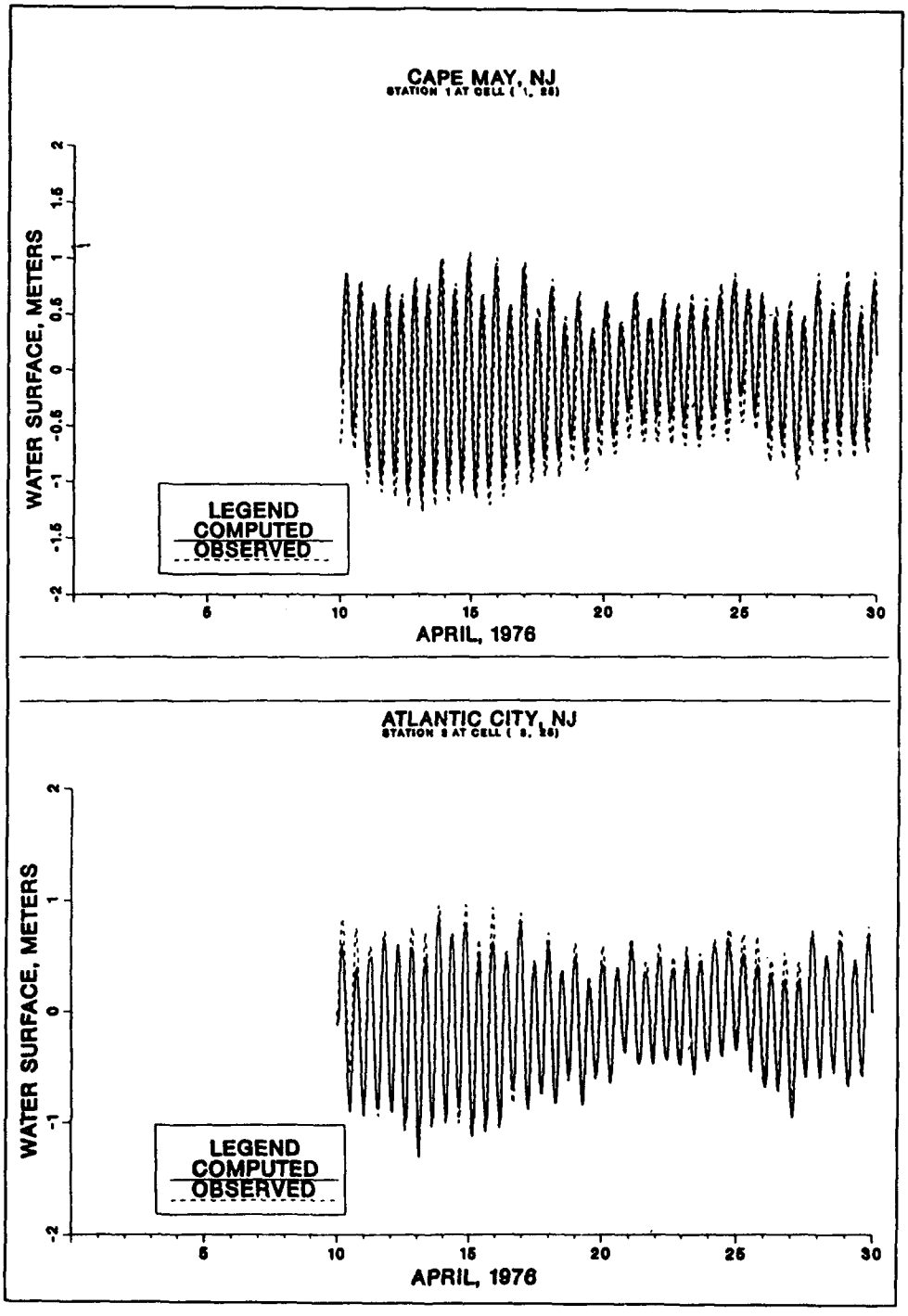

Figure B1. April 1976 tidal elevation comparisons (Sheet 1 of 5)

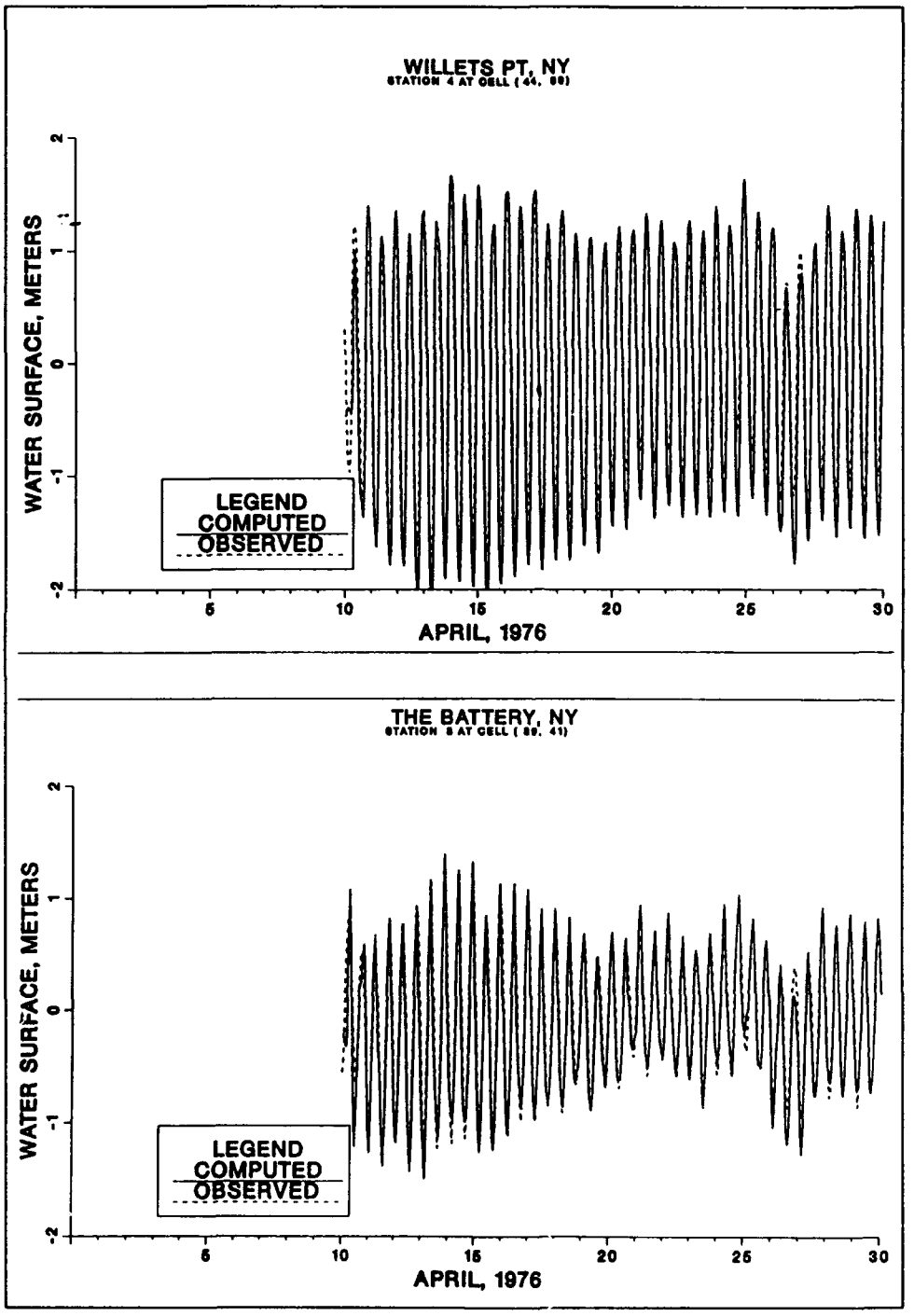

Figure B1. (Sheet 2 of 5)

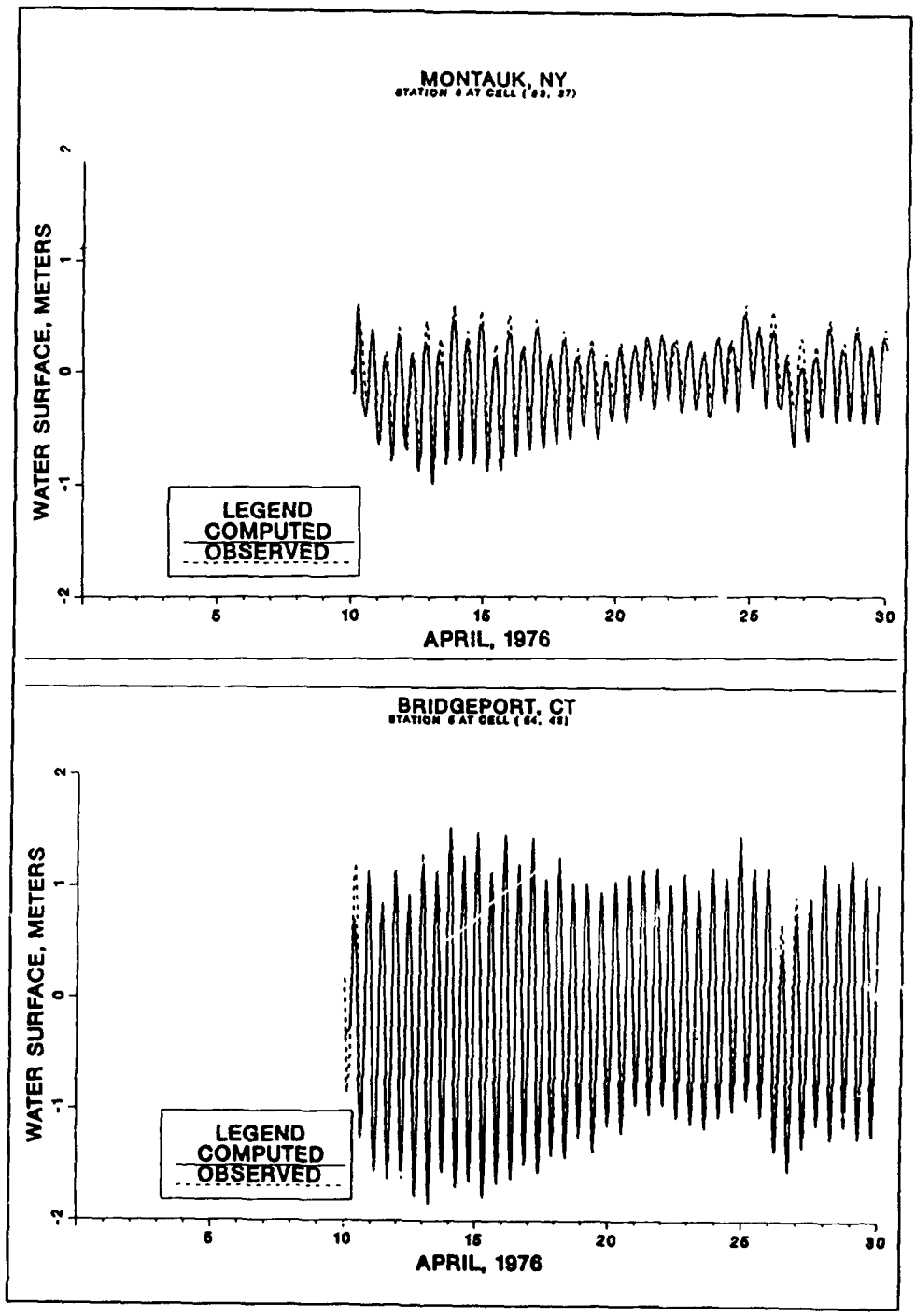

Figure B1. (Sheet 3 of 5)

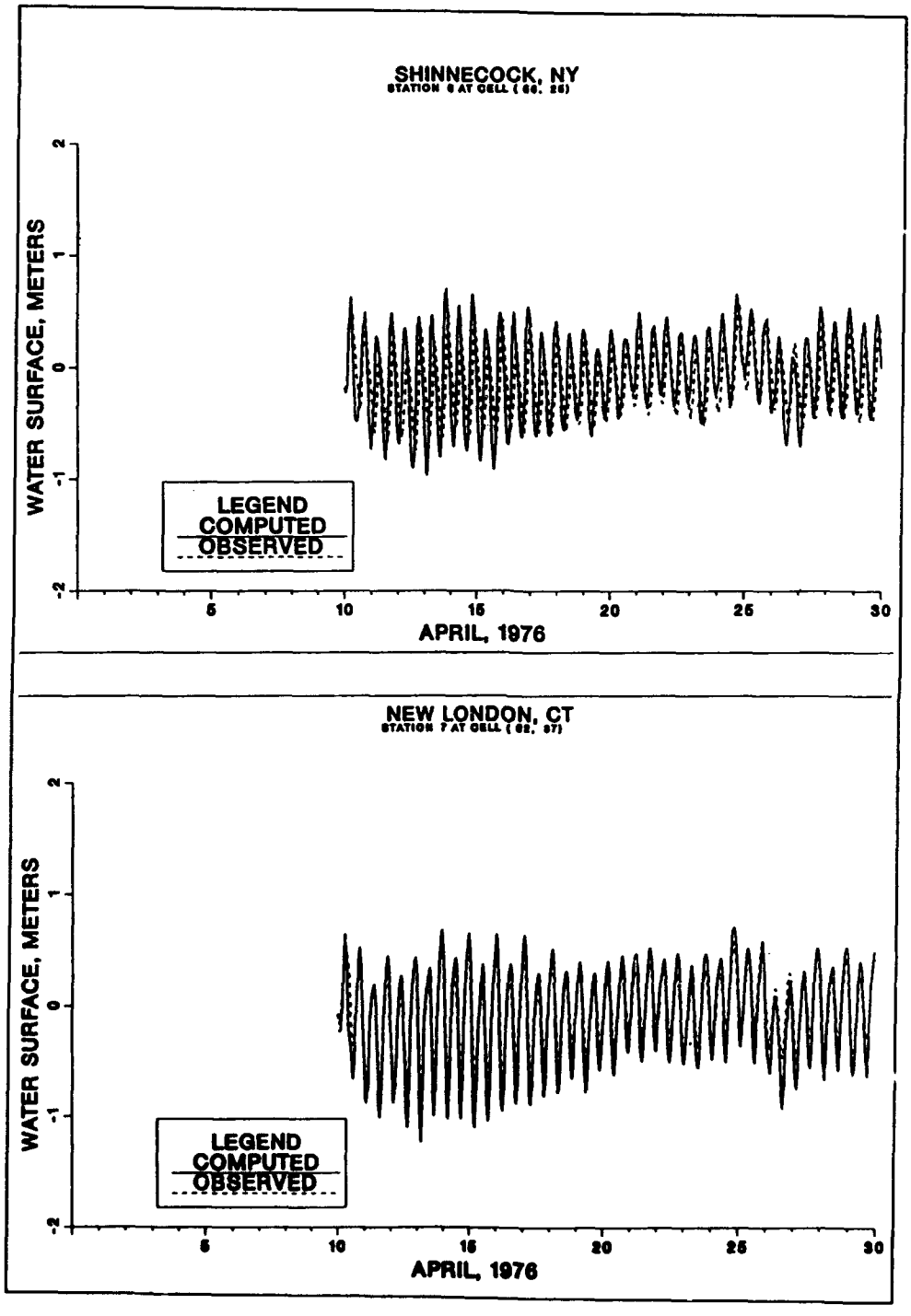

Figure B1. (Sheet 4 of 5)

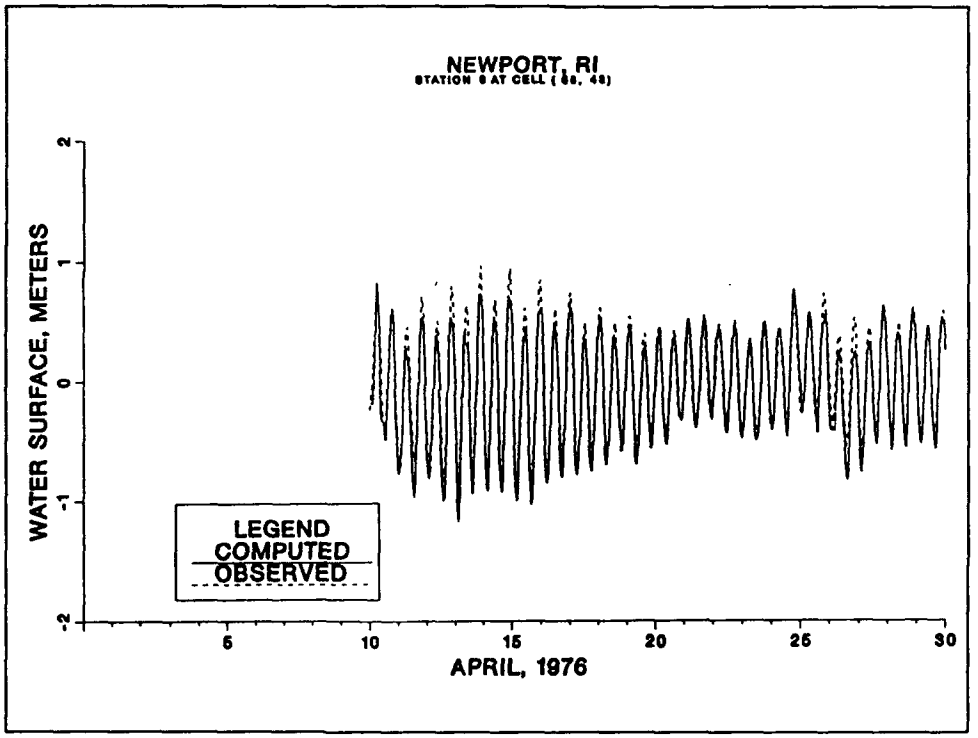

Figure B1. (Sheet 5 of 5)

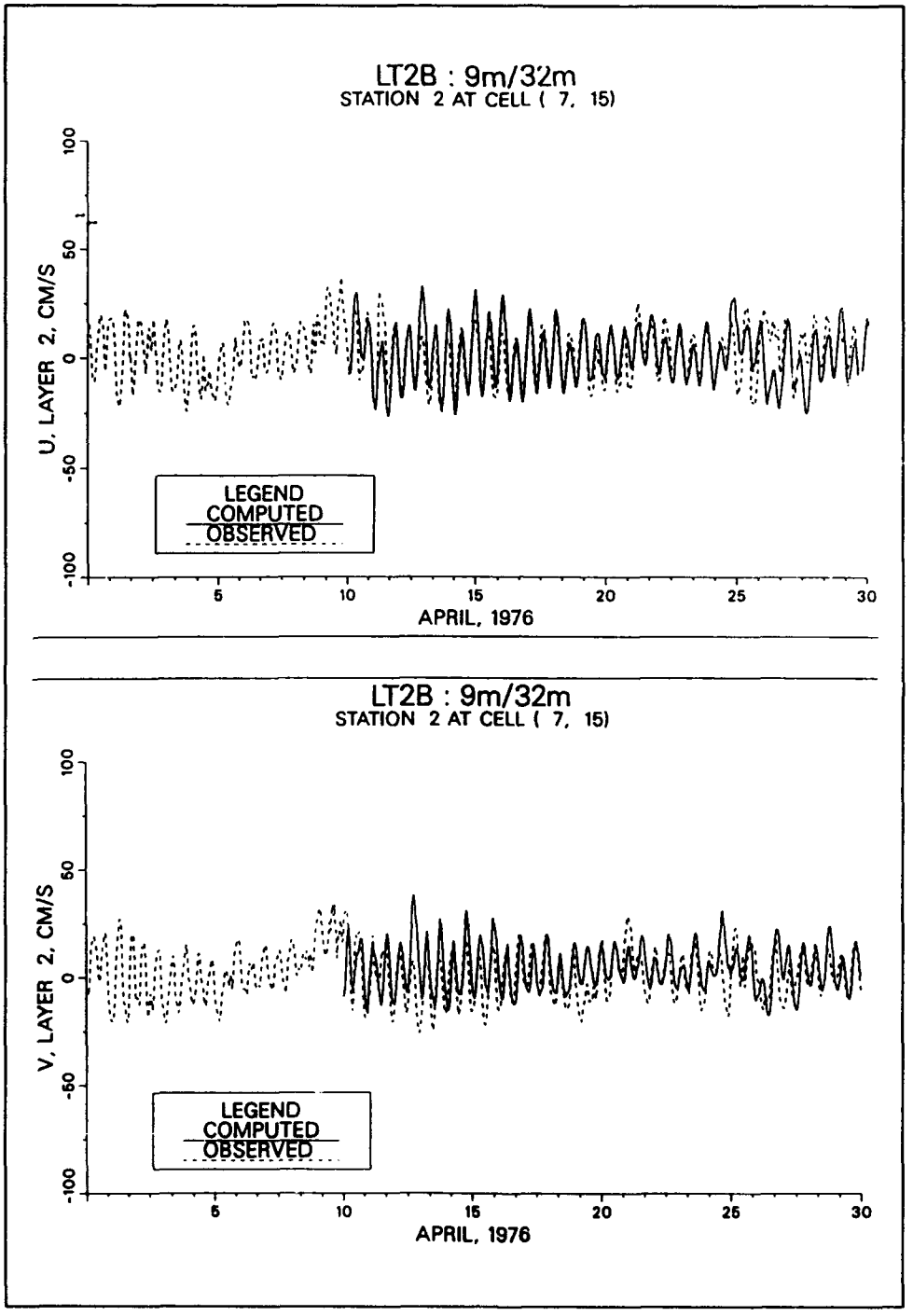

Figure B2. April 1976 current comparisons (Sheet 1 of 12)

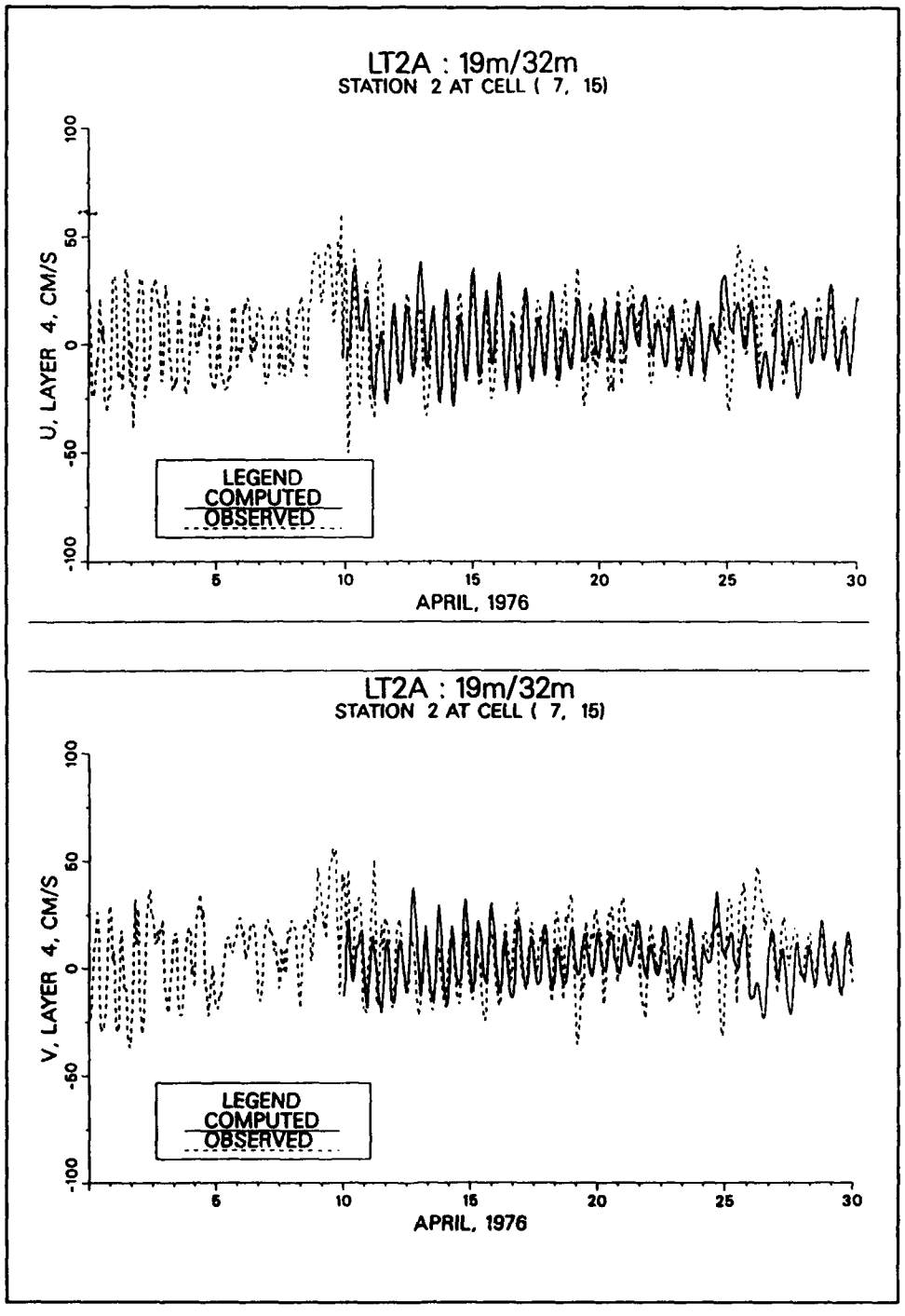

Figure B2. (Sheet 2 of 12)

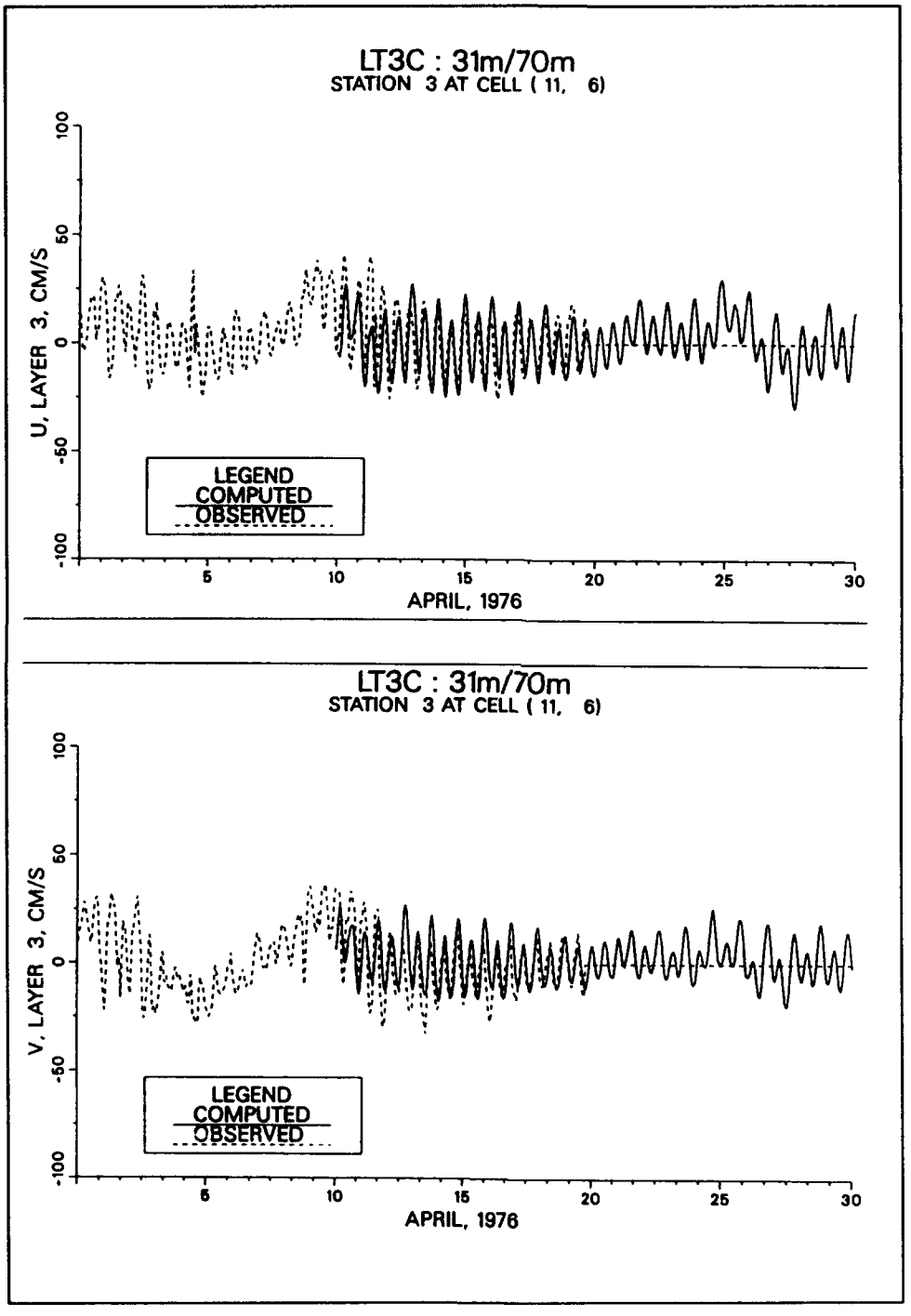

Figure B2. (Sheet 3 of 12)

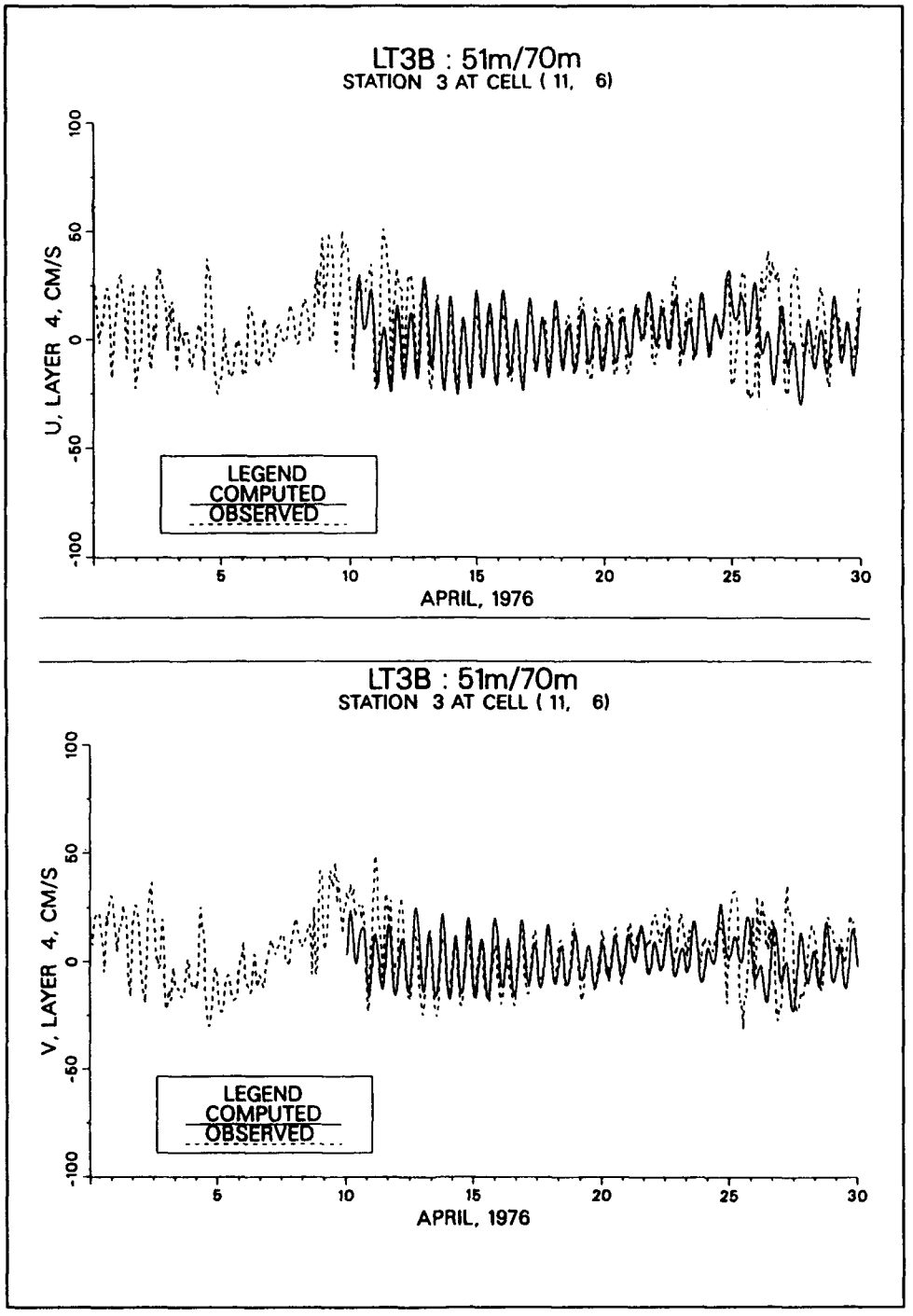

Figure B2. (Sheet 4 of 12)

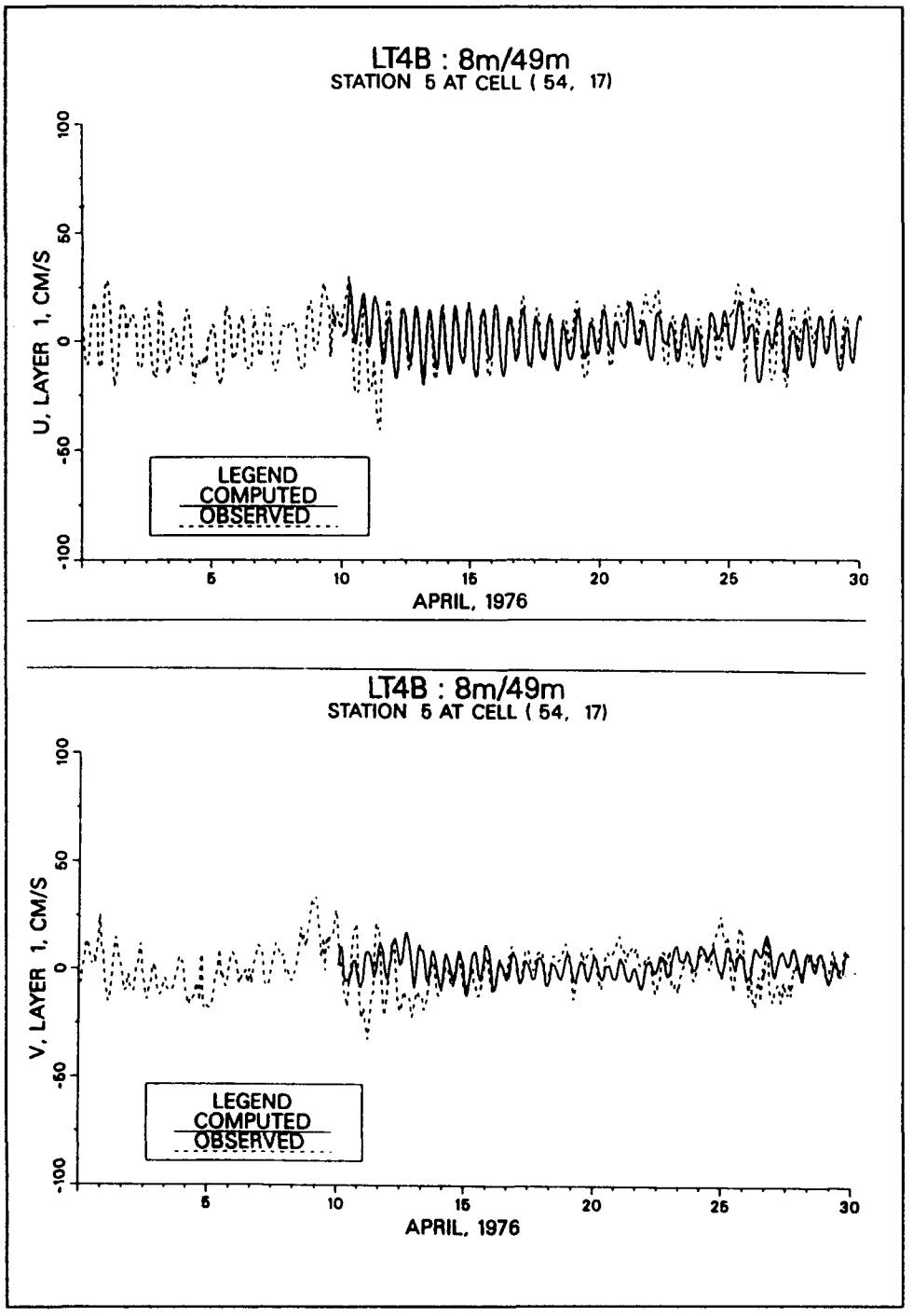

Figure B2. (Sheet 5 of 12)

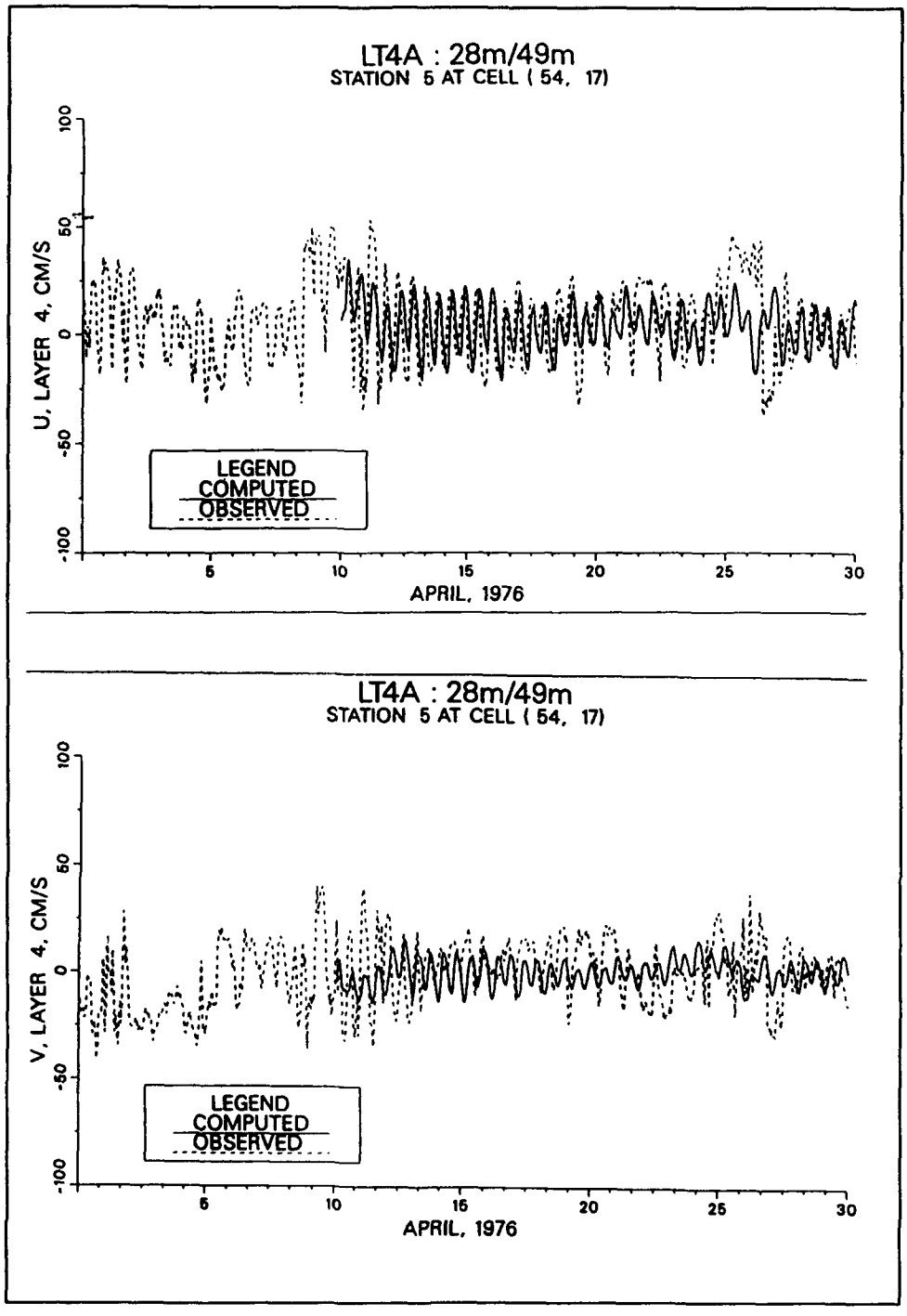

Figure B2. (Sheet 6 of 12)

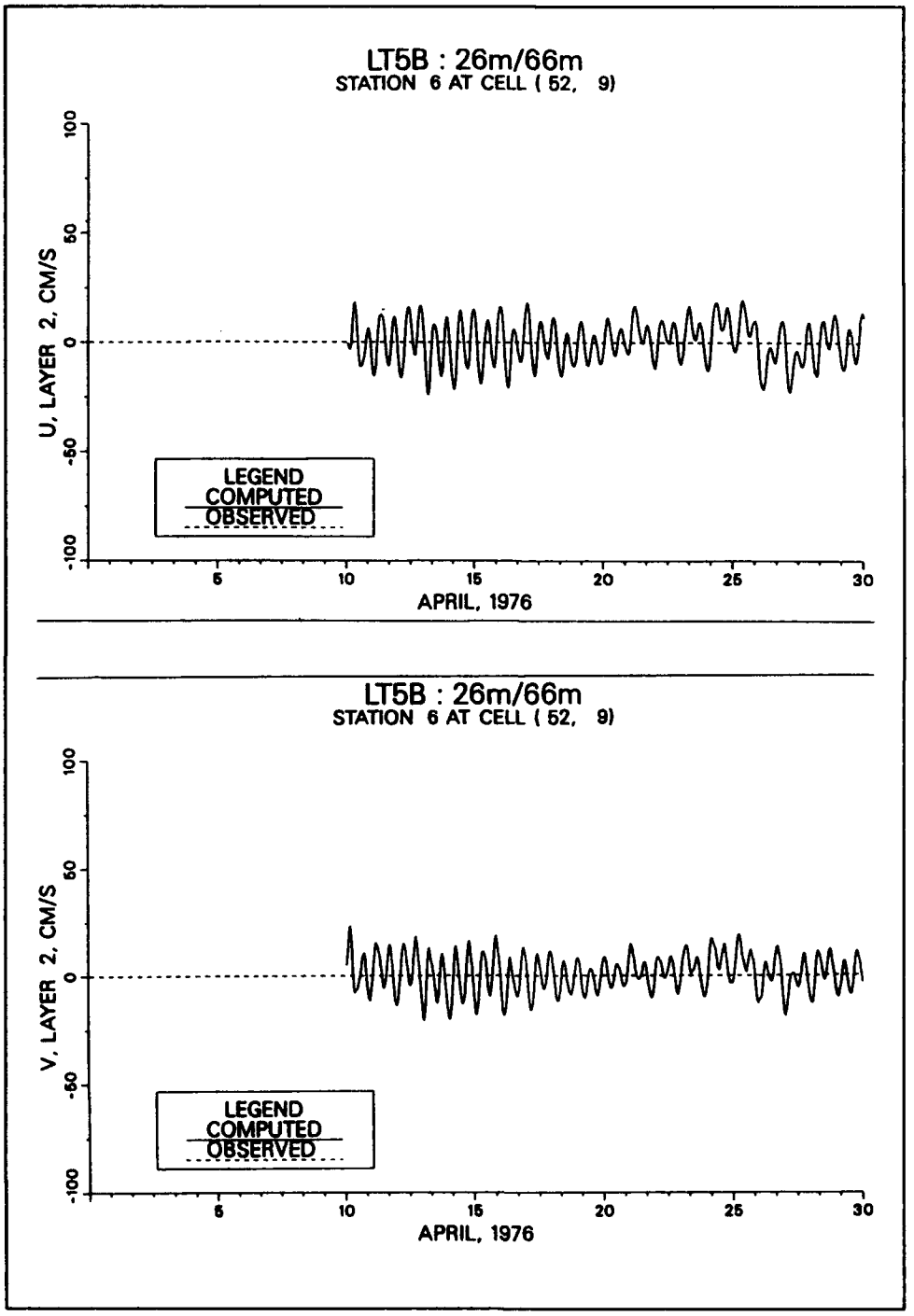

Figure B2. (Sheet 7 of 12)

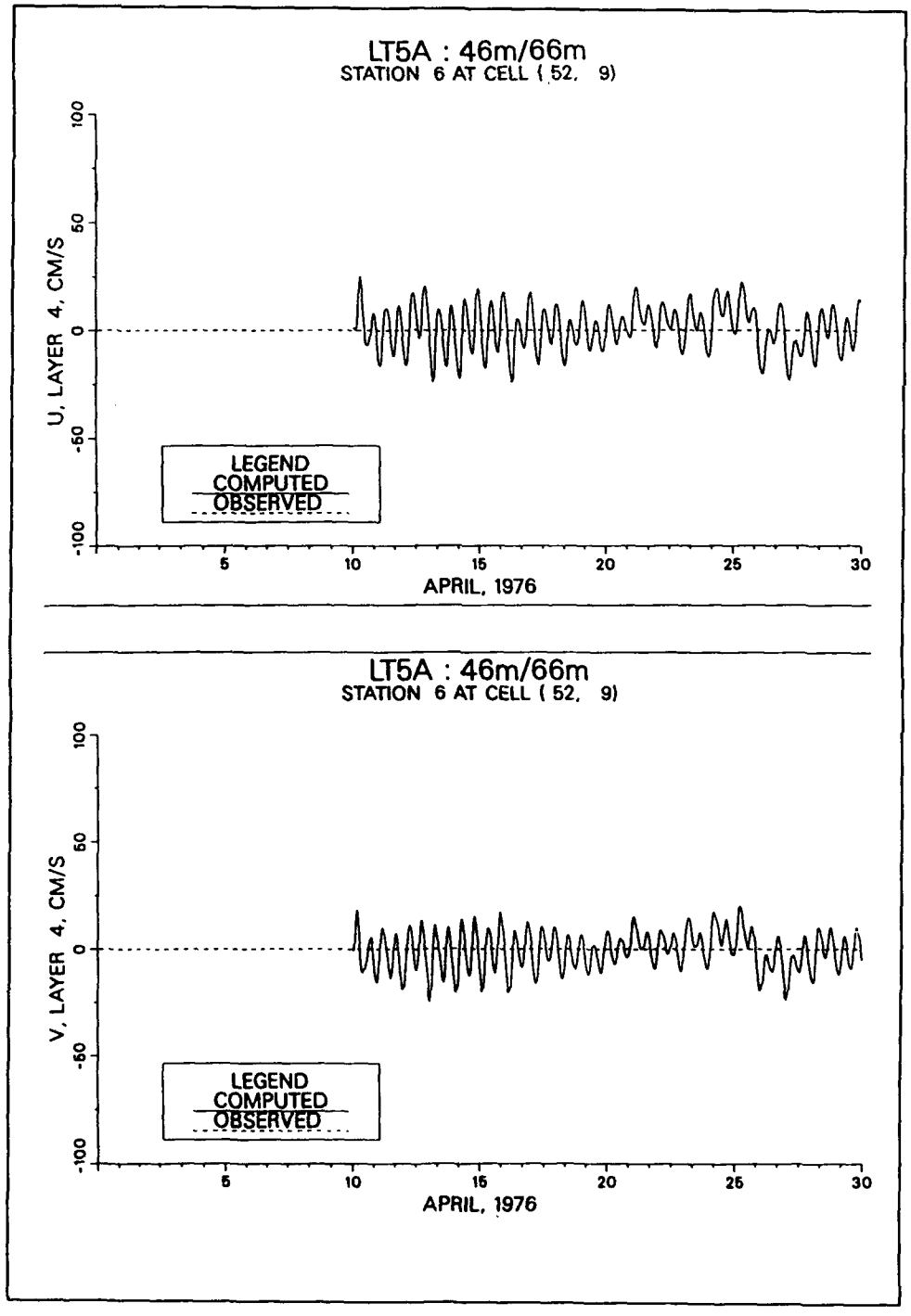

Figure B2. (Sheet 8 of 12)

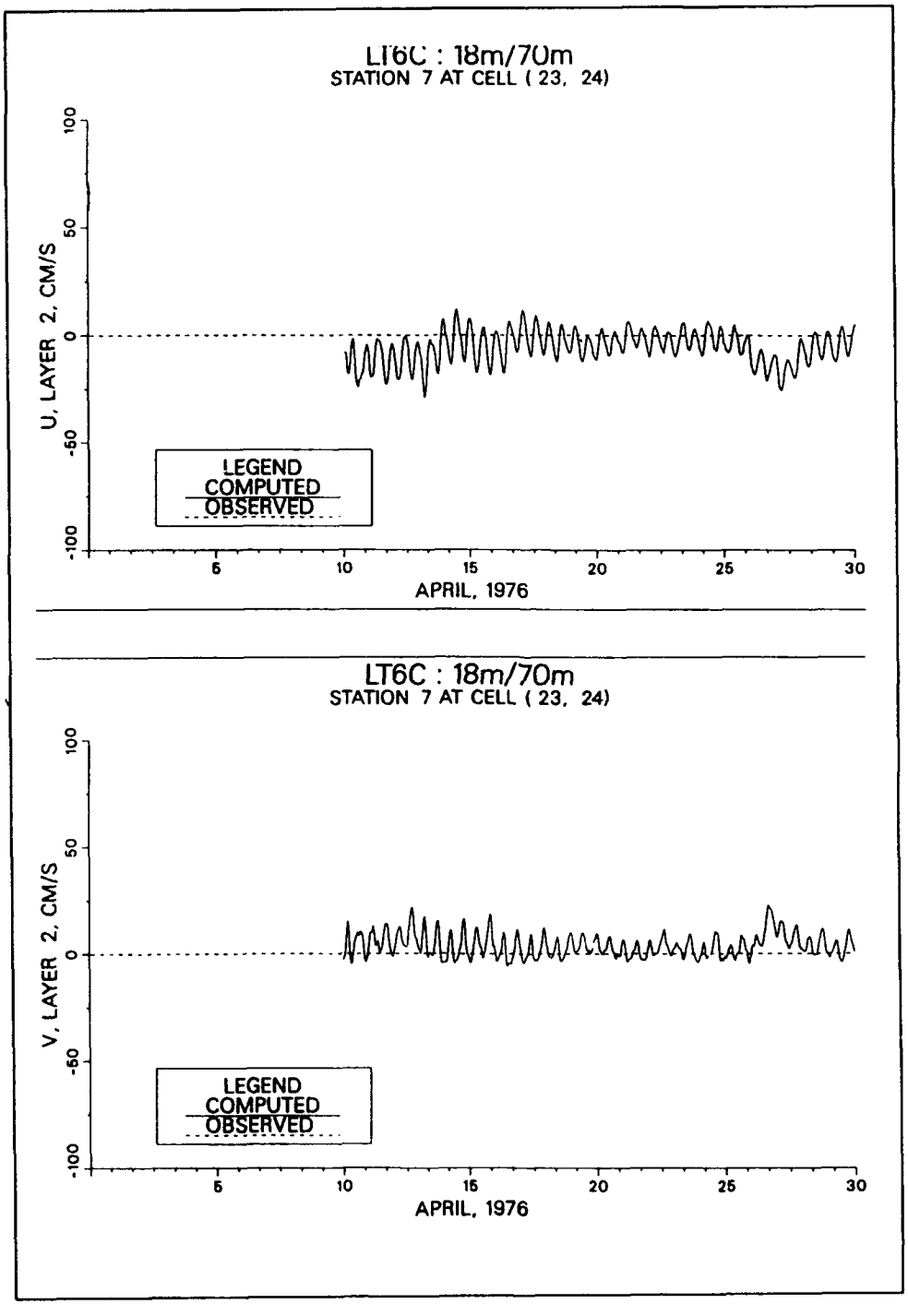

Figure B2. (Sheet 9 of 12)

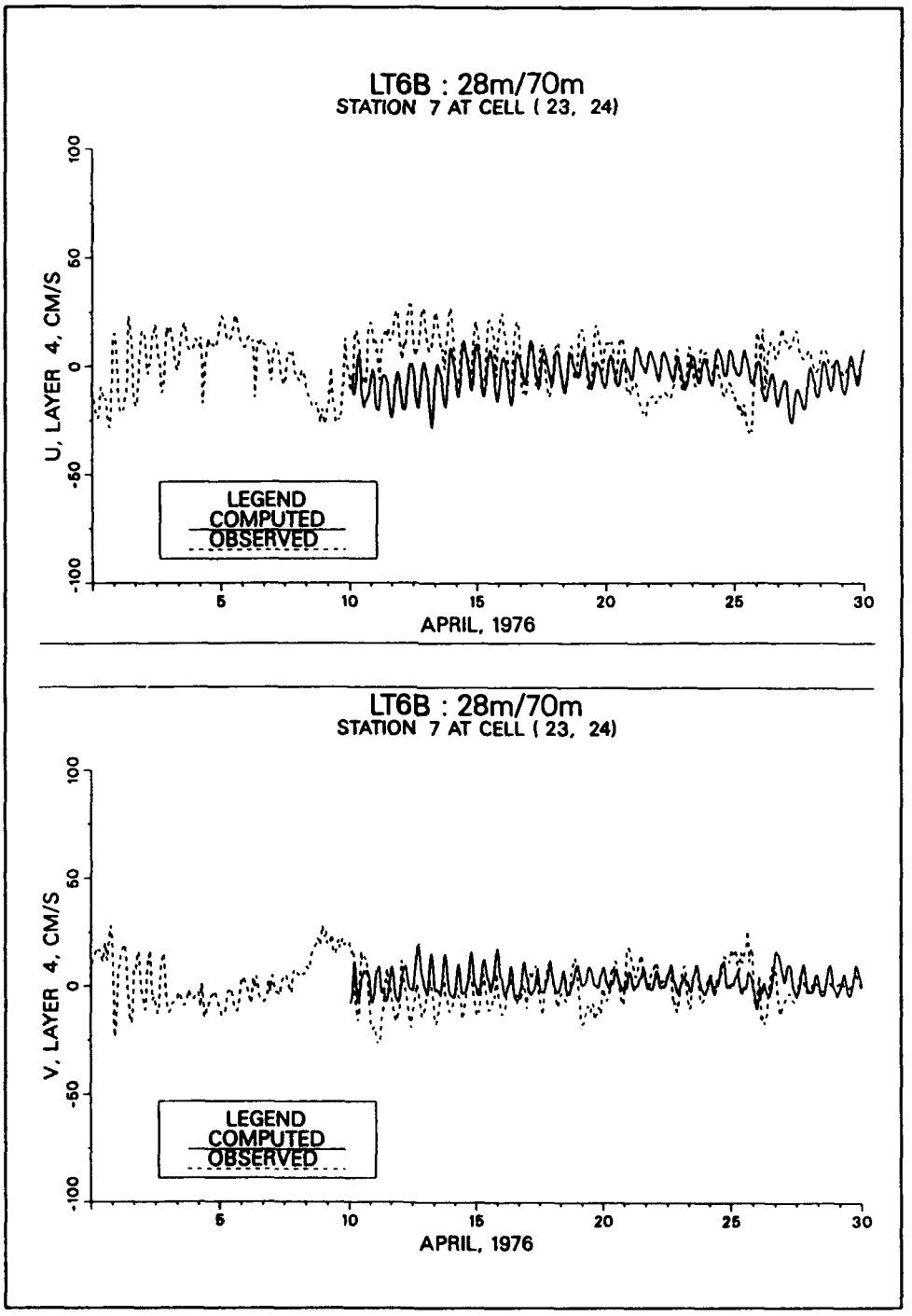

Figure B2. (Figure 10 of 12)

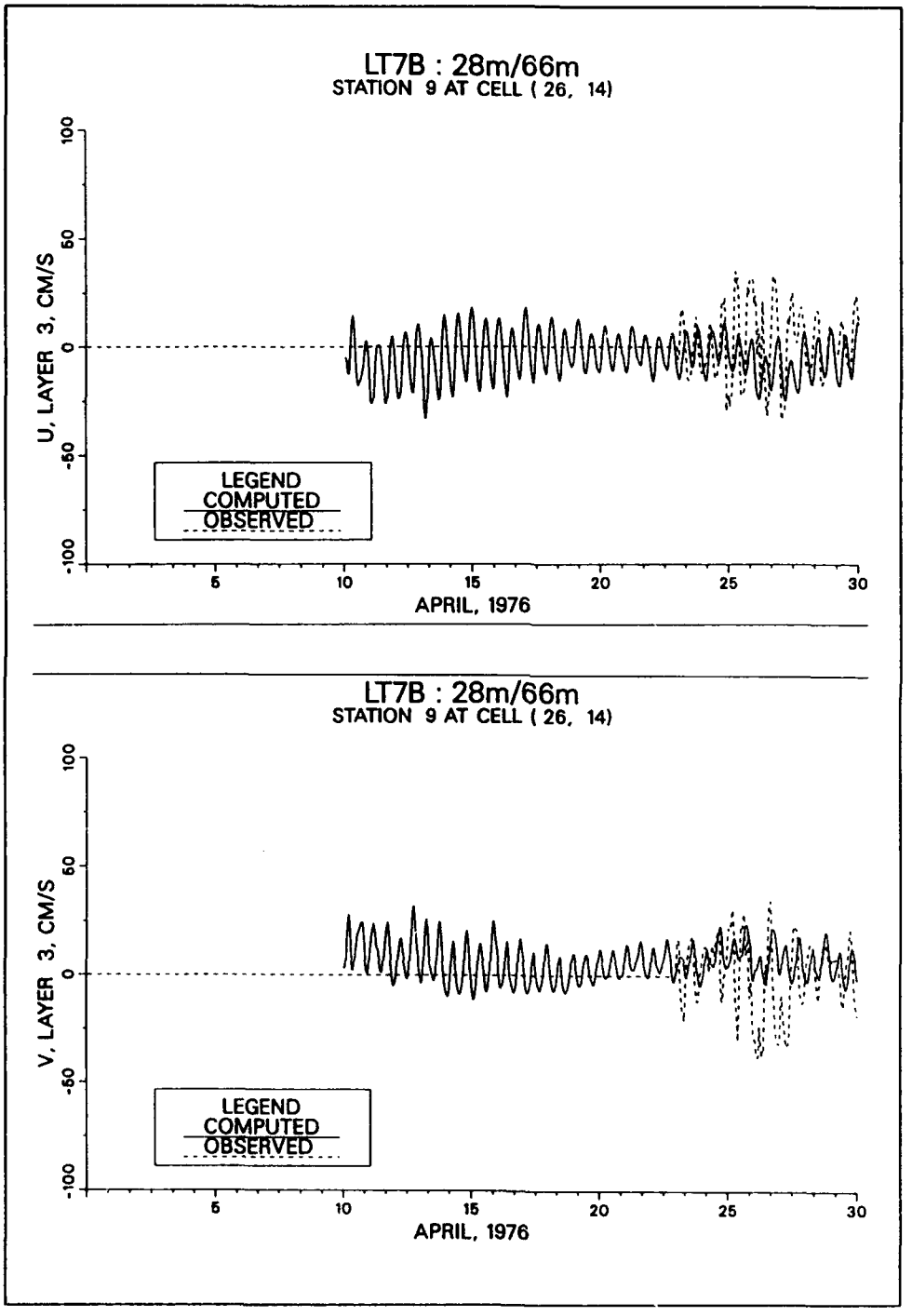

Figure B2. (Sheet 11 of 12)

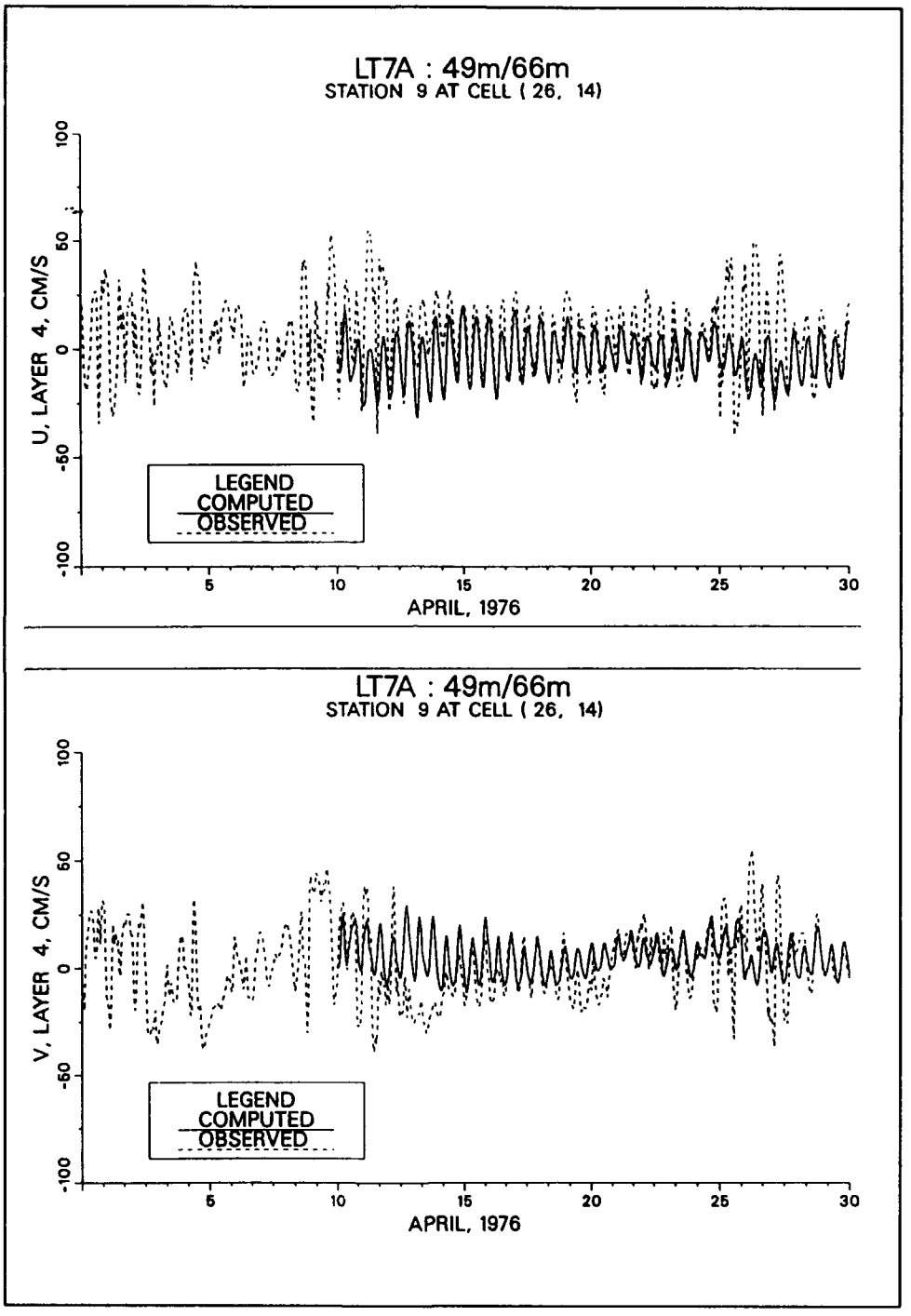

Figure B2. (Sheet 12 of 12)

Appendix C
Verification Comparisons

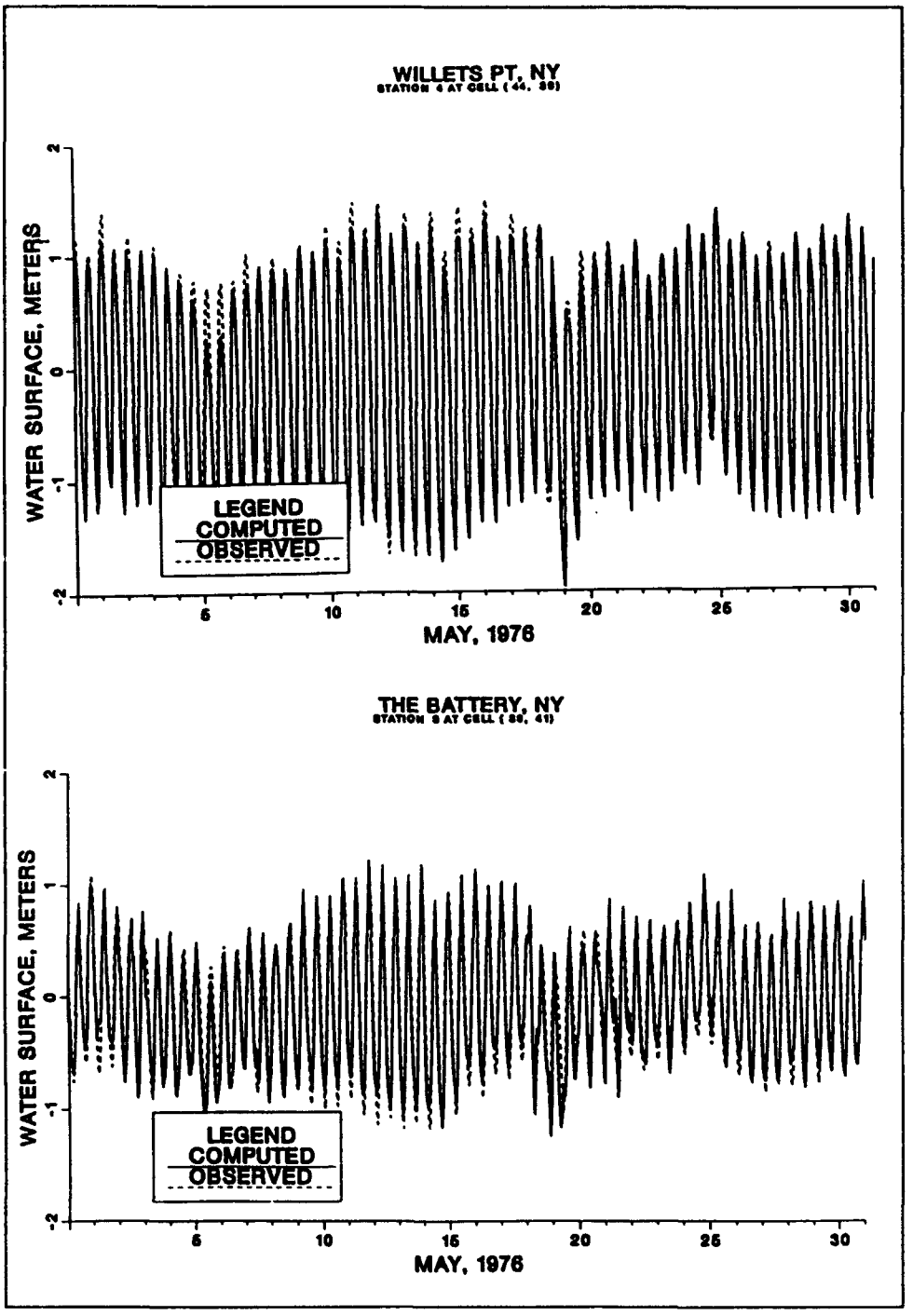

Figure C1. May 1976 tidal elevation comparisons (Sheet 1 of 5)

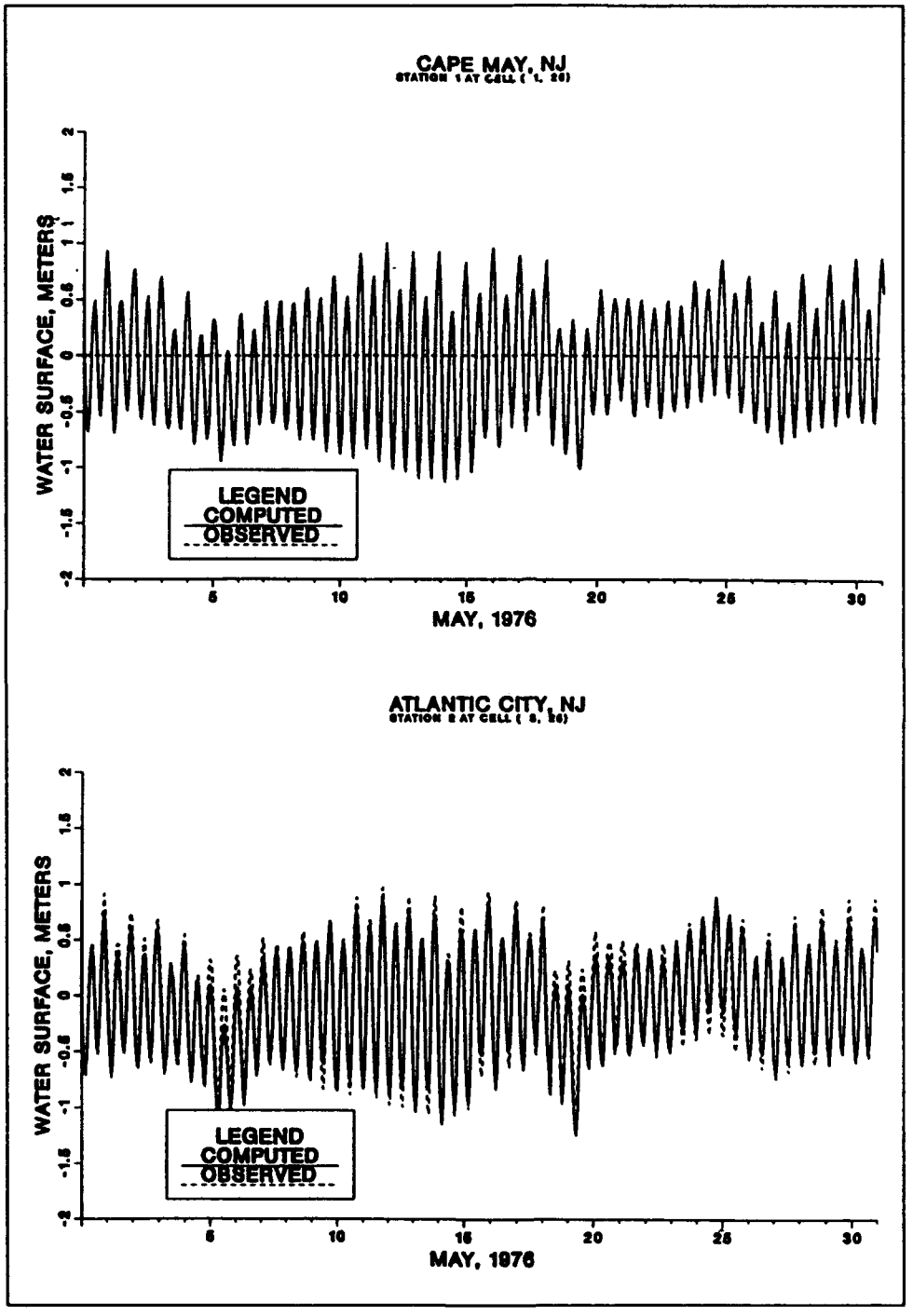

Figure C1. (Sheet 2 of 5)

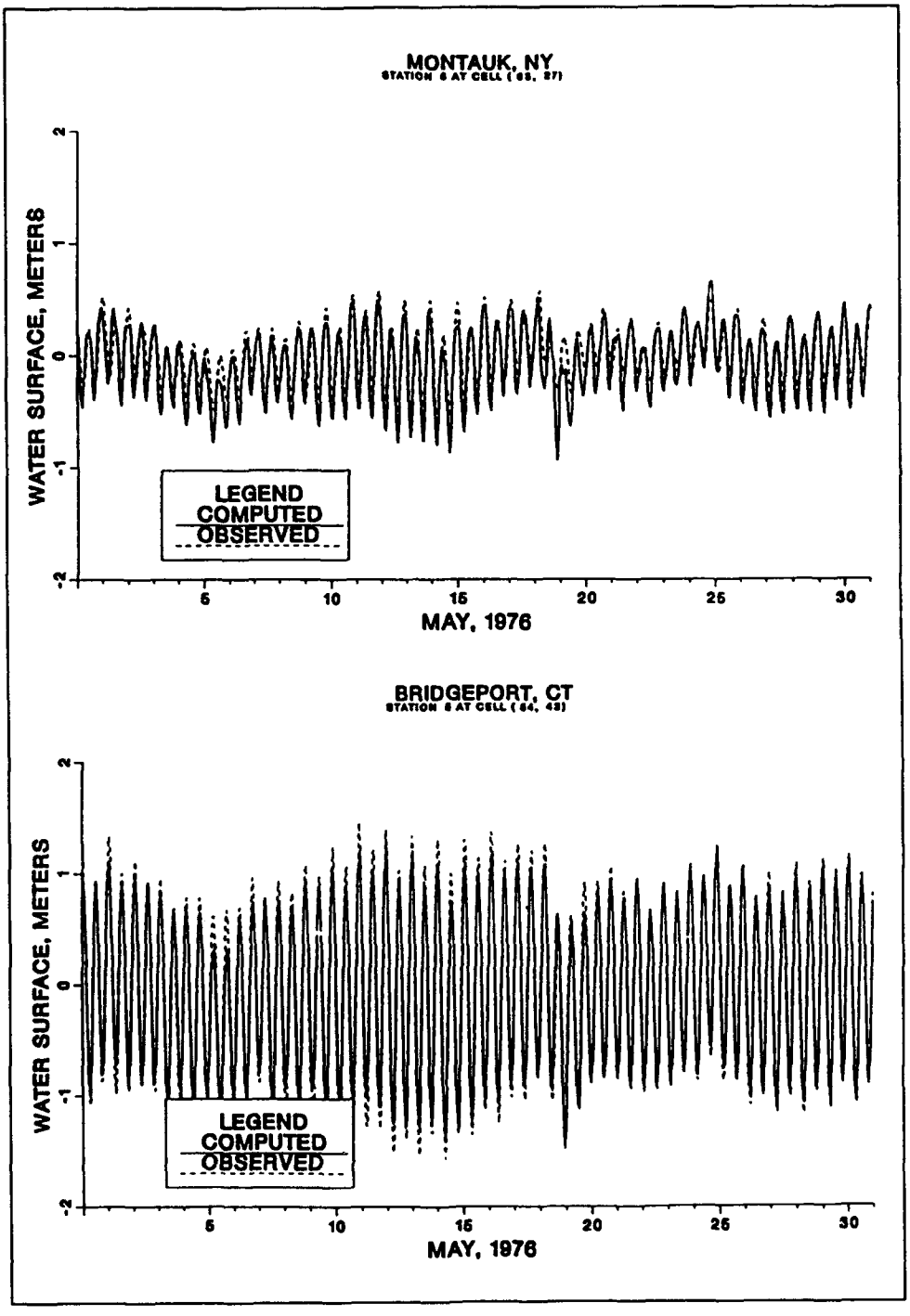

Figure C1. (Sheet 3 of 5)

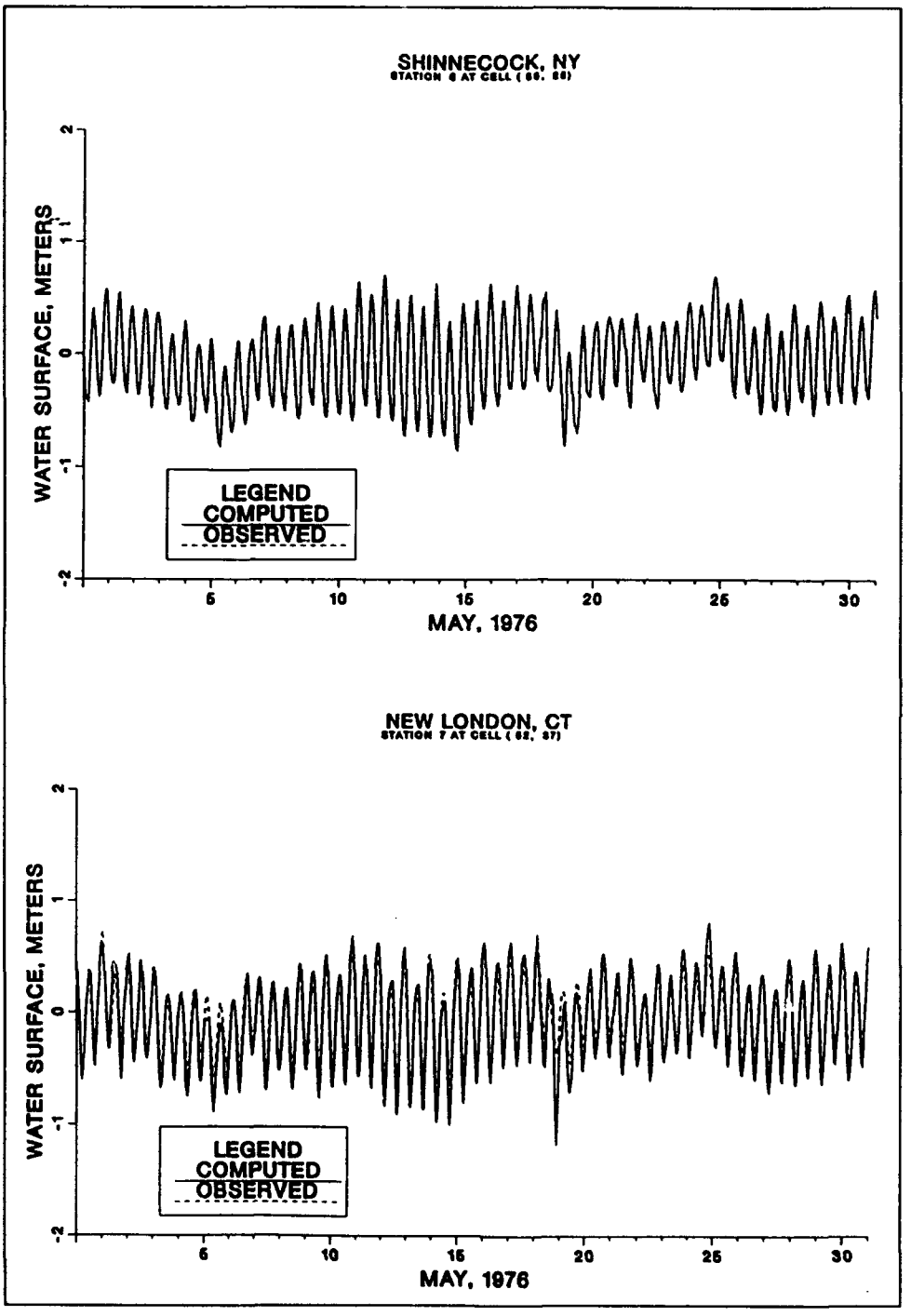

Figure C1. (Sheet 4 of 5)

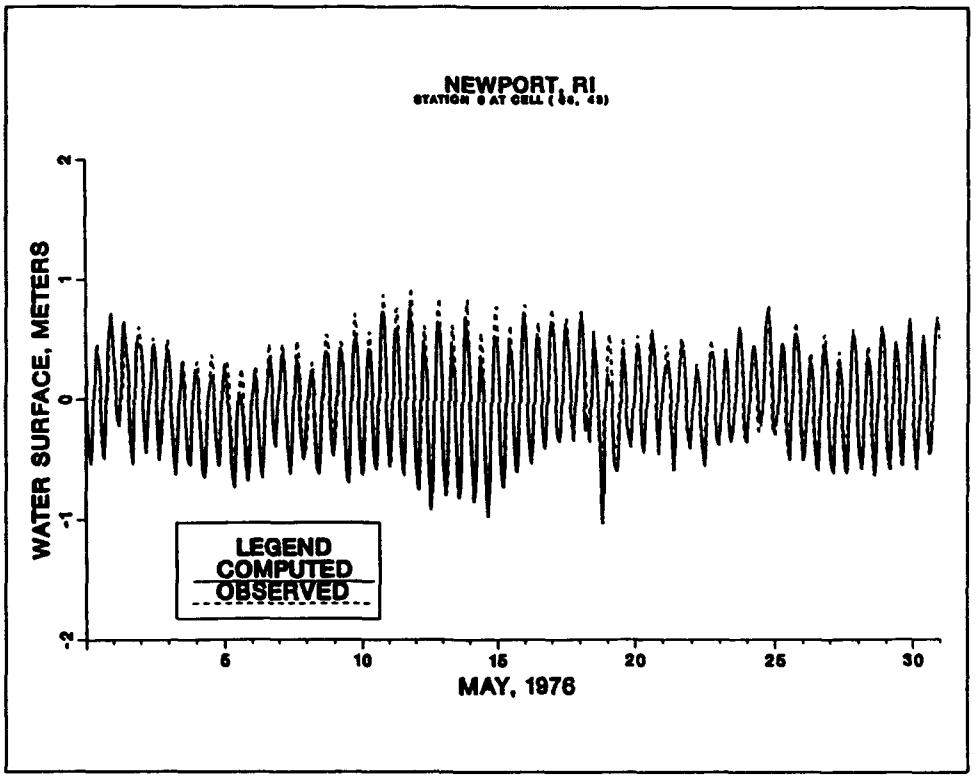

Figure C1. (Sheet 5 of 5)

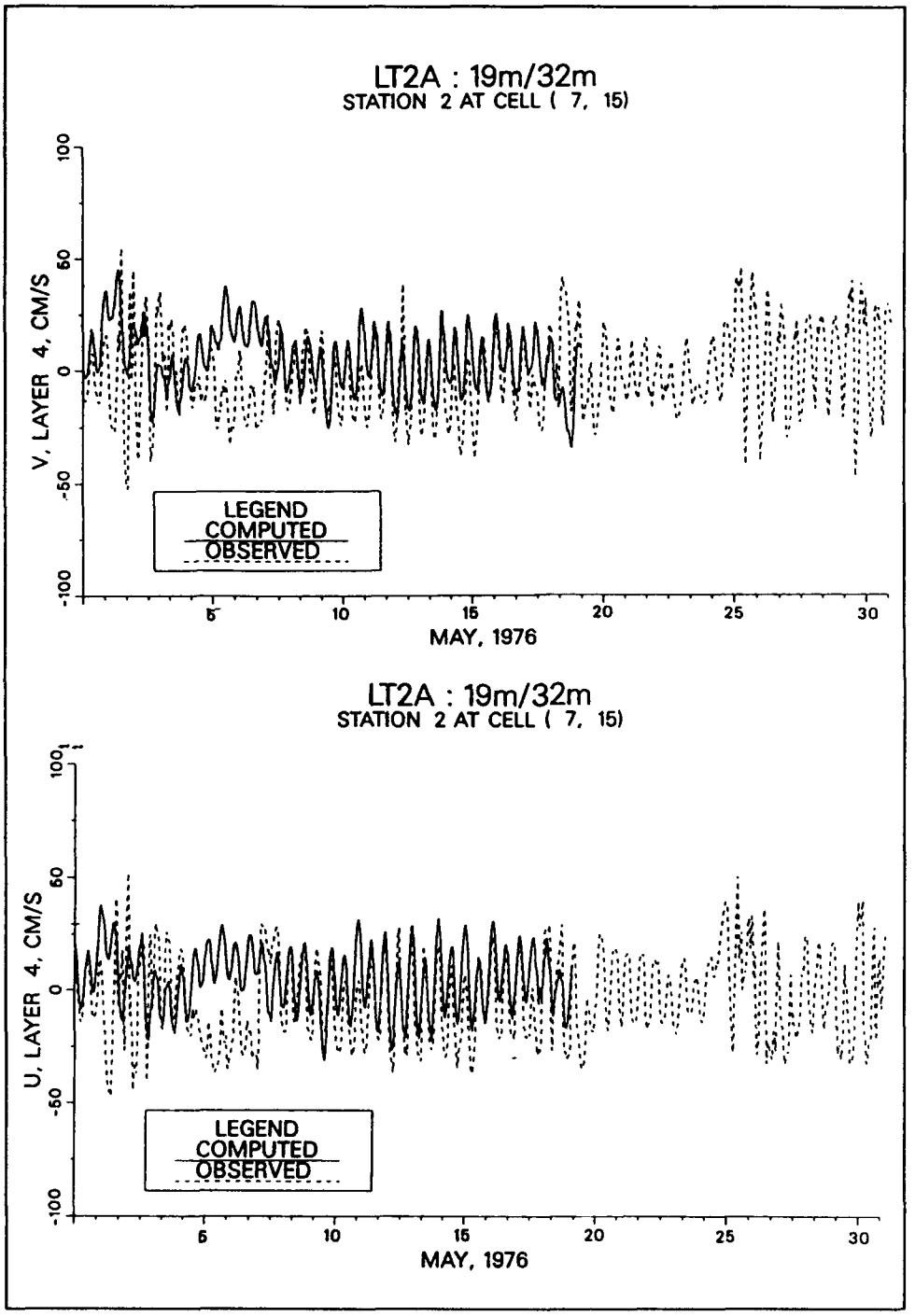

Figure C2. May 1976 current comparisons (Sheet 1 of 13)

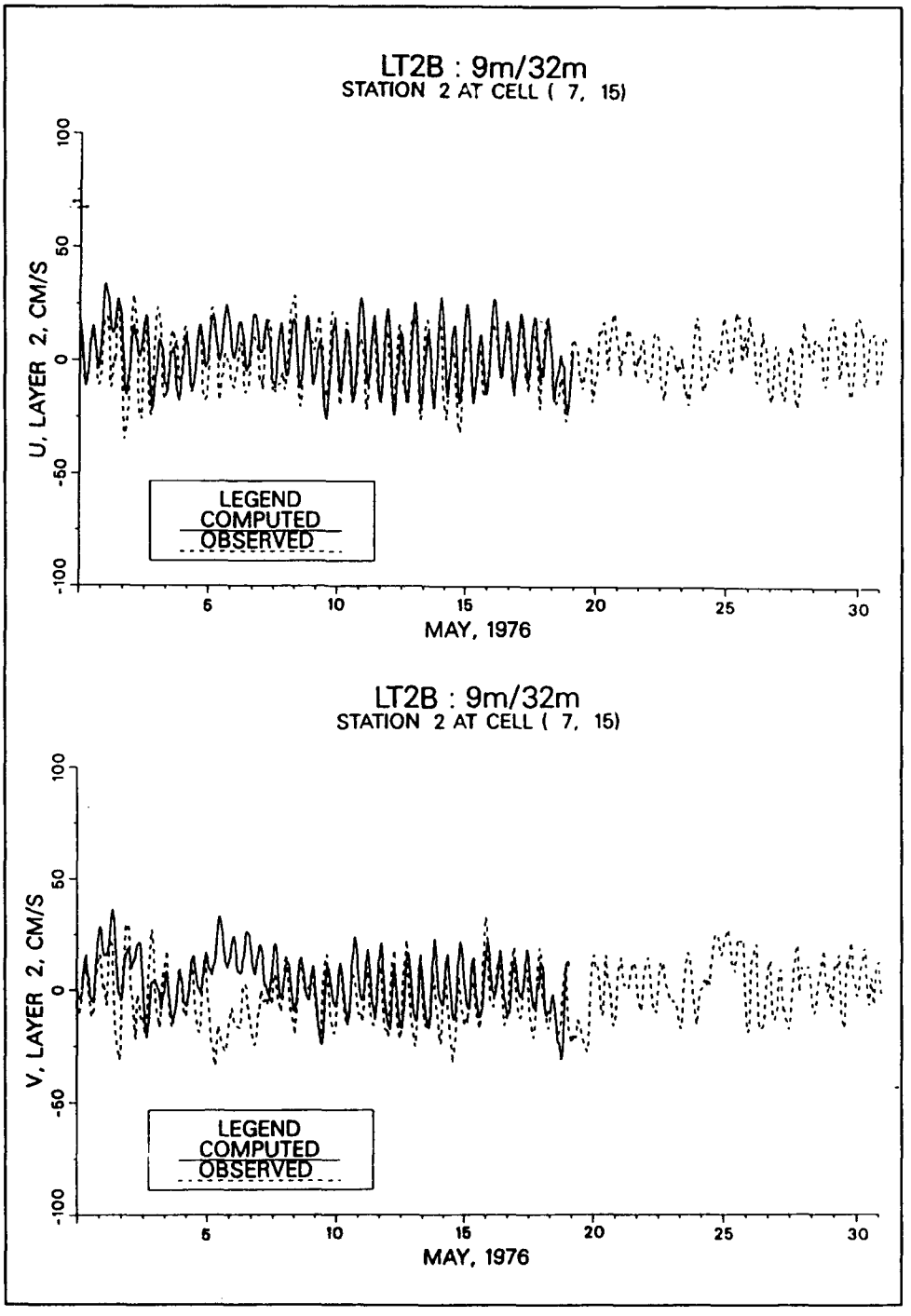

Figure C2. (Sheet 2 of 13)

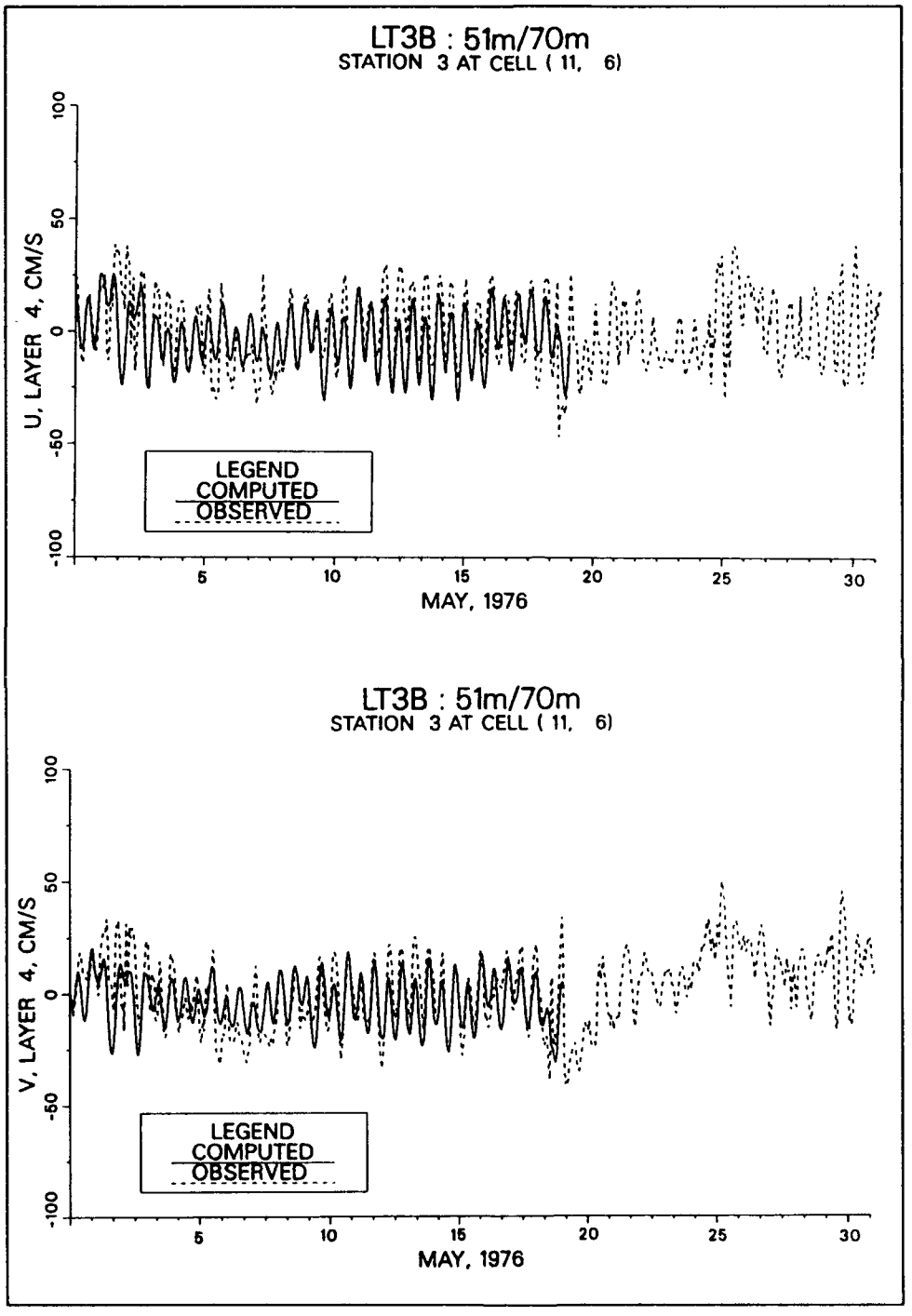

Figure C2. (Sheet 3 of 13)

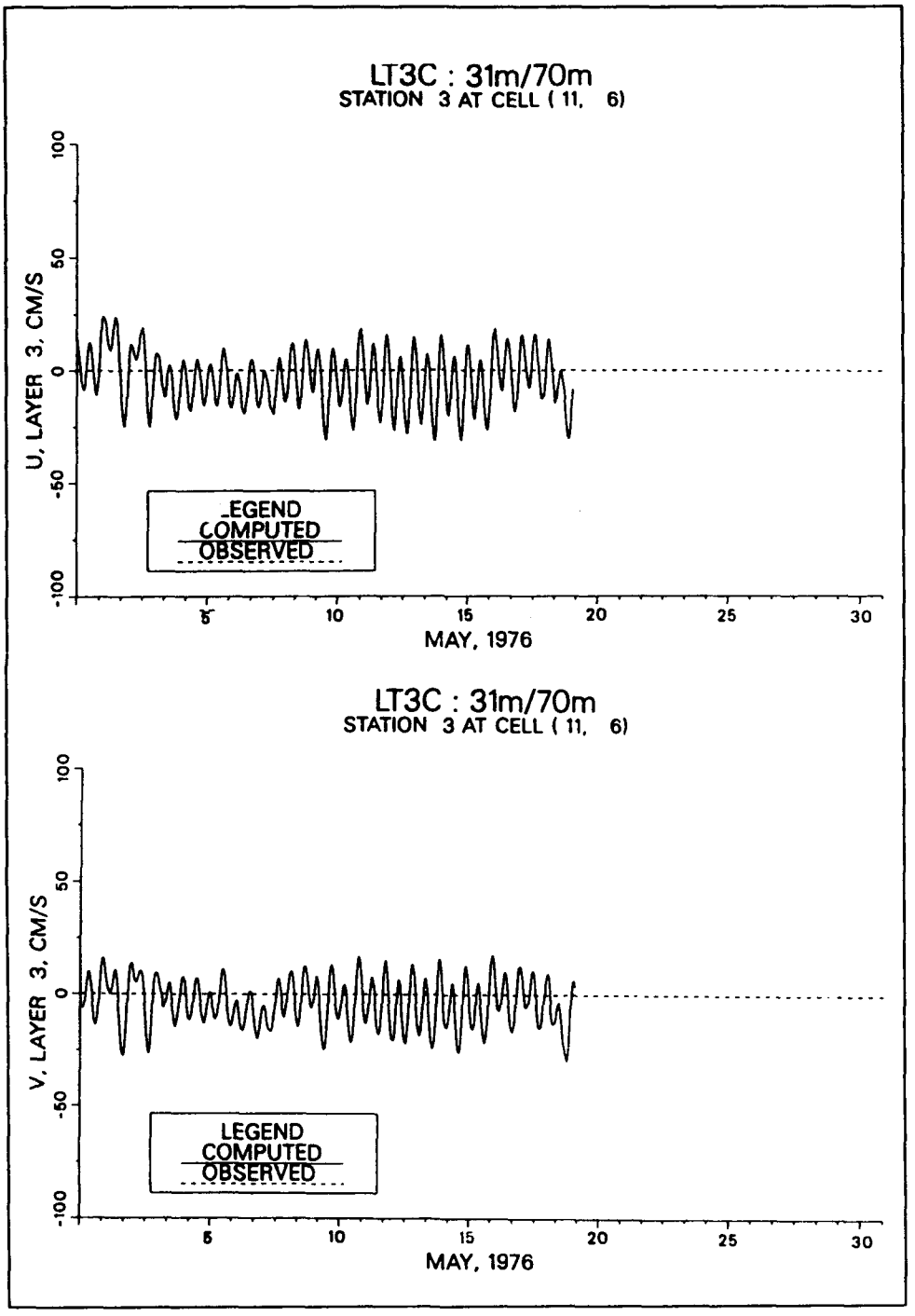

Figure C2. (Sheet 4 of 13)

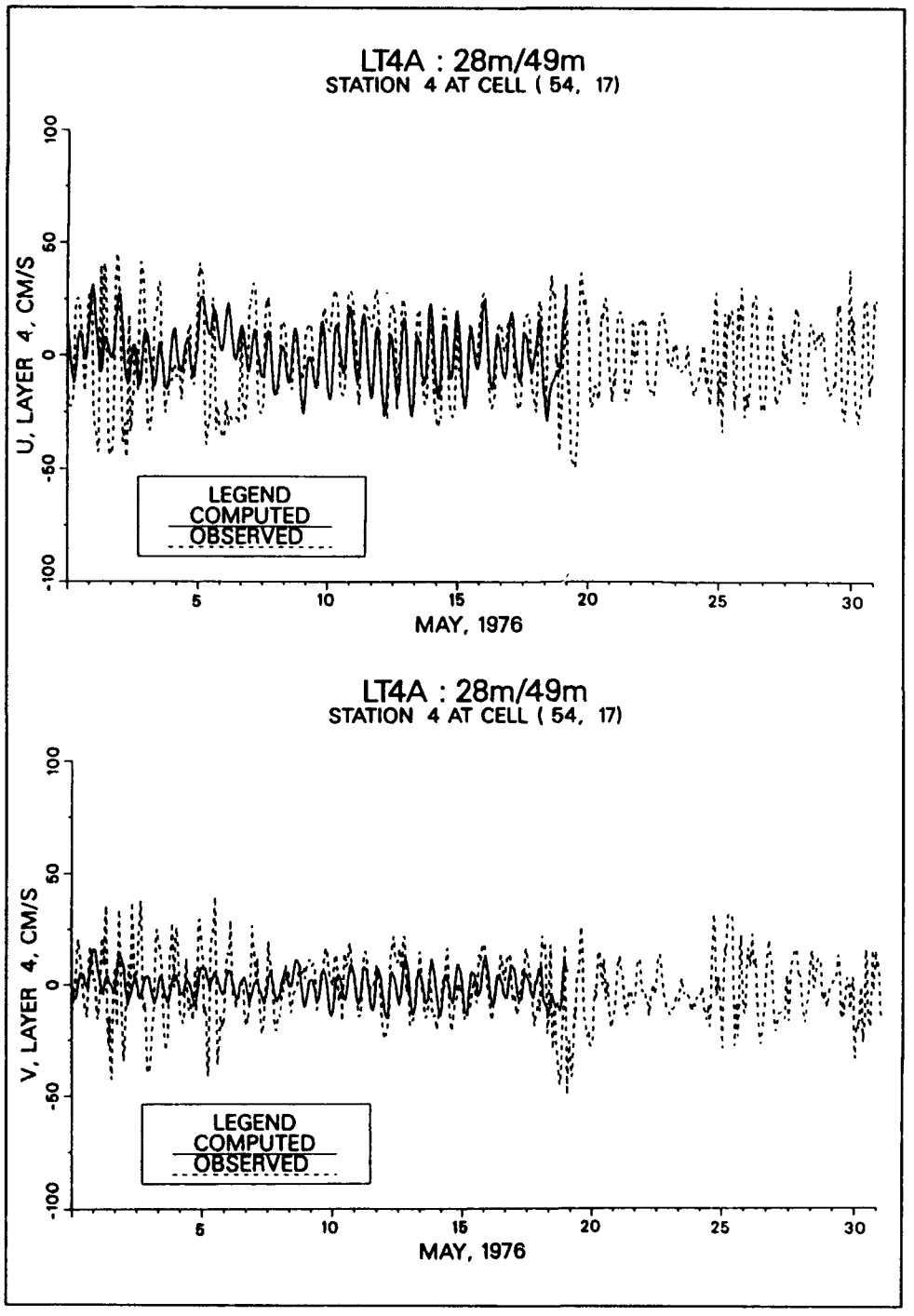

Figure C2. (Sheet 5 of 13)

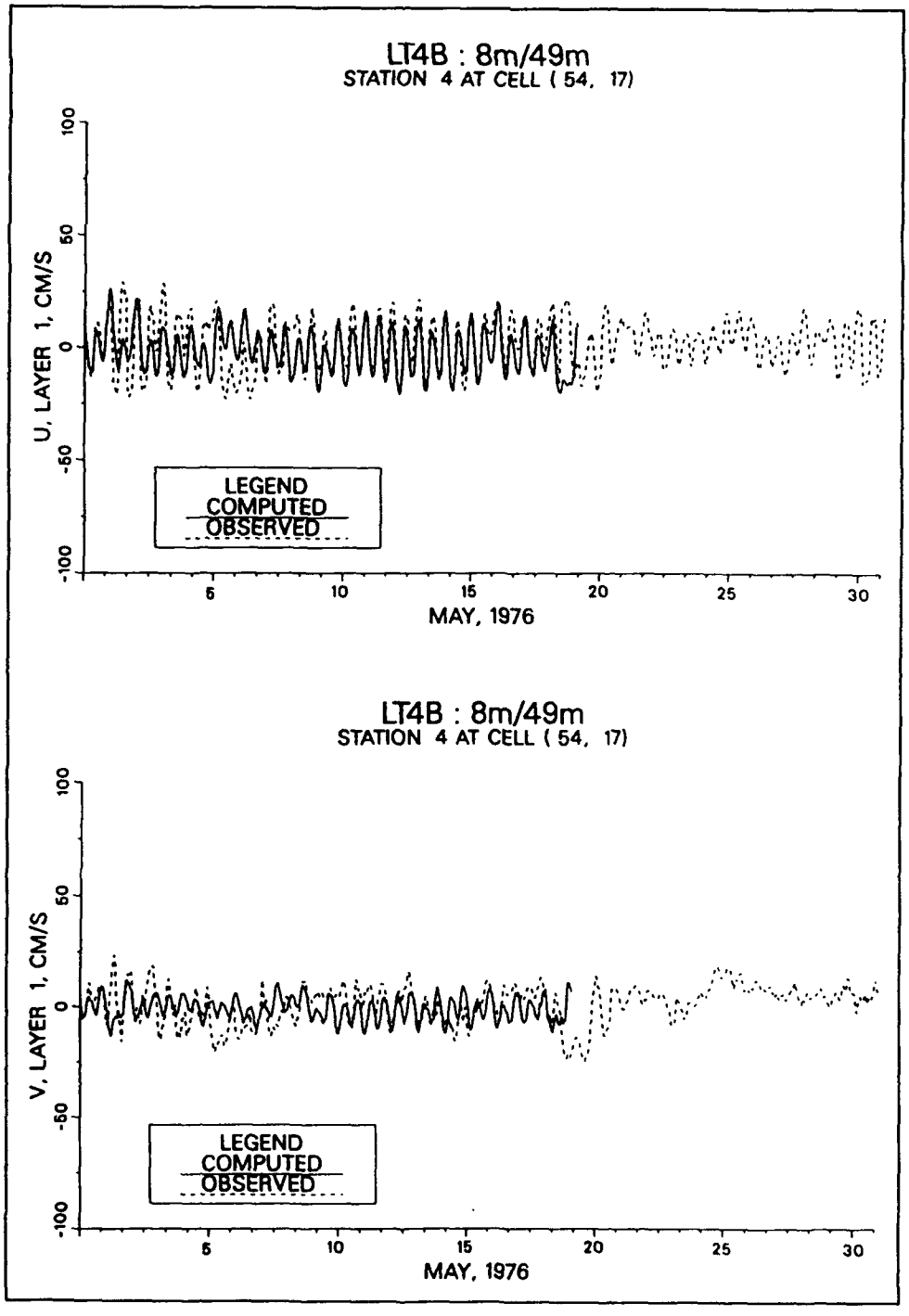

Figure C2. (Sheet 6 of 13)

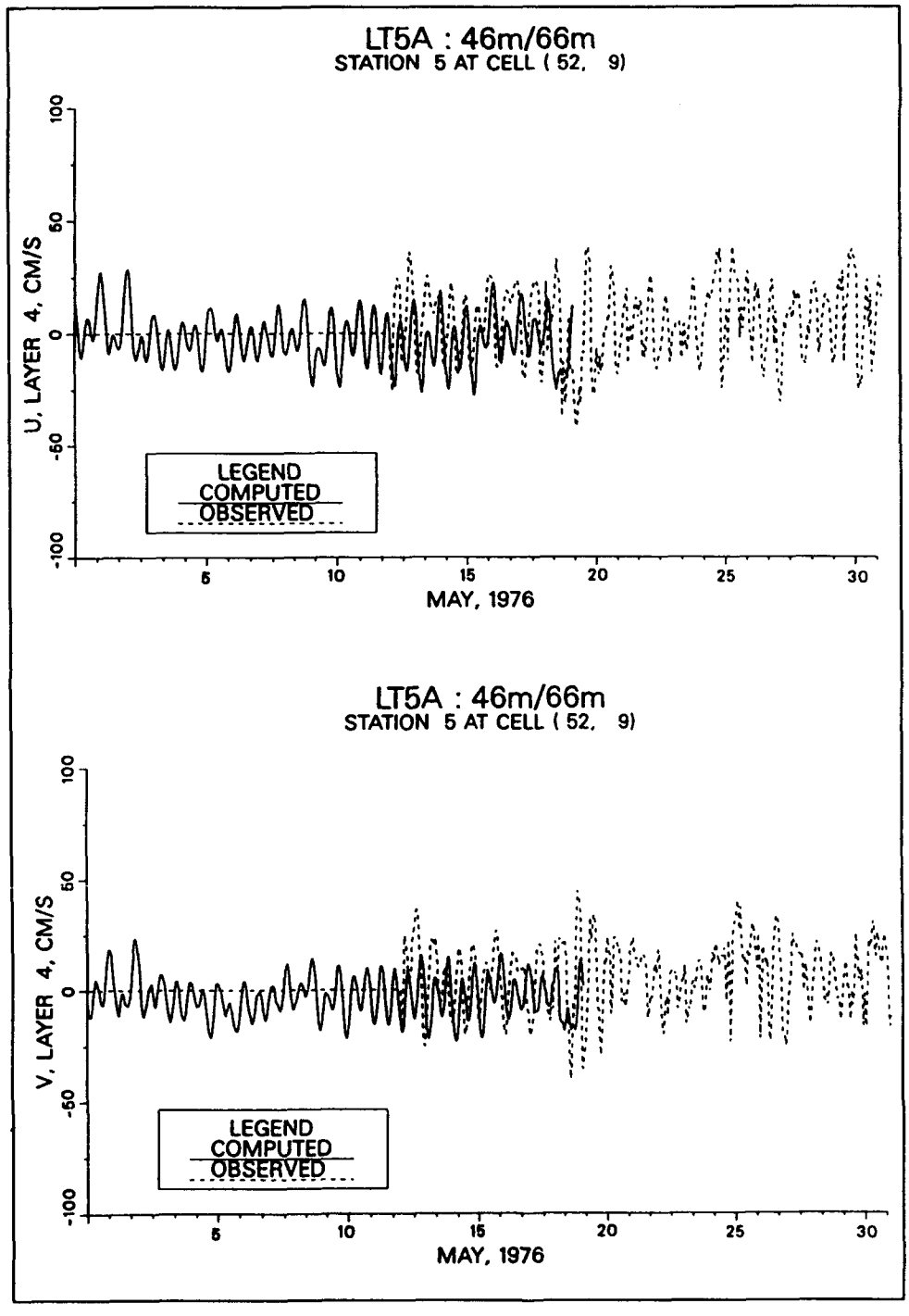

Figure C2. (Sheet 7 of 13)

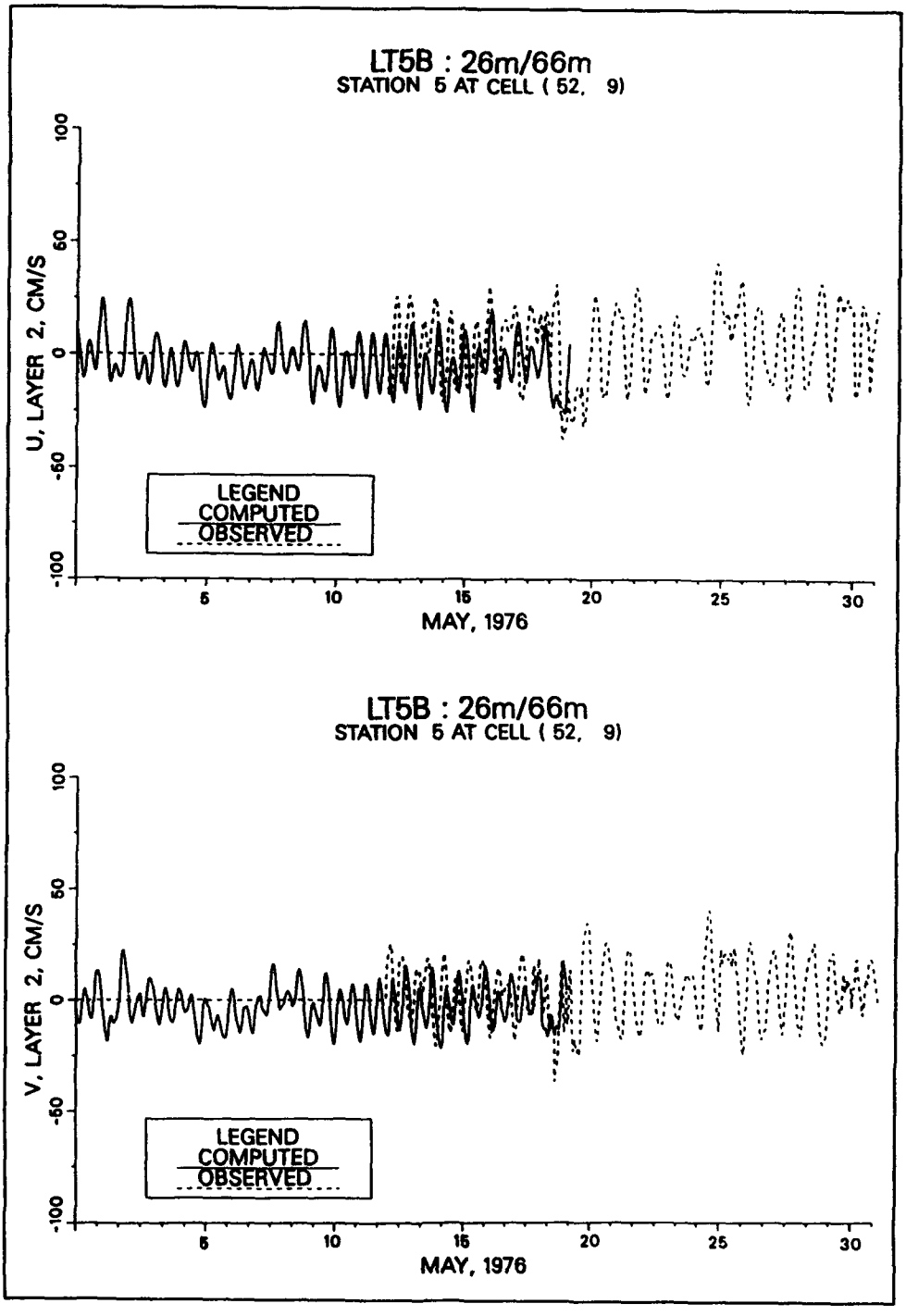

Figure C2. (Sheet 8 of 13)

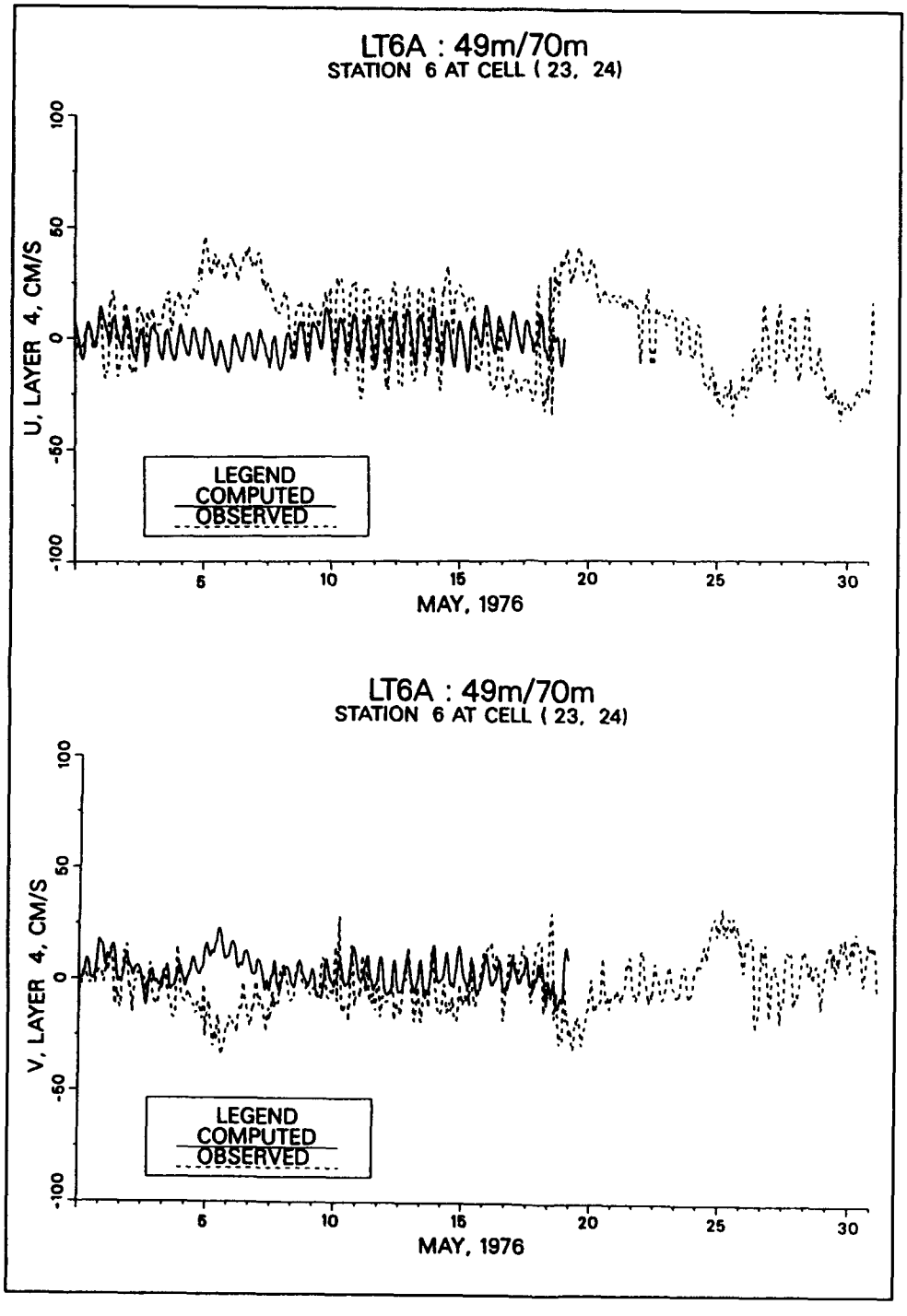

Figure C2. (Sheet 9 of 13)

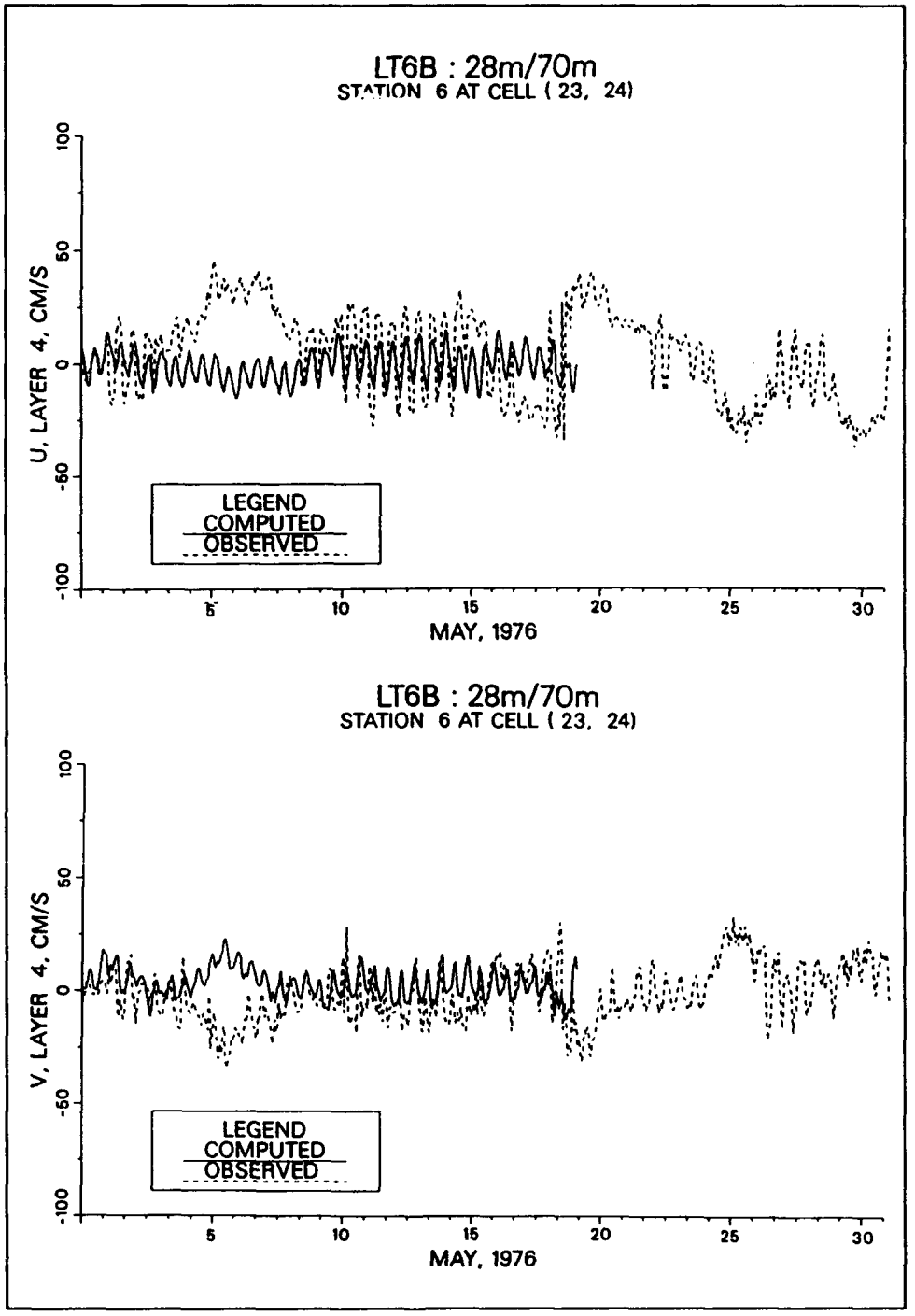

Figure C2. (Sheet 10 of 13)

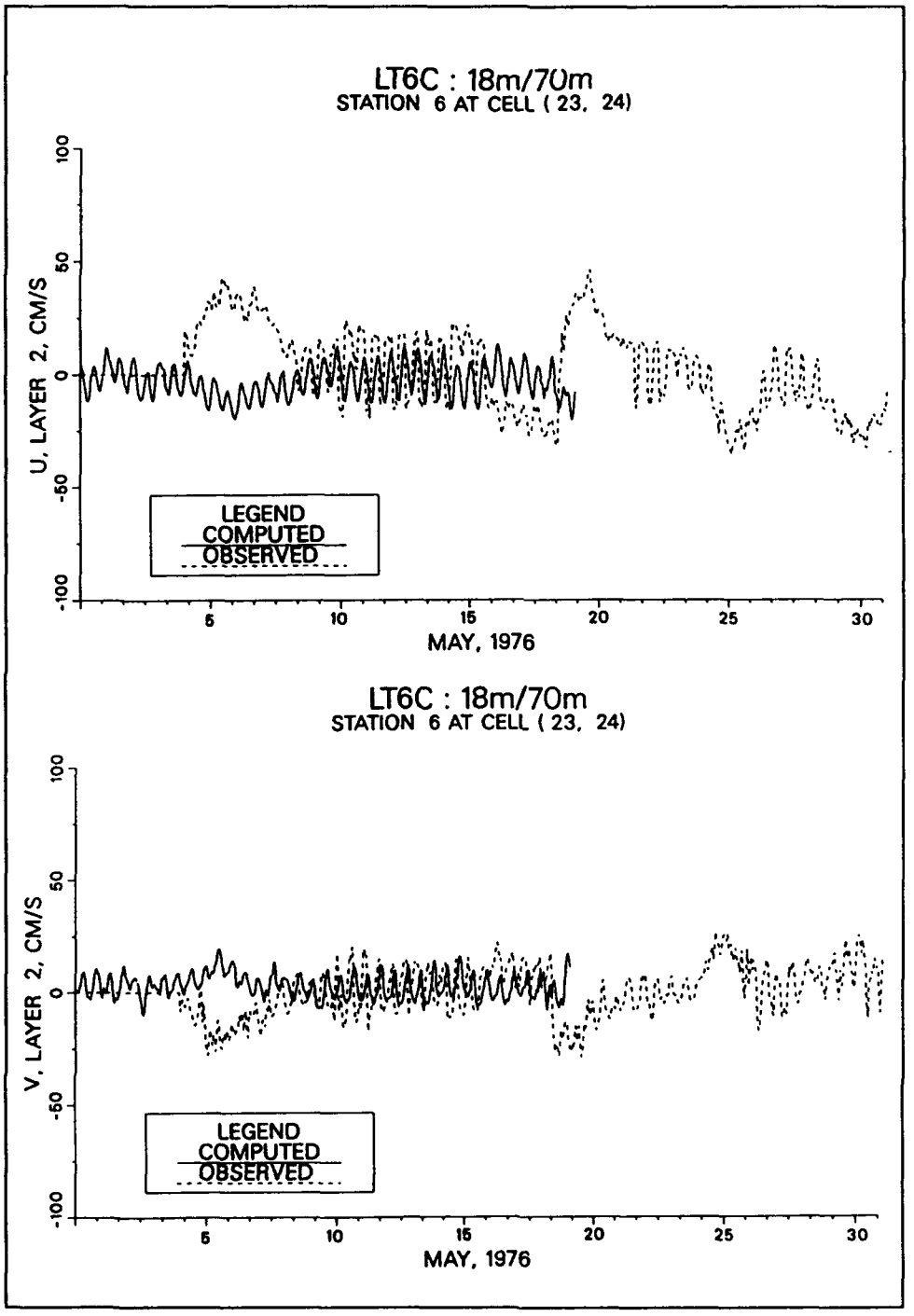

Figure C2. (Sheet 11 of 13)

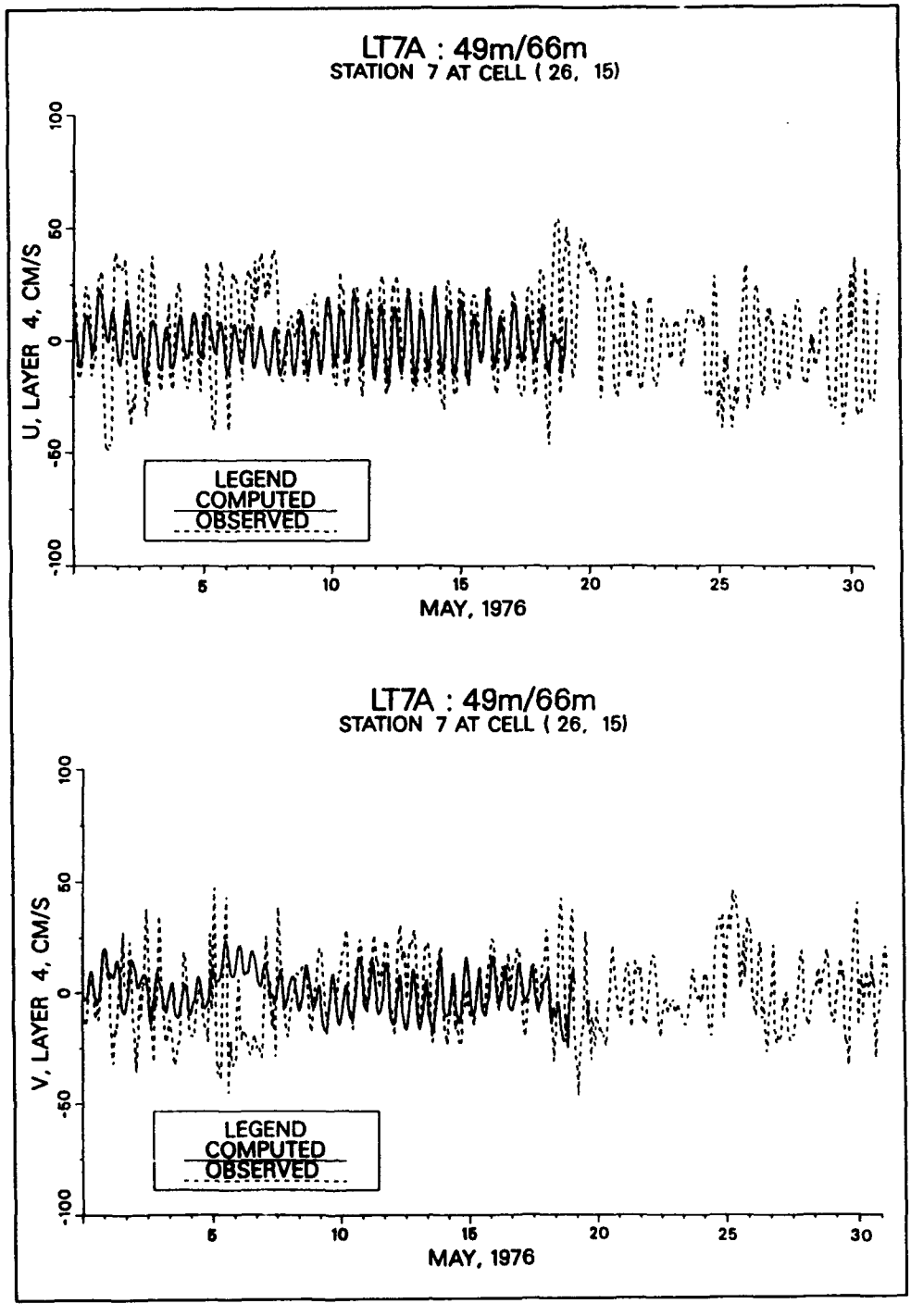

Figure C2. (Sheet 12 of 13)

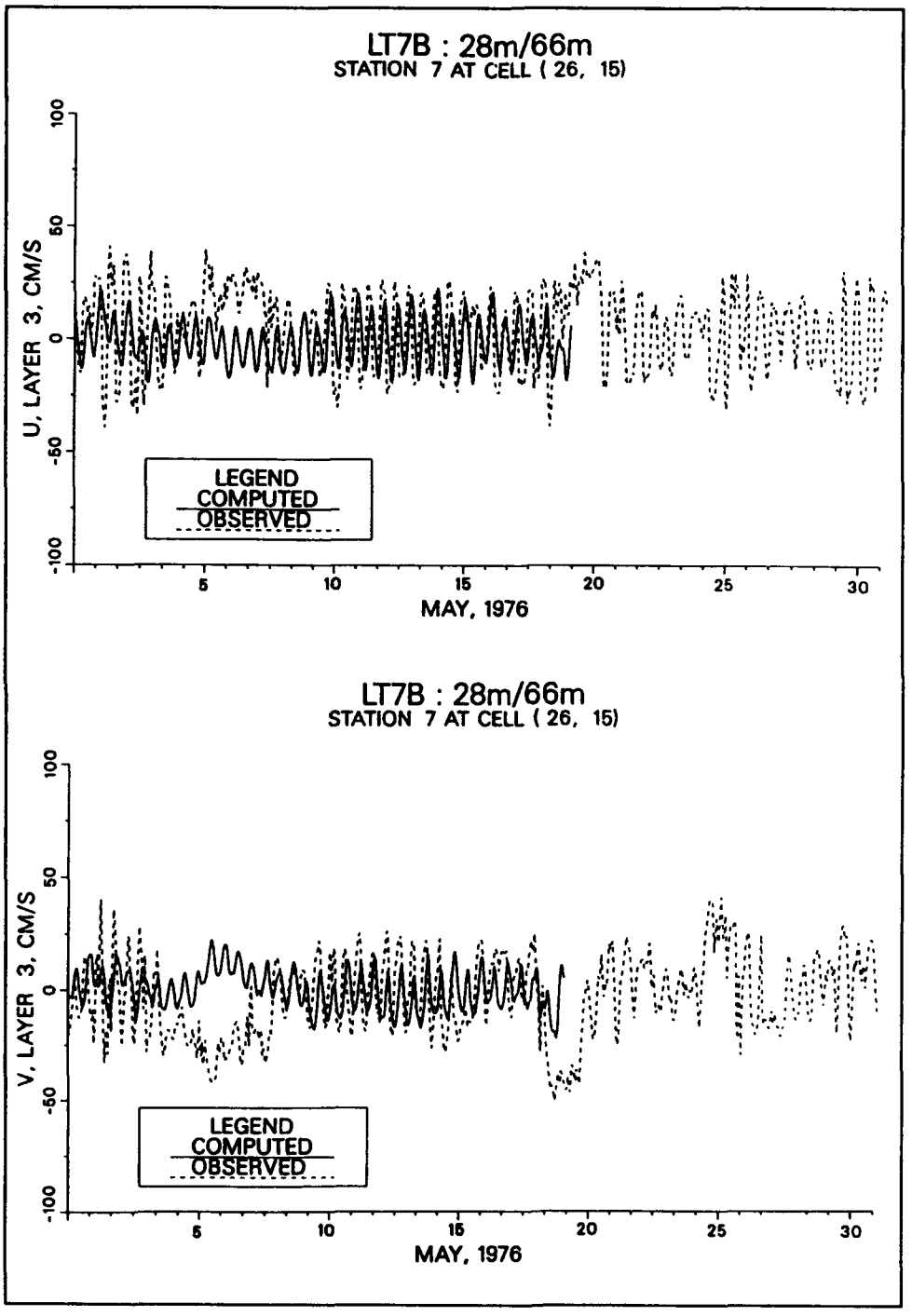

Figure C2. (Sheet 13 of 13)

Appendix D
Long-Term Simulation Comparisons

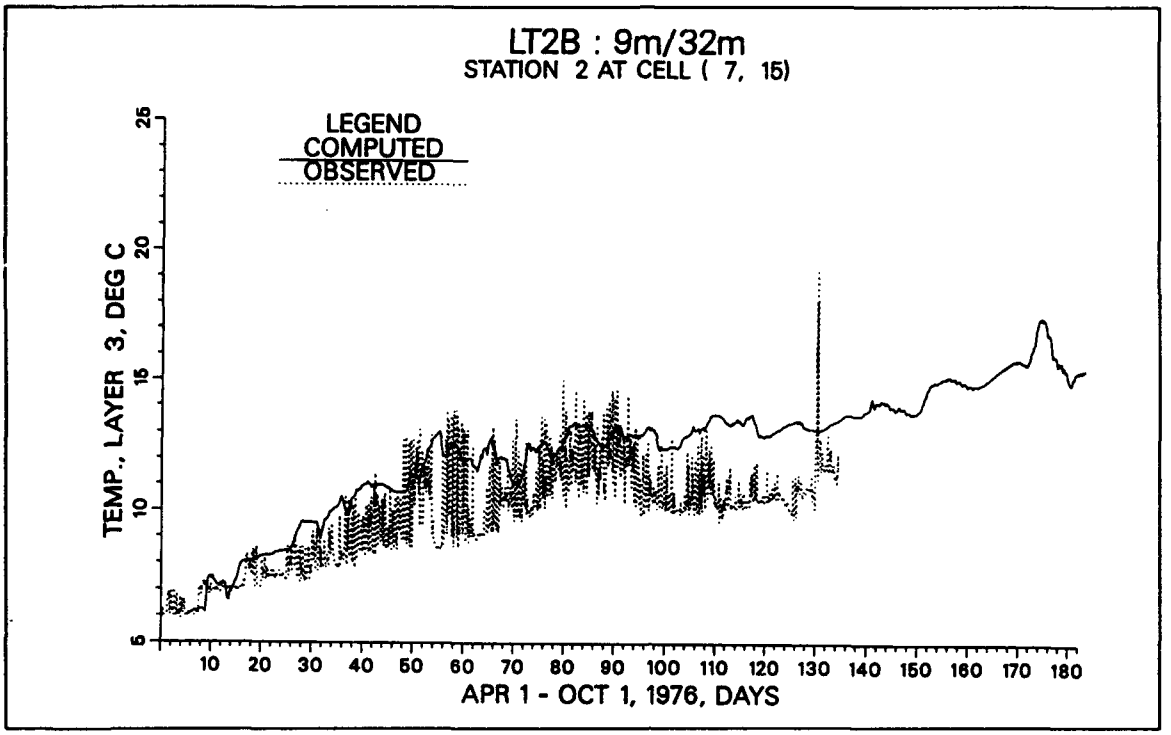

Figure D1. Temperature comparison at LT2B

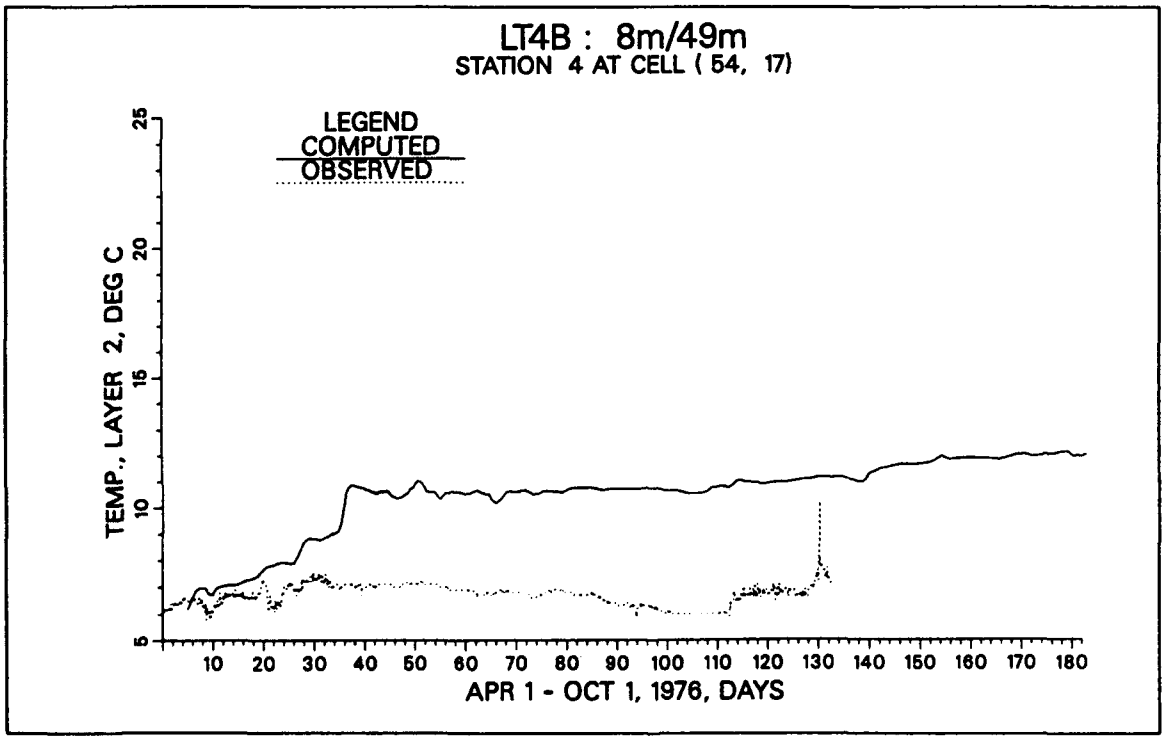

Figure D2. Temperature comparison at LT4B

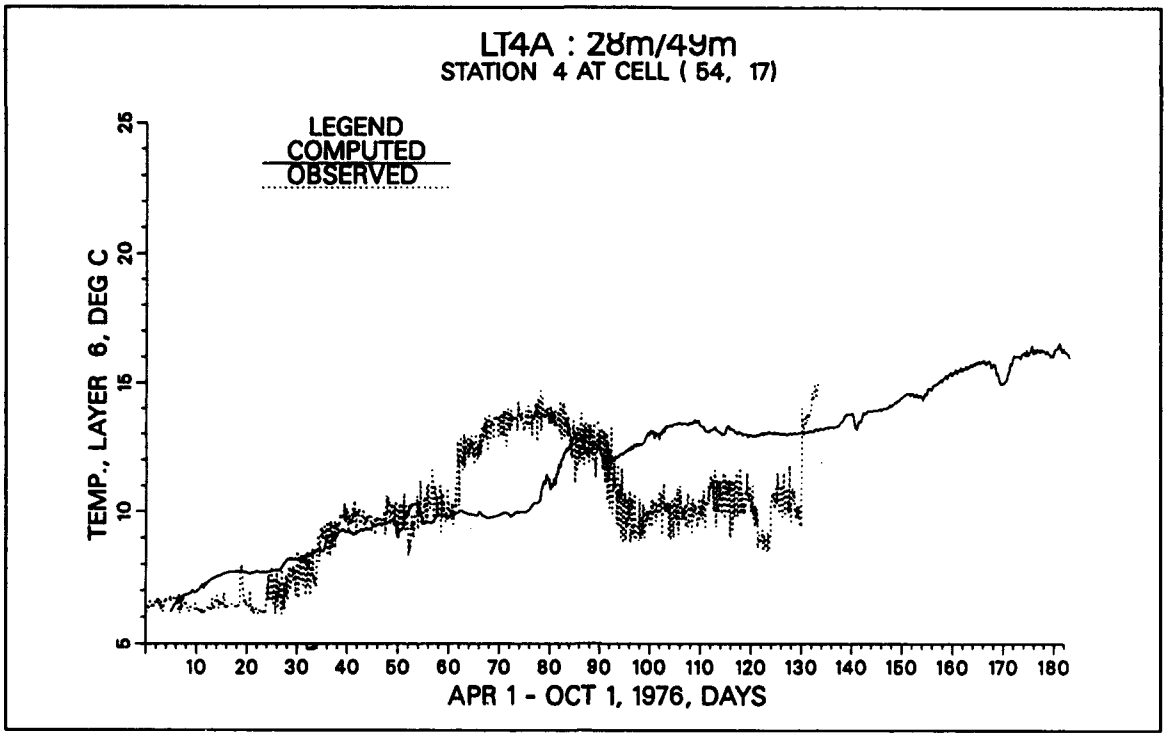

Figure D3. Temperature comparison at LT4A

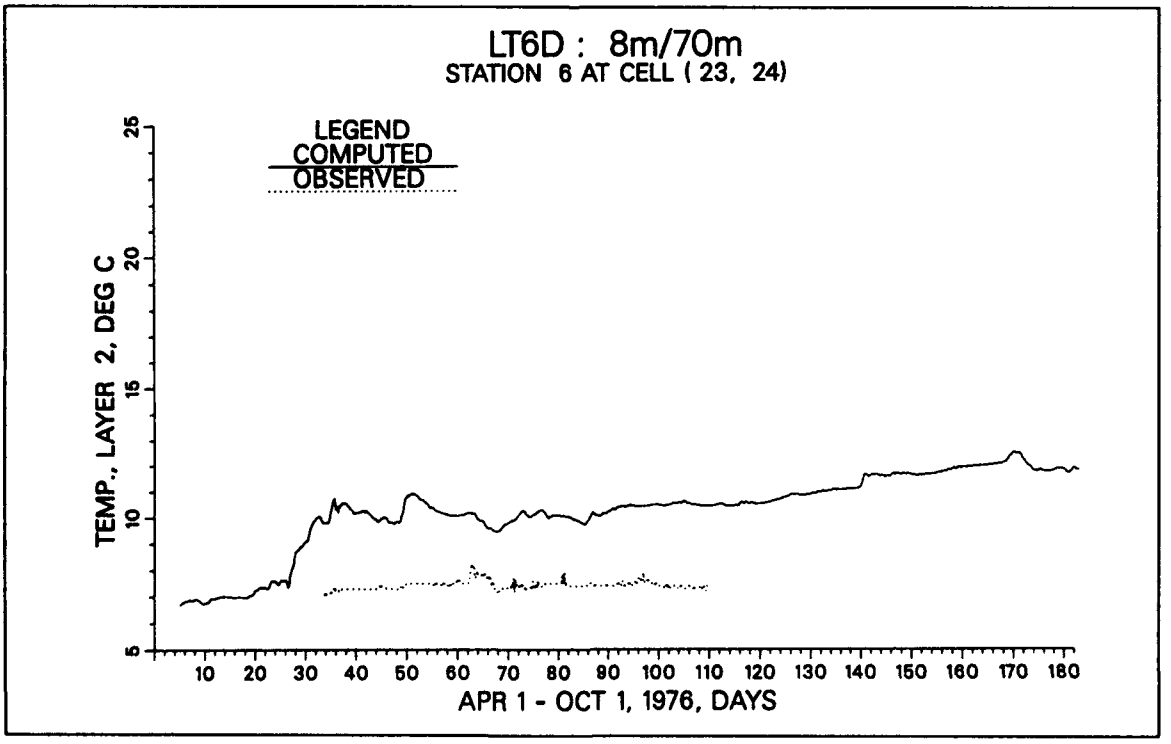

Figure D4. Temperature comparison at LT6D

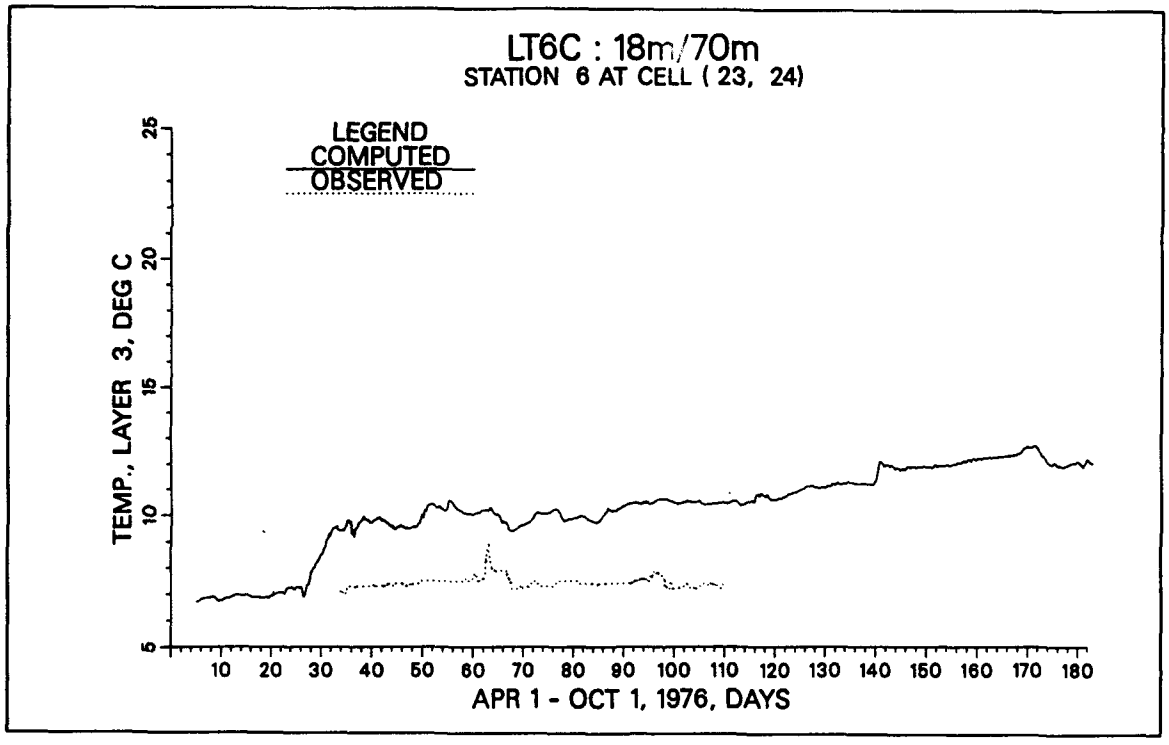

Figure D5. Temperature comparison at LT6C

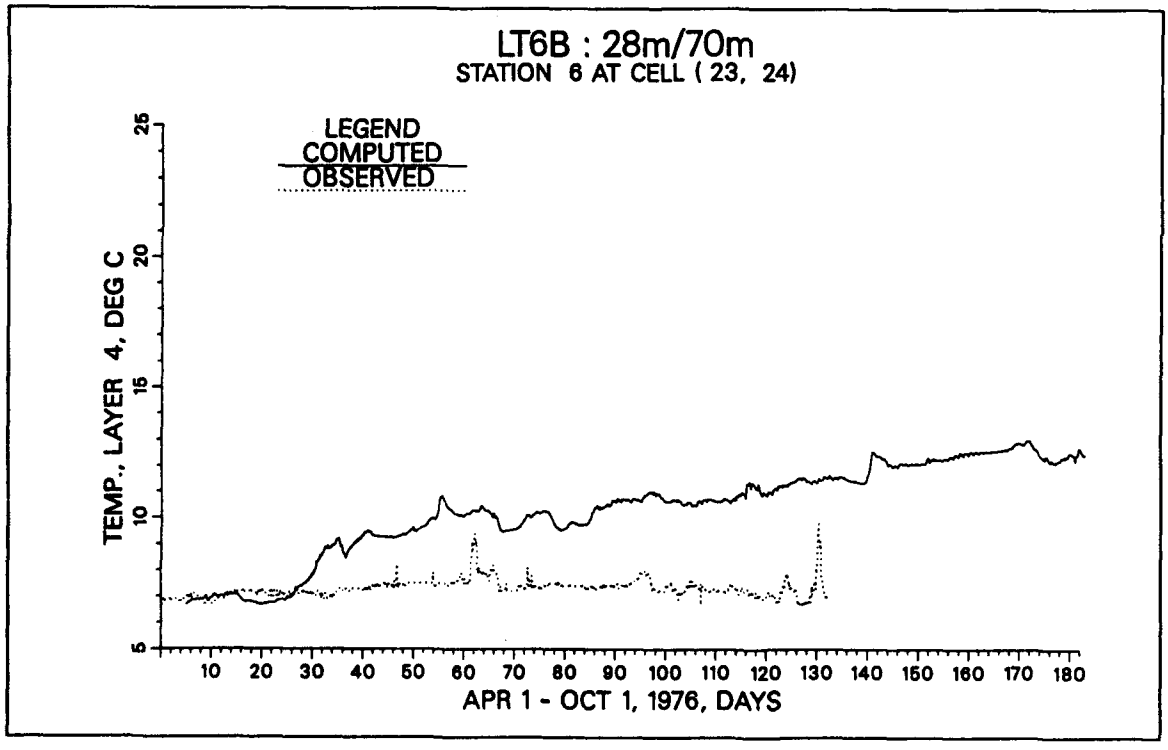

Figure D6. Temperature comparison at LT6B

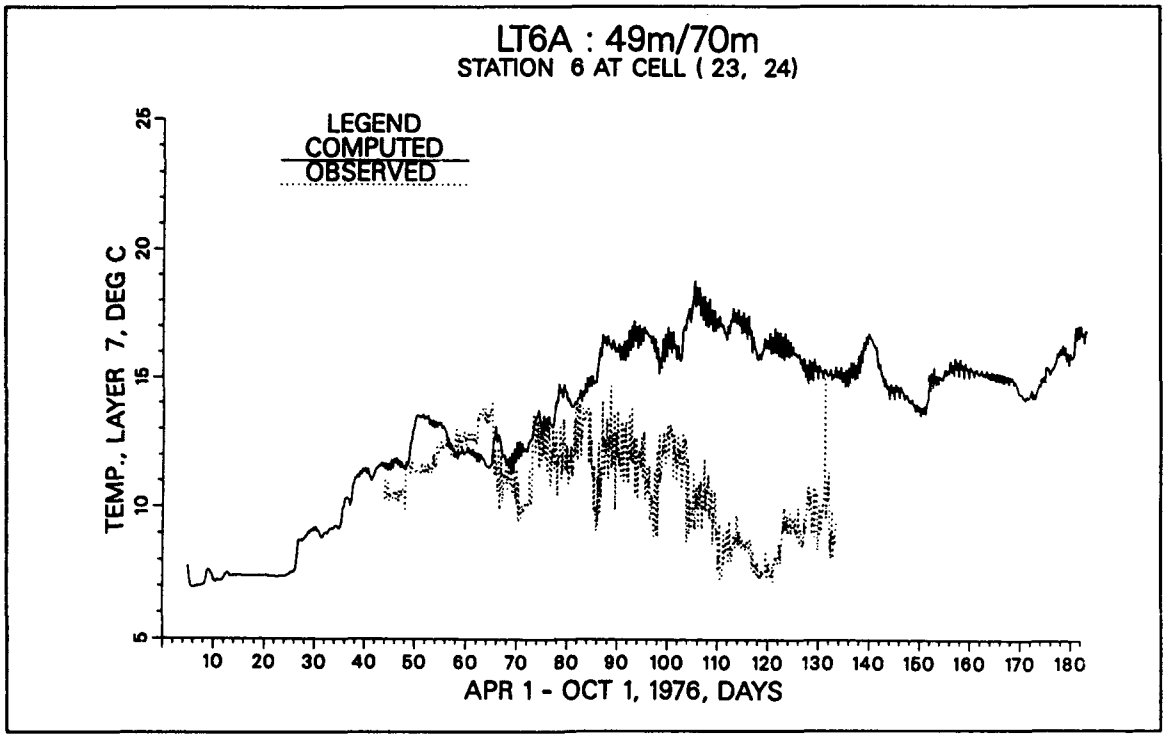

Figure D7. Temperature comparison at LT6A

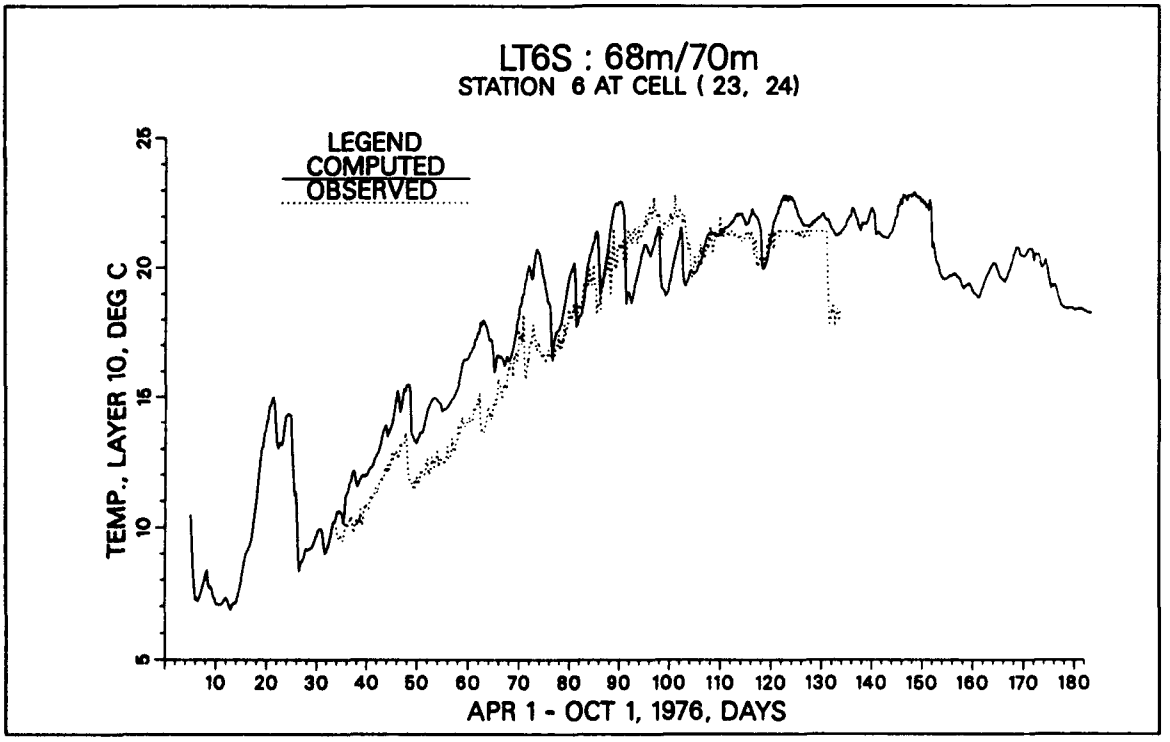

Figure D8. Temperature comparison at LT6S

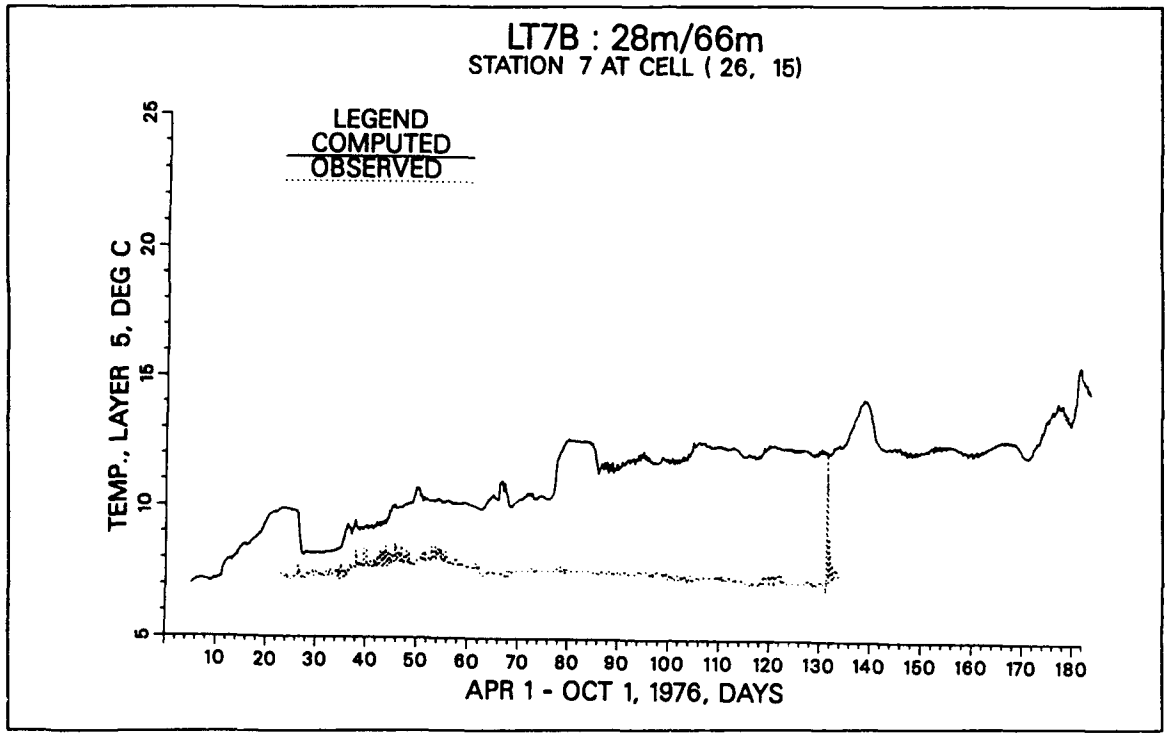

Figure D9. Temperature comparison LT7B

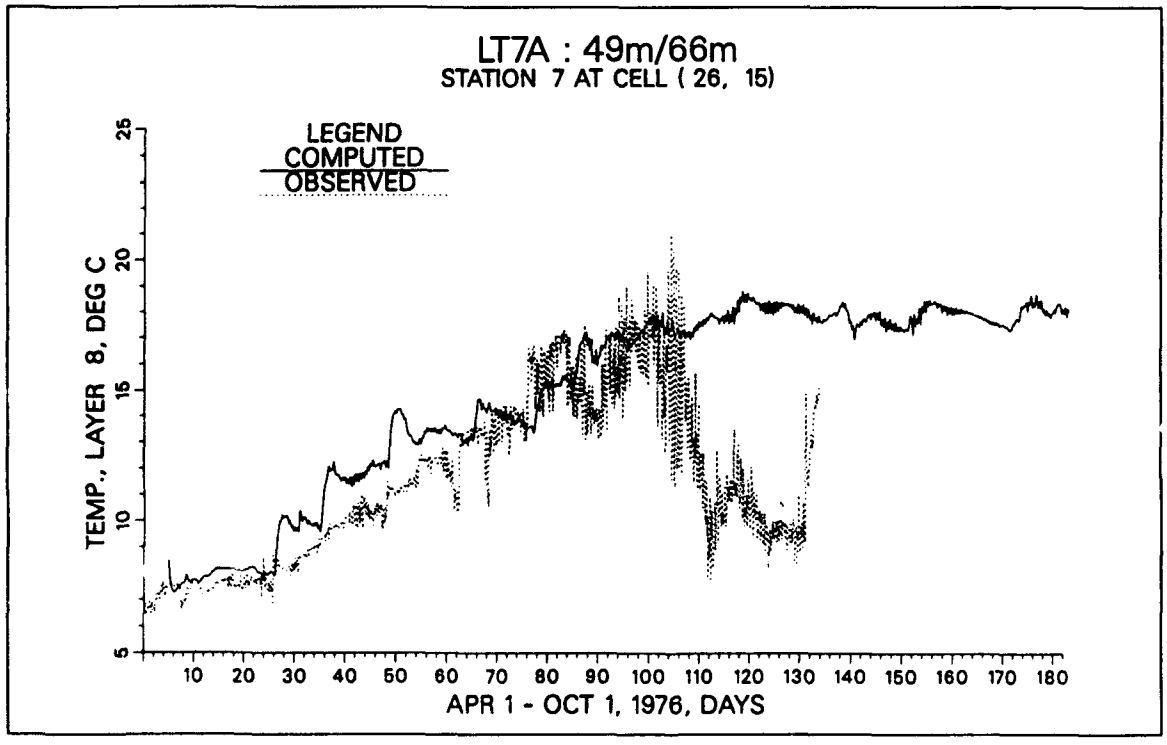

Figure D10. Temperature comparison at LT7A

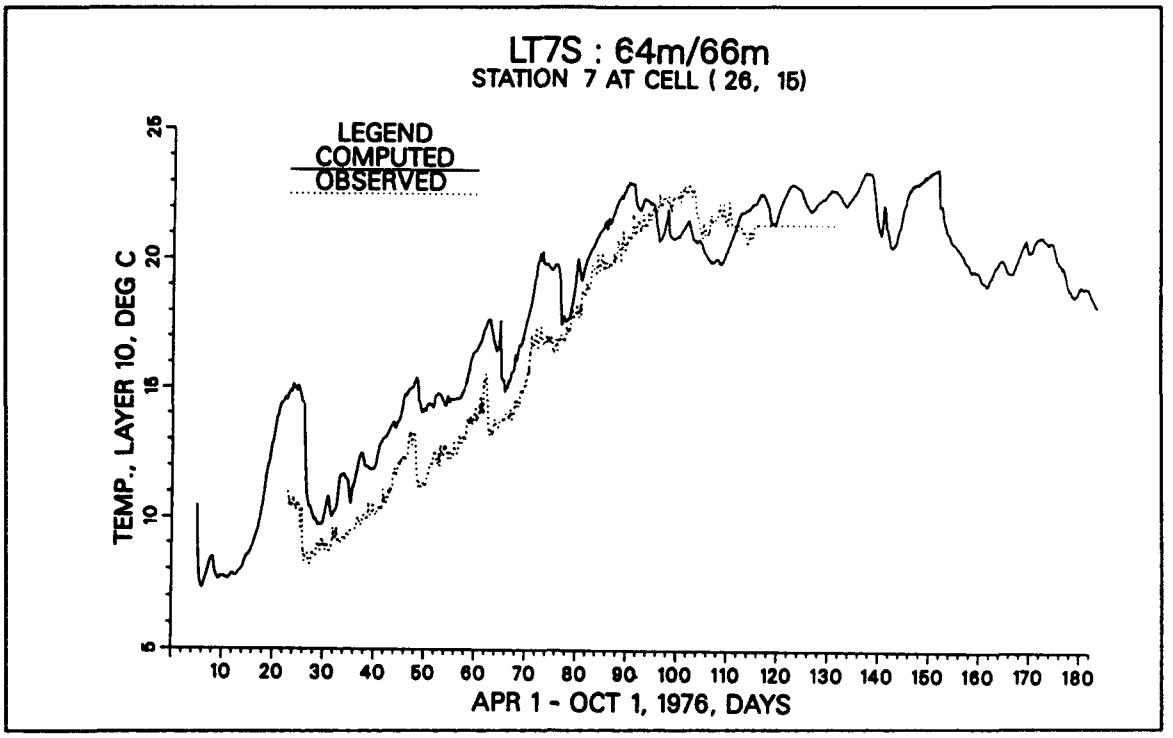

Figure D11. Temperature comparison at LT7S

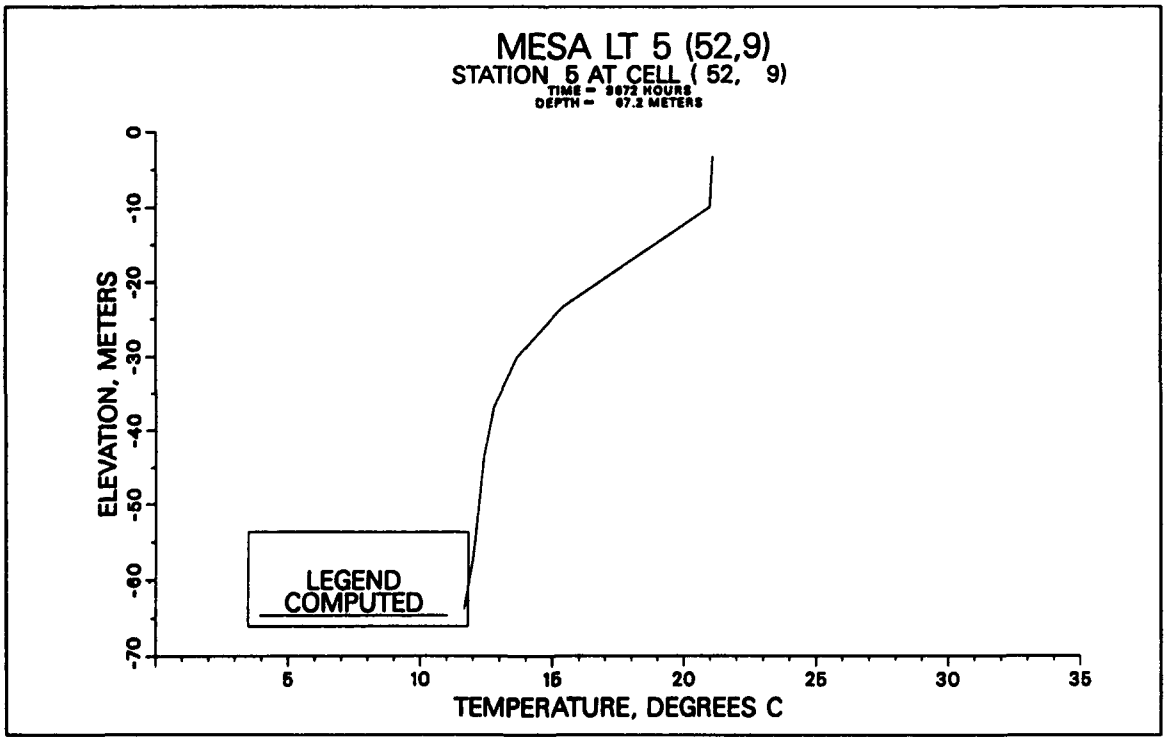

Figure D12. Temperature profile at LT5 at 3672 hours

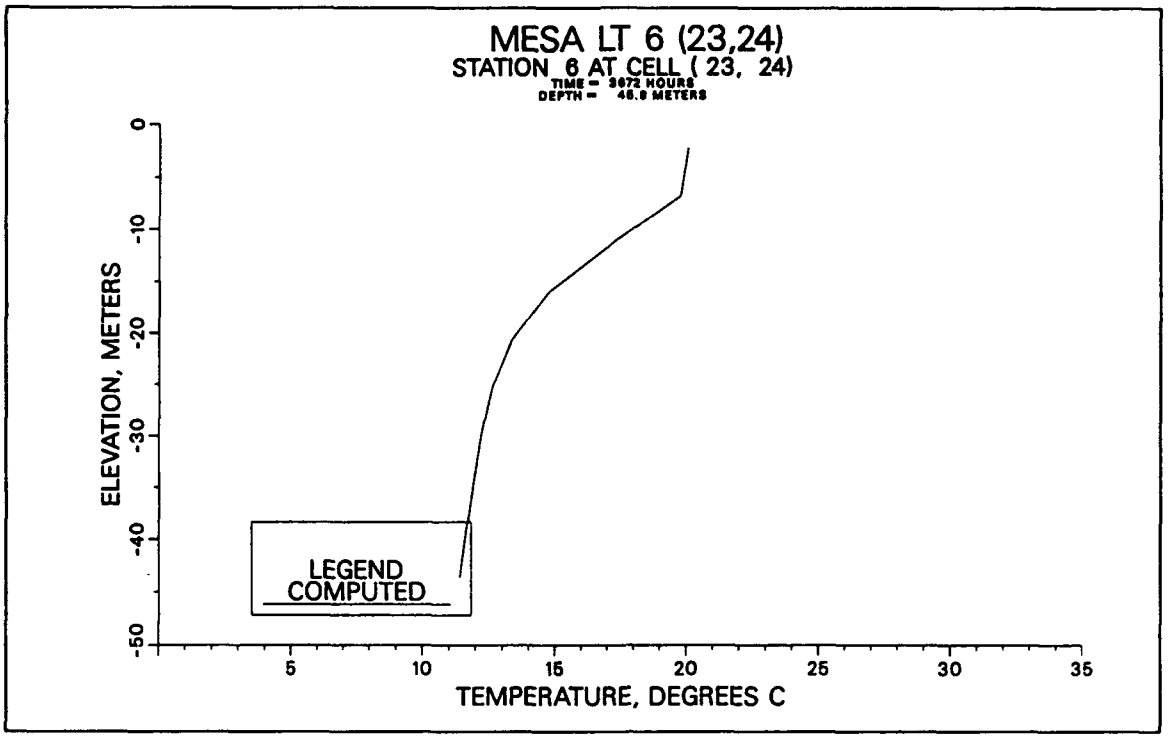

Figure D13. Temperature profile at LT6 at 3762 hours

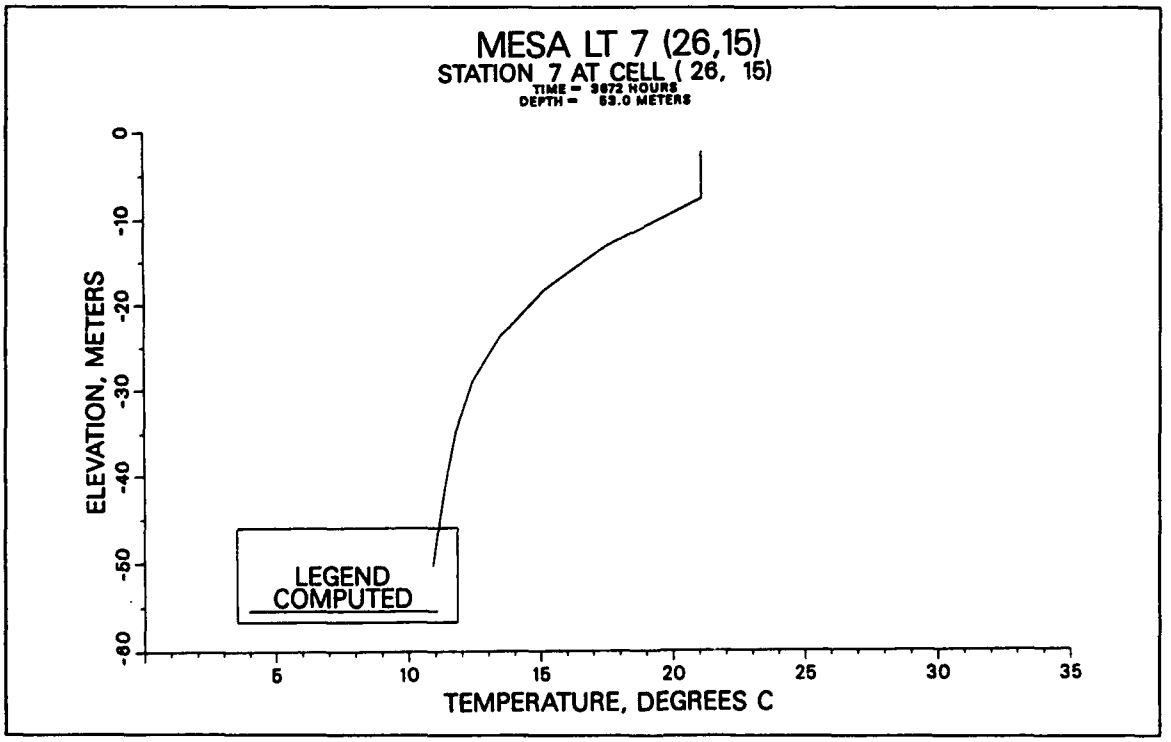

Figure D14. Temperature profile at LT7 at 3672 hours

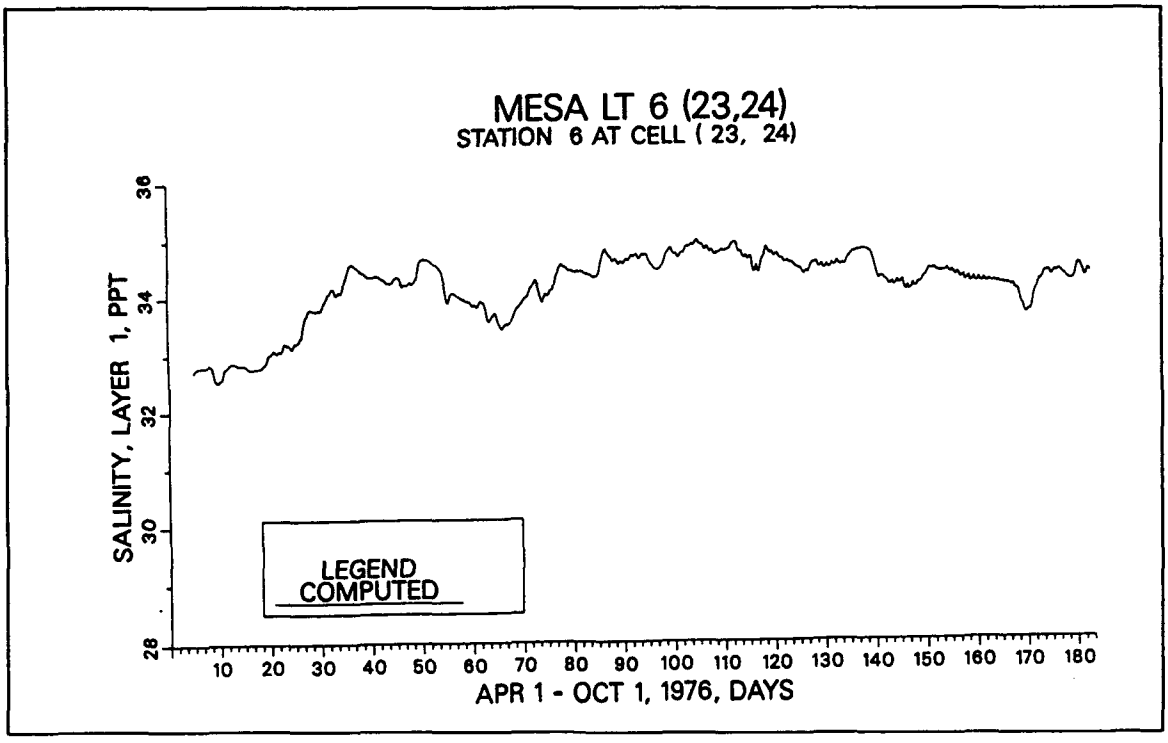

Figure D15. Variation of computed salinity at LT6, layer 1

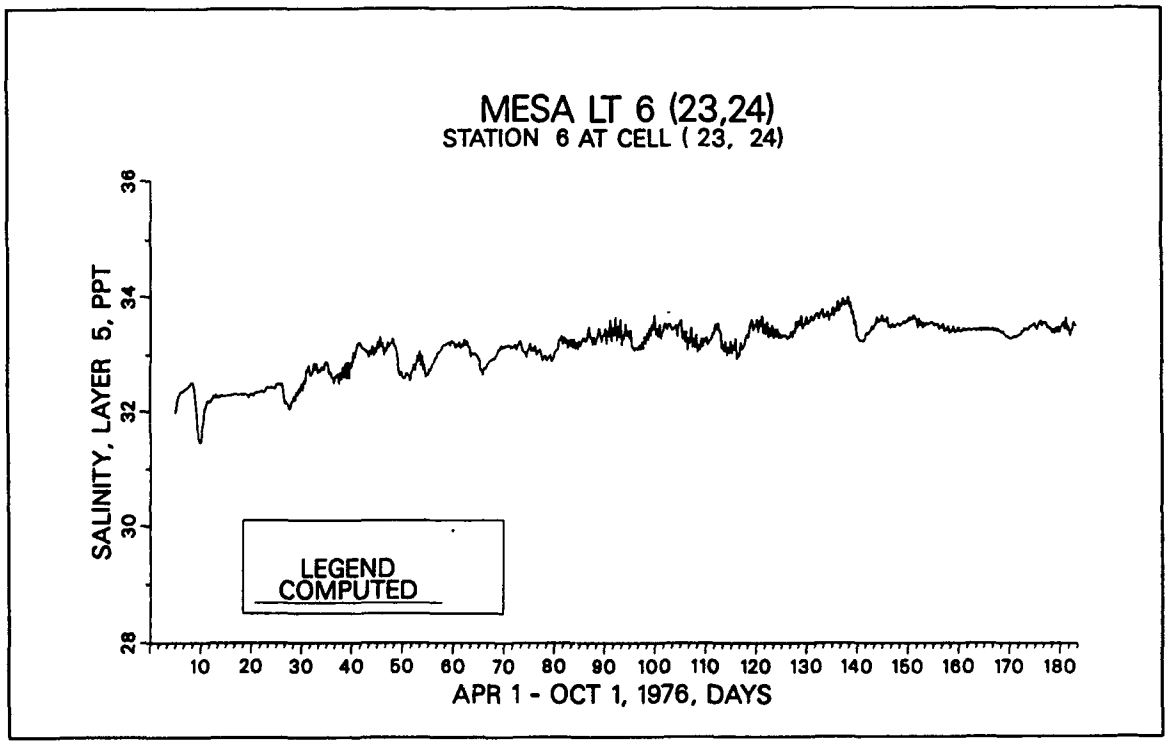

Figure D16. Variation of computed salinity at LT6, layer 5

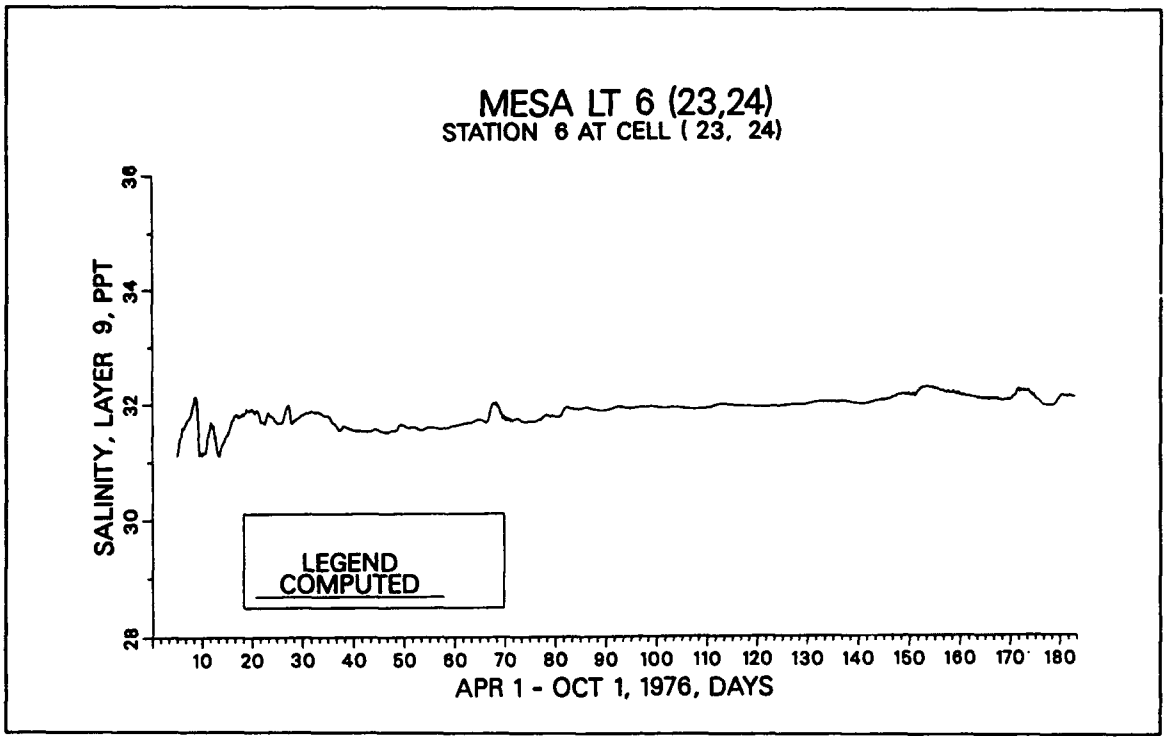

Figure D17. Variation of computed salinity at LT6, layer 9

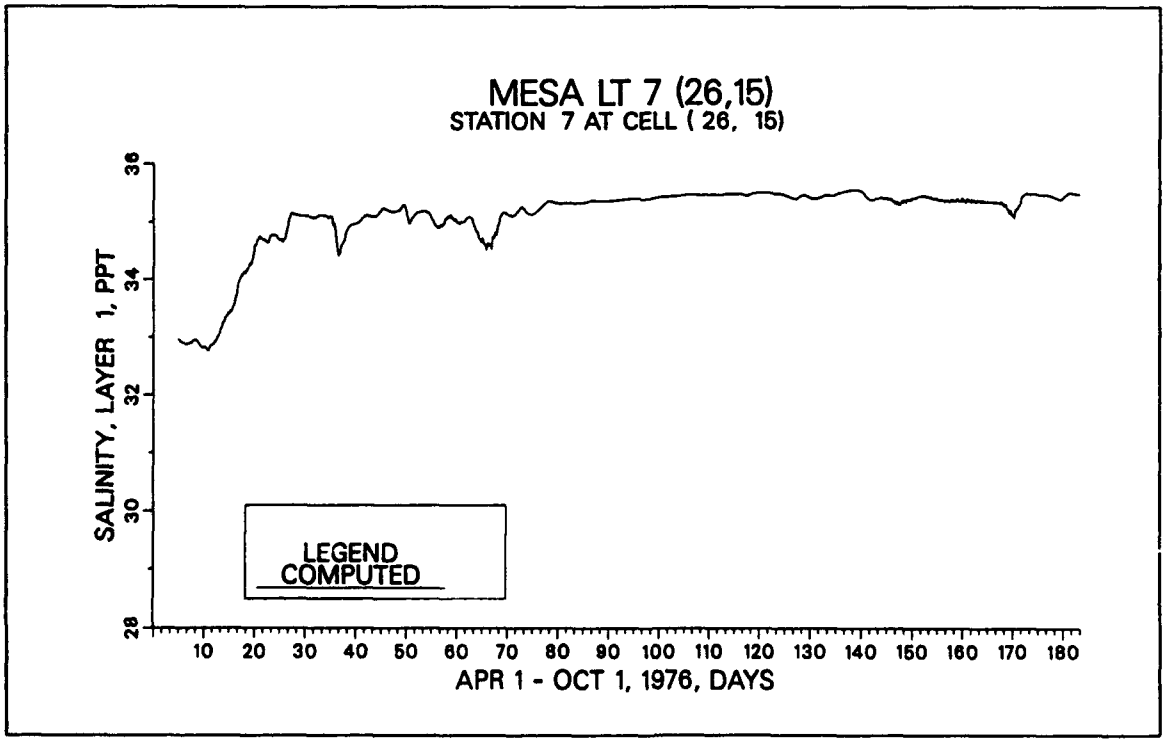

Figure D18. Variation of computed salinity at LT7, layer 1

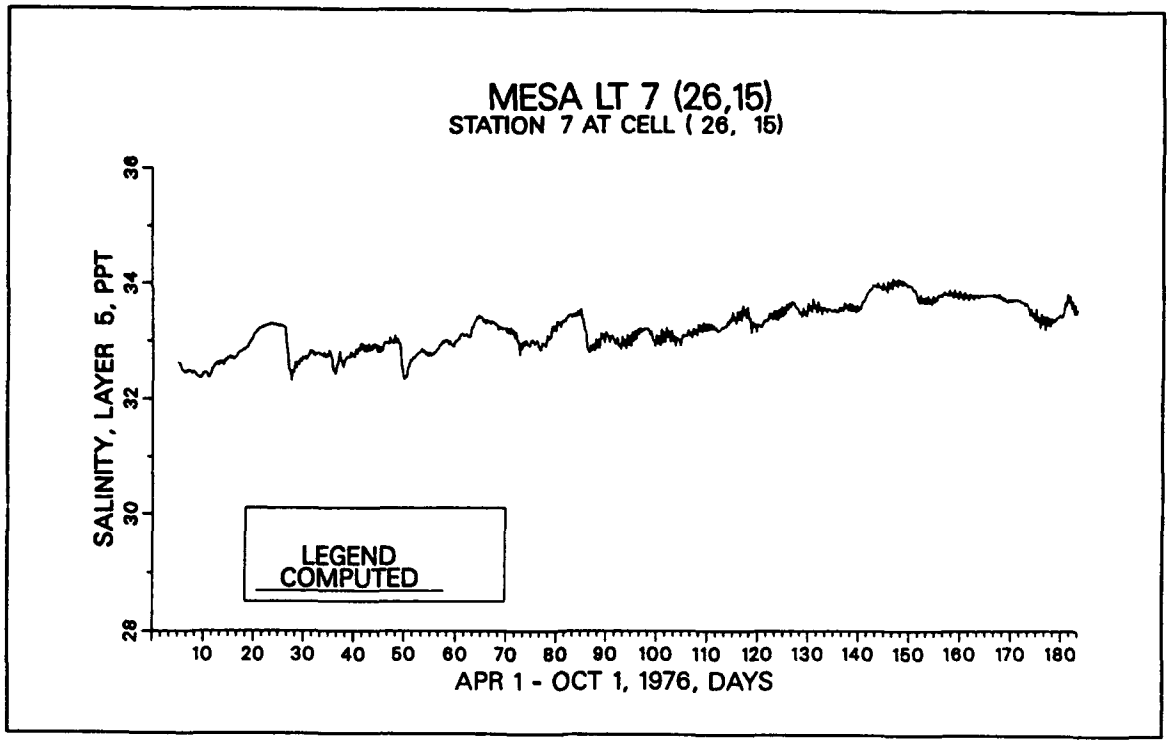

Figure D19. Variation of computed salinity at LT7, layer 5

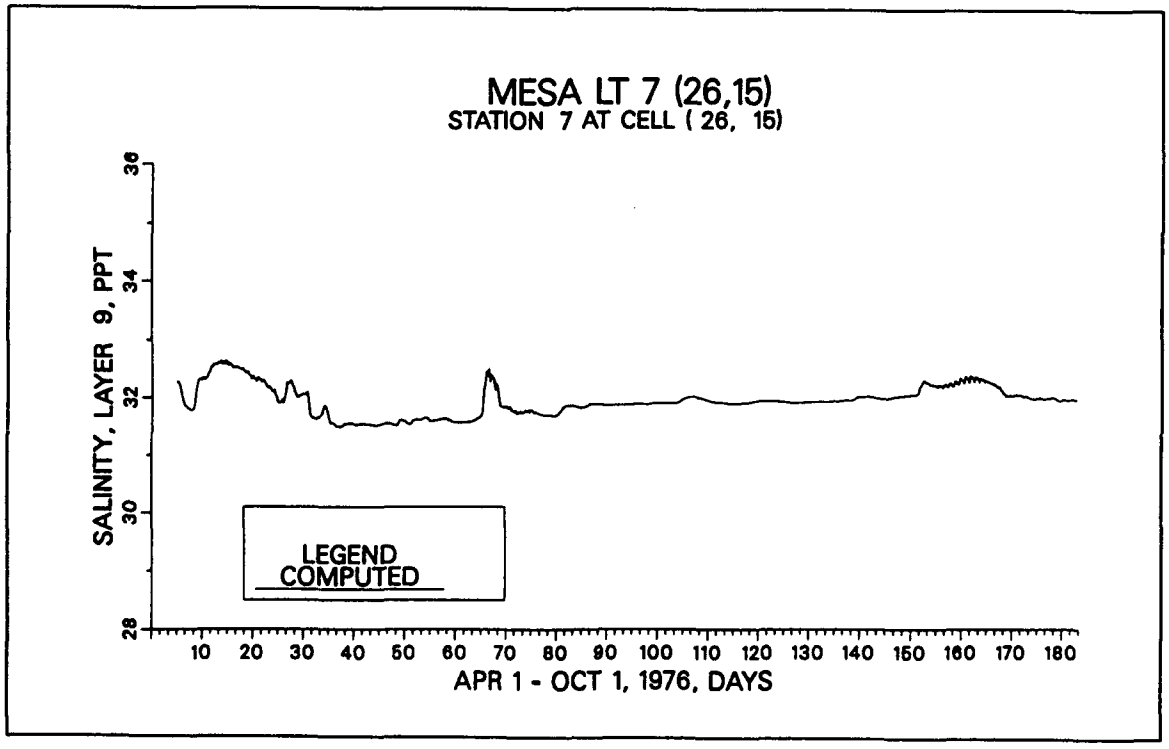

Figure D20. Variation of computed salinity at LT7, layer 9

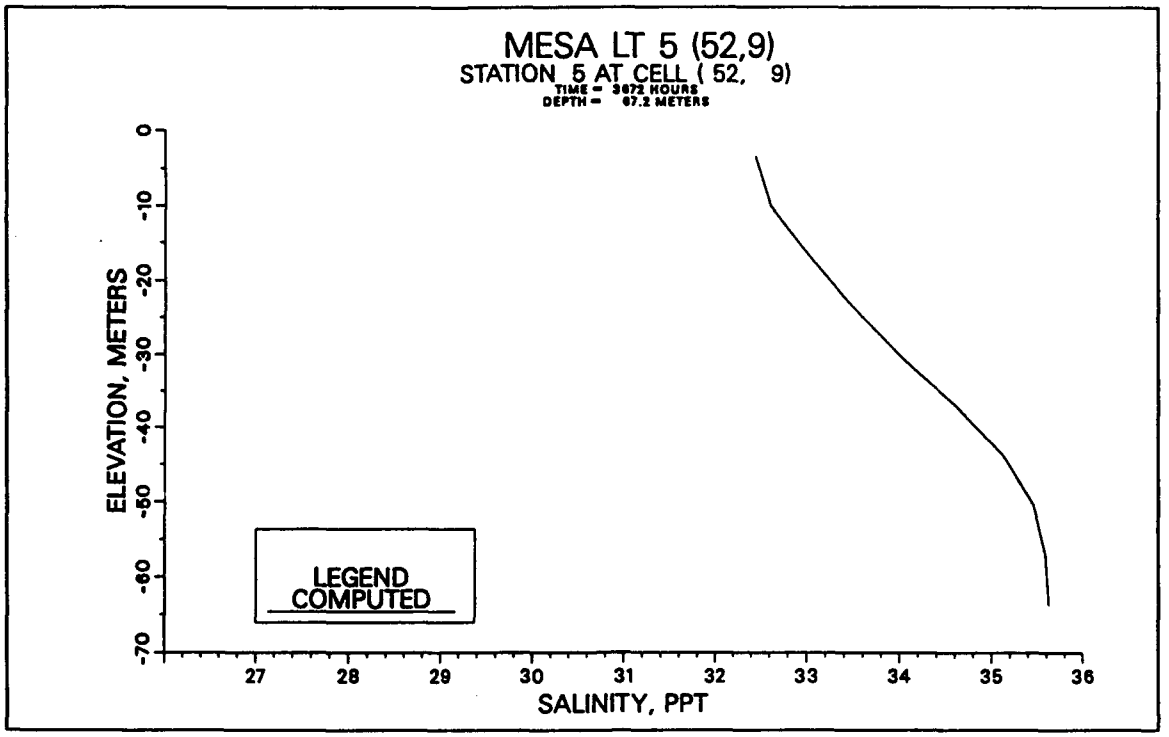

Figure D21. Salinity profile at LT5 at 3672 hours

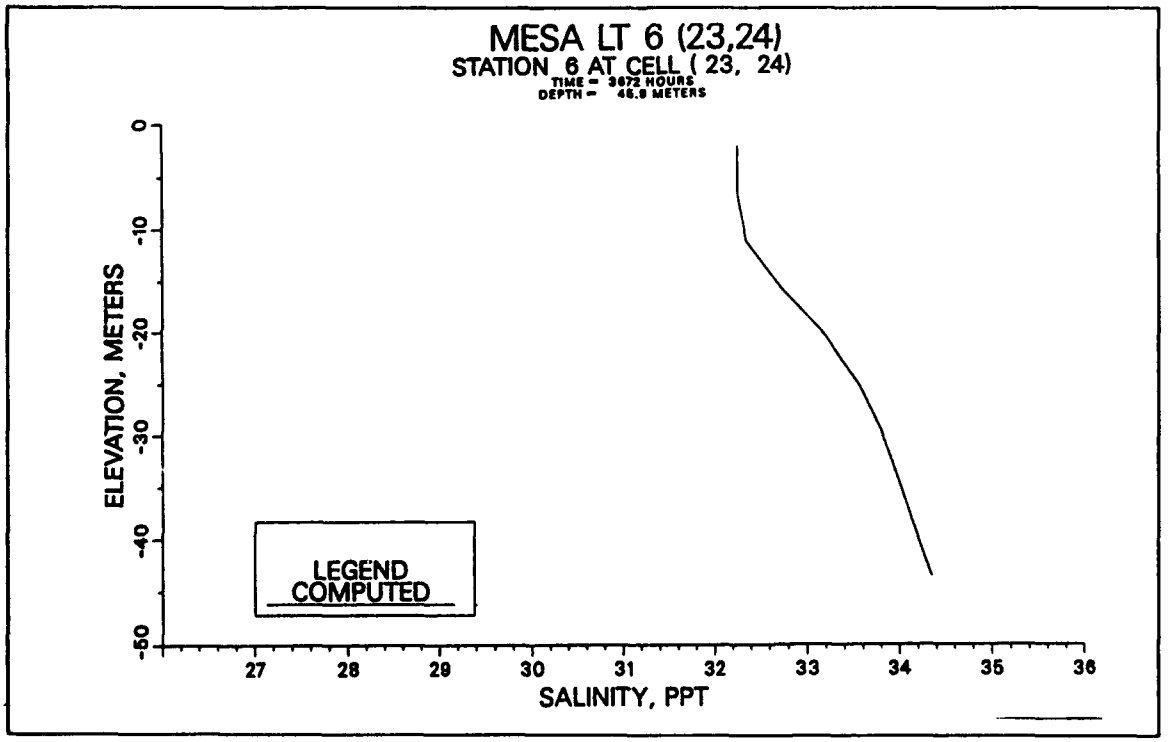

Figure D22. Salinity profile at LT6 at 3672 hours

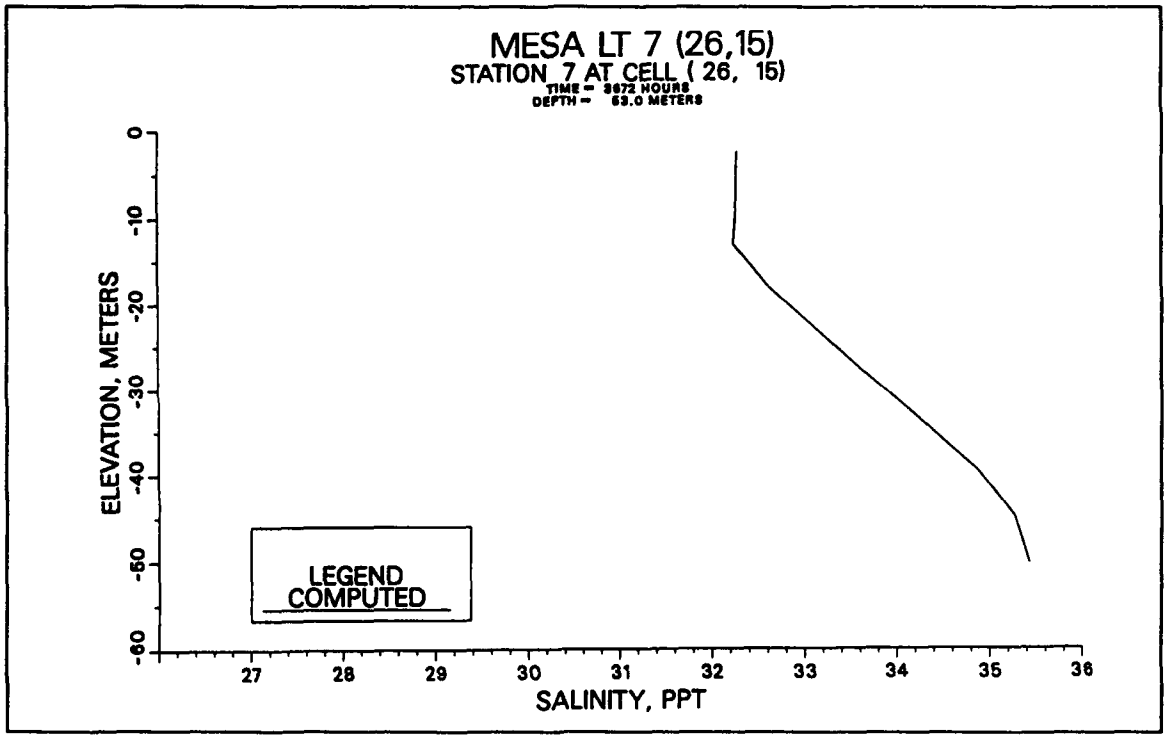

Figure D23. Salinity profile at LT7 at 3672 hours

Appendix E
Extended Validation Comparisons

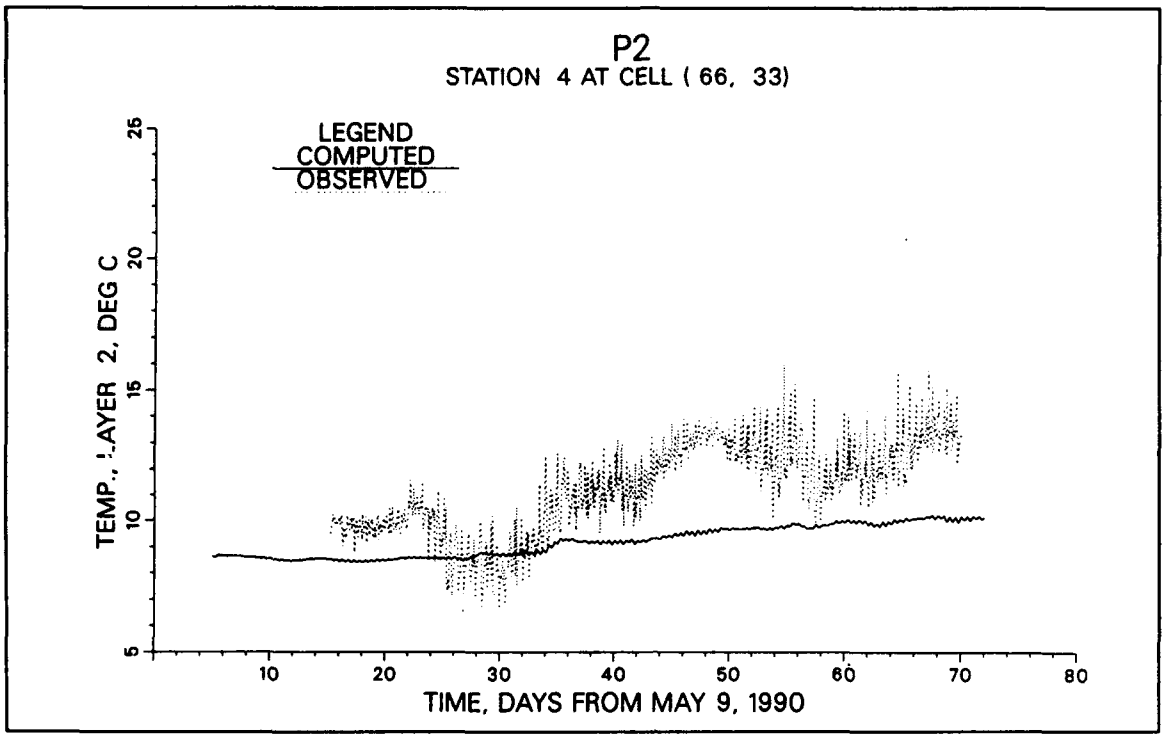

Figure E1. Temperature comparison at P2, lower level

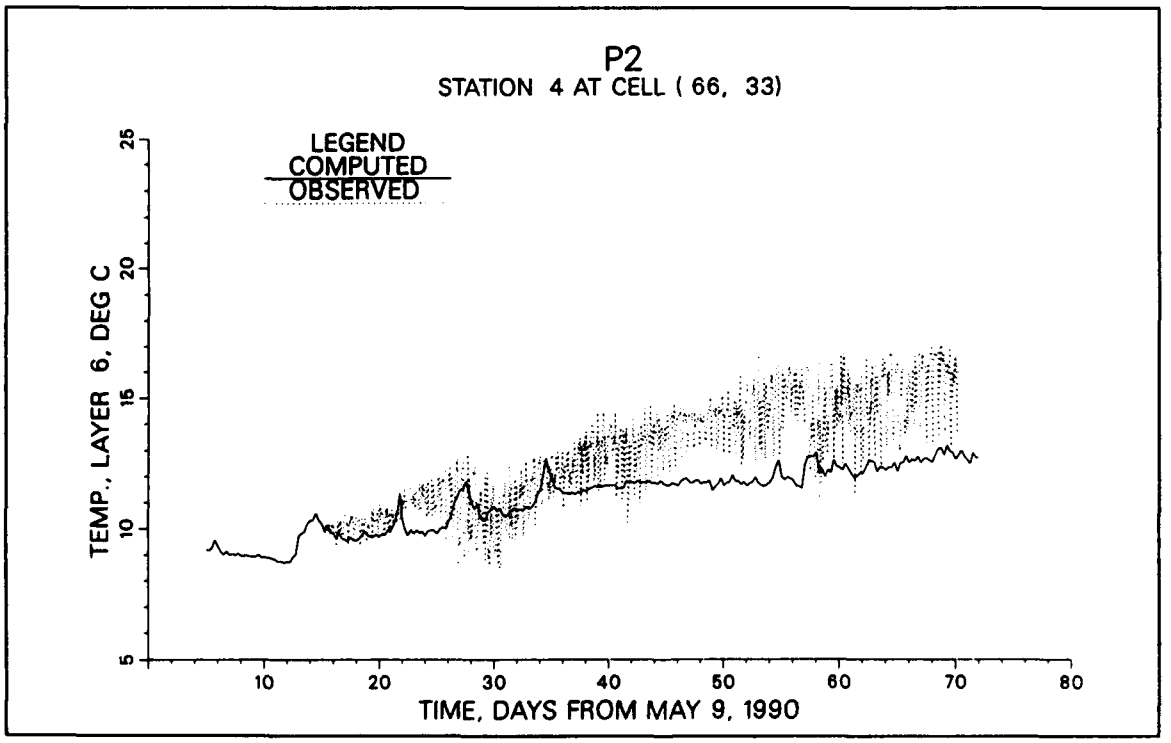

Figure E2. Temperature comparison at P2, upper level

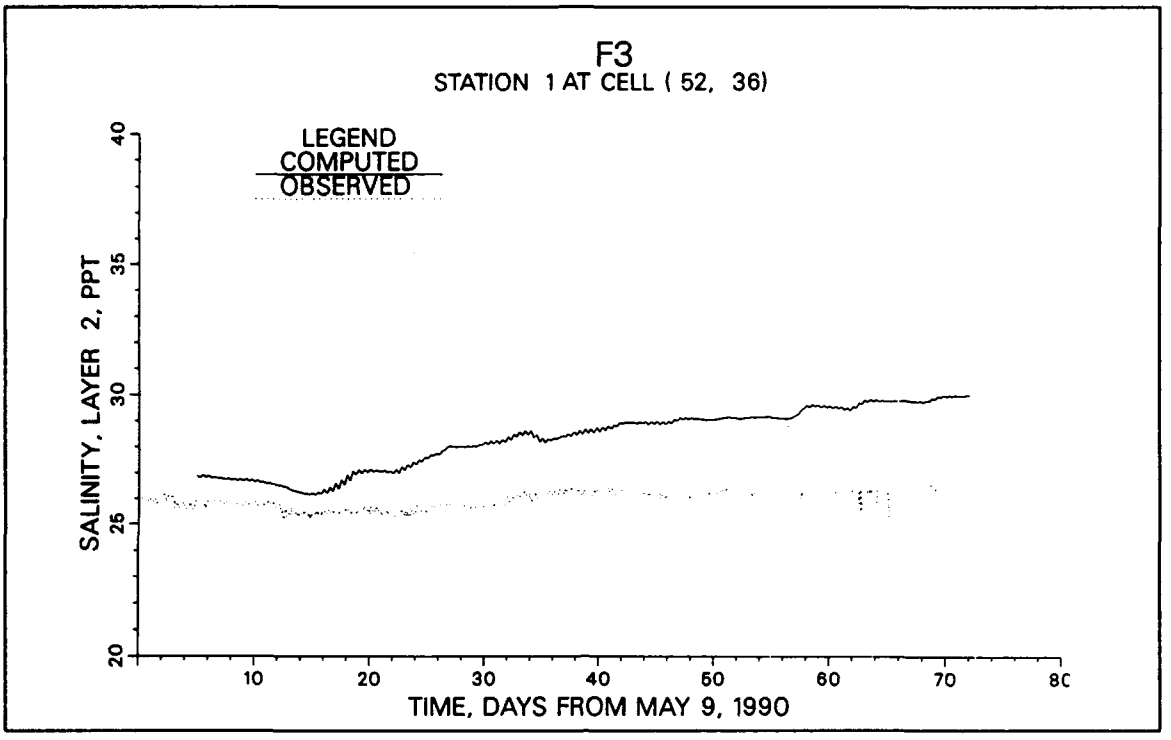

Figure E3. Salinity comparison at F3, lower level

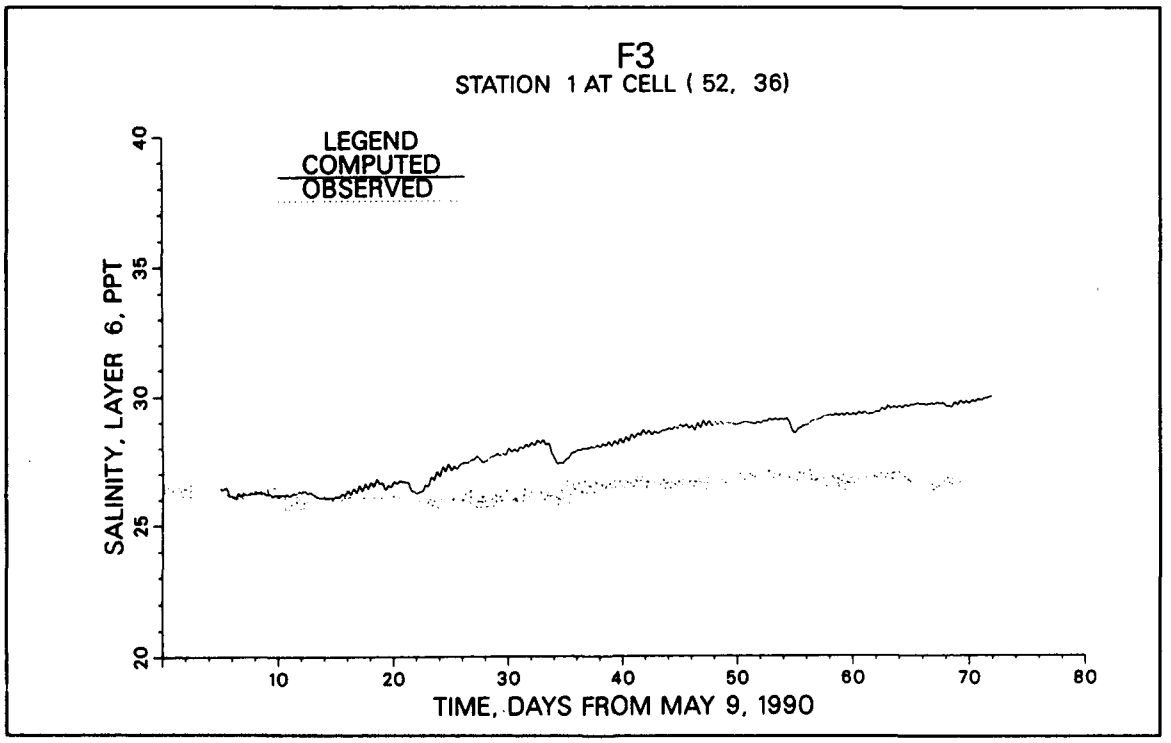

Figure E4. Salinity comparison at F3, upper level

REPORT DOCUMENTATION PAGE

Form Approved
OMB No. 0704-0188

1. AGENCY USE ONLY (Leave blank)	2. REPORT DATE	3. REPORT TYPE AND DATES COVERED
	August 1994	Report 1 of a series

4. TITLE AND SUBTITLE

New York Bight Study; Report 1:
Hydrodynamic Modeling

5. FUNDING NUMBERS

6. AUTHOR(S)

Norman W. Scheffner, S. Rao Vemulakonda
David J. Mark, H. Lee Butler, Keu W. Kim

7. PERFORMING ORGANIZATION NAME(S) AND ADDRESS(ES)

U.S. Army Engineer Waterways Experiment Station
3909 Halls Ferry Road, Vicksburg, MS 39180-6199

8. PERFORMING ORGANIZATION REPORT NUMBER

Technical Report
CERC-94-4

9. SPONSORING/MONITORING AGENCY NAME(S) AND ADDRESS(ES)

U.S. Army Engineer District, New York
New York, NY 10278

10. SPONSORING/MONITORING AGENCY REPORT NUMBER

11. SUPPLEMENTARY NOTES

Available from National Technical Information Service, 5285 Port Royal Road, Springfield, VA 22161.

12a. DISTRIBUTION/AVAILABILITY STATEMENT

Approved for public release; distribution is unlimited.

12b. DISTRIBUTION CODE

13. ABSTRACT *(Maximum 200 words)*

As a part of the New York (NY) Bight Feasibility Study, a three-dimensional hydrodynamic model of the NY Bight was developed and applied by the Coastal Engineering Research Center of the U.S. Army Engineer Waterways Experiment Station. The study used the three-dimensional hydrodynamic model CH3D-WES for this purpose. A 76 x 45 cell boundary-fitted curvilinear grid was employed in the horizontal and five to ten sigma layers were used in the vertical. Steady-state and diagnostic tests were initially performed, using M_2 and mixed tides, cross-shelf gradients, winds, and freshwater flows in the Hudson River. All of the tests were successful in reproducing known circulation patterns of the NY Bight system. The model was next successfully calibrated and verified against prototype tidal elevations and currents measured during April and May 1976.

As a demonstration of the feasibility of long-term modeling, the hydrodynamics, including salinity and temperature, were simulated for the period April-October 1976. Model results compared favorably with available prototype temperature measurements. Model output was furnished to a water quality model of the NY Bight, which successfully reproduced the hypoxic event of 1976. Model results also were used successfully to run particle tracking and oil spill models of the NY Bight. Finally, the model was demonstrated for the Long Island Sound

(Continued)

14. SUBJECT TERMS	15. NUMBER OF PAGES
See reverse.	228
	16. PRICE CODE

17. SECURITY CLASSIFICATION OF REPORT	18. SECURITY CLASSIFICATION OF THIS PAGE	19. SECURITY CLASSIFICATION OF ABSTRACT	20. LIMITATION OF ABSTRACT
UNCLASSIFIED	UNCLASSIFIED		

13. (Concluded).

and East River areas, for the period of May-July 1990. Computed results for elevation, velocity, salinity, and temperature in the Sound as well as net flux in the East River matched measurements reasonably. On the basis of the study results, recommendations are made for monitoring in the NY Bight to improve model predictions in the future.

14. (Concluded).

Feasibility study	Models	Three-dimensional
Hydrodynamics	Monitoring	Water quality
Long Island Sound	New York Bight	

Destroy this report when no longer needed. Do not return it to the originator.